

UC Berkeley

UC Berkeley Electronic Theses and Dissertations

Title

Gas-Phase Organic Carbon and Tropospheric Pollution: Sources, Emissions, and Implications for Air Quality

Permalink

<https://escholarship.org/uc/item/66c0z37x>

Author

Gentner, Drew Roland

Publication Date

2012

Peer reviewed|Thesis/dissertation

Gas-Phase Organic Carbon and Tropospheric Pollution:
Sources, Emissions, and Implications for Air Quality

by

Drew Roland Gentner

A dissertation submitted in partial satisfaction of the
requirements for the degree of

Doctor of Philosophy

in

Engineering - Civil and Environmental Engineering

with a Designated Emphasis

in

Energy Science and Technology

in the

Graduate Division

of the

University of California, Berkeley

Committee in charge:

Professor Allen H. Goldstein, Chair

Professor Robert A. Harley

Professor Daniel M. Kammen

Fall 2012

Gas-Phase Organic Carbon and Tropospheric Pollution:
Sources, Emissions, and Implications for Air Quality

Copyright © 2012

by

Drew Roland Gentner

Abstract

Gas-Phase Organic Carbon and Tropospheric Pollution: Sources, Emissions, and Implications for Air Quality

by

Drew Roland Gentner

Doctor of Philosophy in Engineering - Civil and Environmental Engineering
with a Designated Emphasis in Energy Science and Technology
The University of California, Berkeley
Professor Allen H. Goldstein, Chair

The troposphere is comprised of a complex mixture of molecules with trace amounts of over 10,000 organic compounds in the gas and particle phase. These compounds play important roles in the chemistry of the troposphere and the formation of detrimental secondary air pollution that impacts human health, climate, and the environment. This dissertation describes the development of novel ambient measurement techniques and statistical modeling methods, and their use to provide in-depth characterization of emissions from several prominent anthropogenic and biogenic sources. These results are used to assess the potential of the studied sources to form secondary organic aerosol (SOA) and tropospheric ozone. The objectives of this dissertation are accomplished using data from 6 measurement campaigns in the state of California, which includes some of the worst regions for air quality in the United States.

An automated *in situ* instrument with a gas chromatograph coupled to a mass spectrometer and a flame ionization detector was modified to measure a broad range of gas-phase organic compounds. This included a mixture of traditionally measured chemical species and numerous compounds for which no previous *in situ* measurements exist and have otherwise been relatively unstudied. Many of these compounds were in the intermediate-volatility range (i.e. IVOCs), which have previously been hypothesized to have a considerable effect on the formation of SOA. The rest of the compounds measured were in the volatile organic compound (VOC) range, but many of the least volatile compounds in this range had not been sufficiently studied, such as C₁₀ aromatic hydrocarbons from motor vehicles.

Source receptor modeling techniques with chemical mass balancing were developed in several forms and used in this dissertation to assess emissions of gasoline exhaust, non-tailpipe gasoline, diesel exhaust, and unrefined petroleum gas emissions from petroleum operations. A statistical analysis using meteorological data (Flexpart) and ambient ground site measurements was developed to examine the spatial distribution of emissions in a region and is used in this dissertation to examine emissions from several point and area sources. Techniques are also developed to estimate bulk SOA yields of the complex mixtures in gasoline and diesel emissions.

A comparison of gas-phase organic carbon emissions from gasoline and diesel vehicles concludes that diesel emissions form 15 times more SOA than gasoline exhaust per liter of fuel burned, but given the extensive use of gasoline and varied fuel use depending on region, diesel is responsible for 65-90% of vehicular SOA. The non-tailpipe gasoline and unrefined petroleum gas sources examined in this dissertation are significant in abundance, but are comprised largely of relatively small hydrocarbons and thus form negligible amounts of SOA. Biogenic emissions of terpenoid and benzenoid compounds were measured in this work and are highly reactive. In regions with extensive agricultural operations, such as California's San Joaquin Valley,

summertime emissions of biogenic compounds have the potential to form a similar amount of SOA and ozone as motor vehicle emissions. Additionally, seasonal emission events, such as flowering, produce an order of magnitude increase in emissions of ozone and SOA precursors. In all, the advancements in source characterization and secondary pollution formation potential in this dissertation provide important insights for future studies, models, and air pollution control policies.

Table of Contents

| | <u>Page</u> |
|--|-------------|
| List of Figures | ii |
| List of Tables | v |
| Acknowledgements | vii |
| Chapter 1: Introduction | 1 |
| Chapter 2: Materials and methods | 10 |
| Chapter 3: Diurnal and seasonal variability of gasoline-related volatile organic compound emissions | 27 |
| Chapter 4: Elucidating secondary organic aerosol from diesel and gasoline vehicles through detailed characterization of organic carbon emissions | 48 |
| Chapter 5: Evidence for emissions of gas-phase organic carbon from petroleum operations in California's San Joaquin Valley | 103 |
| Chapter 6: Emissions of biogenic gas-phase organic carbon from agriculture and their implications for air quality | 118 |
| Chapter 7: Conclusions | 158 |

List of Figures

| | <u>Page</u> | |
|------|---|----|
| 2.1 | Example chromatogram from Bakersfield, CA showing distribution of organic compounds across volatility classes from multiple channels/instruments | 23 |
| 2.2 | Example chromatogram from Bakersfield, CA from gas-phase instrument showing the alkanes, aromatics, and PAHs measured | 24 |
| 2.3 | Example chromatogram from channel 1 at Bakersfield, CA showing the m/z 57 signal | 24 |
| 2.4 | Example chromatogram from Bakersfield, CA showing the separation and measurement of naphthalene and its' small alkylated isomers | 25 |
| 2.5 | Example chromatogram from the Lindcove orange orchard in spring 2010 during flowering | 26 |
| 3.1 | Plots of ambient concentrations of n-butane and isopentane versus carbon monoxide at Riverside for summer and fall 2005 | 36 |
| 3.2 | Diurnal variation of ambient CO concentration at Riverside (weekdays only during summer 2005) and collocated variations in ambient temperature and wind speed | 37 |
| 3.3 | Distributions of summer wind speed and direction at Riverside, CA. | 38 |
| 3.4 | Source contributions to ambient VOC at Riverside from whole gasoline and gasoline vapor emissions | 39 |
| 3.5 | Plot of gasoline-related VOC concentrations versus carbon monoxide concentrations during summer 2005 | 40 |
| 3.6 | Sample chromatograms for SOAR measurements | 41 |
| 3.7 | Weekly diurnal ozone and ambient temperature profiles at Riverside, CA | 42 |
| 3.8 | Diurnal EMFAC-derived evaporative emissions during summer 2005 | 42 |
| 3.9 | Daytime vapor contribution fraction from weekday summer measurements compared to EMFAC model results | 43 |
| 3.10 | Gasoline-related VOC to CO ratios for weekday and weekend including EMFAC results | 43 |
| 4.1 | Distributions of chemical classes for diesel and gasoline as shown via gas chromatography/mass spectrometry | 65 |
| 4.2 | Distribution of mass and SOA formation potential in diesel and gasoline fuel and non-tailpipe gasoline emissions | 67 |
| 4.3 | Percent contribution of gasoline and diesel exhaust to SOA over 0-50% diesel fuel use | 68 |
| 4.4 | Comparisons of organic aerosol vs. carbon monoxide for vehicular OA and total OA, and the diurnal pattern of Δ OA/ Δ CO ratios | 69 |
| 4.5 | Demonstration of compositional consistency between gasoline and diesel fuel to gasoline and diesel exhaust at Bakersfield and the Caldecott tunnel | 70 |
| 4.6 | Verification of model performance at CalNex-Bakersfield by comparing | 71 |

| | | |
|------|--|-----|
| | predicted compound concentrations with observations of independent compounds | |
| 4.7 | Verification of model performance at the Caldecott tunnel by comparing predicted compound concentrations with observations of independent compounds | 72 |
| 4.8 | Internal model diagnostics for CalNex-Bakersfield site | 73 |
| 4.9 | Internal model diagnostics for the Caldecott tunnel site | 73 |
| 4.10 | Distributions of SOA yield uncertainties from each gas and diesel source | 74 |
| 4.11 | Volatility basis set distribution of diesel fuel broken down by chemical class | 75 |
| 4.12 | Weekday/weekend diurnal profiles of diesel exhaust, gasoline exhaust, and non-tailpipe gasoline source contributions, and the ratio of diesel to gasoline exhaust at Bakersfield | 76 |
| 4.13 | Overall, weekday, and weekend diurnal patterns for total and vehicular organic aerosol, and their respective $\Delta\text{OA}/\Delta\text{CO}$ ratios at Bakersfield, CA | 77 |
| 4.14 | Weekday/weekend behavior of $\Delta\text{OA}/\Delta\text{CO}$ ratios in Los Angeles, CA | 78 |
| 4.15 | Observed organic aerosol vs. carbon monoxide at Bakersfield, CA with contributions for major non-vehicular sources as determined by factor analysis of AMS data | 79 |
| 4.16 | Percent contribution of diesel exhaust to gas-phase organic carbon and SOA versus percent diesel fuel use | 80 |
| 4.17 | Vehicular organic aerosol vs. carbon monoxide at Bakersfield, CA with weekday/weekend and day/night differences shown | 81 |
| 5.1 | 6 and 12 hour statistical footprints determined using Flexpart meteorological data for the Bakersfield ground site averaged across the entire CalNex campaign | 111 |
| 5.2 | Observations of ethane vs. propane using canister measurements at Bakersfield | 112 |
| 5.3 | Comparison of methylcyclohexane and isooctane at the Bakersfield ground site | 112 |
| 5.4 | The average unexplained concentration of each compound and the percentage of unexplained mass out of total observations shown with examples of exceedances of observed over predicted values | 113 |
| 5.5 | Average diurnal pattern for the petroleum gas source contribution | 113 |
| 5.6 | The sum of unexplained compounds vs. the petroleum gas source | 114 |
| 5.7 | The diurnal average of the ratio of petroleum gas to the sum of motor vehicle emissions | 114 |
| 5.8 | Maps of southern part of the San Joaquin Valley with the location of oil and gas wells, the spatial distribution of petroleum gas emissions determined using statistical footprint analysis, and aircraft canister measurements of propane | 115 |
| 5.9 | Observations of methane vs. the petroleum gas source | 116 |
| 5.10 | Observations of methane vs. non-vehicular ethanol | 116 |

| | | |
|------|---|-----|
| 6.1 | Average diurnal patterns of different compound classes shown on a logarithmic scale during flowering at the Lindcove site | 143 |
| 6.2 | Comparison of total observed flowering compounds to the sum of monoterpenes during the spring at the Lindcove site | 144 |
| 6.3 | Comparison of observed sesquiterpenes to monoterpenes during the spring at Lindcove | 145 |
| 6.4 | Diurnal pattern of sesquiterpenes to monoterpenes during the spring at Lindcove | 145 |
| 6.5 | Diurnal pattern and composition of monoterpenes in spring during flowering | 146 |
| 6.6 | Diurnal pattern and composition of monoterpenes in summer | 146 |
| 6.7 | Seasonal comparison of diurnal monoterpene concentrations at Lindcove | 147 |
| 6.8 | Seasonal comparison of diurnal limonene concentrations at Lindcove | 148 |
| 6.9 | Seasonal comparison of diurnal p-cymene concentrations at Lindcove | 149 |
| 6.10 | Diurnal patterns of the sum of biogenic compounds vs. anthropogenic compounds from motor vehicles at the Lindcove site in the spring | 149 |
| 6.11 | Sum of biogenic compounds (largely monoterpenes) observed at the urban Bakersfield site vs. the sum of compounds from motor vehicles | 149 |
| 6.12 | Comparison of motor vehicle compound concentrations between the urban Bakersfield site and the rural Lindcove site | 150 |
| 6.13 | Observations of Δ -limonene vs. α -pinene at the Bakersfield site with evidence of aging | 151 |
| 6.14 | Comparison of α -pinene vs. camphene at Bakersfield shows evidence of aging by O ₃ and NO ₃ | 152 |
| 6.15 | Spatial distribution of monoterpene sources in the southern San Joaquin Valley | 153 |
| 6.16 | Spatial distribution of monoterpene sources in the southern San Joaquin Valley shown for individual monoterpene species | 154 |
| 6.17 | The components of the net ozone flux for the Lindcove orange grove shown over the full year | 155 |
| 6.18 | Ambient ozone data over a full year at sites in and near the San Joaquin Valley shown with the weekly net effect of the orange grove on ozone | 156 |

List of Tables

| | <u>Page</u> | |
|------|--|-----|
| 2.1 | Summary of compounds quantified across campaigns | 18 |
| 3.1 | 2005 gasoline-related VOC emission inventory for Riverside county (South Coast air basin) | 44 |
| 3.2 | Most abundant compounds in gasoline and headspace vapors | 45 |
| 3.3 | Compounds measured during SOAR 2005 | 46 |
| 3.4 | Percent vapor contribution to gasoline-related VOC emissions at Riverside, CA | 47 |
| 3.5 | VOC/CO ratios at Riverside, CA | 47 |
| 4.1 | Distribution of mass and SOA potential by chemical class for diesel exhaust, gasoline exhaust, and non-tailpipe gasoline | 66 |
| 4.2 | Sales of on-road gasoline and diesel fuel in California and its counties | 82 |
| 4.3 | Chemical class distribution of gasoline and diesel sources by total mass | 83 |
| 4.4 | Summary of compounds used in source receptor modeling at Bakersfield | 84 |
| 4.5 | Summary of compounds used in source receptor modeling at the Caldecott tunnel | 84 |
| 4.6 | Mass and chemical class distribution of diesel fuel | 85 |
| 4.7 | Mass and chemical class distribution of liquid gasoline | 86 |
| 4.8 | Mass and chemical class distribution of non-tailpipe gasoline | 87 |
| 4.9 | Average high-NO _x SOA yields with uncertainties constructed from scenarios and Monte Carlo analysis | 88 |
| 4.10 | Compound specific liquid gasoline speciation for California in Summer 2010 | 89 |
| 4.11 | Compound specific diesel fuel speciation for California in Summer 2010 | 96 |
| 4.12 | Compound specific non-tailpipe gasoline speciation for California in Summer 2010 | 99 |
| 5.1 | Unrefined natural gas profile for thermogenic wet wells in the San Joaquin Valley from U.S.G.S. samples | 108 |
| 5.2 | Interquartile ranges and MIRs for alkanes | 109 |
| 5.3 | Quartiles for ambient concentrations from major petroleum-based sources measured at the Bakersfield site | 110 |
| 6.1 | Planted areas for permanent crops with largest land cover in the San Joaquin Valley | 132 |
| 6.2 | Plants studied during greenhouse enclosure campaign | 133 |
| 6.3 | Basal emission factors and beta values for monoterpenes, oxygenated monoterpenes and sesquiterpenes from enclosure studies | 134 |
| 6.4 | Statistics for modeling methods using light and temperature and temperature only from enclosure studies | 135 |
| 6.5 | Composition of monoterpene emissions measured in enclosure studies | 136 |
| 6.6 | Composition of oxygenated monoterpene emissions measured in enclosure | 137 |

| | | |
|------|--|-----|
| | studies | |
| 6.7 | Composition of sesquiterpene emissions measured in enclosure studies | 138 |
| 6.8 | Interquartile ranges for measured BVOC in spring and summer | 139 |
| 6.9 | Novel compounds from measurements of ambient air during flowering | 140 |
| 6.10 | Compounds highly correlated with flowering emissions | 141 |
| 6.11 | Source profile for flowering emissions from citrus trees | 142 |
| 6.12 | Summary of monoterpene composition for both seasonal campaigns at Lindcove | 142 |

Acknowledgements

It has been a remarkable and fulfilling journey over the past five years. I would like to foremost thank Allen Goldstein and Rob Harley for their mentorship, confidence, support, and the opportunity to work on engaging impactful projects. For all his time spent educating me in the lab and his technical advice, I would like to thank, my friend, Dave Worton. I would also like to express my gratitude to Robin Weber, Elena Ormeno-Lafuente, Gabriel Isaacman, and all my other colleagues at UCB in engineering and environmental sciences that have provided assistance, research tools, collaboration, camaraderie, and a great working environment (Arthur Chan, Tim Dallmann, Brian McDonald, Silvano Fares, Dylan Millet, Nicole Bouvier-Brown, Brent Williams, Yunliang Zhao, Tom Kirchstetter, Bev Coleman, Arman Shehabi, Bret Strogon, Rudi Schuech, Josh Apte, Sharon Shearer, Seema Bhangar, Nasim Mullen, Dev Millstein, Sally Pusede, Chelsea Preble, Jeong-Hoo Park, Pawel Misztal, Chris Ruehl, Rachel O'Brien, Abhinav Guha, & Megan McKay). I would like to acknowledge and thank my undergraduate researchers for all of their hard work and trust in me (Raymond Lo, Laura Davis, Sara Forestieri, Josh Pepper, Luis Mendez, Kelsey Boulanger, & Trevor Ford); it has been a pleasure to be a part of your education and professional development.

I would like to thank my collaborators at NOAA (Joost de Gouw, Jessica Gilman, David Parrish, and Jerome Brioude) for their assistance and contributions to my research. There are many collaborators at other institutions that deserve recognition: John Karlik, Lynn Russell, Kevin Wilson, Izadyar Dalvand, Shang Liu, Doug Day, Don Blake, and Elliot Atlas. I would like to thank the members of my committees: Allen, Rob, Dan Kammen, Bill Nazaroff, Ron Cohen, and Tina Katopodes-Chow. I would like to thank the U.S. EPA, NOAA, the Citrus Research Board, and the California Air Resources Board for funding my research. For infrastructure and project assistance, I would like to acknowledge the Gorden Family and the staff of UCB Oxford Tract greenhouse, Caldecott tunnel, CalTrans, and the U.C. Cooperative Extension centers at Lindcove and Kern County.

I don't think I would have found myself at U.C. Berkeley without the guidance and support of the educators throughout my life who encouraged my dreams and had confidence in my abilities; for this I would specifically like to thank Kim Gray and Mike Welty. A big thanks goes to those who helped me survive fieldwork and have a bit fun along the way: Trevor VandenBoer, Milos Markovic, and many of those already mentioned above. There are many other people who have helped me during my time at Berkeley, and I thank all of you for your assistance and friendship—Shelley Okimoto, Joan Chamberlain, Jamie Hampton, Mike Branzel, Brian Lesters and all those I apologetically cannot recall.

To my parents, family and friends, I can only begin to convey the power of your love, support, and encouragement throughout my life and over the past five years. Much love and appreciation goes to my brothers, Greg and Eric. Finally, to Brenda, an acknowledgement in my dissertation is beyond insufficient to show my gratitude for everything you have done for me. Thank you for all the big things, all the little things, and your enduring love.

In loving memory of my mother,
for her endless love, support and
steadfast commitment to my education

Chapter 1: Introduction

Organic compounds are ubiquitous throughout the atmosphere and include over 10,000 individual chemical species that exist in the gas phase, particle phase, or distributed between the two phases (1). Many gas-phase organic compounds are important precursors to the formation of secondary organic aerosol (SOA) and tropospheric ozone (1). Some compounds are also of concern as primary pollutants due to their acute and chronic health effects, influence on climate change, and/or ability to deplete stratospheric ozone (2, 3, 4). Both tropospheric ozone and SOA have detrimental effects on human health and implications for climate change (3, 5, 6). Many aspects regarding the emissions of gas-phase organic carbon and the formation mechanisms leading to SOA and ozone are poorly understood and regulatory agencies lack sufficient information to develop effective control strategies for regions affected by detrimental air quality.

Organic carbon in the gas-phase can be classified by vapor pressure and is generally divided into Volatile Organic Compound (VOC), Intermediate Volatility Organic Compound (IVOC), and Semi-Volatile Organic Compound (SVOC) classes, or ranges (7). Gas-phase organic carbon exists over a wide range of molecular sizes (containing 1-25 carbon atoms) and functionalities, which together determine their volatility (i.e. their partitioning between the gas and particle phase) (1). A large fraction of organic compounds have rarely, or never, been measured in the atmosphere, especially those in the IVOC range, as historically gas-phase measurements have typically been limited to compounds with volatilities higher than alkanes with 8-10 carbon atoms. This can be attributed to the difficulty of measuring these compounds compared to much smaller compounds with greater abundances in the atmosphere. Additionally, it is much easier to sample and analyze light VOCs or much lower vapor pressure compounds that are entirely in the particle phase. Organic compounds can also be classified by chemical type and include, but are not limited to, alkanes, alkenes, alkynes, aromatics, polycyclic aromatic hydrocarbons (PAHs), and those with functional groups containing one or more oxygen, nitrogen, or halogen species (1). Sources are both biogenic and anthropogenic with varying degrees of characterization and uncertainty depending on historical importance and extent of research on individual source categories (1).

Tropospheric ozone

Elevated concentrations of ozone have been shown to cause increased mortality and have been linked to both acute and chronic cardiovascular and respiratory health problems (5). Ozone is formed as a product of the photochemical processing of VOCs via NO to NO₂ catalytic cycling (8). Emissions of VOCs and nitrogen oxides (NO_x) are both essential for ozone formation and, depending on regional atmospheric composition, emissions reductions for one or both may be required to reduce ambient ozone (8).

In regions where VOCs are the limiting reactant, emissions from anthropogenic sources can be controlled to reduce ozone (8). One prominent historical example is the South Coast air basin, which includes Los Angeles, Orange County, Anaheim, and Riverside (12). Regulatory efforts in the South Coast air basin, and nationally, began in the mid-1960's and focused on decreasing emissions of anthropogenic VOCs (9). Starting in the 1970's emissions of NO_x were targeted and a major step came with the development of catalytic converters in the late 1970's, which simultaneously reduced emissions of NO_x, VOCs, and carbon monoxide (9, 10). Significant progress has been made in most regions, including the South Coast air basin with reductions in peak ozone and the number of exceedance days annually (9). However, the South

Coast air basin is still not in compliance with current ozone standards and progress has slowed, suggesting a potential transition from a VOC-limited regime (9, 11).

Many regions are NO_x-limited, such as much of the southeastern U.S. owing to the large magnitude of BVOC emissions (8). In these areas, control of NO_x is the only viable option, but may not lead to immediate reductions in ozone due to decreased NO_x scavenging of ozone (8). NO_x emissions are dominated by anthropogenic sources with the largest sources being on- and off-road vehicles (12). NO_x concentrations in California have decreased by 4-9 % yr⁻¹ over 2005-2008 because of control measures on these mobile sources and continued efforts to control NO_x emissions in California are focused on installing NO_x control devices in heavy-duty diesel trucks (13).

Maximum concentrations of ozone will typically occur downwind of primary pollutant peaks once there has been adequate photochemical processing time and less NO_x scavenging of ozone (8). The formation of ozone is heavily influenced by temperature and solar irradiance due to enhanced photochemical processing and increased emissions of VOCs and, to a smaller extent, NO_x (8). For this reason, ambient concentrations tend to peak in the afternoon and are much greater in the summer than any other season.

One of the main challenges concerning the mitigation of ozone is assessing the VOC or NO_x sensitivity of ozone production for a specific region and then identifying the most important sources of VOCs that lead to ozone formation. The characterization of these sources and estimation of emission rates is critical to understand their ozone formation potential and improve model performance and develop effective regulatory measures (8). In particular for California's San Joaquin Valley, one of the major challenges is differentiating between biogenic and anthropogenic VOC contributions to ozone production.

Secondary organic aerosol

Atmospheric aerosols have important impacts on both climate change and human health; they remain the most uncertain anthropogenic forcing of climate change and can be expected to vary with changes in future climate and energy use (3). Organic aerosol (OA) comprises a significant and variable fraction (20-90%) of total aerosol mass and is composed of both primary organic aerosol (POA) and SOA (14). POA is largely a product of combustion processes, while SOA is chemically formed in the atmosphere from the oxidation of gaseous precursors including both biogenic and anthropogenic VOCs (1, 14). SOA is not directly regulated, but as a component of "smog" with ozone, concentrations have been reduced indirectly with VOC and NO_x controls over the past several decades. Particulate matter under 2.5 μm in diameter (PM_{2.5}) has been regulated since 1997 in the U.S. and is partially comprised of SOA (10).

Globally, biogenic contributions from vegetation are considered the dominant source of SOA precursors (1, 15). However, laboratory, field, and modeling studies have difficulty predicting SOA in urban areas and downwind (1, 15, 16, 17, 18, 19, 20, 21, 22). Multiple studies cite the importance of oxidized AVOC emissions in these underestimates, yet biogenic emissions may still play a significant role in unresolved urban SOA due to possible interactions with NO_x, SO₂, or other anthropogenic emissions (15, 16, 17, 23).

Organic compounds with lower volatilities (i.e. IVOCs and SVOCs) are now considered dominant contributors to SOA in urban and rural environments as several studies have shown their efficacy for SOA formation (7, 16, 17, 20, 24, 25). Research on the sources and photochemical aging of these low-volatility organics is crucial in order to account for all observed SOA (26). IVOCs and SVOCs are present in both the gas and particle phase with

effective saturation vapor pressures ranging from 10 to 10^6 $\mu\text{g}/\text{m}^3$ (7, 16). Many IVOCs are co-emitted with VOCs, but lack sufficient characterization from either anthropogenic or biogenic sources. Suggested sources of SVOCs include volatilized POA emitted during anthropogenic and biogenic combustion, and also from the gas-phase oxidation of more volatile organics in the atmosphere (7, 14, 16, 17, 20). The primary organic particles emitted during the combustion of either fossil fuels or biomass evaporate via atmospheric dilution in accordance with gas-to-particle partitioning theory, which is sensitive to both organic particle loadings and temperature (16, 27, 28). The photo-oxidation of gas-phase organics in the intermediate and semi-volatile range are important for SOA production and are termed non-traditional precursors (16, 29). In particular, diesel combustion emissions are expected to be a considerable source due to the high molecular weight characteristics of diesel fuel and the significant contribution of lubricating oil in diesel exhaust (30). Smog chamber simulations show rapid photo-oxidation of low-volatility diesel exhaust and adding parameterizations for these compounds to traditional modeling methods improves mass closure as previously models could only explain $\sim 10\%$ of SOA formation (22, 31).

The presence of low-volatility organics in both the gas and particle-phase emphasizes the importance of reactions in both phases, as they affect volatility and thus SOA formation potential (32, 33). Gas-phase oxidation (initiated by atmospheric oxidants: OH, NO_3 , and O_3) can lower volatility by adding polar functional groups, but oxidation can also increase volatility by triggering molecular decompositions at carbon-carbon double bonds. Several urban studies using an aerosol mass spectrometer (AMS) show that a considerable fraction of OA is not primary, but rather oxygenated organic aerosol (OOA) and thus secondary in nature (21, 34, 35, 36). OOA, therefore SOA formation, coincides with greater VOC oxidation, which occurs during active photochemical periods accompanied by high oxidant concentrations, solar irradiation, and temperature (29, 34, 37). Improved understanding of photochemical aging will help to resolve unaccounted SOA, which increases with age of an air parcel (15, 16, 21, 34).

Numerous studies have demonstrated the critical need for further research to measure and understand the sources and chemical transformations of SOA precursors with lower volatilities than historically studied compounds. Globally, measurements of traditional SOA precursors and model studies have substantially underestimated observed SOA formation; de Gouw et al. estimated that 63% of SOA in urban plumes in the northeastern U.S. is unexplained by traditional SOA precursors and may be due to low-volatility organics. Volkamer et al. similarly observed large unaccounted SOA contributions from AVOC in Mexico City, while Takegawa et al. and Johnson et al. saw similar results in Tokyo and London, respectively (15, 17, 18, 19, 20).

SOA & ozone in the San Joaquin Valley

Concentrations of ozone and $\text{PM}_{2.5}$ (comprised largely of OA) exceed air-quality standards in many locations throughout the developed and developing world. The problems, while substantial, are dependent on similar fundamental chemistry, atmospheric composition, and regional emission inventories. Concentrations of both $\text{PM}_{2.5}$ and ozone frequently exceed federal and state standards in California's San Joaquin Valley, placing several of its cities among the worst for air quality in the U.S.; all counties are designated non-attainment areas by the U.S. Environmental Protection Agency for 1-hour ozone, 8-hour ozone, and 24-hour $\text{PM}_{2.5}$ (11). These standard-violating concentrations of secondary pollutants are responsible for numerous health problems and excess deaths in the San Joaquin Valley (5, 6). The San Joaquin Valley is an important location to examine gas-phase organic carbon emissions and their effects on SOA and

ozone in conjunction with the nearby South Coast air basin. While the number of ozone exceedance days annually has improved markedly in the South Coast air basin over the past 30 years, the San Joaquin Valley shows minor, if any, improvement (11). A better understanding of the sources and composition of organic carbon emissions in the San Joaquin Valley and their potential to form SOA and ozone is essential to inform air quality policy in this region.

Gas-phase organic carbon, energy, & climate

There is a strong interconnection between air quality, climate change, and the production/consumption of energy. They are fundamentally intertwined as climate change is a product of changes in atmospheric composition and air quality, which is largely due to energy-related emissions. A better understanding of primary emissions from energy-related sources is necessary to inform decisions on energy/fuels with regard to mitigating both climate change and air quality.

Ozone and some VOCs are greenhouse gases causing positive radiative forcing, while aerosols can have either a warming or cooling effect (3). SOA typically has a negative radiative forcing (i.e. a cooling effect) through direct effects of the aerosol's high albedo and also indirectly effects on cloud formation and persistence (3). The multigenerational oxidative transformations that accompany photochemical aging play a critical role in determining aerosol hygroscopicity, which in turn increases the aerosol's ability to alter cloud formation and precipitation (14, 21, 34, 38).

A substantial amount of anthropogenic gas-phase organic carbon emissions are related to energy production or consumption. There are significant point and area source emissions from operations involving the drilling, refining, and delivery of fossil fuels, but mobile sources using gasoline and diesel account for over 50% of anthropogenic gas-phase organic carbon emissions in California (12). Mobile source emissions can be due to engine exhaust, or the escape of fuel vapors, which is somewhat temperature dependent (39). Additionally, hydrocarbons emitted in exhaust are affected considerably by engine design, operation, and control technologies, which stresses the importance of combustion technology in mitigating air quality. Emissions of gas-phase organic carbon are highly dependent on the types of fuel used and associated regulations. In the past, regulatory fuel standards have caused changes in gas-phase organic carbon emissions from mobile sources, and current/future regulation will have similar effects (40).

Biogenic VOC emissions will be affected by climate change; increased temperatures will lead to more emissions from plants and will thus increase SOA formation and ozone formation in VOC-limited regions (3). Several positive and negative feedbacks exist in between climate change and air quality (3). Increased SOA formation owing to increases in BVOC emissions is an example of a negative feedback in climate change since the cooling SOA caused by climate change will offset a fraction of the warming (3). Positive feedbacks will actually exacerbate the warming effect, such as increased temperatures leading to increases in NO_x emission due to greater energy use for cooling purposes, which when coupled with increased VOC emissions will produce more of the greenhouse gas ozone (3). Many co-benefits exist in between air quality and climate change. One very pertinent example is the relationship between ozone and climate change since anthropogenic VOC control efforts will not only reduce the positive radiative forcing from ozone and VOCs, but it will also improve air quality and human health (3).

Sources of gas-phase organic carbon

It has been estimated that the global production rate of non-methane VOCs is ~1300 TgC/yr with ~90% being biogenic, mainly from terrestrial plants (1). Anthropogenic VOCs, while only accounting for 10% of total emissions, are still extremely important as emissions typically occur in or near urban areas and will thus disproportionately affect local and regional populations (1, 15). Dominant sources of biogenic VOC (BVOC) emissions include plant growth and decay, as well as microbial activity. The compound isoprene (C_5H_8), which accounts for ~500 TgC of BVOC emissions annually, is an important precursor to ozone and SOA (1, 15). Biogenic emissions of terpenes are equally important; emissions of monoterpenes ($C_{10}H_{16}$) and sesquiterpenes ($C_{15}H_{24}$) are highly uncertain, but both are on the order of 100 TgC yr^{-1} and have significant implications for SOA and ozone since they are highly reactive and have considerable SOA and ozone formation potentials (15, 41).

Anthropogenic emissions of gas-phase organic carbon are ubiquitous and originate from point, area, and mobile sources (12). Fossil fuel-related sources, including on-road, off-road, and non-mobile sources, account for the dominant fraction of anthropogenic emissions and play crucial roles in the formation of SOA and ozone particularly in and downwind of urban areas (8, 12, 15). Other important sources include solvents and coatings involved in commercial products and industrial processes (12). Agricultural emissions, which are biogenic by definition yet caused by anthropogenic activity are considerable but highly uncertain and thus of great interest in agricultural regions of California (e.g. the Central Valley) given the substantial planted acreage of crops (42).

Research Objectives

The research presented in this dissertation is motivated by the goal of providing useful information for air quality models and control policy to reduce concentrations of tropospheric ozone and organic aerosol. This is accomplished through an increased understanding of the sources and emissions of gas-phase organic carbon from prominent sources, some of which have previously been insufficiently characterized. Using California, including the San Joaquin Valley, as a case study I developed an instrument to make novel field measurements and examined emissions and potential contributions to SOA and ozone formation. This work will aid the development of effective control strategies for the mitigation of air pollution in California and elsewhere, while also informing future research directions. The objectives are summarized as follows:

I develop instrumentation to measure traditional and under-studied compounds in the VOC and IVOC range and deploy it to make measurements of gas-phase organic carbon from a mix of anthropogenic and biogenic sources at 5 field campaigns: U.C. Berkeley greenhouse plant enclosures, the CalNex (California at the Nexus of Air Quality and Climate Change) supersite in Bakersfield, CA, the Caldecott Tunnel in Oakland, CA, and two sets of seasonal measurements over an orange orchard in the rural area of Lindcove in California's San Joaquin Valley.

I develop and refine several statistical methods to assess the relative contributions of sources to gas-phase organic carbon in the atmosphere and the spatial distribution of emissions. This includes a source receptor model based on chemical mass balancing with effective accounting of uncertainty and errors. Using Flexpart meteorological model outputs over the whole CalNex campaign in conjunction with ground site data, I evaluate the spatial distribution of sources via statistical footprint modeling.

With liquid fuel-based source profiles for gasoline sources and ambient data from Riverside, CA, I use a chemical mass balance source receptor model to examine the relative contributions of gasoline exhaust and non-tailpipe emissions and compare the results to California's emission factor model.

Using data from the CalNex Bakersfield ambient site and on-road measurements at the Caldecott Tunnel, I characterize gas-phase organic carbon emissions from gasoline and diesel vehicles. I chemically speciate gasoline and diesel fuel, use source receptor modeling to assess their relative contributions to total mass in the atmosphere, and combine these with bulk SOA yield modeling to determine the relative importance of gasoline and diesel sources for SOA formation.

An additional source of petroleum-related hydrocarbons is observed and characterized in Bakersfield, and is attributed to petroleum operations, which are prominent in the southern San Joaquin Valley. Statistical footprint modeling with Flexpart meteorological data and ground-based hydrocarbon measurements are used to estimate the spatial distribution of emissions. The importance of this source, in terms of total mass and for atmospheric chemistry, is determined for the region.

Emissions of gas-phase organic carbon from agriculture, a major part of the San Joaquin Valley are estimated for a suite of biogenic terpenoid compounds from ~25 crops studied using enclosures in the greenhouse. Additionally, two seasons of ambient measurements of terpenoids and other biogenic compounds are used from an orange orchard in the San Joaquin Valley. The potential of emissions to form ozone and secondary organic aerosol is assessed, including the impact of seasonal emission events and deposition of ozone into crop canopies.

References

- 1 A.H. Goldstein and I.E. Galbally, Known and Unexplored Organic Constituents in the Earth's Atmosphere. *Environ. Sci. Technol.*, **41**, 1514-1521 (2007)
- 2 U.S. Environmental Protection Agency, 2002 National-Scale Air Toxics Assessment. Available at: <http://www.epa.gov/ttn/atw/nata2002/index.html> (Accessed January 2010)
- 3 S. Solomon, D. Qin, M. Manning et al., 2007: Technical Summary. In: Climate Change 2007: The Physical Science Basis. Contribution of Working Group I to the Fourth Assessment Report of the Intergovernmental Panel on Climate Change [Solomon, S., D. Qin, M. Manning, Z. Chen, M. Marquis, K.B. Averyt, M. Tignor and H.L. Miller (eds.)]. Cambridge University Press, Cambridge, United Kingdom and New York, NY, USA.
- 4 The United Nations Environmental Program, The Montreal Protocol on substances that deplete the ozone layer (and subsequent amendments). Montreal, Quebec, Canada (1999)
- 5 M. Jerrett, R.T. Burnett, C.A. Pope III et al., Long-Term Ozone Exposure and Mortality. *N. Eng. J. Med.*, **360**, 1085-95 (2009)
- 6 R.B. Schlesinger, N. Kunzli, G.M. Hidy et al., Health Relevance of Ambient Particulate Matter Characteristics: Coherence of Toxicological and Epidemiological Inferences. *Inhal. Toxicol.*, **18**, 95-125 (2006)

- 7 N.M. Donahue, A.L. Robinson, and S.N. Pandis, Atmospheric organic particulate matter: From smoke to secondary organic aerosol. *Atmos. Env.*, **43**, 94-106 (2009)
- 8 S. Sillman, The relation between ozone, NO_x, and hydrocarbons in urban and polluted rural environments. *Atmos. Environ.*, **33**, 1821-1845 (1999)
- 9 D.D. Parrish, H.W. Singh, L. Molina, et al., Air quality progress in North American megacities: a review. *Atmos. Env.*, **45**, 7015-7025 (2011)
- 10 M.Z. Jacobson, 2002: Chapter 8: International regulation of urban smog since the 1940's. In: Atmospheric pollution: history, science, and regulation. Cambridge University Press, Cambridge, United Kingdom and New York, NY, USA.
- 11 U.S. Environmental Protection Agency. Air Quality System Database. Available at: <http://www.epa.gov/air/data/aqsdb.html> (Accessed November 2010)
- 12 California Air Resources Board, Estimated annual average emission, 2008. Available at: <http://www.arb.ca.gov/ei/emsmain/emsmain.htm> (accessed January 2010).
- 13 A.R. Russell, L.C. Valin, E.J. Bucsela et al., Space-based Constraints on Spatial and Temporal Patterns of NO_x Emissions in California, 2005-2008. *Environ. Sci. Technol.* **44**, 3608-3615 (2010)
- 14 M. Kanakidou, J.H. Seinfeld, S.N. Pandis et al., Organic aerosol and global climate modeling: a review. *Atmos. Chem. Phys.*, **5**, 1053–1123 (2005)
- 15 R. Volkamer, J.L. Jimenez, F .S. Federico et al., Secondary organic aerosol formation from anthropogenic air pollution: Rapid and higher than expected. *Geophys. Res. Lett.*, **33**, L17811 (2006)
- 16 A.L. Robinson, N.M. Donahue, M.K. Shrivastava et al., Rethinking Organic Aerosols: Semivolatile Emissions and Photochemical Aging. *Science*, **351**, 1259-1262 (2007)
- 17 J.A. de Gouw, C.A. Brock, E.L. Atlas et al., Sources of particulate matter in the northeastern United States in summer: 1. Direct emissions and secondary formation of organic matter in urban plumes. *J. Geophys. Res.*, **113**, D08301 (2008)
- 18 N. Takegawa, T. Miyakawa, Y. Kondo et al., Evolution of submicron organic aerosol in polluted air exported from Tokyo. *Geophys. Res. Lett.*, **33**, L15814 (2006)
- 19 D. Johnson, S.R. Utembe, M.E. Jenkin et al., Simulating regional scale secondary organic aerosol formation during the TORCH 2003 campaign in the southern UK. *Atmos. Chem. Phys.*, **6**, 403-418 (2006)

- 20 C.L. Heald, D.J. Jacob, R.J. Park et al., large organic aerosol source in the free troposphere missing from current models. *Geophys. Res. Lett.*, **32**, L18809 (2005)
- 21 L.I. Kleinman, S.R. Springston, P.H. Daum et al., The time evolution of aerosol composition over the Mexico City plateau. *Atmos. Chem. Phys.*, **8**, 1559-1575 (2008)
- 22 A. Hodzic et al., Modeling organic aerosols in a megacity: potential contribution of semi-volatile and intermediate volatility primary organic compounds to secondary organic aerosol formation. *Atmos. Chem. Phys.* **10**, 5491-5514 (2010).
- 23 R.J. Weber, A.P. Sullivan, R.E. Peltier et al., A study of secondary organic aerosol formation in the anthropogenic-influenced southeastern United States. *J. Geophys. Res.*, **112**, D13302 (2007)
- 24 J.A. de Gouw et al., Organic Aerosol Formation Downwind from the Deepwater Horizon Oil Spill. *Science* **331**, 1295-1299 (2011).
- 25 A. Presto et al., Intermediate-Volatility Organic Compounds: A Potential Source of Ambient Oxidized Organic Aerosol. *Environ. Sci. Technol.* **43**, 4744-4749 (2009).
- 26 J.L. Jimenez et al., Evolution of Organic Aerosols in the Atmosphere. *Science* **326**, 1525-1529 (2009)
- 27 E.M. Lipsky and A.L. Robinson, Effects of Dilution on Fine Particle Mass and Partitioning of Semivolatile Organics in Diesel Exhaust and Wood Smoke. *Environ. Sci. Technol.* **40**, 155-162 (2006)
- 28 T. Kuhn, S. Biswas, P.M. Fine et al., Physical and Chemical Characteristics and Volatility of PM in the Proximity of a Light-Duty Vehicle Freeway. *Aerosol Sci. Technol.*, **39**, 347-357 (2005)
- 29 M.K. Shrivastava, T.E. Lane, N.M. Donahue et al., Effects of gas particle partitioning and aging of primary emissions on urban and regional organic aerosol concentrations. *J. Geophys. Res.*, **113**, D18301 (2008)
- 30 D.B. Kittelson, W.F. Watts, and J.P. Johnson, On-road and laboratory evaluation of combustion aerosols—Part 1: Summary of diesel engine results. *J. Aerosol Sci.*, **37**, 913 – 930 (2006)
- 31 E.A. Weitkamp, A.M. Sage, J.R. Pierce et al., Organic Aerosol Formation from Photochemical Oxidation of Diesel Exhaust in a Smog Chamber. *Environ. Sci. Technol.*, **41**, 6969-6975 (2007)
- 32 N.M. Donahue, A.L. Robinson, C.O. Stanier et al., Coupled partitioning, dilution, and chemical aging of semivolatile organics. *Environ. Sci. Technol.*, **40**, 2635-2643 (2006)

- 33 J.H. Kroll and J.H. Seinfeld, Chemistry of secondary organic aerosol: Formation and evolution of low-volatility organics in the atmosphere. *Atmos. Environ.*, **42**, 3593-3624 (2008)
- 34 T.S. Bates, P.K. Quinn, D. Coffman et al., Boundary layer aerosol chemistry during TexAQS/GoMACCS 2006: Insights into aerosol sources and transformation processes. *J. Geophys. Res.*, **113**, D00F01 (2008)
- 35 Q. Zhang, D.R. Worsnop, M.R. Canagaratna et al., Hydrocarbon-like and oxygenated organic aerosols in Pittsburgh: insights into sources and processes of organic aerosols. *Atmos. Chem. Phys.*, **5**, 3289-3311 (2005)
- 36 Q. Zhang, J.L. Jimenez, M.R. Canagaratna et al., Ubiquity and dominance of oxygenated species in organic aerosols in anthropogenically-influenced Northern Hemisphere midlatitudes. *Geophys. Res. Lett.*, **34**, L13801 (2007)
- 37 O. Favez, H. Cachier, J. Sciare, et al., Characterization and contribution to PM_{2.5} of semi-volatile aerosols in Paris (France). *Atmos. Environ.*, **41**, 7969-7976 (2007)
- 38 V. Ramanathan, P.J. Crutzen, J.T. Kiehl et al., Aerosols, Climate, and the Hydrological Cycle. *Science*, **294**, 2119-2124 (2001)
- 39 D.R. Gentner, R.A. Harley, A.M. Miller, A.H. Goldstein, Diurnal and Seasonal Variability of Gasoline-Related Volatile Organic Compound Emissions in Riverside, California. *Environ. Sci. Technol.*, **43**, 4247-4252 (2009)
- 40 T.W. Kirchstetter, B.C. Singer, and R.A. Harley, Impact of California reformulated gasoline on motor vehicle emissions. 2. volatile organic compound speciation and reactivity. *Environ. Sci. Technol.*, **33**, 329-336 (1999)
- 41 A. Lee, A.H. Goldstein, M.D. Keywood et al., Gas-phase products and secondary aerosol yields from the ozonolysis of ten different terpenes. *J. Geophys. Res.*, **111**, D7 (2006)
- 42 T. Sakulyanontvittaya, T. Duhl, C. Wiedinmyer et al., Monoterpene and Sesquiterpene Emission Estimates for the United States. *Environ. Sci. Technol.* **42**, 1623-1629 (2008)

Chapter 2: Materials and methods

The research objectives of this dissertation were achieved through a mix of instrument development to measure previously understudied compounds; field measurements; and detailed analyses using novel statistical methods to elucidate sources, emissions, and impacts on air quality. This chapter describes the refinement of a custom-made *in situ* gas chromatography/mass spectrometry instrument to measure compounds in the VOC and IVOC range at 5 field campaigns and the development of statistical techniques to analyze the resulting data.

The range of VOCs measured in the atmosphere has been increasing rapidly since the first VOCs were measured as part of studies in the South Coast air basin during the 1950s in response to hazardous air quality (1). Continuous *in situ* gas-chromatography systems for measuring atmospheric VOCs were first used in the 1990's, but focused on a small number of compounds that included mainly C₂₋₆ hydrocarbons (2). By the late 1990's, the range of measureable compounds was expanded to include oxygenated VOCs, halocarbons, and monoterpenes as it became clearer that these measurements were important for understanding emissions and atmospheric chemical processes (3, 4). Further development to measure sesquiterpenes became necessary as they were hypothesized to be important for chemistry in the forest canopy and as precursors to SOA (5). At the onset of this dissertation research, published work hypothesized the importance of IVOCs and SVOCs for SOA formation (6, 7). It was apparent that measurements of these compounds were critically important to understand SOA formation, but current capabilities were insufficient. In response to this need for expanded measurement capabilities and a better understanding of the concentrations and emissions of these compounds, I further developed the ability to measure compounds with lower volatilities in the gas-phase than had previously been measured *in situ*.

Since historical atmospheric measurements focused on a limited range of compounds including a mix of oxygenated, halogenated and aromatic compounds, major modifications were necessary to collect, detect, and quantify the broad range of hydrocarbons necessary for my research. These measurements include a mix of historically studied compounds as well as compounds with limited, or no, prior measurements, such as those in the VOC range with lower volatilities (e.g. C₁₀ aromatics, naphthalenes) and compounds in the IVOC range (e.g. C₁₃₋₁₇ *n*-alkanes). Necessary modifications are summarized as follows: the optimization of adsorbent material for sample preconcentration tuned to capture all compounds of interest; the selection and evaluation of GC capillary columns for a broad range of compounds; the elimination of condensation points throughout the entire system in order to preserve the ambient sample; the development of effective standardization techniques; and the design of an adequate temperature ramping program in the GC oven to separate all the compounds of interest for analysis by the detectors.

1. Site descriptions

Emissions from gasoline and diesel vehicles were measured as part of a field sampling campaign to characterize on-road mobile sources. Measurements were made July 13-29, 2010 at the Caldecott tunnel, on Highway 24 in Oakland, CA, which has been used previously for on-road emission studies. The tunnel is 1 km in length and consists of three 2-lane traffic bores, which have a 4% grade. Sampling for the data presented here was taken in the uphill eastbound traffic bore with all vehicle types and traffic rates of approximately 2,000 light-duty vehicles and 30-140 medium and heavy-duty trucks per hour running on a mixture of gasoline and diesel fuel.

Sample inlets were located in a ventilation aperture in the tunnel roof approximately 50 m prior to the tunnel exit and extended ~0.1 m into the tunnel traffic bore.

Ambient *in-situ* measurements were made in Bakersfield, CA at the CalNex (California Research at the Nexus of Air Quality and Climate Change) supersite as part of a larger study with an additional supersite in the South Coast air basin and several mobile platforms (e.g. planes). The Bakersfield supersite (35.3463° N, 118.9654° W) was located in southeast Bakersfield, a city in the southern San Joaquin Valley whose total metropolitan population is roughly 800,000. The measurement site was typically downwind of the urban core and the nearby (<0.5 mile) state highway 58 that is used by both gasoline and diesel vehicles, including substantial use as a long-haul trucking route both during the night and over the weekend. Sampling of gas-phase organics and supporting gas measurements took place May 18 - June 30, 2010 from the top of an 18 m tower.

To examine emissions from agricultural vegetation, over 20 different crops were studied in the partially controlled environment of the Oxford Tract greenhouse at U.C. Berkeley during the summer of 2008. The crops were a mixture of woody and non-woody trees, scrubs, and annuals that are prominent in California (a full list can be found in Chapter 7). Branches or whole plants were enclosed in Teflon chambers outfitted with temperature and light monitors for several days at a time with several replicates of each species. To avoid any biases caused by plant damage during enclosure, plants were given time to equilibrate before measurements were used to assess emissions and chemical speciation. In addition to chemically-speciated measurements of VOCs via gas chromatography/mass spectrometry, several other instruments were used to measure ozone, carbon dioxide, water and other VOCs via Proton Transfer Resonance Mass Spectrometry (PTR-MS) and cartridge sampling for offline analysis.

Based on the results of the greenhouse study, a year-long measurement site was set-up in an orange orchard in the San Joaquin Valley (36°21'23.68"N and 119°5'32.14"W), located east of Visalia in the foothills of the Sierra Nevada mountains. The local area around the site had a large planted acreage of various citrus trees and some other crops. In addition to biogenic emissions from nearby agriculture, the site had considerable influence from natural vegetation and anthropogenic sources in the San Joaquin Valley. I took two sets of 10+ day measurements at this site during two different seasons; in April-May 2010 during citrus flowering and summer 2010. Measurements were made at the top of the canopy (4 m), and the site had a similar suite of supporting measurements as the greenhouse study.

2. *In situ* gas-phase organic carbon measurements

At both the tunnel and ambient measurement sites, chemical speciation of gas-phase organic carbon was achieved using a gas chromatograph (Hewlett Packard 5890 Series II) that was equipped with a quadrupole mass selective detector (Hewlett Packard 5971) and a flame ionization detector. The instrument was operated *in situ* with a custom system that automated the collection and analysis of samples. Ambient and on-road samples were collected for the first 30 minutes of every hour. At CalNex and the orange orchard, the inlet was located at the top of a tower with the instrument located in a temperature-controlled trailer at ground level. To prevent line losses and accurately preserve compounds, ozone and particulate matter were removed at the inlet using 47 mm glass fiber filters (Pall, type A/E) that were coated in sodium thiosulfate according to the method vetted by Pollmann et al. (8). At the Caldecott tunnel, a longer inlet was used for multiple instruments that could not be operated in the ventilation duct. This 45 m shared inlet was constructed of aluminum and was 6" in diameter. Laminar flow was maintained with a

volumetric flow rate of 200 L min⁻¹. For the VOC/IVOC measurements presented in this paper, a subsample was taken from the flow centerline, and particles were removed using the same filters used in the CalNex set-up. When possible, filters were changed daily in the morning to reduce any potential artifacts. After ozone and particulate removal, the sample traveled at ~1 L min⁻¹ down a 1/4" insulated Silcosteel line heated to >80°C to a preconcentration system, where two separate channels sampled off the main flow, each at ~20 mL min⁻¹. Ozone removal was confirmed by measuring the remainder of the main flow with a spectroscopic ozone analyzer (Dasibi model 1008-AH). During the tunnel study, minor losses of oxygenated and intermediate-volatility hydrocarbons occurred due to adsorption in the shared 6" inlet owing to its lack of passivation and heating.

This instrument, modified from previous use by Millet et al. (9) and Bouvier-Brown et al. (5), was equipped with two independent measurement channels sampling from the same inlet line. Channel 1 focused on a broad range of VOCs including those with lower volatilities (ranging from isopentane to n-heptadecane). Channel 2 measured more volatile, low-molecular weight compounds (e.g. propene – isopentane). For ambient measurements, prior to subsampling from the inlet line for the 2 channels, an internal standard (n-octane, 5.0 ppm) was constantly added to the sample flow at 2 mL/min, such that after the dynamic dilution its concentration was ~2 ppb. The internal standard was used to correct for any drift in the sensitivity of the mass selective detector and to assess overall instrument analytical stability. The entire main sampling line and all other elements of the sampling/preconcentration system that pertain to Channel 1 were constructed with passivated steel or other highly inert materials that were heated to constant temperatures at or above 90°C using resistive heaters. This was done to minimize losses of any VOC due to adsorption, absorption, or condensation, especially for compounds with lower volatility.

The Channel 2 sub-sample went through a custom-made water trap to remove water that could adsorb onto the channel 2 adsorbent trap. This was accomplished by passing the Channel 2 Teflon sample line through an aluminum block that was cooled to 0°C and routinely heated and purged between samples.

Ambient samples for both channels were concentrated on custom-made multilayer adsorbent traps using a system of three 12-port rotary valves (Valco, Valcon E) to automate sampling and injection. Adsorbent traps were constructed out of 1/8" Sulfinert steel tubing and contained the following sequences of adsorbent materials secured by glass wool at each end; Channel 1: 60 mg glass beads (Alltech, 60/80 mesh, DCMS-treated), 20 mg Tenax TA (Supelco, 60/80 mesh), 30 mg Carbopak B (Supelco, 60/80 mesh), and 40 mg Carbopak X (Supelco, 60/80 mesh); Channel 2: 60 mg glass beads, 30 mg Carbopak B, 40 mg Carbopak X, and 40 mg Carboxen 1000 (Supelco, 60/80 mesh). During sample collection adsorbent traps were thermoelectrically cooled to a constant 15°C and 5°C for channel 1 and 2, respectively. Following the preconcentration of ~1 L on each adsorbent trap, analytes were thermally desorbed at 320°C with a reverse flow of helium and injected directly onto their respective capillary columns where chromatographic separation was assisted by a ramped temperature program in the GC oven. The effluent from the traps was injected onto a DB-624 capillary column (60 m × 0.32 mm × 1.8 μm) and a HP-Plot-Q capillary column (30 m × 0.32 mm × 20.0 μm) for channel 1 and 2, respectively. The analytes are separated based on differences in volatility and polarity in the columns and then quantified/characterized by either the mass selective detector or the flame ionization detector.

All flows were measured and controlled using mass-flow controllers (MKS Instruments), and system temperatures were monitored using T-type thermocouples (Thermo Scientific). All system data were recorded on a data-logging system (Campbell-Scientific).

The instrument was calibrated for more than 100 individual hydrocarbons using a combination of standard gas mixtures and liquid standards. Three gas standard cylinders with ppm concentrations (Apel-Riemer, Scotty Gas) were dynamically diluted into a $\sim 1 \text{ L min}^{-1}$ flow of pure air supplied from a zero air generator (Aadco Inc.) to get pptv to ppbv-level concentrations. At CalNex, liquid standards were introduced into the system at the top of the tower to account for any losses in the sample lines or preconcentration system. Multi-point calibrations were run at the beginning and end of the measurement campaign, and daily single-point standards were run to verify the calibrations. Pure air from the zero air generator was also used to run daily blank runs to check for any artifacts or biases in the system. For identified compounds without standards, their response factors on the MSD were determined by multiplying the fraction of the quantifying ion in a representative mass spectrum by the total ion response factor calculated from known compounds of similar chemical classes. This method, while approximate, provides concentration data with a reasonable amount of uncertainty when standards are not available for relatively unstable hydrocarbons.

We quantified hourly concentrations for over 250 compounds, including linear alkanes, branched alkanes, cyclic alkanes, alkenes, aromatics, polycyclic aromatic hydrocarbons (PAHs), terpenoids, halogenated compounds, species containing sulfur, oxygenates, and alcohols (Table 2.1). Detection limits for most compounds were at or near 1 pptv with accuracies determined by standards ($\pm 5\%$) and MKS flow controllers ($\pm 5\%$). Numerous compounds reported have limited or no prior *in situ* ambient measurements. This includes compounds in the intermediate-volatility range (IVOCs), such as the methylnaphthalenes and dimethylnaphthalenes. Some compounds are reported together as groups because it was infeasible to accurately separate them on the chromatographic column used while measuring such a wide range of compounds. A selection of chromatograms are shown in Figures 2.1-5.

3. Statistical methods to model gas-phase organic carbon emissions

Statistical methods and analyses have been used to assess atmospheric data of various forms and can effectively be used to examine sources of gas-phase organic carbon. These methods include basic exploration of data by testing the correlation of measured compounds through linear regressions, which provides valuable information about the composition and behavior of sources. More complex analyses, known as multivariate receptor modeling, combine these basic statistical analyses on a larger set of compounds to assess the suite of sources and processes that determine observed concentrations of measured compounds. These modeling methods vary in the amount of *a priori* information they require about the composition of sources. Factor analysis (a derivative of principal component analysis) and positive matrix factorization (PMF) require no input information about sources and produces a result by minimizing residuals through covariance in measured compounds. Source receptor models such as those using chemical mass balancing require *a priori* information about the composition of sources also known as source profiles, in which each compound is expressed as a mass fraction (i.e wt%) of emissions from the source. Much of the work presented in this dissertation uses chemical mass balance source receptor modeling to examine emission from petroleum sources, such as gasoline and diesel exhaust, non-tailpipe gasoline emissions from vehicles and service stations, and fugitive unrefined natural gas emissions from petroleum extraction operations. The

source profiles used as inputs in the model were derived from the compound-specific fuel profiles presented in this work, with liquid fuels representing exhaust profiles and vapor-liquid equilibrium calculations determining the non-tailpipe profile. Previous work has shown compositional consistency for non-combusted gas-phase organics in liquid gasoline and gasoline exhaust (10). In addition to confirming this finding for gasoline, we also demonstrate compositional consistency for diesel fuel and exhaust (Chapter 4).

Chapter 3 uses a fully-constrained system where the number of compounds was equal to the number of sources being modeled. Chapters 4-5 use an over-constrained system where more compounds than sources are used and more sophisticated methods are used to account for uncertainties in measurements and source profiles.

For each hourly sample in the Caldecott tunnel (N=114) and at CalNex-Bakersfield (N=476), an over-constrained matrix system was constructed with 6 to 10 compounds to represent the source profiles of the 3 sources. For each site, several confirmation model runs with different sets of compounds were used in the model to assess sensitivity of results. A summary of compounds used for modeling can be found in Chapter 4. All compounds used in the model have authentic standards.

The gas-phase organic carbon data have numerous VOCs and IVOCs that act as source tracers either independently or in tandem with other compounds. With regards to gasoline and diesel emissions, emissions of most observed tracer compounds had not undergone significant photochemistry that could bias the model over the timescales observed between emission and measurement at either field site. This is evidenced by roughly identical ratios for gasoline-related compounds in the ambient measurements compared to liquid gasoline collected in Bakersfield during the campaign (Fig. 4.5). If considerable aging with the ability to bias our model had occurred, these comparisons would be poor for compounds that have large differences in OH reaction rate constants. Chemical losses were only really a concern at the Bakersfield site since the on-road emissions study was in close proximity to the source. At Bakersfield, evidence of chemical losses in the fresh emissions can occasionally be seen in comparisons of model results to independent compounds that are highly reactive, which is only an issue with the most reactive compounds that are not used in modeling for that reason. This lack of observable photochemical processing of the primary emissions used in the model allows us to effectively assess emissions from gasoline and diesel sources. Additionally, any minor biases that could be introduced due to chemical losses are minimized by selecting compounds for the model that have relatively similar reaction rates with OH and negligible reaction rates with ozone.

For Bakersfield, a fourth source representing fugitive light hydrocarbon (C₁₋₆) emissions from petroleum extraction and refining was necessary to properly model non-tailpipe gasoline emissions; data for this source came from U.S. geological surveys. Using IGOR Pro 6.22, a least-squares solution was determined for each over-constrained system to determine each hourly source contribution in ppbC using effective variance weighting methods described by Watson *et al.* and used by the U.S. EPA in their CMBv8.2 modeling platform (11, 12). To assess model performance, I calculated normalized biases and root mean squared errors for each compound used in the model and each independent compound. I also calculated the reduced chi-squared test and model R-squared for each hourly sample; results can be seen in Chapter 4. I verified the predictive capability of all compounds to independent compounds to confirm the ability of the model to predict the behavior of reactive VOCs and IVOCs that are emitted by both gasoline and diesel at both measurement sites. Minor inconsistencies for reactive compounds are due to a combination of oxidation losses during the most photochemically-active periods of the day, other

non-vehicular sources, and, in the case of IVOCs in the tunnel study, adsorptive losses on walls of the shared inlet.

Additional considerations have been made throughout the work in this dissertation to accurately present reported values and the appropriate uncertainty and/or variability associated with them. Where appropriate uncertainties have been propagated through calculations to accurately represent the uncertainty of a given number. Additionally, many of the averages reported in this work are reported as geometric means when dealing with atmospheric data that are typically logarithmically distributed. The geometric mean and its uncertainty are calculated as follows:

$$\mu_{geo} = \frac{1}{N} \sum_{i=1}^N [\ln(x_i)]$$

$$\sigma_{geo} = \frac{1}{2} \mu_{geo} \left(\exp \left[\frac{\sum_{i=1}^N [\ln(x_i/\mu_{geo})^2]}{N} \right] - \exp \left[\frac{-\sum_{i=1}^N [\ln(x_i/\mu_{geo})^2]}{N} \right] \right)$$

Meteorological modeling and assessment of source distribution

Several methods are used in this work to assess the spatial distribution of organic carbon sources. In addition to the use of aircraft data collected from the NOAA P3 mobile platform during the CalNex campaign, I developed a method to use a meteorological model (Flexpart) that estimates the distribution of air parcels (i.e. back trajectory footprints) prior to measurement at a ground site and combine it with ambient compound data to assess the spatial distribution of emissions for a compound in a region. Just looking at the average distribution of wind direction when high concentrations of a compound are observed is not always sufficient when complex meteorology affects the transport of air masses in a region such as California's central valley. Similarly, basic HYSPLIT back-trajectory analysis can oversimplify the footprint of measurements into one single path and not accurately represent the residence time of an air parcel at ground level.

We generated 6- and 12-hour back-trajectory footprints with 4 km resolution for each hourly sample using the Flexpart meteorological modeling package developed by the NOAA Earth Sciences Research Laboratory. Simulations for Bakersfield were initiated from the top of the 18 m tower and further details of Flexpart modeling can be found elsewhere (13, 14). We present the first integration of this meteorological modeling method with statistical back-trajectory analysis to explore the distribution of VOC sources. Utilizing concentration weighted trajectory analysis allows us to find the average concentration of a compound in a cell, \overline{C}_{ij} :

$$\overline{C}_{ij} = \frac{1}{\sum_0^t (\tau_{ijt})} \sum_0^t (c_{ijt} \cdot \tau_{ijt})$$

where τ_{ij} is the time the trajectory spends at ground level (<100 m) in the ij th cell and c_{ij} is the concentration of a compound in each trajectory. Each cell has a corresponding n_{ij} value, the number of t_{ij} values contributing to a cell (15). To correct for the exaggerated contributions of low n_{ij} values, a weighting function multiplies \overline{C}_{ij} with n_{ij} values above the Q_{90} , Q_{75} , Q_{50} and

below the Q_{50} percentiles by 1, 0.7, 0.4, and 0.05 respectively (16). Contour maps were then plotted using these final $\overline{C_{ij}}$ values and appended on top of a 1 arc second elevation map obtained from the USGS National Map Seamless Server.

Maps are presented in Chapters 5-7 to demonstrate this tool and also show the dominant meteorological patterns in the central valley.

References

- 1 Eggertsen, F.T. and F.M. Nelsen (1958) Gas Chromatographic Analysis of Engine Exhaust and Atmosphere—Determination of C-2 to C-5 Hydrocarbons. *Anal. Chem.*, 30, 1040–1043.
- 2 Goldstein, A.H., B.C. Daube, J.W. Munger, and S.C. Wofsy (1995) Automated in-situ monitoring of atmospheric non-methane hydrocarbon concentrations and gradients", *J. Atmos. Chem.*, 21, 43-59.
- 3 Lamanna, M.S., and A.H. Goldstein (1999) In-situ measurements of C2-C10 VOCs above a Sierra Nevada ponderosa pine plantation, *J. Geophys. Res.*, 104, D17, 21247-21262.
- 4 Millet, D.B., A.H. Goldstein, J.D. Allan et al. (2004) VOC measurements at Trinidad Head, CA during ITCT 2K2: Analysis of sources, atmospheric composition and aerosol residence times, *J. Geophys. Res.*, 109, D23, D23S16, 10.1029/2003JD004026.
- 5 Bouvier-Brown, N.C., A.H. Goldstein, J.B. Gilman et al. (2009) In-situ ambient quantification of monoterpenes, sesquiterpenes, and related oxygenated compounds during BEARPEX 2007: implications for gas- and particle-phase chemistry, *Atmos. Chem. Phys.*, 9:5505-5518.
- 6 Goldstein A.H. and I.E. Galbally (2007) Known and Unexplored Organic Constituents in the Earth's Atmosphere. *Environ. Sci. Technol.*, 41, 1514-1521.
- 7 Robinson, A.L., N.M. Donahue, M.K. Shrivastava et al. (2007) Rethinking Organic Aerosols: Semivolatile Emissions and Photochemical Aging. *Science*, 351, 1259-1262.
- 8 Pollmann J., J. Ortega, and D. Helmig (2005) Analysis of atmospheric sesquiterpenes: Sampling losses and mitigation of ozone interferences, *Environ. Sci. Technol.*, 39:9620-9629.
- 9 Millet D.B., N.M. Donahue, S.N. Pandis et al. (2005) Atmospheric volatile organic compound measurements during the Pittsburgh Air Quality Study: Results, interpretations, and quantification of primary and secondary contributions. *J. Geophys. Res.* 110:D07S07.
- 10 Leppard W.R., R.A. Gorse, L.A. Rapp et al. (1992) Effects of gasoline composition on vehicle engineout and tailpipe hydrocarbon emissions. *SAE Tech. Pap. Ser.* No. 920329.

- 11 Watson J.G., J.A. Cooper, and J.J. Huntzicker (1984) The effective variance weighting for least squares calculations applied to the mass balance receptor model. *Atmos. Env.* 18:1347-1355.
- 12 U.S. Environmental Protection Agency, *EPA-CMB8.2*
(http://www.epa.gov/scram001/receptor_cmb.htm)
- 13 Brioude, J., W.M. Angevine, S.A. McKeen, and E.Y. Hsie (2012) Numerical uncertainty at mesoscale in a Lagrangian model in complex terrain, *Geosci. Model Dev. Discuss.*, 5, 967–991, doi:10.5194/gmdd-5-967-2012.
- 14 Metcalf, A.R., J.S. Craven, J.J. Ensberg et al. (2012) Black carbon aerosol over the Los Angeles Basin during CalNex, *J. Geophys. Res.*, 117, D00V13, doi: 10.1029/2011JD017255.
- 15 Seibert, P., H. Kromp-Kolb, U. Baltensperger et al. (1994) Trajectory analysis of aerosol measurements at high alpine sites. In: B.P. M., B. P., C. T. and S. W. (Editors), *Transport and Transformation of Pollutants in the Troposphere*. Academic Publishing, Den Haag, pp. 689-693, 1994.
- 16 Polissar, A.V., P.K. Hopke and J.M. Harris(2001) Source regions for atmospheric aerosol measured at Barrow, Alaska, *Environ. Sci. Technol.*, 35:4214-4226.

Tables and Figures

Table 2.1: Summary of compounds quantified across campaigns

| Compound | CalNex - Bakersfield | Caldecott Tunnel | Lindcove Orange Orchard | Greenhouse Enclosures |
|--|-------------------------|---------------------|----------------------------|--------------------------|
| Straight-chain alkanes | | | | |
| propane | X | X | X | |
| n-butane | X | X | X | |
| n-pentane | X | X | X | |
| n-hexane | X | X | X | |
| n-heptane | X | X | X | |
| n-octane | | X | X | |
| n-nonane | X | X | X | |
| n-decane | X | X | X | |
| n-undecane | X | X | X | |
| n-dodecane | X | X | X | |
| n-tridecane | X | X | X | |
| n-tetradecane | X | X | X | |
| n-pentadecane | X | X | X | |
| n-hexadecane | | | X | |
| n-heptadecane | | | X | |
| Branched alkanes | | | | |
| Iso-butane | | X | X | |
| iso-pentane | X | X | X | |
| 2-2-dimethylbutane | X | X | X | |
| 2-methylpentane & 2,3- dimethylbutane | X | X | X | |
| 3-methylpentane | X | X | X | |
| 2,4- & 2,2-dimethylpentane | X | X | X | |
| 3,3-dimethylpentane | X | X | | |
| 2,3-dimethylpentane | X | X | X | |
| 2-methylhexane | X | X | X | |
| 3-methylhexane | X | X | X | |
| 2,2-dimethylhexane | X | X | | |
| 2,5-dimethylhexane | X | X | X | |
| 2,4-dimethylhexane | X | X | X | |
| 2,2,3-trimethylpentane | X | X | | |
| iso-octane | X | X | X | |
| 2,3,4-trimethylpentane & ctc-1,2,3- trimethylcyclopentane | X | X | X | |
| 2,3,3-trimethylpentane & 2,3- dimethylhexane | X | X | | |
| 2-methylheptane | X | X | | |
| 4-methylheptane | X | X | | |
| 3-methylheptane | X | X | X | |
| 2,2,5-trimethylhexane | X | X | | |
| 2,6-dimethylheptane | X | X | | |
| 3,5-dimethylheptane | X | X | | |
| 2,3-dimethylheptane | X | X | | |
| 2- & 4-methyloctane | X | X | | |
| 3-methyloctane & 4-ethylheptane | X | X | X | |
| 2,2,5-trimethylheptane | X | X | | |
| 2,2,4-trimethylheptane | X | X | | |

| | | | | |
|--|---|---|---|--|
| C10 branched alkanes (5 unknown isomers) | x | x | | |
| 2,6-dimethyloctane | x | x | | |
| 2- & 3- & 4-methylnonane & 3- & 4-ethyloctane & 2,3-dimetyloctane | x | x | | |
| C11 branched alkanes (3 unknown isomers) | x | x | | |
| C11 branched alkanes (10 unknown isomers) | x | x | | |
| dimethylundecane isomer #1 | x | x | x | |
| dimethylundecane isomer #2 | x | x | x | |
| C13 branched alkanes (2 unknown isomers) | x | x | | |
| C14 branched alkanes (6 unknown isomers) | x | x | | |
| C16 branched alkane (unknown) | x | x | | |
| Cycloalakanes | | | | |
| cyclopentane | x | x | x | |
| methylcyclopentane | x | x | x | |
| cis-1,3-dimethylcyclopentane | x | x | | |
| trans-1,3-dimethylcyclopentane | x | x | | |
| ethylcyclopentane | x | x | | |
| ctc-1,2,4-trimethylcyclopentane | x | x | | |
| ctt-1,2,4 trimethylcyclopentane | x | x | | |
| Unknown methylethylcyclopentane | x | x | | |
| iso-propylcyclopentane | x | x | | |
| n-propylcyclopentane | x | x | | |
| cyclohexane | x | x | x | |
| methylcyclohexane | x | x | x | |
| cis-1,3- & 1,1-dimethylcyclohexane | x | x | | |
| trans-1,2-dimethylcyclohexane | x | x | | |
| trans-1,3-dimethylcyclohexane | x | x | | |
| cis_1_2 dimethylcyclohexane | x | x | | |
| ethylcyclohexane | x | x | | |
| ccc-1,3,5-trimethylcyclohexane | x | x | | |
| 1,1,3-trimethylcyclohexane | x | x | | |
| 1,1,4-trimethylcyclohexane | x | x | | |
| ctt-1,2,4- & cct-1,3,5-trimethylcyclohexane | x | x | | |
| ctc-1,2,4-trimethylcyclohexane | x | x | | |
| 1,1,2-trimethylcyclohexane and isobutylcyclopentane | x | x | | |
| methylethylcyclohexane isomer #1 | x | x | | |
| methylethylcyclohexane isomer #2 | x | x | | |
| iso-propylcyclohexane | x | x | | |
| n-propylcyclohexane | x | x | | |
| unidentified C10 cyclohexane | x | x | | |
| unidentified C10 cyclohexanes | x | x | | |
| unidentified C9 cycloalkane | x | x | | |
| Alkenes | | | | |
| propene | x | x | x | |
| 1-butene | x | x | | |
| isobutene | x | x | | |

| | | | | |
|--------------------------------------|---|---|---|--|
| 1,3-butadiene | | X | | |
| trans-2-butene | X | X | | |
| cis-2-butene | X | X | | |
| 1-pentene | X | X | | |
| cis-2-pentene | X | X | | |
| 1-hexene | X | X | | |
| 2-methyl-2- & cis-3-methyl-2-pentene | X | X | | |
| 1-methylcyclopentene | X | X | | |
| C7 cyclopentenes (2 unknown isomers) | X | X | | |
| 1-methylcyclohexene | X | X | | |
| unidentified C9 cycloalkene | X | X | | |
| 1-heptadecene | | | X | |
| 8-heptadecene | | | X | |
| Alkynes | | | | |
| propyne | | X | | |
| Single-ring aromatics | | | | |
| benzene | | X | X | |
| toluene | X | X | X | |
| ethylbenzene | X | X | X | |
| m- & p-xylene | X | X | X | |
| o-xylene | X | X | X | |
| cumene | X | X | X | |
| n-propyl-benzene | X | X | X | |
| 1,2,3-trimethylbenzene | X | X | X | |
| 1,3,5-trimethylbenzene | X | X | X | |
| 1,2,4-trimethylbenzene | X | X | X | |
| 1-ethyl-3- & 1-ethyl-4-methylbenzene | X | X | X | |
| 1-ethyl-2-methylbenzene | X | X | X | |
| 1-methylethenylbenzene | X | X | | |
| 1-ethenyl-2(or3)-methylbenzene | X | X | | |
| Iso-butyl-benzene | X | X | | |
| n-butyl-benzene | X | X | | |
| m-cymene | X | X | | |
| p-cymene | X | X | X | |
| m-diethylbenzene | X | X | | |
| p-diethylbenzene | X | X | | |
| o-diethyl-benzene | X | X | | |
| 1-methyl-3-n-propyl-benzene | X | X | | |
| 1-methyl-2-n-propyl-benzene | X | X | | |
| 1,4-dimethyl-2-ethyl-benzene | X | X | | |
| 1,3-dimethyl-4-ethyl-benzene | X | X | | |
| 1,2-dimethyl-4-ethyl-benzene | X | X | | |
| 1,3-dimethyl-2-ethyl-benzene | X | X | | |
| 1,2-dimethyl-3-ethyl-benzene | X | X | | |
| trans-2-butenyl-benzene | X | X | | |
| 1,2,4,5-tetramethyl-benzene | X | X | | |
| 1,2,3,5-tetramethyl-benzene | X | X | | |
| 1,2,3,4-tetramethyl-benzene | X | X | | |
| C11 aromatics (5 unknown isomers) | X | X | | |

| | | | | |
|---|---|---|---|---|
| Polycyclic Aromatic Hydrocarbons (PAHs) | | | | |
| indan | x | x | | |
| indene | x | x | | |
| 1-methyl-indan | x | x | | |
| 2-methyl-indan | x | x | | |
| naphthalene | x | x | x | |
| 1-methylnaphthalene | x | x | | |
| 2-methylnaphthalene | x | x | | |
| dimethylnaphthalenes | x | x | | |
| trimethylnaphthalenes | x | | | |
| Alcohols and carbonyls | | | | |
| methacrolein | x | | | |
| methanol | x | | x | |
| ethanol | x | | x | |
| acetaldehyde | | x | x | |
| isopropyl alcohol | x | | x | |
| acetone | x | x | x | |
| methyl ethyl ketone | x | | x | |
| methyl isobutyl ketone | x | | x | |
| methyl n-butyl ketone | x | | x | |
| propanal | x | x | | |
| butanal | x | x | | |
| pentanal | x | | | |
| hexanal | x | x | x | |
| heptanal | x | | | |
| nonanal | x | | | x |
| phenol | x | | | |
| acetophenone | x | | | |
| Terpenoids | | | | |
| Isoprene | x | | x | x |
| alpha-pinene | x | | x | x |
| d-limonene | x | | x | x |
| nopinone | x | | x | x |
| alpha-thujene | x | | x | x |
| camphene | x | | x | |
| sabinene | x | | x | x |
| beta-myrcene | x | | x | x |
| beta-pinene | x | | x | x |
| d2-carene | | | | x |
| d3-carene | x | | x | x |
| trans-beta-ocimene | x | | x | x |
| cis-beta-ocimene | | | x | x |
| gamma-terpinene | x | | x | x |
| alpha-terpinene | | | x | x |
| eucalyptol | | | | x |
| terpinolene | | | x | x |
| alpha-phellandrene | | | x | x |
| beta-phellandrene | | | | x |
| alpha-humulene | | | | x |
| beta-caryophyllene | | | x | x |
| trans-beta-farnesene | | | x | |
| aromadendrene | | | x | |

| | | | | |
|------------------------------------|---|--|---|---|
| valencene | | | X | |
| trans-nerolidol | | | X | |
| unknown sesquiterpene | | | X | |
| Other biogenic compounds | | | | |
| diacetyl | | | X | |
| ethyl acetate | | | X | |
| perillene | | | | X |
| 2-trans-hexenyl formate | | | X | |
| cis-3-hexenyl acetate | | | X | X |
| benzaldehyde | | | X | X |
| gamma-valeroactone | | | X | |
| linalool | | | X | X |
| trans-linalool oxide | | | X | |
| cis-linalool oxide | | | X | |
| benzeneacetaldehyde | | | X | |
| lavender lactone | | | X | |
| methyl-benzoate | | | X | |
| benzene ethanol | | | X | |
| benzyl nitrile | | | X | |
| indole | | | X | |
| methyl anthranilate | | | X | |
| 4-methylene-5-hexenal | | | X | |
| sabina ketone | | | X | |
| neryl acetone | | | X | |
| 2-amino-benzaldehyde | | | X | |
| Halocarbons | | | | |
| CFC-11 | X | | | |
| chloroform | X | | X | |
| tetrachloroethylene | X | | | |
| 1,1-dichloroethene | X | | | |
| cis-1,2-dichloroethylene | X | | | |
| 1,2-dichloroethane | X | | | |
| trichloroethylene | X | | | |
| 1,2-dichloropropane | X | | | |
| trans-1,3-dichloropropene | X | | | |
| cis-1,3-dichloropropene | X | | | |
| 1,3-dichlorobenzene | X | | | |
| para-chlorobenzotrifluoride | X | | X | |
| Other | | | | |
| carbon disulfide | X | | | |
| ethanethiol | X | | | |

Note: Identified compounds for which these are the first *in situ* measurements are shown in bold

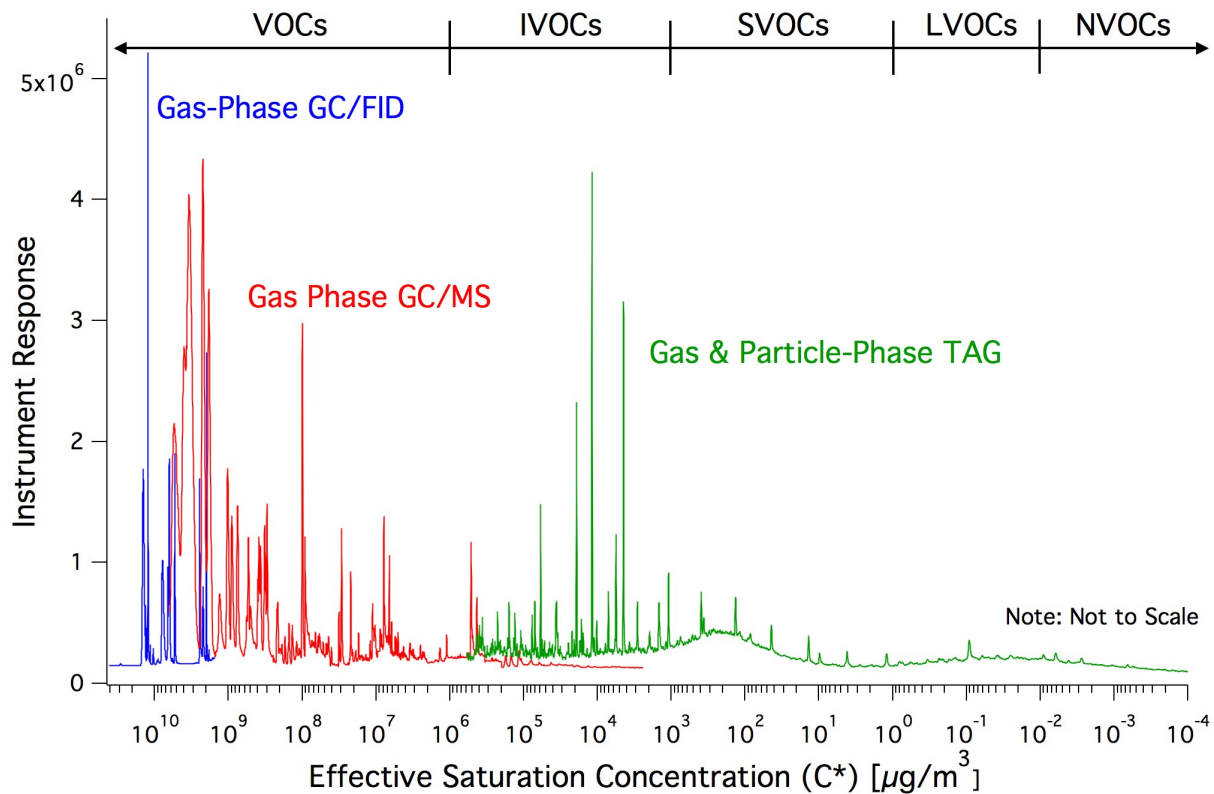


Figure 2.1: Example chromatogram from Bakersfield, CA showing distribution of organic compounds across volatility classes measured using both channels of the gas-phase instrument and a companion instrument (GC-TAG) which measures aerosols and partitioned compounds

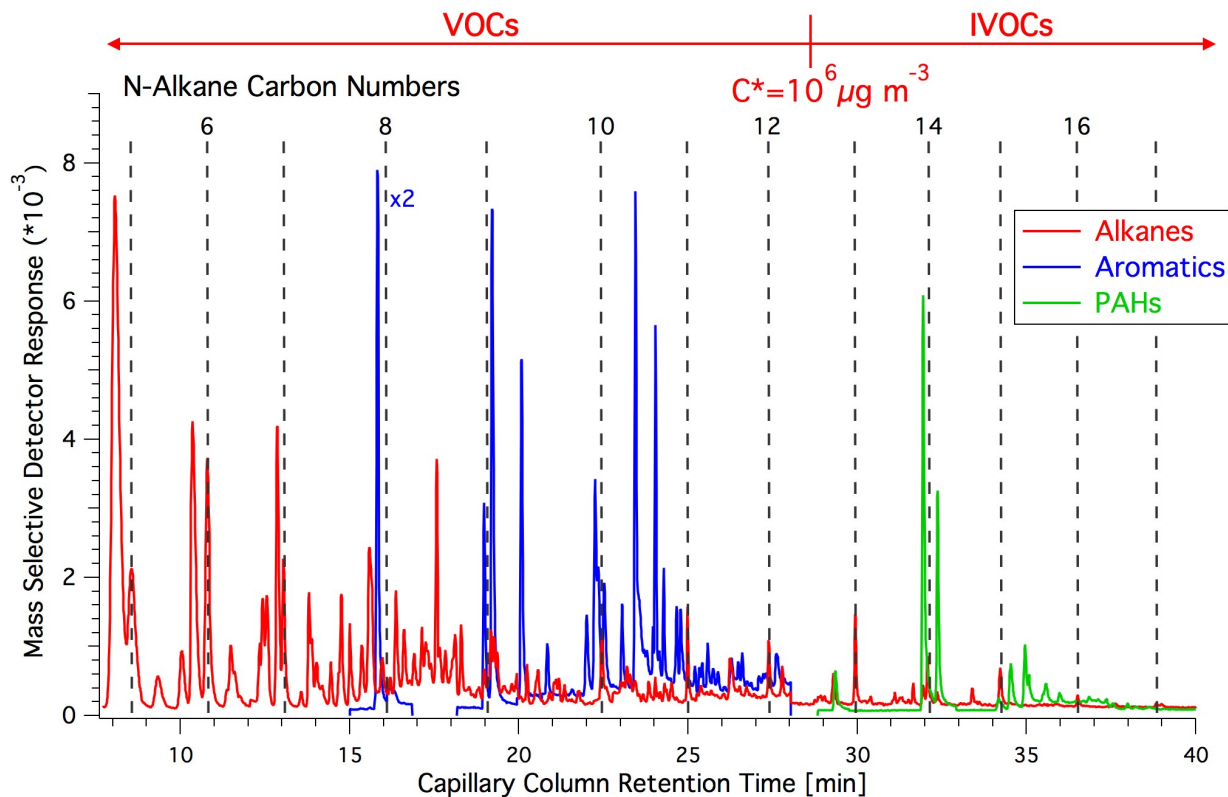


Figure 2.2: Example chromatogram from Bakersfield, CA from gas-phase instrument showing the alkanes, aromatics, and PAHs measured, many of which fall in the IVOC range. The location of n-alkane carbon numbers is shown as a reference.

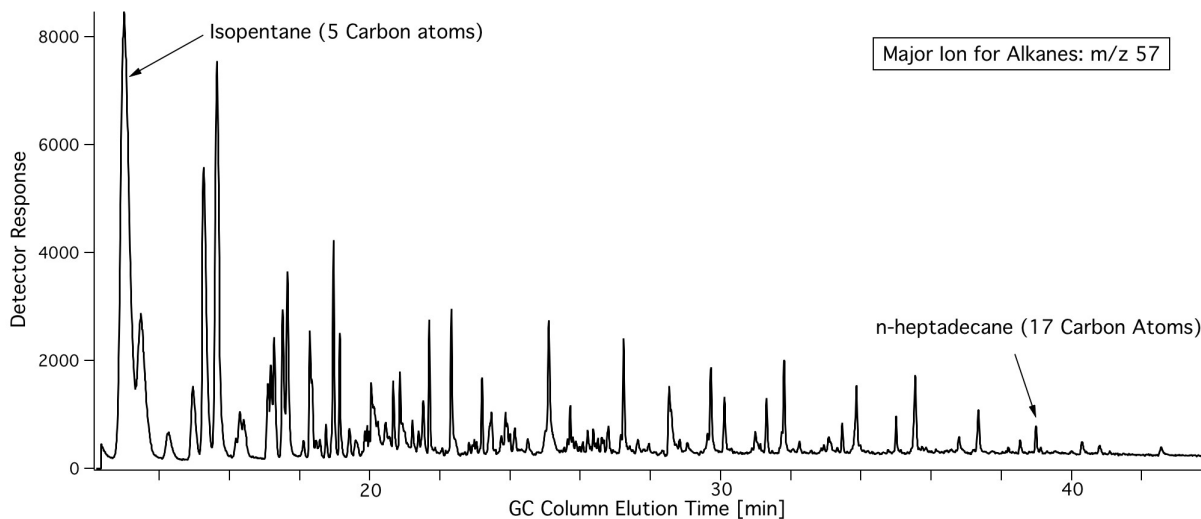


Figure 3.3: Example chromatogram from channel 1 at Bakersfield, CA showing the m/z 57 signal, which shows the prevalence of straight, branched, and cyclic alkanes with up to 17 carbon atoms

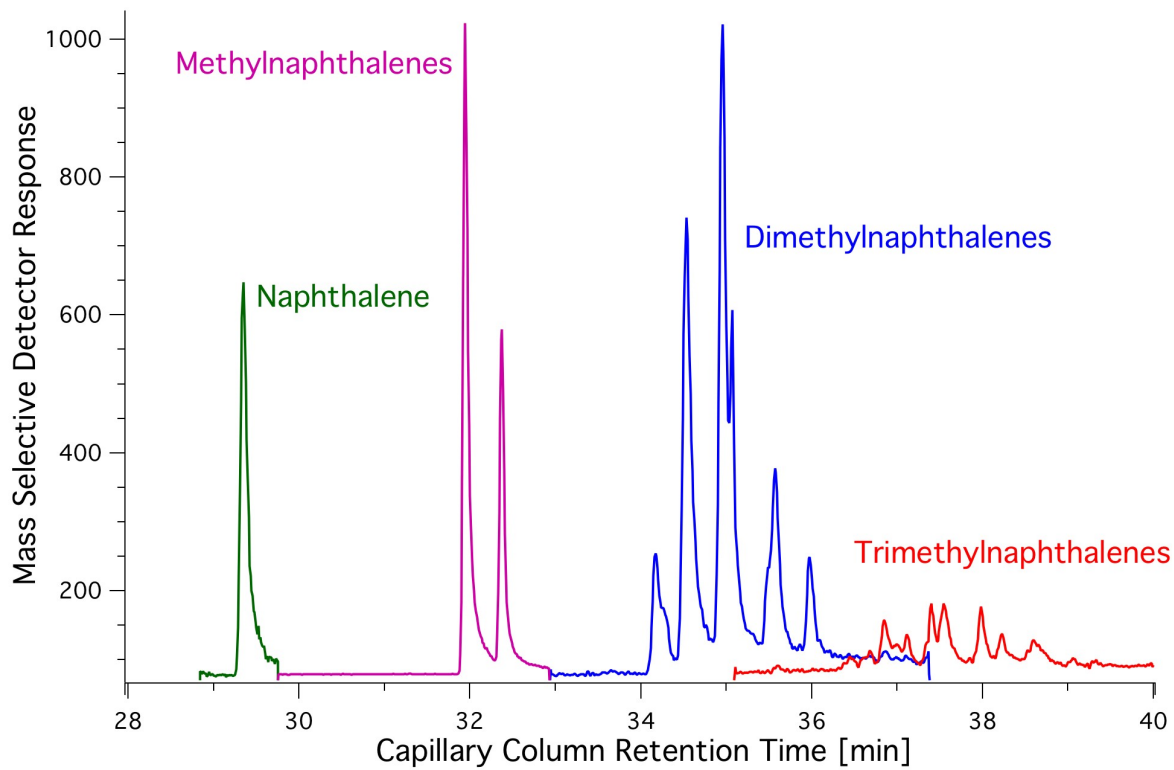


Figure 2.4: Example chromatogram from Bakersfield, CA showing the separation and measurement of naphthalene and its' small alkylated isomers.

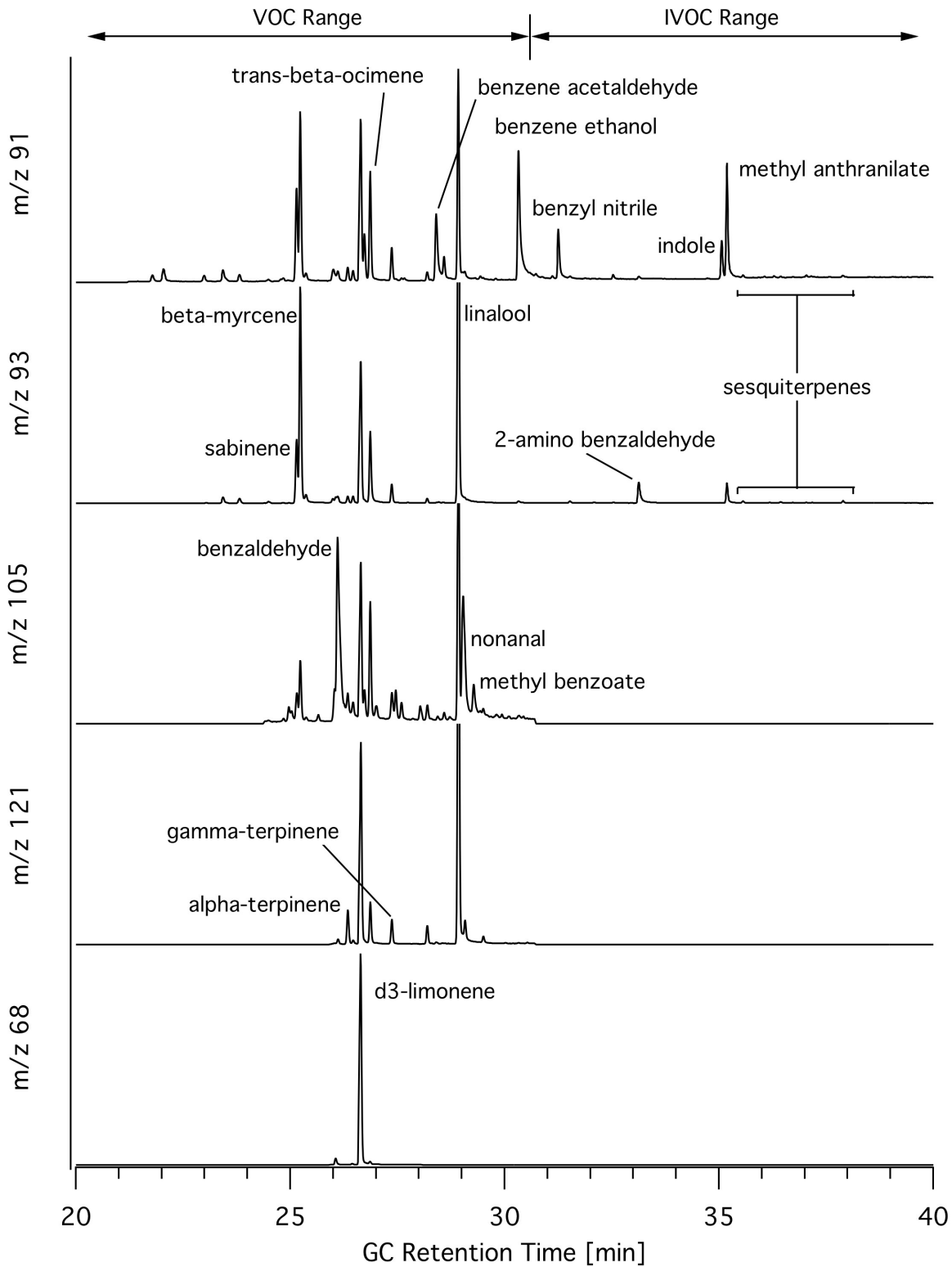


Figure 2.5: Example chromatogram from the Lindcove orange orchard in spring 2010 during flowering. A selection of the most prominent biogenic compounds are shown on representative mass to charge (m/z) ratios.

Chapter 3: Diurnal and seasonal variability of gasoline-related volatile organic compound emissions

Reproduced from: D.R. Gentner, R.A. Harley, A.M. Miller, A.H. Goldstein (2009) “Diurnal and Seasonal Variability of Gasoline-related Volatile Organic Compounds in Riverside, California,” *Environmental Science and Technology*, 43 (12), 4247–4252. with permission from the American Chemical Society.

Abstract

On and off-road mobile sources are the dominant contributors to urban anthropogenic volatile organic compound (AVOC) emissions. Analyses of gasoline samples from California for both summer and winter indicate significant differences in liquid fuel and vapor chemical composition due to intentional seasonal adjustments. Ambient concentrations of 55 VOCs were measured via in-situ gas chromatography in the 2005 Study of Organic Aerosols at Riverside (SOAR) during both summer and fall. A chemical mass balance analysis was used to differentiate vapor pressure-driven VOC emissions from other motor vehicle-related emissions such as tailpipe exhaust. Overall, fuel vapor emissions accounted for $31 \pm 2\%$ of gasoline-related VOC in Riverside; California’s emission factor model similarly estimates 31% of gasoline-related VOC emissions are fuel vapor. The diurnal pattern of vapor pressure-driven VOC source contributions is relatively stable around $10 \mu\text{g}/\text{m}^3$, while whole gasoline (i.e. tailpipe) contributions peak at $\sim 60 \mu\text{g}/\text{m}^3$ during the morning commute. There is no peak in whole gasoline source contributions during the afternoon, due to rapid dilution associated with high mixing heights and wind speeds in the Riverside area. The relationship between estimated gasoline-related VOC and observed carbon monoxide concentrations in this study is similar to California’s 2005 emission inventory; we calculated a VOC to CO mass ratio of 0.086 ± 0.006 (95% CI) compared to 0.097 in the emission inventory for all gasoline-related sources.

1. Introduction

Volatile organic compound (VOC) emissions, both biogenic and anthropogenic, are important precursors to the formation of ozone and secondary organic aerosols (1). Anthropogenic volatile organic compound (AVOC) emissions in urbanized areas are predominantly from gasoline-related sources (2). Gasoline use occurs in both on and off-road engines, which together are responsible for the majority of both VOC and carbon monoxide (CO) emissions in urban environments (2). California actively regulates gasoline formulation to reduce environmental and human health effects of air pollution; recently methyl tert-butyl ether (MTBE) was replaced by ethanol as the main oxygenated additive in gasoline.

VOC emissions from the tailpipe contain compounds of all volatilities and include running exhaust, engine idling, and engine start up; these emissions are attributable to incomplete combustion of gasoline during various modes of vehicle operation. The composition of the resulting VOC emissions is a function of engine design, operating conditions, and vehicle maintenance. Evaporative emissions include the release of gasoline vapors resulting from diurnal temperature variations, hot soak (i.e., residual heat at the end of a trip), running losses, and resting losses. In contrast to diurnal and hot soak emissions from parked vehicles, running losses occur only during vehicle operation. Resting losses, due for example to permeation of fuel through plastic and rubber components of the fuel system, occur at all hours whether or not the vehicle is in operation. All forms of evaporative emissions are released into the ambient

atmosphere due to leaks throughout the fuel system, and in the case of older vehicles, uncontrolled atmospheric vents on the gas tank. For emission inventories, liquid fuel leaks/spills originating from on-road vehicles are considered a form of running losses, while leaks/spills occurring at service stations are included under fuel storage and handling as an area source; in terms of our analysis both are grouped in with tailpipe emissions under the larger category of whole gasoline emissions. California regulations and control equipment have emphasized control of both tailpipe and vapor emissions from vehicles. Control technologies include catalytic converters, seasonal changes in gasoline formulation to reduce summertime vapor pressure, and vapor recovery systems on vehicles and at service stations.

Previous studies using dynamometer vehicle fleet tests conclude that 7-35% of motor vehicle non-methane hydrocarbons are non-tailpipe emissions (3). Similarly, an analysis of 2001 ambient data from Granite Bay, CA (near Sacramento) estimated $17.0 \pm 0.9\%$ of total daytime gasoline-related VOC emissions are vapor pressure-driven (4). This new work in Riverside, CA presents a valuable opportunity to study a different location with different geography and meteorological conditions while also considering seasonal variability. Another difference compared to previous work is the incorporation of ethanol into California gasoline, which may affect VOC emissions. A comprehensive understanding of VOC emissions at Riverside is of particular interest because this area has some of the highest levels of ozone and particulate matter (PM) pollution in the United States (5).

Methods for generating emissions estimates are subject to uncertainties. A review of mobile source emission modeling by the National Research Council stresses the importance of model evaluation studies using ambient observations to reduce uncertainties by identifying areas of agreement and those that deserve further study (6). In an effort to evaluate emission inventories, we compare ambient observations to inventories developed by the California Air Resources Board (CARB) for reactive organic gases and CO (7). These inventories are resolved by source category, county, and air basin. Table 3.1 summarizes VOC emissions estimates for the western portion of Riverside County that is included in the South Coast air basin (SoCAB). California's emission inventories (7) and EMFAC model (8) are the sources of the estimates shown in Table 3.1; EMFAC estimates on-road vehicle emissions by calendar year, season, and location.

The objectives of this research were to evaluate changes in AVOC emissions resulting from seasonal variations in gasoline formulation; to distinguish vapor pressure-driven AVOC emissions from other gasoline-related AVOC emission sources; to develop diurnal profiles of AVOC emissions, meteorology, and source contributions; and finally to examine the consistency of AVOC and CO emission inventories with measured ambient pollutant concentrations.

2. Methods

2.1. Ambient Measurements

Ambient concentrations of 55 VOCs (Table 3.3) were measured during the 2005 Study of Organic Aerosols at Riverside (SOAR) campaign in Riverside, CA. The measurement site ($33^{\circ}\text{N } 58^{\circ} 18''/117^{\circ}\text{W } 19^{\circ} 17''$) was located on the University of California, Riverside campus in an urban area within the South Coast air basin, east of Los Angeles and Orange County. The site was located 1 km east (typically downwind) of a major highway—Interstate 215. Month-long sampling campaigns were conducted in the summer (July 15 - August 15) and in the fall (October 31 - November 30).

Hourly-resolved VOC concentrations were measured on-site using a gas chromatograph (HP model 5890) equipped with both a mass-selective detector (HP model 5971) and a flame ionization detector; example chromatograms can be found in the supporting information section (Figure 3.6). The instrument pre-concentrated 450 mL samples of ambient air on adsorbent traps over a 30 minute period and thermally desorbed them onto capillary columns; the FID-analyzed sample was collected on a glass bead/Carbopak B/Carboxen 1000 adsorbent mix and injected onto a RT-Alumina Plot column, while the MSD-analyzed sample was collected on a glass bead/Carbopak B/Carbosieves SIII mix, then injected onto a DB-Wax column. Further detail on the GC/MS-FID system can be found in Millet et al. (9). Meteorological data, including ambient temperature and wind speed/direction were recorded on-site throughout the campaign. CO was measured using non-dispersive infrared absorption (TEI, model 48c) and ground-level ozone (O₃) was measured using an UV photometric analyzer (Dasibi Inc., model 1008-RS); CO and O₃ data were averaged to match the temporal resolution of the VOC data.

2.2. Liquid Gasoline

Liquid gasoline composition was measured by the California Air Resources Board during both summer and winter 2005-06 by collecting fuel samples from the tanks of 20 in-use vehicles during both summer (April - October) and winter (November - March) months. Individual gasoline samples were combined into aggregate samples for each season and then a detailed hydrocarbon analysis was performed to measure fuel composition (10). For specific compound weight fractions reported in this study, averages (and ranges) of the two seasonal mixtures were calculated.

2.3. Gasoline Headspace Vapors

Vapor-liquid equilibrium calculations were performed using speciated liquid gasoline measurements to predict gasoline vapor composition:

$$P_i = x_i \gamma_i P_i^o(T) \quad (3.1)$$

$$y_i = P_i / \sum_i P_i \quad (3.2)$$

$$w_i = y_i MW_i / \sum_i y_i MW_i \quad (3.3)$$

where P_i represents the partial pressure of compound i and $P_i^o(T)$ is the vapor pressure of the pure liquid i at a specified temperature ($T = 298$ K in this analysis). γ_i denotes the liquid phase activity coefficient of compound i . California gasoline now contains significant amounts of ethanol and behaves as a non-ideal solution ($\gamma \neq 1$); liquid-phase activity coefficients were specified as described in Harley et al. (11). The vapor-phase mol fractions and weight fractions of species in the gasoline headspace vapor are represented by y_i and w_i , respectively. Vapor-liquid equilibrium calculations considered all species with up to 8 carbons; the heavier molecules are minor contributors to gasoline vapor pressure and headspace composition.

2.4. Chemical Mass Balance Analysis

Source-receptor modeling using a chemical mass balance method was performed following Rubin et al. (4). We used tracers present in both liquid gasoline and headspace vapors to distinguish between whole gasoline and vapor pressure-driven VOC emissions. Isopentane and the sum of methylpentane isomers were used as tracers in this study. Emissions of these VOC are dominated by gasoline-related sources, and they have defined and distinctly different signatures in vapor versus liquid fuel. Both tracers were measured at Riverside during SOAR and have similar atmospheric lifetimes. Tracer weight fractions in the headspace vapor represent vapor pressure-driven evaporative emissions, whereas whole gasoline emissions are estimated using the tracer weight fractions in liquid gasoline. The colinearity of vehicular tailpipe VOC emissions and liquid gasoline composition has been reported previously (12). This approach provides an upper bound on the vapor pressure-driven contribution as we neglect products of incomplete combustion such as ethane, ethene, propene, acetylene, isobutene, and all aldehydes in tailpipe emissions; which were not measured at Riverside. We estimate, from previous on-road measurements (13), that ~17% of the non-methane organic carbon mass emissions are products of incomplete combustion, with the precise fraction varying depending on engine type, age, and operation mode. Isopentane's high vapor pressure makes it considerably more abundant in vapor pressure-driven emissions and changes in its abundance, relative to the heavier methylpentanes, allow us to differentiate vapor from liquid fuel sources.

The chemical mass balance equation can be written as follows:

$$C_i = \sum_j w_{ij} S_j \quad (3.4)$$

Hourly source contributions (S_j) were calculated from measured ambient concentrations (C_i) and the chemical fingerprint matrix (w_{ij}) generated from the liquid fuel and headspace vapor composition profiles described above. Source contribution results from this method were used to analyze the diurnal variations in fuel vapor and whole gasoline emissions as well as the vapor pressure-driven contribution to total gasoline-related VOC emissions. In addition, we examined variations in wind speed and direction to determine meteorological effects on ambient concentrations and source contributions. Measurements were separated into weekday and weekend subgroups to control for differences in traffic patterns (14).

2.5. Emission Inventories

County and air basin-resolved emission inventories for 2005 were compared to our ambient CO data and total gasoline-related VOC (the sum of fuel vapor and whole gasoline source contributions) (7). We evaluated the correlation of gasoline-related VOC to CO concentrations via linear regression using our data and compared them to model estimates developed using California's emission inventory tools. The model-based gasoline-related VOC/CO ratios were estimated by dividing the sum of on and off-road gasoline-related VOC emissions by the total CO emissions in the region to be consistent with the sources included in our ambient sampling-based method. For the purposes of comparison, biogenic CO emissions were excluded due to the absence of forest fires during the field studies in 2005 and the relatively low biogenic VOC emissions in the Riverside and Los Angeles areas. VOC/CO emission inventory ratios were calculated for the portion of Riverside County within the South Coast air

basin and the entire South Coast air basin for comparison to results derived using our ambient data.

The EMFAC model was used to generate daily and hourly-resolved estimates of gasoline vapor contributions to total gasoline-related VOC emissions and VOC/CO ratios during summer 2005. One caveat to the ratios developed using EMFAC is that they are limited to on-road emissions for both VOC and CO, and do not include off-road emissions or any other sources of CO observed in ambient air. California's emission inventory suggests that ~30% of gasoline-related VOC and ~20% of CO emissions have therefore been excluded from the comparison. For comparison to the hourly EMFAC results, we also generated a diurnal profile of VOC/CO ratios by performing linear regressions over 3-hour intervals of our data (Table 3.5 & Figure 3.10).

3. Results and Discussion

3.1. Gasoline Seasonality

Seasonal changes in gasoline formulation are reflected in differences between summer and winter headspace vapor composition. Isopentane comprises a smaller fraction of winter gasoline vapors compared to summer, while the n-butane vapor fraction increases significantly and the ethanol fraction decreases in winter. Table 3.2 summarizes the seasonal variation of abundant compounds in gasoline in both liquid fuel and headspace vapors. The inclusion of high-volatility compounds is intentionally limited during the summer to reduce AVOC emissions, which leads to observed decreases in ambient mixing ratios of such VOCs in the summer (See Figure 3.1) (15). The molar ratio of n-butane to CO more than doubles from $(1.8 \pm 0.2) \times 10^{-3}$ in the summer to $(4.1 \pm 0.2) \times 10^{-3}$ in the fall, while the isopentane ratio to CO exhibits less variation, increasing modestly from 0.0038 ± 0.0002 in the summer to 0.0045 ± 0.0002 in the fall. Similar seasonality of ambient n-butane concentrations was observed by Lee et al. in the northeastern U.S. during much of the 1990's and isopentane concentrations were more stable with no statistically significant seasonal variation observed between summer and fall (16).

The most dramatic compositional effect of seasonal gasoline reformulation is the large variation of n-butane in the liquid fuel, headspace vapors, and ambient measurements. This result is expected since n-butane has a higher vapor pressure than isopentane and is preferentially removed by refiners during summer months due to seasonal limits on gasoline vapor pressure. Despite strong vapor/liquid and seasonal contrasts in n-butane abundance, we did not include this compound in the chemical mass balance analysis. Our primary concern is the presence of n-butane in other VOC emission sources (17). In summer especially, when n-butane is greatly reduced in liquid gasoline, it should not be assumed that gasoline-related sources will dominate the atmospheric concentration of n-butane. The high vapor pressure of n-butane and its very low abundance in summer gasoline also makes this compound especially susceptible to fuel weathering (aging) effects, which would be an added source of uncertainty in the analysis.

3.2. Dilution Effects

The diurnal concentration profile of vehicle-related pollutants during the summer sampling period consistently showed a large peak from morning commuter traffic and a gradual accumulation of pollution during nighttime hours in the shallow inversion layer. Riverside's location is far enough inland to not be limited by marine boundary layer effects, thus the afternoon concentration minima is attributed to atmospheric dilution associated with increased mixing heights and horizontal wind speeds. Figure 3.2 shows the concentration of CO plotted with wind speed and ambient temperature; increases in both correspond to enhanced dilution and

vertical mixing. Even with this dilution, the summertime daily minimum in Riverside is significantly above background at ~400 ppbv CO compared to the hemispheric background of ~100 ppbv CO (18).

An analysis of wind speed and direction in the summer (Figure 3.3) indicates that the wind is consistently blowing from the west (LA/Orange County) during the afternoon. This precludes wind direction from being responsible for the lack of an afternoon peak in pollutant concentration by changing boundary inflow conditions with cleaner air. Dilution effects are responsible for attenuating local concentrations associated with the higher emissions during the afternoon commute. The same winds that dilute nearby primary emissions also transport ozone formed further upwind. The diurnal ozone cycle coincides with ambient temperature, peaking at an average of ~90 ppb around 15:00 PST (Figure 3.7).

3.3. Source Contributions

The chemical mass balance results for the summer sampling period showed a consistent diurnal pattern (Figure 3.4). Similar to the CO profile (Figure 3.2), the peak in tailpipe contributions (~60 $\mu\text{g}/\text{m}^3$) coincides with the morning commute, and the gradual increase in tailpipe contributions throughout the nighttime hours can be attributed to some nighttime traffic, but more importantly decreased dilution. In the afternoon, dilution offsets the expected increase in source contributions from both whole gasoline and fuel vapor VOC emissions, which we would expect due to increased traffic and temperature. The relatively stable vapor pressure-driven source contributions (~10 $\mu\text{g}/\text{m}^3$) with increasing temperatures throughout the day indicate a balance between evaporative emissions and atmospheric dilution in the South Coast air basin. A comparison of our temperature observations to evaporative emissions estimated using EFMAC yields an expected increase in evaporative emissions with temperature (Figure 3.8), which is offset in our ambient observations by enhanced afternoon dilution. Similar stability of vapor source contributions throughout the day was observed near Sacramento, CA, in a previous study (4).

Vapor pressure-driven contributions to gasoline-related VOC emissions averaged $31 \pm 2\%$ during the summer portion of SOAR 2005 and did not vary significantly from weekday to weekend ($30 \pm 2\%$ on weekdays versus $33 \pm 3\%$ during the weekend). Similar to previous results (4), the percent vapor contribution to total gasoline-related VOC is statistically stable after the morning commute. At Riverside, it peaks in the early afternoon (~40%) due to increased temperatures and reduced traffic volumes compared to commuter peak periods (Figure 3.9). The percent vapor contribution is lowest during the morning commute (~20%) due to the large volume of whole gasoline (presumably tailpipe) emissions. Diurnal patterns of the vapor contribution exhibited statistically insignificant variation between weekdays and weekends (Table 3.4). The relative vapor contribution to total gasoline-related VOC is significantly higher than previous results from Granite Bay, which ranged from 7-22% during daytime hours on weekdays, compared to 19-44% during daytime hours on weekdays at Riverside in the present study; both sites had similar diurnal patterns in vapor fraction and at similar afternoon temperatures the percent contribution of fuel vapor was greater at Riverside than Granite Bay (4). Possible contributing factors include reductions in tailpipe hydrocarbon emissions between 2001 and 2005, differences in emissions and meteorology at Granite Bay and Riverside, increases in evaporative emissions since 2001 due to the switch from MTBE to ethanol, and uncertainties in VOC source speciation profiles.

Simulations using the EMFAC emission factor model indicate 31% of total gasoline-related VOC is vapor pressure-driven, which is in agreement with our overall value of $31 \pm 2\%$.

The comparison of our data to the model's diurnal profile of percent vapor contribution (Figure 3.9) shows reasonable agreement during the day considering the uncertainties involved in both approaches.

Our results highlight the importance of VOC emission control for both tailpipe and vapor pressure-driven emissions. Both are significant contributors and will need to be controlled to successfully reduce ozone and secondary organic aerosol formation in the South Coast air basin.

3.4. Gasoline-related VOC to Carbon Monoxide Emission Ratio

Our estimated molar emission ratio for Riverside is 0.086 ± 0.006 for gasoline-related VOC to CO emissions (Figure 3.5). Ratios estimated using California's emission inventory are slightly greater; ranging from 0.097 to 0.106 depending on the spatial scale considered. Our molar emission ratio is consistent with the 0.087 ratio estimated using EMFAC. One caveat to our inventory is that the ambient CO measurements may be greater than that expected from emissions due to inflow from upwind urban areas and formation of secondary CO from the oxidation of AVOC in the late morning and afternoon (19). This may explain why our value is slightly lower than values from the emission inventory.

A comparison of diurnal patterns in gasoline-related VOC to CO ratios between our data and the EMFAC model (Figure 3.10) indicates good agreement between the two, given that the model includes only 80% of CO emissions. Our results show no significant difference between weekdays and weekends, and the ratio is relatively stable as expected (Table 3.5).

3.5 Implications for Emissions Studies

A caveat to this and similar studies is that it assumes liquid gasoline composition is representative of actual combustion (i.e. whole gasoline) emissions and does not account for all products of incomplete combustion. In actuality, the compositional fraction of prominent hydrocarbons (e.g. tracers) in tailpipe exhaust is lower than in liquid fuel. This implies that analyses may underestimate contributions from exhaust and the total AVOC emissions from gasoline, and thus the percent contribution from vapor pressure-driven emissions is likely an upper bound. Accounting for this effect, we estimate that tailpipe source contributions may be underestimated by up to 20%. Additionally, designations for motor vehicle emission mechanisms merit reflection as it is not always clear if an evaporative pathway is vapor pressure-driven and thus temperature dependent or if all the components of the liquid gasoline are being evaporated. In some cases evaporative emissions may appear to be more representative of tailpipe emissions, for example with hot soak emissions and running losses from older vehicles, or liquid fuel spillage at service stations. Nevertheless, our upper-limit results are in agreement with California's emission factor model and their emission inventories.

Notes on EMFAC Model Calculations:

The model (EMFAC 2007 v2.3) was run for the summer season constrained to the portion of Riverside County in the South Coast air basin using model years 1965-2005 and all classes of gasoline-powered vehicles in the enhanced interim method (8). To calculate the percent vapor contribution, vapor and whole gasoline emissions are grouped as defined in the introduction; with the exception that running losses were halved between whole gasoline and fuel vapor emissions to account for liquid fuel spills, which is in accordance with previous work (4).

References

1. Goldstein, A.H.; Galbally, I.E. Known and unexplored organic constituents in the earth's atmosphere. *Environ. Sci. Technol.* **2007**, 41, 1514-1521.
2. Sawyer, R.F.; Harley, R.A.; Cadle, S.H.; Norbeck, J.M.; Slott, R.; Bravo, H.A. Mobile sources critical review: 1998 NARSTO assessment. *Atmos. Environ.* **2000**, 34, 2161-2181.
3. Pierson, W.R.; Schorran, D.E.; Fujita, E.M.; Sagebiel, J.C.; Lawson, D.R.; Tanner, R.L. Assessment of nontailpipe hydrocarbon emissions from motor vehicles. *J. Air Waste Manage. Assoc.* **1999**, 49, 498-519.
4. Rubin, J.I.; Kean, A.J.; Harley, R.A.; Millet, D.B.; Goldstein, A.H. Temperature dependence of volatile organic compound evaporative emissions from motor vehicles. *J. Geophys. Res., [Atmos.]* **2006**, 111 (D3), D03305.
5. American Lung Association. *State of the Air 2008*; New York, 2008
6. National Research Council. *Modeling Mobile-Source Emissions*; National Academy Press: Washington, DC, 2000.
7. California Air Resources Board: Estimated annual average emissions, 2005. Available at <http://www.arb.ca.gov/ei/emsmain/emsmain.htm> (accessed June-August 2008).
8. California Air Resources Board: Motor Vehicle Emission Factor/Emission Inventory Model, EMFAC 2007 version 2.3, Available at <http://www.arb.ca.gov/msei/msei.htm> (downloaded July 2008).
9. Millet, D.B.; Donahue, N.M.; Pandis, S.N.; Polidori, A.; Stanier, C.O.; Turpin, B.J.; Goldstein, A.H. Atmospheric volatile organic compound measurements during the Pittsburgh Air Quality Study: Results, interpretations, and quantification of primary and secondary contributions. *J. Geophys. Res., [Atmos.]* **2005**, 110 (D7), D07S07.
10. Standard test method for determination of individual components in spark ignition engine fuels by 50-metre capillary high resolution gas chromatography, ASTM D-6733, performed July 2006. Available at: <http://www.astm.org/Standards/D6733.htm> (accessed April 2009).
11. Harley, R.A.; Coulter-Burke, S.C.; Yeung, T.S. Relating liquid fuel and headspace vapor composition in California reformulated gasoline samples containing ethanol. *Environ. Sci. Technol.* **2000**, 34, 4088-4094.
12. Leppard, W.R.; Gorse, R.A.; Rapp, L.A.; Knepper, J.C.; Burns, V.R.; Koehl, W.J. Effects of gasoline composition on vehicle engineout and tailpipe hydrocarbon emissions. *SAE Tech. Pap. Ser.* **1992**, no. 920329.
13. Kirchstetter, T.W.; Singer, B.C.; Harley, R.A. Impact of California reformulated gasoline on motor vehicle emissions. 2. volatile organic compound speciation and reactivity. *Environ. Sci. Technol.* **1999**, 33, 329-336.
14. Harley, R.A.; Marr, L.C.; Lehner, J.K.; Giddings, S.N. Changes in motor vehicle emissions on diurnal to decadal time scales and effects on atmospheric composition. *Environ. Sci. Technol.* **2005**, 39, 5356-5362.
15. California Air Resources Board: Reid Vapor Pressure (RVP) Control Periods for California Air Basins and Counties, 2008. Available at <http://www.arb.ca.gov/fuels/gasoline/rvp/rvp.htm> (accessed January-February 2009).
16. Lee, B.H.; Munger, J.W.; Wofsy, S.C.; Goldstein, A.H. Anthropogenic emissions of nonmethane hydrocarbons in the northeastern United States: measured seasonal

- variations from 1992-1996 and 1999-2001. *J. Geophys. Res., [Atmos.]* **2006**, 111 (D20), D20307.
17. U.S. Environmental Protection Agency. *SPECIATE 4.0: Speciation Database Development Documentation: Final Report*; Research Triangle Park, NC, 2006.
 18. National Oceanic & Atmospheric Administration, Earth System Research Laboratory: Mauna Loa Observatory Carbon Monoxide Measurements. Available at <http://www.esrl.noaa.gov/gmd/ccgg/iadv/> (accessed January-February 2009).
 19. Griffin, R. J.; Chen, J.; Carmody, K.; Vutukuru, S.; and Dabdub, D. Contribution of gas phase oxidation of volatile organic compounds to atmospheric carbon monoxide levels in two areas of the United States, *J. Geophys. Res., [Atmos.]* **2007**, 112 (D10), D10S17.

Figures & Tables

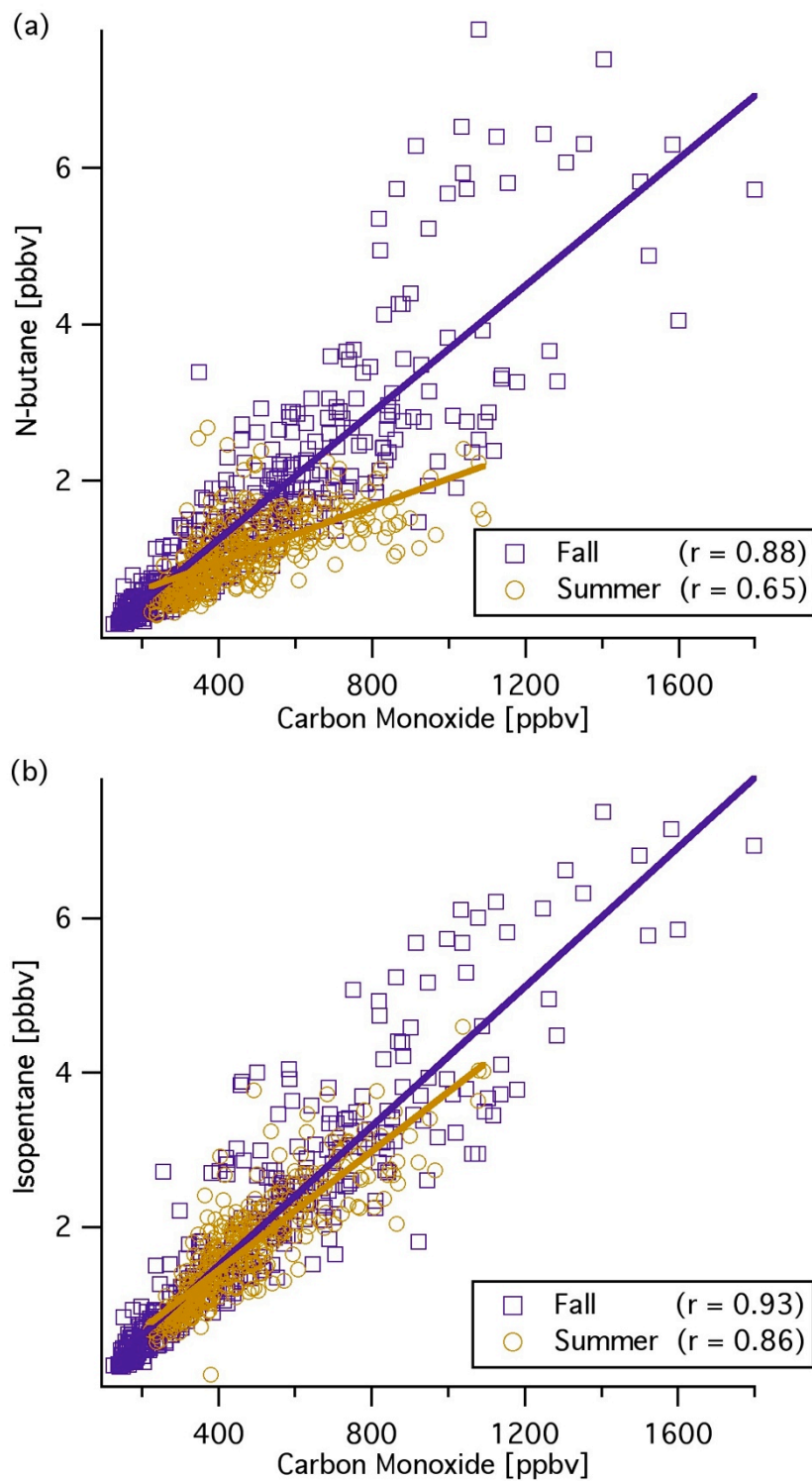


Figure 3.1: Plots of Ambient Concentrations of (a) n-butane and (b) isopentane versus carbon monoxide at Riverside for summer and fall 2005

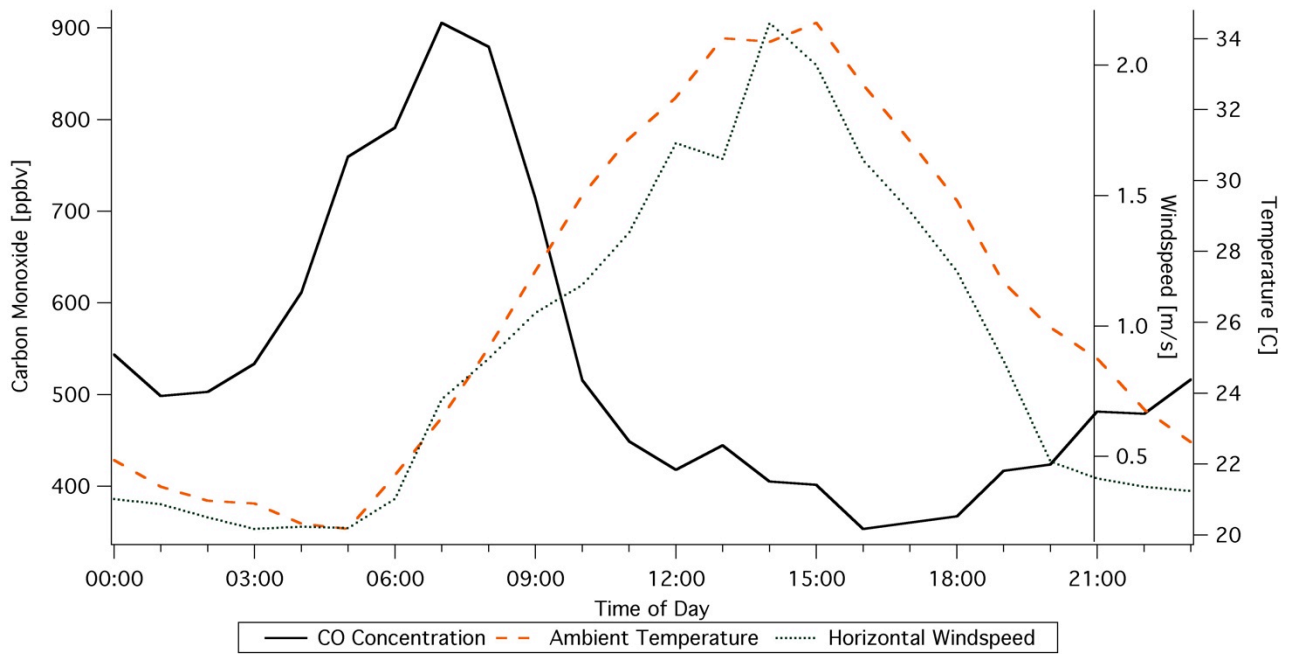


Figure 3.2: Diurnal variation of ambient CO concentration at Riverside (weekdays only during summer 2005) and collocated variations in ambient temperature and wind speed

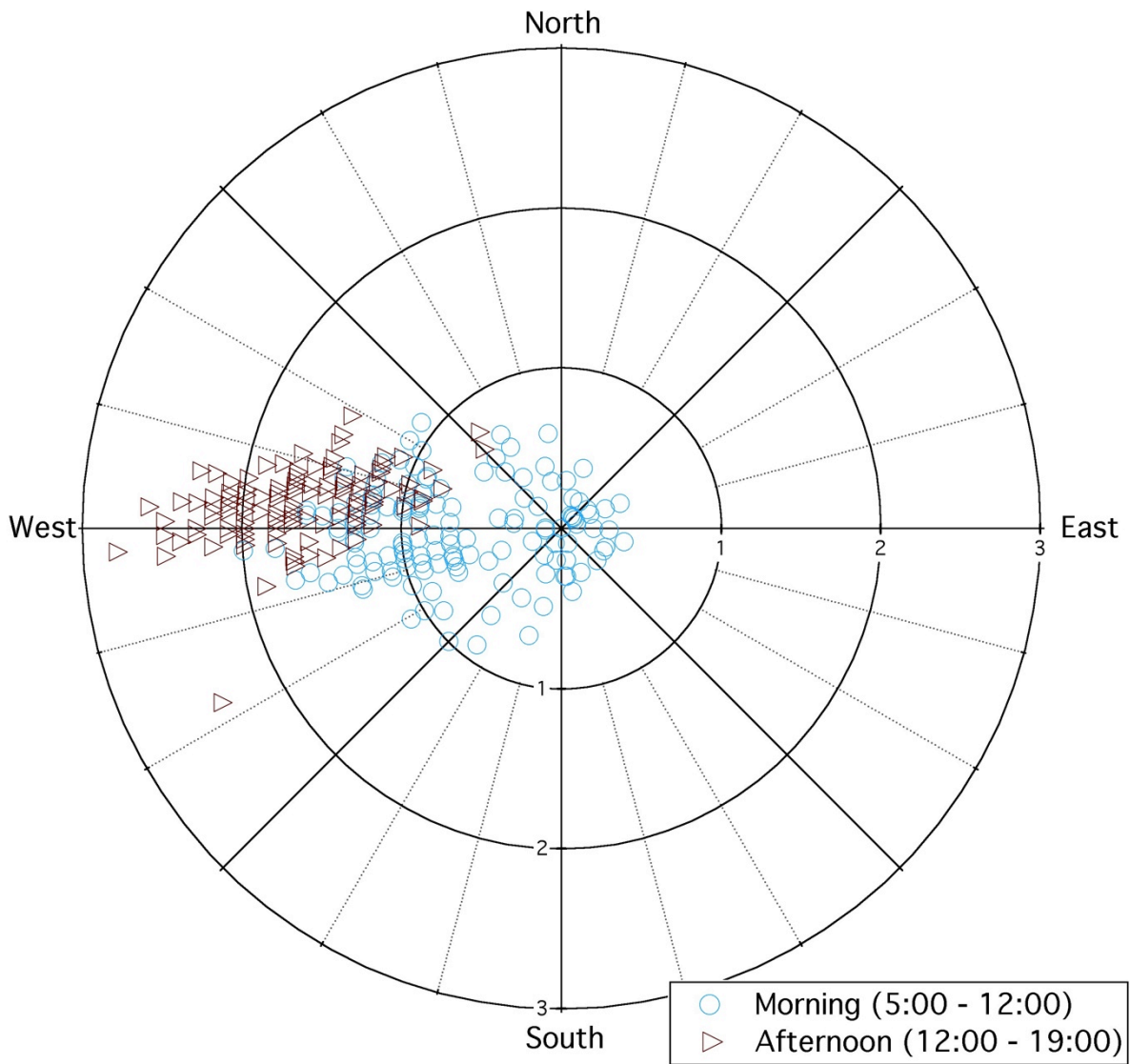


Figure 3.3: Distributions of summer wind speed (m/s) and direction at Riverside, CA. Displayed as individual hourly measurements for the morning and afternoon; overnight ground-level wind (not shown) was relatively calm with no dominant direction.

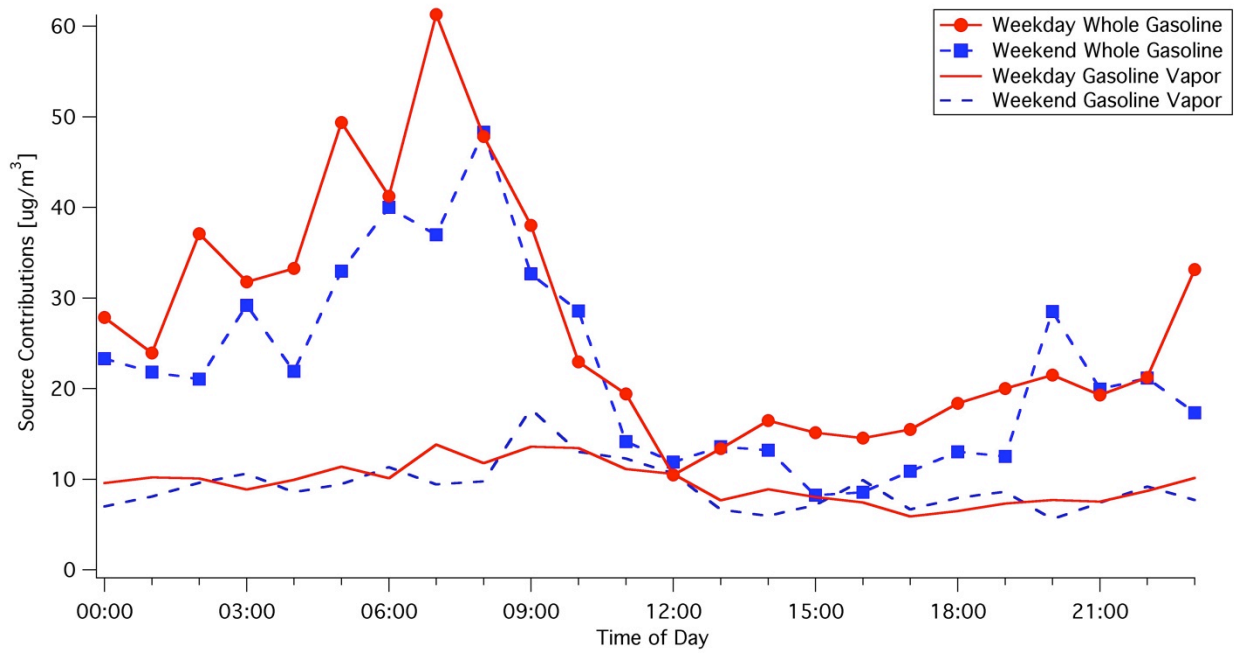


Figure 3.4: Source contributions to ambient VOC at Riverside from whole gasoline and gasoline vapor emissions

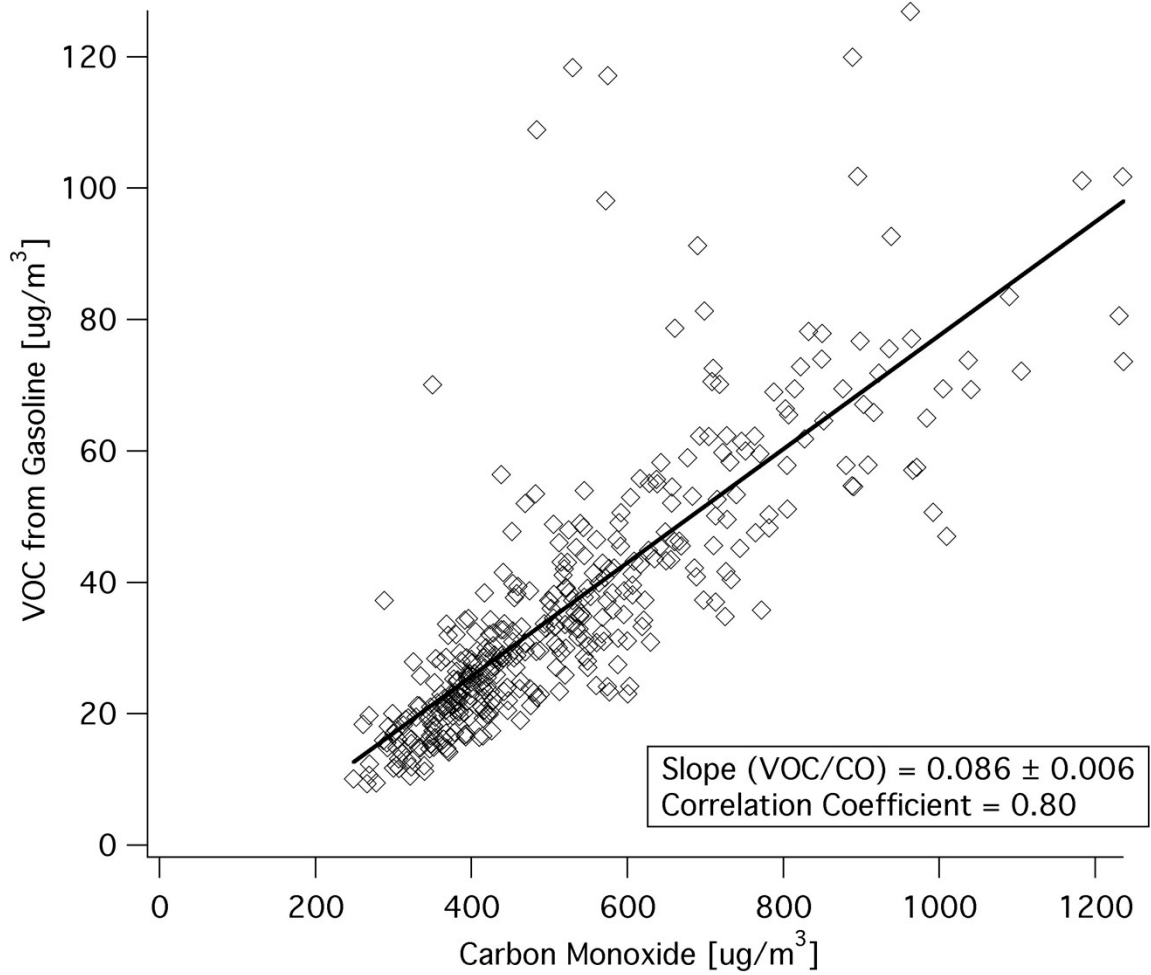


Figure 3.5: Plot of gasoline-related VOC concentrations versus carbon monoxide concentrations during summer 2005

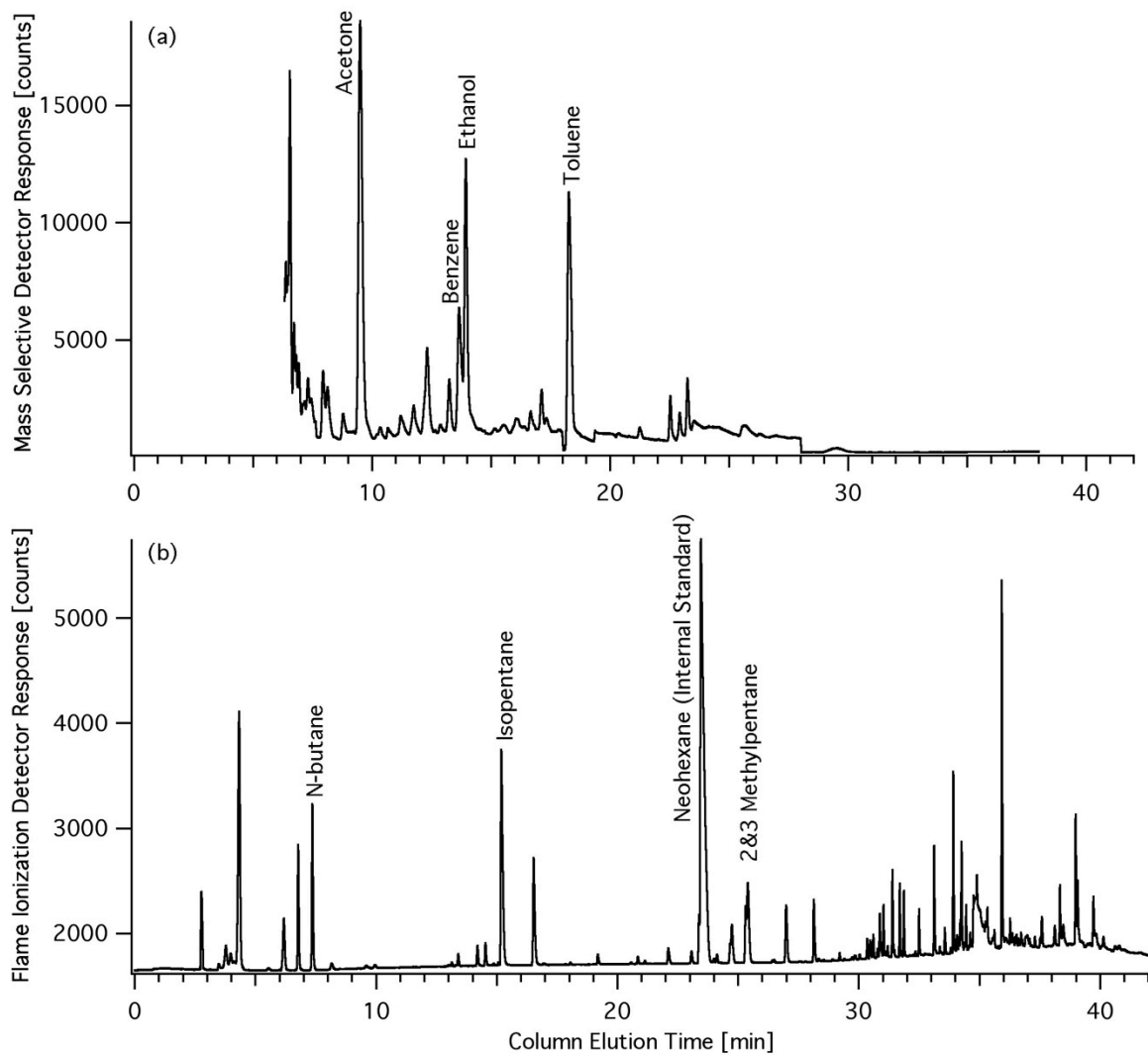


Figure 3.6: Sample chromatograms from Summer SOAR measurements (07:00 7/26/2005) for (a) the mass selective detector and (b) the flame ionization detector

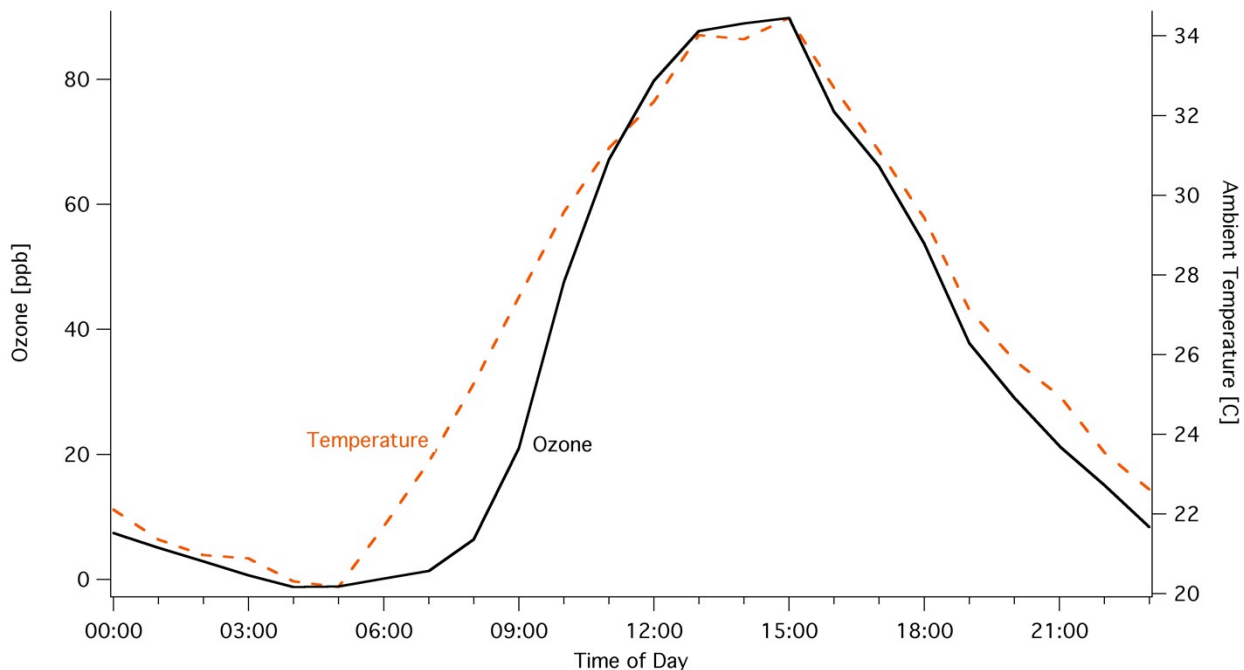


Figure 3.7: Superimposed weekday diurnal ozone and ambient temperature profiles

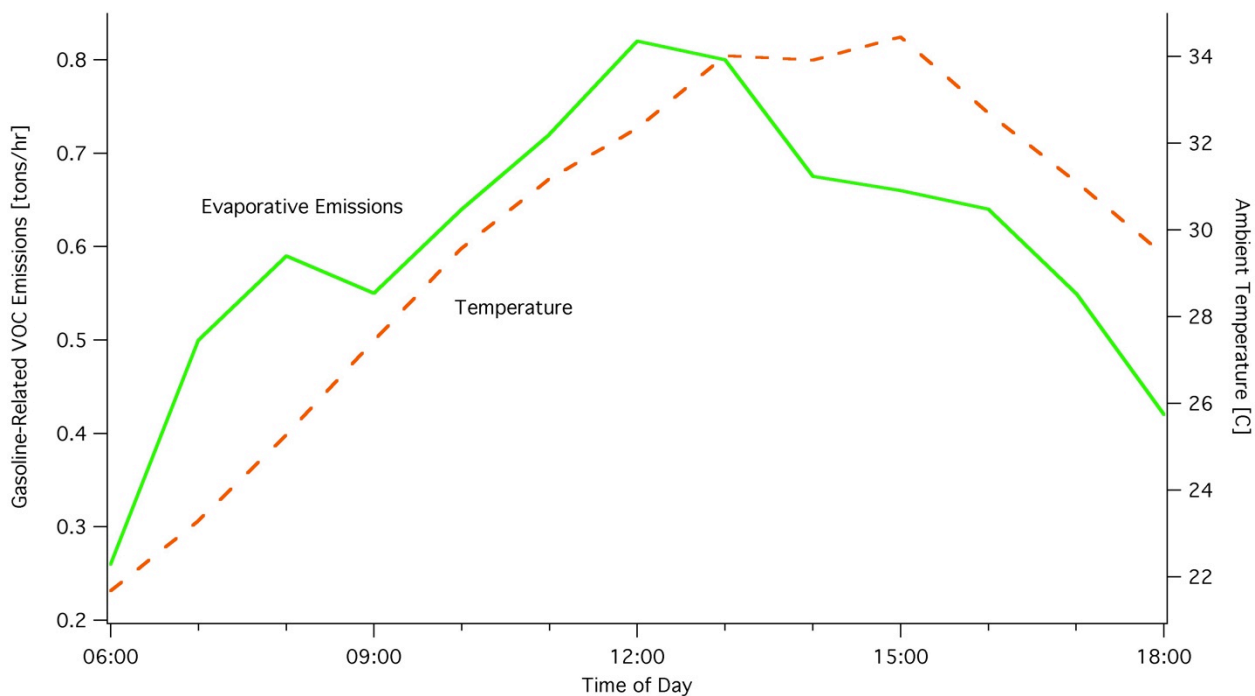


Figure 3.8: Diurnal EMFAC-derived evaporative emissions during summer 2005 with ambient temperature observations superimposed

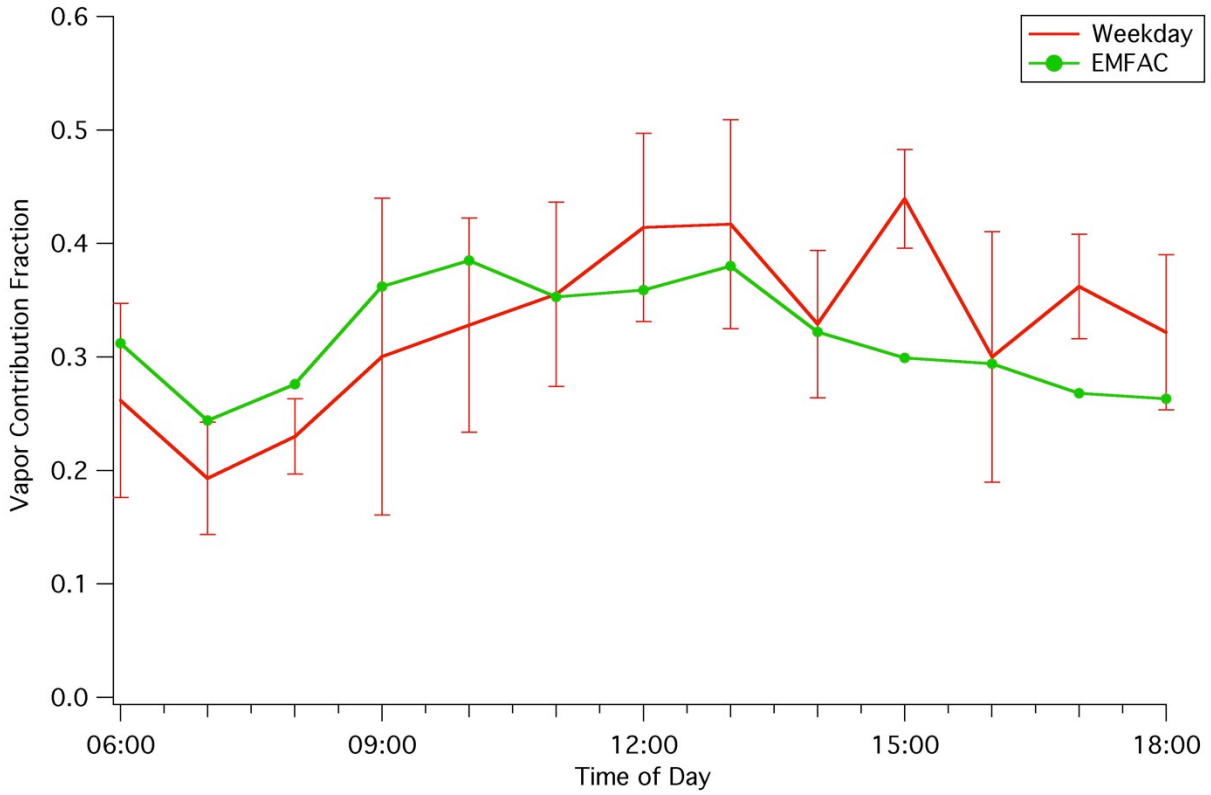


Figure 3.9: Daytime vapor contribution fraction from weekday summer measurements (with 95% confidence intervals) compared to EMFAC model results

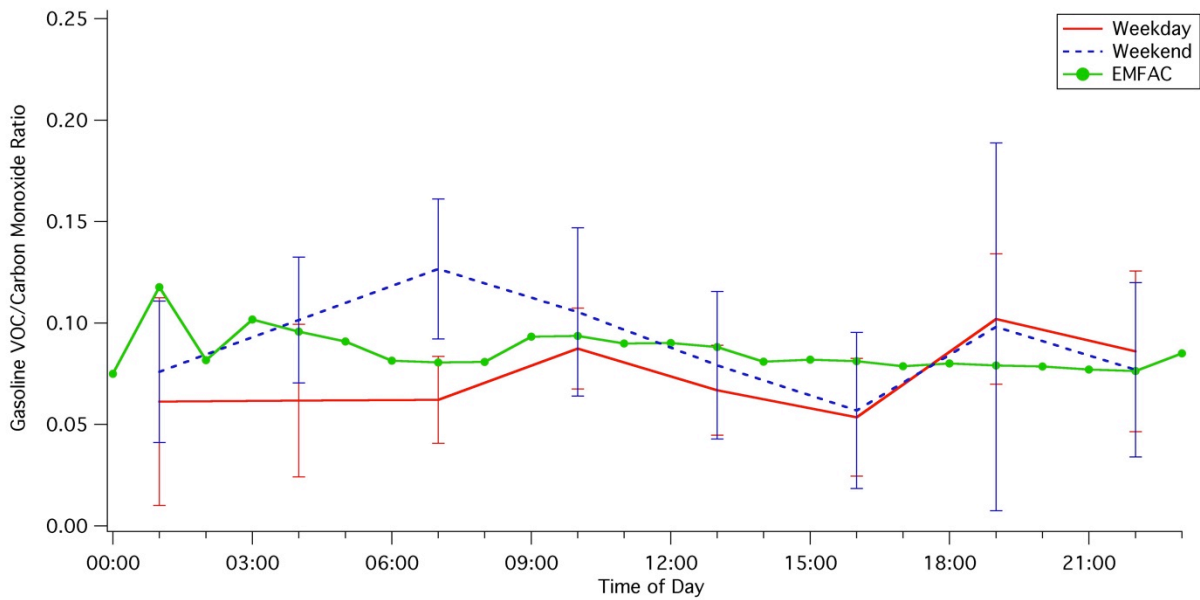


Figure 3.10: Gasoline-related VOC to CO ratios for weekday and weekend (with 95% confidence intervals) including EMFAC model results

**Table 3.1: 2005 Gasoline-related VOC emission inventory
for Riverside County (South Coast air basin)^a**

| Source ^b | Emissions [tons/day] | Percent Contribution |
|------------------------------------|----------------------|----------------------|
| Light Duty Passenger | 11.0 | 26% |
| Light Duty Trucks | 8.4 | 20% |
| Medium Duty Trucks | 2.9 | 7% |
| Heavy Duty Gasoline Trucks & Buses | 3.3 | 8% |
| Motorcycles | 3.3 | 8% |
| Recreational (Off-road & Boats) | 4.6 | 11% |
| Off-Road Equipment ^c | 5.2 | 12% |
| Petroleum Production & Refining | 2.1 | 5% |
| Fuel Storage and Handling | 1.4 | 3% |

^a Estimates are the annual average of daily emissions

^b Train and aircraft emissions are excluded due to fuel differences (2.8 tons VOC/day)

^c Includes farm, lawn & garden, and other commercial/residential equipment

Table 3.2: Most abundant compounds in gasoline and headspace vapors [wt% (range)]^a

| Compound | <i>Headspace Vapor</i> | | <i>Liquid Gasoline</i> | |
|------------------------|------------------------|------------------|------------------------|---------------|
| | Summer | Winter | Summer | Winter |
| Isopentane | 31.7 (30.9-32.6) | 24.2 (23.6-24.8) | 6.9 (6.7-7.1) | 7.4 (7.2-7.5) |
| N-Butane | 4.7 (4.4-5.1) | 24.2 (24.1-24.3) | 0.5 (0.5-0.5) | 3.4 (3.4-3.4) |
| 2-Methylpentane | 6.5 (6.3-6.7) | 4.0 (3.6-4.3) | 3.9 (3.8-3.9) | 3.3 (3.0-3.6) |
| 3-Methylpentane | 3.5 (3.4-3.7) | 2.5 (2.3-2.6) | 2.4 (2.3-2.4) | 2.3 (2.2-2.5) |
| Ethanol | 7.5 (7.5-7.6) | 5.4 (5.4-5.5) | 6.0 (6.0-6.1) | 6.3 (6.2-6.4) |
| N-Pentane | 8.3 (8.2-8.3) | 7.8 (7.1-8.4) | 2.4 (2.4-2.4) | 3.2 (2.9-3.5) |
| Toluene | 2.0 (1.9-2.1) | 1.3 (1.2-1.4) | 8.2 (7.7-8.6) | 7.6 (7.0-8.3) |
| M-xylene | 0.3 (0.3-0.3) | 0.2 (0.2-0.2) | 3.9 (3.9-4.0) | 4.1 (4.0-4.3) |
| 2,2,4-Trimethylpentane | 3.3 (3.2-3.4) | 1.3 (1.0-1.7) | 6.3 (6.0-6.7) | 3.5 (2.6-4.5) |
| Isobutane | 0.7 (0.7-0.7) | 6.2 (4.9-7.5) | 0.05 (0.05-0.05) | 0.6 (0.5-0.7) |

^a Liquid gasoline composition acquired from CARB and is based on 20 liquid gasoline samples collected each season and aggregated into 2 mixtures for detailed hydrocarbon analysis (ranges are over the two aggregates). Some individual liquid samples may have been affected by weathering in the fuel tank.

Table 3.3: Compounds measured during SOAR 2005

| | | |
|---------------------------|-------------------------|-------------------|
| 2-pentanone | isoprene | pentane |
| 3-pentanone | isopropanol | propanal |
| acetone | methacrolein | propane |
| acetonitrile | methyl ethyl ketone | propene |
| alpha-pinene | methyl furan | propyne |
| benzene | methyl nitrate | toluene |
| beta-pinene | methyl tert-butyl ether | trans-2-butene |
| butanal | methyl vinyl ketone | water vapor |
| butane | methyl-1-butene | C2Cl4 |
| butene | methyl-2-butanone | C2HCl3 |
| carbon monoxide | methylbutenol | CCl3F |
| cyclopentane | methylpentane | CH2Cl2 |
| dimethylsulfide | methylpropanal | CH3CCl3 |
| ethyl & isopropyl nitrate | methylpropene | CH3Cl |
| heptane | neopentane | CH3I |
| hexanal | n-propyl nitrate | CHCl3 |
| hexane | o-xylene | CHClF2 |
| isobutane | ozone | Cl2FC-CClF2 |
| isopentane | pentanal | F141b (Cl2FC-CH3) |

**Table 3.4: Percent vapor contribution to gasoline-related VOC emissions
(± 95% confidence intervals)**

| Hour | Weekday | Weekend | EMFAC |
|-------------|----------------|----------------|--------------|
| 0:00:00 | 31 ± 13 | 23 ± 1 | 41 |
| 1:00:00 | 30 ± 5 | 27 ± 7 | 58 |
| 2:00:00 | 34 ± 19 | 32 ± 13 | 59 |
| 3:00:00 | 38 ± 23 | 29 ± 6 | 75 |
| 4:00:00 | 26 ± 2 | 29 ± 5 | 53 |
| 5:00:00 | 21 ± 4 | 24 ± 3 | 47 |
| 6:00:00 | 26 ± 9 | 22 ± 6 | 31 |
| 7:00:00 | 19 ± 5 | 22 ± 5 | 24 |
| 8:00:00 | 23 ± 3 | 23 ± 11 | 28 |
| 9:00:00 | 30 ± 14 | 37 ± 8 | 36 |
| 10:00:00 | 33 ± 9 | 33 ± 9 | 39 |
| 11:00:00 | 36 ± 8 | 46 ± 10 | 35 |
| 12:00:00 | 41 ± 8 | 49 ± 22 | 36 |
| 13:00:00 | 42 ± 9 | 34 ± 13 | 38 |
| 14:00:00 | 33 ± 6 | 31 ± 12 | 32 |
| 15:00:00 | 44 ± 4 | 47 ± 11 | 30 |
| 16:00:00 | 30 ± 11 | 52 ± 13 | 29 |
| 17:00:00 | 36 ± 5 | 37 ± 6 | 27 |
| 18:00:00 | 32 ± 7 | 39 ± 11 | 26 |
| 19:00:00 | 29 ± 6 | 42 ± 9 | 26 |
| 20:00:00 | 27 ± 8 | 28 ± 6 | 26 |
| 21:00:00 | 34 ± 13 | 27 ± 9 | 28 |
| 22:00:00 | 33 ± 10 | 32 ± 14 | 23 |
| 23:00:00 | 23 ± 8 | 32 ± 16 | 29 |

Table 3.5: VOC/CO ratios (± 95% confidence intervals)

| Time of Day | Weekday | Weekend | EMFAC |
|--------------------|----------------|----------------|--------------|
| 0:00-3:00 | 0.061 ± 0.051 | 0.076 ± 0.035 | 0.091 |
| 3:00-6:00 | 0.062 ± 0.038 | 0.101 ± 0.031 | 0.096 |
| 6:00-9:00 | 0.062 ± 0.021 | 0.127 ± 0.035 | 0.081 |
| 9:00-12:00 | 0.087 ± 0.020 | 0.106 ± 0.041 | 0.092 |
| 12:00-15:00 | 0.067 ± 0.022 | 0.079 ± 0.036 | 0.086 |
| 15:00-18:00 | 0.054 ± 0.029 | 0.057 ± 0.038 | 0.081 |
| 18:00-21:00 | 0.102 ± 0.032 | 0.098 ± 0.091 | 0.079 |
| 21:00-0:00 | 0.086 ± 0.040 | 0.077 ± 0.043 | 0.079 |

Chapter 4: Elucidating secondary organic aerosol from diesel and gasoline vehicles through detailed characterization of organic carbon emissions

Reproduced in part from: D.R. Gentner, G. Isaacman, D.R. Worton, A.W.H. Chan, T.R. Dallmann, L. Davis, S. Liu, D.A. Day, L.M. Russell, K.R. Wilson, R. Weber, A. Guha, R.A. Harley, A.H. Goldstein (2012) “Elucidating secondary organic aerosol from diesel and gasoline vehicles through detailed characterization of organic carbon emissions” *Proceedings of the National Academy of Sciences*, in press.

Abstract

Emissions from gasoline and diesel vehicles are predominant anthropogenic sources of reactive gas-phase organic carbon and key precursors to Secondary Organic Aerosol (SOA) in urban areas. Their relative importance for aerosol formation is a controversial issue with implications for air quality control policy and public health. We characterize the chemical composition, mass distribution, and organic aerosol formation potential of emissions from gasoline and diesel vehicles, and find diesel exhaust is 7 times more efficient at forming aerosol than gasoline exhaust. Yet, both sources are important for air quality; depending on a region’s fuel use, diesel is responsible for 65-90% of vehicular-derived SOA, with substantial contributions from both aromatic and aliphatic hydrocarbons. Including these insights on source characterization and SOA formation will improve regional pollution control policies, fuel regulations, and methodologies for future measurement, laboratory, and modeling studies.

1. Introduction

Organic Aerosol (OA) in the atmosphere is detrimental to human health and represents a highly uncertain forcing of climate change (1). The use of petroleum-derived fuels is an important source of reactive gas-phase organic carbon that provides key precursors to the formation of Secondary Organic Aerosol (SOA) and tropospheric ozone (1). Controlling these emissions from gasoline and diesel vehicles is central to air quality mitigation policies in urban areas (2). Previous work has concluded that further research is necessary to elucidate all organic sources of SOA precursors (3-4). Significant controversy exists over the contributions of precursors from gasoline and diesel vehicles, and the relative importance of each for SOA formation remains in question, in part, due to insufficient chemical characterization of fuels and emissions, and the difficulty of ambient measurements of gas-phase compounds emitted from diesel sources (1, 4-8).

In the U.S., diesel fuel accounts for 21% of on-road fuel use (by volume), with off-road sources increasing total use to 28% diesel. In California, the diesel share of on-road use ranges from around 10% in coastal cities to over 30% in agricultural regions (Table 4.2) (2, 9-11). Non-combusted hydrocarbons from the fuels are emitted in the exhaust of gasoline and diesel engines, and also via evaporation from gasoline vehicles and service stations. These compounds in unburned gasoline and diesel fuel dominate vehicular emissions of reactive gas-phase carbon that have the potential to form SOA (12-13). Previous work has shown non-tailpipe emissions account for ~30% of gasoline-related emissions in urban regions, but limited work exists constraining the emissions and SOA formation potential of gas-phase organic carbon from gasoline and diesel sources (14). Using extensive fuel analyses and field data from 2 sites that include many compounds with no prior *in situ* measurements, we present the most comprehensive data to date on the chemical composition, mass distribution, emissions, and SOA

formation potential of non-tailpipe gasoline, gasoline exhaust, and diesel exhaust. We determine the relative importance of gasoline and diesel sources for SOA formation in, and downwind of, urban regions. We assess these results in the context of other studies over the past decade and discuss their significant implications for air pollution measurement, modeling, and control.

2. Results & Discussion

Forty gasoline and twelve diesel fuel samples from California were collected (coincident with field data) and characterized using several gas-chromatography methods, yielding the first comprehensive speciation of the “unresolved complex mixture” in diesel fuel. This was accomplished using soft photoionization techniques, and provides unprecedented detail on the molecular identification and mass distribution of hydrocarbons in diesel fuel (15). Gasoline and diesel fuel, and thus their emissions of unburned hydrocarbons, can be classified by vapor pressure and span the Volatile Organic Compound (VOC) range and the less volatile Intermediate-Volatility Organic Compound (IVOC) range (Figure 4.1). Gasoline hydrocarbons fall mostly within the VOC range with some aromatics extending into the IVOC range, whereas only 30% of diesel fuel hydrocarbons are in the VOC range. Diesel fuel is widely distributed across molecules containing 8 to 25 carbon atoms with a peak around 10-13 carbon atoms (Figure 4.2A). This peak is due to aromatics and cycloalkanes since straight and branched alkanes are evenly distributed between 10 and 20 carbon atoms. Aromatic and aliphatic hydrocarbons make up 23 and 68% of diesel fuel, respectively. By comparison, gasoline contains ~30% aromatics with the remainder of the non-ethanol fraction dominated by straight and branched alkanes with less than 10 carbon atoms (Table 4.1, Figure 4.2A).

In order to examine contributions from each source to reactive gas-phase organic carbon in both the ambient atmosphere and on-road emissions measured in a roadway tunnel, we used a chemical mass balance model with effective variance weighting on over-constrained least squares regressions (9, 16). The model uses a subset of measured compounds and capitalizes on differences in the chemical composition of sources to assess the magnitude of total non-combusted hydrocarbon emissions from each source (9). The source profiles used as *a priori* information are constructed from liquid fuel data to represent gasoline and diesel exhaust, and vapor-liquid equilibrium calculations to represent non-tailpipe gasoline emissions. Equivalent chemical composition in exhaust and liquid fuel has been reported previously for gasoline and is demonstrated in this work for gasoline and diesel at both measurement sites (Figure 4.5) (17). Extensive diagnostics were used to assess model performance, including comparisons against independent compounds to confirm the model’s ability to predict the behavior of reactive VOCs and IVOCs emitted by both gasoline and diesel sources (Figures 4.6-4.9) (9).

Emission factors for non-combusted gas-phase organic carbon in exhaust were determined to be 0.38 ± 0.11 gC L⁻¹ for gasoline and 0.86 ± 0.25 gC L⁻¹ for diesel, which are consistent with values calculated using California’s emissions model for the same period (18). With respect to contributions of non-combusted hydrocarbons from gasoline and diesel exhaust, diesel accounted for 24% at the tunnel study in a coastal city compared to 57% in the urban center of an agricultural region. Accounting for differences in emission factors and fuel densities, this is consistent with on-road fuel sales data in both regions—11 and 33% diesel fuel by volume, respectively (Table 4.2) (9, 11).

To assess the importance of gasoline and diesel sources for SOA in urban areas, we calculated bulk SOA yields for all 3 sources and compared them in context of our emission factors and source contributions. Data on SOA yields are limited for many of the hydrocarbons;

the mass fraction of diesel, gasoline, and non-tailpipe gasoline emissions that have unknown yields are 66, 25, and 7%, respectively. Thus, we modeled high-NO_x SOA yields using published data (where available) and an estimation of yields and uncertainties for unknown values based on best estimates from various plausible scenarios (Figures 4.2B, 4.10) (9).

For the same mass of unburned fuel emissions reacted, diesel exhaust forms 6.7 ± 2.9 times more SOA than gasoline exhaust (bulk SOA yields of 0.15 ± 0.05 and 0.023 ± 0.007 $\mu\text{gSOA } \mu\text{g}^{-1}$, respectively). Considering differences in emission factors, diesel exhaust is expected to form 15 times more SOA than gasoline per liter of fuel burned. For populated regions with 10 to 30% diesel fuel use, this implies that diesel exhaust is responsible for 2 to 7 times more SOA than gasoline exhaust (Figure 4.3). Non-tailpipe gasoline emissions were 39-77% lower than gasoline exhaust emissions and produce negligible SOA due to a substantially lower yield (0.0024 ± 0.0001).

Our methods also allowed us to examine the most important chemical classes and mass distribution of SOA formation. The vast majority of SOA from gasoline sources is due to its aromatic content, whereas diesel SOA is predicted to be $47 \pm 7\%$ from aliphatics with the remainder from aromatics (Figure 4.2B, Table 4.1).

Regional estimates of daytime SOA concentrations from both diesel and gasoline using our model results and calculated SOA yields are consistent with independent positive matrix factor analysis results for aromatic and aliphatic SOA from fossil fuel combustion in the San Joaquin Valley using Aerosol Mass Spectrometer (AMS) and Fourier Transform Infrared spectroscopy (FTIR) measurements. Based on our model results, we expect an average of 1.3 ± 0.4 $\mu\text{gOA } \text{m}^{-3}$ from motor vehicles compared to average PM_{1.0} factor concentrations of 1.8 to 2.1 $\mu\text{gOA } \text{m}^{-3}$ from FTIR and AMS data, respectively (19). These independent data also support the predominance of diesel SOA in the San Joaquin Valley as young aerosol (oxygen:carbon (O:C) ratio = 0.27-0.36) was 58% aliphatic and 42% aromatic (19).

SOA models have made considerable progress using a parameterization known as the *volatility basis set* to estimate contributions from unmeasured intermediate and semi-volatile compounds (5, 20). Together with traditional explicit models for individual hydrocarbons in the VOC range, models are better able to predict the magnitude of observed SOA, but not all temporal patterns or physical/chemical characteristics (3, 20, 28). Here we evaluate the inclusion of SOA precursors in these models and their distribution in gasoline and diesel exhaust. Aromatics with single or multiple rings have rightfully received considerable attention historically, but their distribution between gasoline and diesel emissions has been relatively unexplored. Gasoline exhaust dominates emissions of C₇ and C₈ aromatics. C₉ aromatic content is 4 times greater in gasoline than diesel and there are nearly equivalent amounts of C₁₀ aromatics. For an urban region with 15% diesel fuel use, this implies that gasoline emits over 90% of the C₉ aromatics and 75% of the C₁₀ aromatics. Gasoline SOA from C₉ and C₁₀ aromatics represent 26% and 14% of total SOA from gasoline, respectively, and C₉₋₁₁ aromatics represent 5% of SOA from diesel exhaust (Table 4.1). Emissions of naphthalene and similar small Polycyclic Aromatic Hydrocarbons (PAHs) are shared by both gasoline and diesel vehicles, but represent only a minor contribution to potential SOA formation due to their minor weight fractions in the fuels (Figure 4.2, Tables 4.10-4.11).

We examined the compounds included in SOA models and found that 20-30% of the SOA formed from gasoline exhaust was not included in recent urban studies (9, 21-23). Given the contributions of C₉₋₁₁ aromatics to SOA formation from gasoline and diesel vehicles, it is important that they are better represented in either explicit traditional SOA models or the

extension of volatility basis set modeling to include the 10^7 and 10^8 $\mu\text{g m}^{-3}$ C° bins that fall in the VOC range (Figure 4.11) (5, 9, 20, 22). For recent urban studies, scaling up traditional compound-explicit SOA models (without the volatility basis set) to include the missing 20-30% of gasoline SOA and contributions from diesel (assuming 15% diesel fuel use) produces a 5x increase in modeled SOA from vehicular exhaust. Such an inclusion dramatically improves model closure which has typically underestimated SOA in urban regions by 80-90% (20), but additional contributions from other sources of SOA precursors remain critical to model all observed SOA. Further chamber and modeling studies on SOA yields of aromatics with 9 or more carbon atoms are important to reduce uncertainties in the SOA-forming potential of gasoline and diesel exhaust emissions and their overall contribution to SOA in urban regions. Additional studies on the SOA yields of cyclic alkanes with 5- and 6-membered rings are also of interest since they are unstudied and comprise 37% of diesel and 11% of gasoline fuel.

In 1993, with the goal of mitigating emissions of particulates and nitrogen oxides, California regulated diesel fuel to have less than 10% single-ring aromatics and 1.4% PAHs, but concerns about engine performance and the cost of fuel production led the state to allow higher aromatic levels in diesel fuel (9, 24). It is evident from our data (Table 4.1) that the vast majority of diesel fuels sold in California are certified alternative formulations that contain nearly double the aromatic content than initial regulations intended. While the fuel regulations were designed to help control primary particulate emissions (i.e. black carbon), this enhancement of aromatic content in diesel fuel increases the SOA potential of diesel emissions, especially for hydrocarbons with 9 to 17 carbon atoms. Significant progress is being made to improve heavy-duty diesel engine performance with post-combustion control technology, and may affect emissions of gas-phase organic carbon, but it is clear that attention to both gasoline and diesel fuel composition and emissions of reactive organic gases is necessary to control SOA precursor contributions from all vehicle classes. Furthermore, this work has focused on organic carbon emissions originating from fuels, but emissions of unburned motor oil from both gasoline and diesel vehicles represent an additional source of organic carbon. While total consumption of oil is minor relative to fuel, oil contributes gas and particle-phase compounds with lower volatilities than diesel fuel and should continue to be monitored in field, laboratory, and modeling studies.

Comparing observed concentrations of OA to carbon monoxide (CO) is a popular method for assessing the formation and behavior of SOA in the atmosphere (6, 21, 25-26, 31-34). Using derived SOA yields and emission factors for reactive gas-phase organic carbon and CO, we predict $\Delta\text{OA}/\Delta\text{CO}$ ratios for a mixture of gasoline and diesel fuel use for comparison to our observations in the San Joaquin Valley (Bakersfield) and other urban studies over the past decade (Figure 4.4) (9). Predicted $\Delta\text{OA}/\Delta\text{CO}$ slopes for a range of typical fuel use are consistent with observed $\Delta\text{OA}/\Delta\text{CO}$ values in Los Angeles, Tokyo, and Mexico City after initial SOA formation occurring in the first 6 hours of processing (Figure 4.4A) (6, 25-26). We predict “young” $\Delta\text{OA}/\Delta\text{CO}$ ratios well, but as air masses develop from a relatively young photochemical age of ~ 6 hours to ~ 1 day, $\Delta\text{OA}/\Delta\text{CO}$ ratios increase. A 3-4x increase was observed in Mexico City, and the effect of increased processing can also be observed in Tokyo, where $\Delta\text{OA}/\Delta\text{CO}$ slopes for multiple seasons depict a clear seasonal trend with the greatest slope occurring in the summer for processed air parcels while less-processed parcels remain consistent with expected ratios for a mix of gasoline and diesel emissions (20, 25-26).

In the San Joaquin Valley, the increase in $\Delta\text{OA}/\Delta\text{CO}$ ratios appears to be coincident with the transition of young semi-volatile aerosols to more aged aerosols with lower volatility as shown by the increase in O:C ratios that peaks with $\Delta\text{OA}/\Delta\text{CO}$ ratios in the afternoon (Figure

4.4) (3, 20, 26). Similarly, a greater fraction of low-volatility organic aerosol was observed in the summertime in Tokyo (3). Aged $\Delta\text{OA}/\Delta\text{CO}$ ratios exceed our predictions despite our ability to predict overall observed vehicular OA concentrations. This suggests that the comprehension of all OA transformation processes is incomplete and further work remains to understand the development of low-volatility OA observed in urban plumes globally, a conclusion supported by recent observations and consideration of other mechanisms. (3, 28-30).

Examining differences between weekdays and weekends is another common and insightful metric for assessing emissions and chemical processes. We observed no weekday/weekend difference in the distribution of emissions between gasoline and diesel exhaust in Bakersfield as daytime values of both decreased by ~40% over the weekend (Figure 4.12). Yet, weekend OA concentrations (total and vehicular) were greater due to increased photochemical aging evidenced by higher $\Delta\text{OA}/\Delta\text{CO}$ ratios (Figures 4.4C, 4.13). Recent work focused on Los Angeles reported that gasoline is vastly more important than diesel as a source of SOA precursors based on the observation that weekend $\Delta\text{OA}/\Delta\text{CO}$ slopes were marginally similar to weekday slopes with similar photochemical ages despite large differences in diesel activity (6). Similar to Los Angeles, OA concentrations and $\Delta\text{OA}/\Delta\text{CO}$ ratios are higher in Bakersfield over the weekend, but occurs despite no change in the relative use of gasoline and diesel, suggesting that increased OA at both locations over the weekend is a function of decreased diesel NO_x emissions leading to faster photochemical processing and is independent of changes in the mix of fuel use (27). The ubiquitous increase in $\Delta\text{OA}/\Delta\text{CO}$ ratios with increased processing for both vehicular and total OA is independent of the mixture of gasoline and diesel, and $\Delta\text{OA}/\Delta\text{CO}$ slopes alone are insufficient to discern organic SOA precursor contributions from gasoline vs. diesel given the variability in Los Angeles measurements (Figure 4.14) (6, 9).

Non-vehicular anthropogenic and biogenic sources also lead to elevated $\Delta\text{OA}/\Delta\text{CO}$ ratios with higher slopes occurring in regions with large non-vehicular sources, such as Mexico City, the Southeast U.S., and the Po Valley (Figure 4.4B). $\Delta\text{OA}/\Delta\text{CO}$ ratios in the San Joaquin Valley span a broad range of values observed at other sites and the importance of other SOA sources is supported by elevated $\Delta\text{OA}/\Delta\text{CO}$ ratios in aged air masses and episodic contributions of low O:C OA from other sources (Figures 4.4B, 4.15) (6, 9, 21, 25-26, 31-33).

Our expanded measurement capabilities for gasoline and diesel compounds in both the liquid fuels and the ambient atmosphere produce a more complete picture of SOA formation from motor vehicles. We provide the ability to predict emissions of SOA precursors and SOA formation that is consistent with fuel use data and ambient measurements. SOA from diesel sources outweighs gasoline contributions, and other sources provide significant precursors in many urban regions. The inclusion of our insights will allow for the development of more effective pollution control policies and inform the design of future studies in the ambient atmosphere, laboratory experiments, and modeling efforts.

3. Supporting materials and methods

3.1 Supporting in situ measurements

An extensive suite of instrumentation was deployed to both field studies to characterize gas and particle species. In the Caldecott tunnel, Black Carbon (BC), carbon monoxide (CO), and carbon dioxide (CO_2) were measured at inlets co-located with gas-phase organic sampling. After passing through a 2.5 μm cyclone (URG Corporation, model 2000-30EN), BC was measured using an aethalometer (McGee Sci. model AE-16) and post-processed as described elsewhere (37). CO and CO_2 were measured via an infrared spectrometer (TECO Inc. Model 48)

and non-dispersive infrared absorption (LI-COR, Lincoln, NE; model LI-820), respectively, with twice daily zero and calibration checks. Uncertainties are estimated to be ± 3 and 2%, respectively. Raw data was recorded at high-time resolution, but was averaged for this analysis to 30-min periods coincident with the VOC measurements.

At CalNex-Bakersfield, aerosol measurements were made using an Aerosol Mass Spectrometer (AMS) and Fourier Transform Infrared spectroscopy (FTIR) analysis of filters to assess $PM_{1.0}$ and $PM_{2.5}$ concentrations and composition; methods have been described elsewhere (19). Carbon monoxide was measured from the top of the tower using a gas filter correlation infrared spectrometer (Teledyne, API M300EU2). Comparisons of Organic Aerosol (OA) to CO were done at 5-min time resolution with a $PM_{1.0}$ cutpoint. Vehicular OA, as presented in the paper, was determined as the sum of the 4 vehicular aerosol factors from the positive matrix factorization analysis of the AMS data: low O:C alkane, low O:C aromatic, high O:C alkane, and high O:C aromatic (19).

3.2 Fuel characterization

Forty samples of regular and premium grade gasoline, and twelve samples of diesel fuel were collected from service stations during summer 2010 (coincident with the field studies) in 4 California locations (Bakersfield, Pasadena, Sacramento, and Berkeley). Gasoline samples were analyzed at Chevron laboratories (Richmond, CA) by gas chromatography with dual flame ionization detectors. Additional analyses were performed to resolve co-eluting peaks. Over 400 compounds were quantified in the fuel samples via this method. Compositional averages for the state and each location were calculated assuming a 80:20 regular to premium usage.

To characterize the full range of compounds in diesel fuel, samples were analyzed by 2 methods. Samples were analyzed via direct injection on a traditional 1-dimensional gas chromatograph (HP 5890 Series II) with a quadrapole mass selective detector (HP 5971) on a DB-624 column ($60\text{ m} \times 0.32\text{ mm} \times 1.8\text{ }\mu\text{m}$). Where available, liquid standards were used to calibrate traditionally-characterized components. Nine of the twelve diesel fuel samples were additionally run on a Rxi-5Sil MS column ($60\text{ m} \times 0.25\text{ mm} \times 0.5\text{ }\mu\text{m}$; Restek) coupled to a time-of-flight mass spectrometer (TOFMS; HTOF model, Tofwerk) with a custom modification to allow single-photon ionization. Effluent from the column was ionized using 10.5 eV vacuum-ultraviolet photons generated by synchrotron radiation at the Chemical Dynamics Beamline of the Advanced Light Source (ALS) at Lawrence Berkeley National Lab. Analysis of this data was performed following methods described previously (15), with improved quantification owing to the use of a more extensive suite of structurally-relevant standards.

Vapor-liquid equilibrium calculations were performed for each liquid gasoline sample to predict gasoline vapor composition, which were then averaged statewide and at each location using the same methodology as the liquid fuel. A detailed description of the non-ideal solution equilibrium calculations for gasoline has been published previously (14, 38). Uncertainties presented with all fuel data in this work have been propagated to reflect all variability in fuel samples.

3.3 Comparison of fuels to ambient and tunnel measurements

In order to compare expected versus measured source profiles for gas-phase organics, we compare gasoline and diesel fuel to both tunnel and ambient VOC/IVOC measurements. Isooctane and *n*-dodecane are selected as tracers for gasoline and diesel exhaust, respectively. Isooctane represents a good tracer for gasoline exhaust since it is a trimethylpentane that is

intentionally produced during the refining process and added to gasoline to comprise 3.6 ± 0.3 wt% of California gasoline (Summer 2010). Additionally, it will only be present as a minor component of evaporative gasoline emissions and diesel exhaust. *n*-dodecane represents a good tracer for diesel exhaust since it is prevalent in diesel fuel and will be emitted only as a non-combusted hydrocarbon, while it makes up only 0.01% of gasoline fuel and diesel emissions will greatly exceed any other minor urban VOC source of *n*-dodecane. From the fuels, expected ratios to tracers are derived by dividing the concentration (i.e. mol%) of a given compound by that of either isooctane or *n*-dodecane. For the tunnel and ambient data we performed linear regressions using a trust-region Levenberg-Marquardt least orthogonal distance method to account for uncertainties in both the compound measurements.

3.4 Emission factor calculations

Emission factors for non-combusted gas-phase organic carbon (expressed as GPOC in equations) were calculated using the modeling results and supporting in-situ measurements from the Caldecott tunnel study. The gasoline emission factor was first calculated by taking the average of hourly emission factors (the source contribution ($SC_{t, \text{gasoline}}$) over total carbon ($\Delta Total C_t$)) during the weekend when diesel traffic and contributions to total carbon were negligible, similar to previous studies (12). Uncertainty is determined from the standard deviation of the emission factor.

$$EF_{GPOC, \text{gasoline exhaust}} = \frac{1}{N} \sum_{t=0}^N \left[\frac{SC_{t, \text{gasoline}}}{\Delta Total C_t} \right] f_{c, \text{gasoline}} d_{\text{gasoline}} \quad (S1)$$

$$\Delta Total C_t = [CO_2]_{t, \text{tunnel}} + [CO]_{t, \text{tunnel}} - [CO_2]_{t, \text{ambient}} - [CO]_{t, \text{ambient}} \quad (S2)$$

where:

$$SC_{t, \text{gasoline}} [=] \text{gC GPOC m}^{-3} (@25^\circ\text{C})$$

$$\Delta Total C_t \text{ and concentrations } [=] \text{kgC m}^{-3}$$

N : number of samples

$f_{c, \text{gasoline}}$: carbon fraction of gasoline

d_{gasoline} : liquid density of gasoline (@25°C)

Assumption: $SC_{t, \text{gasoline}, \text{tunnel}} \gg SC_{t, \text{gasoline}, \text{ambient}}$

The results of this method were compared to a regression method where the slope of the source contribution vs. total carbon is used to calculate the emission factor and the uncertainty is determined from the standard deviation of the slope.

$$EF_{GPOC, \text{gasoline exhaust}} = \left[\frac{SC_{t, \text{gasoline}}}{Total C_t} \right]_{\text{slope}} f_{c, \text{gasoline}} d_{\text{gasoline}} \quad (S3)$$

The diesel emission factor is calculated similarly, but since the total carbon signal is dominated by gasoline in the tunnel, Black Carbon (BC) is used in its place since BC is largely from diesel. To correct for BC contributions from gasoline, BC measurements are adjusted to

isolate the diesel signature using the gasoline source contribution and emission factors for non-combusted gas-phase organic carbon and BC from gasoline derived in this work and elsewhere (37). Data from weekdays and weekends are used in the regression.

$$EF_{GPOC,diesel\ exhaust} = \left[\frac{SC_{t,diesel}}{BC_{t,diesel}} \right]_{slope} EF_{BC,diesel\ exhaust} d_{diesel} \quad (S4)$$

$$BC_{t,diesel} = BC_{t,observed} - \frac{SC_{t,gasoline} EF_{BC,gasoline\ exhaust}}{EF_{GPOC,gasoline\ exhaust}} \quad (S5)$$

where:

$$EF_{BC,gasoline} = 0.020 \pm 0.003 \text{ gBC kg}^{-1} \quad (\text{Caldecott Tunnel Study})$$

$$EF_{BC,diesel} = 0.54 \pm 0.07 \text{ gBC kg}^{-1} \quad (\text{Dallmann et al. (37)})$$

Emission factors are compared to those from the California emission factor model (EMFAC2011); determined from statewide summer 2010 data for running emissions and weighted for all vehicle models using vehicle miles traveled (VMT) (18). The resulting emission factor is in gC GPOC L⁻¹ and must be multiplied by ~0.73 to compare to the derived emission factors for non-combusted gas-phase organic carbon as 27% of reactive organic gas (ROG) emissions from gasoline are products of incomplete combustion (12). The exact ratio of products of incomplete combustion to total ROG emissions will vary depending on fuel type, oxygenate level and driving conditions. The value presented here is intended to check consistency with outside measurements and is not used in any of our calculations.

$$EF_{GPOC,gasoline} = \frac{\frac{\Sigma[EF_{ROG,vehicle\ type} VMT_{vehicle\ type}] f_{c,gasoline} d_{gasoline}}{\Sigma[VMT_{vehicle\ type}]}}{\frac{\Sigma[(EF_{CO,vehicle\ type} \frac{MW_C}{MW_{CO}} + EF_{CO_2,vehicle\ type} \frac{MW_C}{MW_{CO_2}}) VMT_{vehicle\ type}]}{\Sigma[VMT_{vehicle\ type}]}} \quad (S6)$$

$$EF_{CO,gasoline} = \frac{\frac{\Sigma[EF_{CO,vehicle\ type} VMT_{vehicle\ type}] f_{c,gasoline} d_{gasoline}}{\Sigma[VMT_{vehicle\ type}]}}{\frac{\Sigma[(EF_{CO,vehicle\ type} \frac{MW_C}{MW_{CO}} + EF_{CO_2,vehicle\ type} \frac{MW_C}{MW_{CO_2}}) VMT_{vehicle\ type}]}{\Sigma[VMT_{vehicle\ type}]}} \quad (S7)$$

Calculations to determine diesel emission factors for gas-phase organic carbon and CO are the same as for gasoline while using the diesel fuel properties.

3.5 Secondary organic aerosol yield determination methodology and associated calculations

To determine overall SOA yields for each source and the distribution of SOA formation from each source across molecular sizes and chemical classes, we first determined the distribution of mass in each source's emissions and organized it into 25 x 8 matrices ($W_{ij,source}$). The rows of the matrix represent carbon number (i) and the columns, chemical class (j) as shown in Tables 4.6-4.8. With the objective of determining average high-NO_x yields for the subset of isomers in each point in this matrix, we determined which values were well-known in the literature from chamber or modeling data, and which had insufficient data.

For all compounds, high-NO_x SOA yields for known and estimated compounds are calculated or modeled assuming an average organic particle concentration of 10 μg m⁻³. This organic particle loading was used as a value relevant to chamber studies, urban areas, and downwind urban areas. As the organic loading decreases the yields of IVOCs will also decrease slightly due to changes in partitioning of the reaction products. Straight and branched alkanes were considered to have known yields. Yields for *n*-alkanes were calculated using the model reported by Jordan *et al.* (39) and the product yields provided therein. The volatilities of those reaction products are assumed to decrease by a multiplicative factor of 0.35 per carbon number (41). Yields for branched alkanes were calculated using the same model assuming an average 30% alkoxy radical decomposition (42), yielding a product with the volatility of a ketone with 3/4 of the original carbon atoms. For all compounds, volatility was calculated using SIMPOL as described by Pankow *et al.* (43). We assumed branched aliphatic compounds have volatilities similar to an *n*-alkane with similar gas chromatographic retention times, which is a reasonable proxy for volatility within a compound class (44, 45). Modeled SOA yields for straight-chain and branched alkanes are shown in Table 4.9.

Estimates for SOA yields of other compound classes (straight-chain cycloalkanes (e.g. decylcyclohexane), branched cycloalkanes, bicycloalkanes, tricycloalkanes, aromatics, and PAHs) were estimated via a Monte Carlo analysis (discussed below) by combining various scenarios constrained by literature and model data. All unknown compounds are treated as branched. For all compound classes, one possible scenario posits an SOA yield of the *n*-alkane of a similar volatility, similar to the use of a volatility basis set model using *n*-alkanes as surrogate compounds, such as the analysis of Mexico City aerosol performed by Lee-Taylor *et al.* (45). Similarly, branched alkanes can be expected to be a reasonable surrogate for all branched aliphatic compounds, providing an alternate scenario. Furthermore, several additional schemes are available for estimating yields of cyclic aliphatic compounds based on the small amount of laboratory data available on cyclic alkanes (42). Most of these scenarios provide similar estimated SOA yields.

Small aromatic compounds are somewhat better constrained by laboratory data, though data for larger aromatics and PAHs are scarce. Small aromatics (C₆ through C₈) are assumed to be known and have the yields of benzene, toluene, and *m*-xylene found in the literature (47, 48). C₉ and larger aromatics can be estimated using extrapolations of the two-product models of toluene and *m*-xylene, assuming the products decrease in volatility using the carbon number multiplicative factor described above. These models provide conservative estimates as the yield for even the largest aromatics does not exceed 0.17 using these models. The literature model for naphthalene (49) provides yields closer to those expected based on volatility, so is used as an estimate for aromatics and PAHs. Alternate PAH scenarios assume C₁₀ - C₁₂ PAHs to have SOA yields of naphthalene, methylnaphthalene, and dimethylnaphthalene, based on literature values (49). Yields for larger PAHs are based on the extrapolation of these models. Extrapolations of models provide conservative upper and lower bounds for the least volatile aromatic compounds: 0.10 to 1.28 for C₁₉-C₂₅ aromatics, 0.31 to 1.28 for C₁₉-C₂₅ PAHs.

The Monte Carlo estimation does not give preference to any of the scenarios. For clarity, we provide a summary of the scenarios used to model unknown yields. Scenarios 3-6 for the cycloalkanes and scenarios 3-4 for the multi-ring cycloalkanes are based on laboratory data for three measured cyclohexanes (42).

Cycloalkanes:

- 1) Yields of *n*-alkanes of similar volatility (39)
- 2) Yields of branched alkanes of similar volatility
- 3) Yields of branched alkanes with 2 more carbon atoms
- 4) Yields of branched alkanes with 1 less carbon atom
- 5) C₅₋₁₀ have yields of branched alkanes with 2 more carbon atoms, while C₁₆ and larger have yields with 1 less carbon atom. Yields for C₁₁₋₁₅ are interpolated
- 6) Yields extrapolated from C₆ (branched alkane with 2 more carbon atoms) and C₁₆ (branched alkane with 1 less carbon atom)

Bicycloalkanes & Tricycloalkanes:

- 1) Yields of *n*-alkanes of similar volatility (39)
- 2) Yields of branched alkanes of similar volatility
- 3) C₅₋₁₀ have yields of branched alkanes with 2 more carbon atoms, while C₁₆ and larger have yields with 1 less carbon atom. Yields for C₁₁₋₁₅ are interpolated
- 4) Yields extrapolated from C₆ (branched alkane with 2 more carbon atoms) and C₁₆ (branched alkane with 1 less carbon atom)

Aromatics (C₉ and larger):

- 1) Yields of *n*-alkanes of similar volatility (39)
- 2) Yields extrapolated from toluene two-product model (47)
- 3) All yields are 0.10 based on Chan *et al.* (49)
- 4) Yields extrapolated from naphthalene two-product model (49)

PAHs:

- 1) Yields of *n*-alkanes of similar volatility (39)
- 2) Yields extrapolated from naphthalene two-product model (49)
- 3) Yields for C₁₂ and larger extrapolated from methyl naphthalene two-product model with C₁₀₋₁₁ having known yields (49)
- 4) Yields for C₁₂ and larger assumed to be that of dimethylnaphthalene with C₁₀₋₁₁ having known yields (49)

We performed a Monte Carlo analysis to determine both bulk yields for each source and the distribution of those yields in each source to determine the most important compounds for SOA formation. If the yield for a given carbon number and chemical class point in the matrix was well-known, then the known yield did not change and no uncertainty is reported (Table 4.9). For unknown or understudied yields, for each iteration we randomly selected a scenario (*k*) from the constructed scenarios and added up to ±10% Gaussian-distributed noise (represented as $Y_{estimate,ijk} * gnoise(0.1)$ in Equation S8). Each iteration of known and randomly selected unknown yield values (Y'_{ij}) is multiplied by the known and constant weight percent matrix from each source ($W_{ij,source}$). The average of 10,000 iterations provides the distribution of SOA formation across each source ($Y_{ij,source}$) weighted by the chemical composition of the source. Uncertainties for all points in the matrices ($\sigma_{Y_{ij,source}}$) are determined by assessing the deviation of values across the 10,000 simulations (M=10000).

$$Y'_{ij} = \begin{cases} Y_{known,ij}, & \text{if known value exists} \\ Y_{estimate,ijk} + Y_{estimate,ijk} * gnoise(0.1), & \text{if no known value exists} \end{cases} \quad (S8)$$

where *k* is selected by a random number generator

$$Y_{ij,source} = \frac{1}{M} \sum^M [W_{ij,source} * Y'_{ij}] \frac{1}{100} \quad (S9)$$

$$\sigma_{ij,Y_{source}} = \sqrt{\frac{1}{M} (\sum^M [Y_{ij,source}^2] - M \bar{Y}_{ij,source}^2)} \quad (S10)$$

The bulk SOA yield for a source (y_{source}) is calculated by summing the distribution of SOA yields from the entire matrix to provide a value that can be multiplied by total non-combusted organic carbon from a source to determine the predicted SOA. The uncertainty of the bulk yield value ($\sigma_{y,source}$) is determined by assessing the deviation of all values in the simulations and is shown in Figure 4.10.

$$y_{source} = \sum_i \sum_j Y_{ij,source} \quad (S11)$$

$$\sigma_{y_{source}} = \sum_i \sum_j \sqrt{\frac{1}{M} (\sum^M [y_{source}^2] - M \bar{y}_{source}^2)} \quad (S12)$$

Uncertainties presented in Table 4.1 and throughout the analyses have been propagated to reflect all uncertainties associated with the calculation and comparison of values.

The estimation of expected total SOA from gasoline and diesel presented in the paper ($1.3 \pm 0.4 \mu\text{gOA m}^{-3}$) for comparison to AMS data was calculated by taking the daytime (8:00-19:30 PST) average of source contributions from gasoline and diesel (13.5 ± 9.3 and 9.8 ± 7.1 ppbC, respectively (N=270)) and determining the predicted SOA from both using the derived bulk SOA yields. Our CMB modeling method allows us to assess emissions from gasoline and diesel sources within several hours of transport to the site, and compare them to SOA production from a slightly larger scale of regional emissions and photochemistry as measured by the AMS. While, this does not act as a direct comparison since the observed SOA by the AMS is somewhat decoupled from the fresh emissions used to calculate the expected SOA, it does provide supporting evidence for the consistency of our calculations with observations. There were no significant multi-day OA events with accumulation of precursors or aerosol since concentrations decreased substantially on a daily basis due to meteorology. Dry-deposition of $\text{PM}_{1.0}$ OA would not have been a significant loss process, nor would coagulation of particles given particle number concentrations.

In the paper we examine the inclusion of SOA formation from gasoline in several traditional SOA modeling studies (MILAGRO, TORCH, NEAQS) and find that 20% of the SOA from gasoline is missing in the compound explicit models used at the TORCH and NEAQS campaigns, and 30% at the MILAGRO/MCMA studies (21-23). This was determined using the published list of compounds included in their models with our average liquid gasoline profile and determined SOA yields shown in Tables 4.7 and 4.9.

3.6 Calculation of $\Delta\text{OA}/\Delta\text{CO}$ slopes

For the purposes of comparison to a broad set of urban studies, we estimate $\Delta\text{OA}/\Delta\text{CO}$ slopes using derived bulk SOA yields and emission factors for non-combusted gas-phase organic carbon and CO:

$$\left[\frac{\Delta\text{OA}}{\Delta\text{CO}} \right]_{\text{Predicted}} = \left[\frac{\Delta\text{POA}}{\Delta\text{CO}} \right] + \frac{y_{\text{gasoline}} EF_{\text{GPOC,gasoline}} V_{\text{gasoline}} + y_{\text{diesel}} EF_{\text{GPOC,diesel}} V_{\text{diesel}}}{EF_{\text{CO,gasoline}} V_{\text{gasoline}} + EF_{\text{CO,diesel}} V_{\text{diesel}}} \quad (S13)$$

where $V_{gasoline}$ and V_{diesel} are the fraction of gasoline and diesel sold by volume and:

$$V_{gasoline} + V_{diesel} = 1 \quad (S14)$$

The emission factors for non-combusted gas-phase organic carbon and CO were:

$$EF_{VOC,gasoline} = 0.45 \text{ gGPOC } L^{-1} \quad (\text{from this work, consistent with EMFAC2011 (18)})$$

$$EF_{VOC,diesel} = 1.01 \text{ gGPOC } L^{-1} \quad (\text{from this work, consistent with EMFAC2011 (18)})$$

$$EF_{CO,gasoline} = 12750 \text{ ppmv } L^{-1} \quad (\text{from EMFAC2011 (18)})$$

$$EF_{CO,diesel} = 3890 \text{ ppmv } L^{-1} \quad (\text{from EMFAC2011 (18)})$$

The $[\Delta POA/\Delta CO]$ constant is the average observed slope reported previously ($9.4 \mu\text{g m}^{-3} \text{ ppmv}^{-1} \text{ CO}$) and is similar for most urban studies (21, 34).

Additional derivations of the OA/ Δ CO equation that include non-tailpipe gasoline VOC emissions with no associated CO emissions have a negligible effect on predicted Δ OA/ Δ CO values. Similarly, including cold start emissions, which has a slightly different Δ OA/ Δ CO ratio than the running emission factors used (i.e. more CO in cold start emissions), does not have a substantial effect on the predicted ratio. Therefore, the simplified version (Equation S13) was used to calculate Δ OA/ Δ CO ratios.

4. Supporting results

4.1 Characterization of gasoline and diesel fuel

We present the most comprehensive chemical speciation of diesel fuel to date with over 90% mass closure as part of an overall assessment of gasoline and diesel fuel. In this work, we supply unprecedented detail on both the overall mass and chemical distribution of both fuels and in-depth compound specific speciation data for use in future analyses and models such as those presented in this work. Composition data for hundreds of individual hydrocarbons in both fuels is shown in Tables 4.1-4.12 with average values for the state of California and site-specific data for the 4 regions from which fuel was collected. Ten gasoline samples and three diesel samples were analyzed for each location and standard deviations represent the variability between fuel samples. Gasoline, with 10 wt% ethanol additive, had an average density of $740 \pm 7 \text{ g } L^{-1}$, and a carbon fraction of 0.824. Diesel fuel had an average density of $852 \pm 10 \text{ g } L^{-1}$ and a carbon fraction of 0.866. Gasoline composition was relatively homogeneous across the state in terms of mass distribution and percentages of chemical classes with minor differences in concentrations of individual compounds. Diesel fuel showed some heterogeneity with a few samples being slightly shifted in mass distribution. Overall, the composition was similar, but not as homogeneous as gasoline likely due to differences in regulations between gasoline and diesel fuel. The standard deviations in Tables 4.1 and 4.3 reflect this variability. Future work with the supplied data must recognize that both regional and seasonal differences in fuel can significantly affect the ratios of specific compounds and caution should be taken when extrapolating detailed data outside of the timeframe and locations presented here.

The volatility basis set defines VOCs as compounds with saturation concentrations (C°) $> 10^6 \mu\text{g m}^{-3}$, IVOCs as $C^{\circ} = 10^3\text{-}10^6 \mu\text{g m}^{-3}$, and a third class Semi-Volatile Organic Compounds (SVOCs) as $C^{\circ} = 1\text{-}100 \mu\text{g m}^{-3}$ (5). A small fraction (~5%) of diesel fuel extends into the SVOC

range (Figure 4.11). For the purposes of comparison to *a priori* information used in SOA models to represent diesel POA, IVOCs, and SVOCs, we present the composition of diesel fuel in terms of the volatility basis set used in many SOA models (Figure 4.11) (5, 20-22).

Following the U.S. Clean Air Act of 1990, gasoline composition was reformulated numerous times over the following 2 decades. Currently, California reformulated gasoline, similar to U.S. reformulated gasoline, is regulated to contain less than 25% aromatics and 6% alkenes (by volume) largely due to their ozone formation potential (24). Across our 4 locations we measured a range of 24-29 wt% aromatics and 2-5 wt% olefins. During the summer, vapor pressure is also regulated to reduce non-tailpipe evaporative emissions. All of California is required to use reformulated gasoline and most U.S. regions that fail to meet air quality standards are required to use U.S. reformulated gasoline. Across the whole U.S., about a third of the gasoline sold is reformulated (10). Conventional gasoline, compared to reformulated gasoline can contain greater amounts of aromatics and olefins, which are likely to increase its reactivity and SOA formation potential (2).

Diesel fuel has been regulated nationally for sulfur content, but only in California has the organic composition been regulated. Starting in 1993, diesel fuels distributed in California have been regulated to contain less than 10% aromatics by volume and 1.4% PAHs by weight (24). A provision contained within the regulations allows for producers and importers of diesel fuel to sell an alternative diesel formulation if they can prove that emissions from a heavy-duty diesel engine using their fuel are similar or lower for nitrogen oxides, particulate matter, and soluble organic fraction of particulate matter. Such “Certified Diesel Fuel Formulations” contain 15 to 25% aromatics and 2 to 5% PAHs (24).

4.2 CMB analysis results and comparison of emission factors to EMFAC2011

Over a mix of weekdays and weekends, diesel exhaust constituted $24 \pm 14\%$ of gas-phase organic carbon from motor vehicle exhaust emissions at the Caldecott tunnel, and $57 \pm 16\%$ of total exhaust at the Bakersfield supersite in the San Joaquin Valley. Diesel fuel sales data are consistent with model results at both sites when accounting for differences in emission factors since 11% and 33% of on-road fuel use is diesel in the San Francisco bay area and Kern county, respectively (11). It is important to note that off-road use of diesel represents a non-negligible amount of diesel fuel use and will increase total diesel fuel use by a few percent on a state and national level. On-road diesel use is 4-6x greater than off-road on these scales, but county-level data does not exist at this time.

The contributions of non-tailpipe gasoline (i.e. evaporative) emissions were slightly different than previous work showing that non-tailpipe gasoline was responsible for $\sim 30\%$ of gasoline-related VOC emissions in the South Coast Air Basin (14). $17 \pm 9\%$ of gasoline-related emissions were from non-tailpipe sources in the Caldecott tunnel, which is not unexpected since emissions from service stations and resting emissions from vehicles would not play a role in the tunnel environment. In Bakersfield, non-tailpipe gasoline was $38 \pm 20\%$ of emissions from gasoline vehicles—slightly higher than previous work.

In terms of the overall contribution to non-combusted gas-phase organic carbon emissions at Bakersfield, diesel exhaust, gasoline exhaust, and non-tailpipe gasoline comprised $46 \pm 15\%$, $34 \pm 13\%$, and $20 \pm 11\%$ of motor vehicle emissions, respectively. At the Caldecott tunnel, diesel exhaust, gasoline exhaust, and non-tailpipe gasoline comprised $20 \pm 12\%$, $66 \pm 13\%$, and $14 \pm 7\%$ of motor vehicle emissions, respectively.

Atypical of many urban areas, weekday/weekend differences were not strong in Bakersfield with regard to the distribution of emissions between gasoline and diesel exhaust as daytime values of both decreased by ~40% on the weekends (Figure 4.12).

From the tunnel study, emissions of non-combusted gas-phase organic carbon were determined to be $0.38 \pm 0.11 \text{ gC L}^{-1}$ for gasoline exhaust and $0.86 \pm 0.25 \text{ gC L}^{-1}$ for diesel exhaust. Values calculated using California's emissions model for the same period (18) are 0.36 gC L^{-1} and 0.75 gC L^{-1} before adjusting for products of incomplete combustion for gasoline and diesel, respectively. The gasoline emission factor is close to gasoline emission factors calculated by both methods ($0.30 \pm 0.11 \text{ gC L}^{-1}$ using the regression method), but diesel is somewhat different with our value being slightly higher. Differences in gasoline and diesel fleet distribution across varying vehicle classes, ages, and levels of maintenance in the tunnel versus that of EMFAC may be responsible for these differences, as "high-emitters" are sometimes self-selected out of dynamometer testing.

Calculated exhaust emission factors are lower bounds since they do not include products of incomplete combustion or cold start emissions. The calculated values are focused on unburned hydrocarbons, which are considerably more important for SOA formation. While many products of incomplete combustion are highly reactive and important for overall OH reactivity and ozone formation, most of them are not currently expected to form SOA with the exception of larger carbonyls that make up a minor fraction of emissions (12-13). Continued work is necessary to understand their emissions, but for these reasons they are not included in the emission factors derived and used in this study.

The methods applied in this work include the ability to examine emissions and concentrations of individual compounds in addition to overall source contributions. Emission factors for any individual compound in gasoline and/or diesel fuel (or set of compounds) can be estimated by adjusting the reported emission factors for non-combusted gas-phase organic carbon by the compound's compositional fraction in the fuel (e.g. $EF_{\text{n-dodecane,diesel}} = EF_{\text{GPOC,diesel}} * \text{WtC}\%_{\text{n-dodecane,diesel}} / 100$). Similarly, the ambient concentration of any compound can be estimated by multiplying the source contributions (ppbC) by the compound's composition (WtC%) in the sources and summing the terms. Additionally, estimates of SOA from each source can be obtained by multiplying emission factors or calculated emissions by bulk SOA yields.

4.3 $\Delta\text{OA}/\Delta\text{CO}$ ratios

Emissions of SOA precursors are dominated by diesel, whereas CO emissions are dominated by gasoline, so $\Delta\text{OA}/\Delta\text{CO}$ ratios are sensitive to changes in fuel use. In urban areas which have a mixture of diesel and gasoline use, gasoline CO overwhelms the $\Delta\text{OA}/\Delta\text{CO}$ relationship as gasoline mobile sources are responsible for 30x more than diesel (50). In urban regions such as the South Coast Air Basin, 90% of CO emissions are from mobile sources versus 65% statewide (18, 50). The $\Delta\text{OA}/\Delta\text{CO}$ ratio presented for gasoline is an upper bound given the relatively slow reaction rates for benzene and toluene.

Weekday values in Los Angeles were centered on $14 \mu\text{g m}^{-3} \text{ ppmv}^{-1}$ CO and we predict a very similar value of $13 \mu\text{g m}^{-3} \text{ ppmv}^{-1}$ CO for a reported 17% diesel fraction of total fuel use cited in their work. Photochemical ages reported in Los Angeles during the weekend are greater due to faster photochemical processing likely associated with lower NO_x emissions from diesel sources (6, 27). Adjusting observed weekend $\Delta\text{OA}/\Delta\text{CO}$ values from Los Angeles for photochemical aging results in a $\Delta\text{OA}/\Delta\text{CO}$ slope very similar to that expected from a gasoline-dominated fleet (6). Based on previous work, a 3-4x increase in the $\Delta\text{OA}/\Delta\text{CO}$ slope occurs from

photochemical ages of ~6 hours to 1 day at a roughly linear rate (20, 26). Thus, ages of 12 and 24 hours should correspond to increases of 2x and 4x, respectively. Observed weekend ratios ranged from 22 to 70 $\mu\text{g m}^{-3} \text{ppmv}^{-1} \text{CO}$ (Figure 4.14) (6). The corresponding range of photochemical ages shown over the weekend extend from 12 hours to just over 24 hours as determined by toluene/benzene ratios of 2.0 through 1.0 (6, 31). Adjusting the observed $\Delta\text{OA}/\Delta\text{CO}$ values of 22 to 70 $\mu\text{g m}^{-3} \text{ppmv}^{-1} \text{CO}$, by factors of 2 to 4, respectively, produces $\Delta\text{OA}/\Delta\text{CO}$ values around 11 to 17 $\mu\text{g m}^{-3} \text{ppmv}^{-1} \text{CO}$ at ~6 hours of photochemical processing, and does not consider the influence of other sources of SOA precursors. Similarly, in Figure 4.14, we estimate aged weekend $\Delta\text{OA}/\Delta\text{CO}$ values based on a fuel mixture of 5-10% diesel and see general agreement with reported measurements. We contend that $\Delta\text{OA}/\Delta\text{CO}$ slopes alone are not sensitive enough to effectively discern the contributions of gasoline vs. diesel, and given the variability in data from the Los Angeles study, it is difficult to separate the effects of changes in SOA precursor emissions, CO emissions, and increased photochemical processing.

Non-vehicular anthropogenic and biogenic sources contribute SOA precursors without CO and will vary depending on the characteristics of an urban region as shown by enhanced $\Delta\text{OA}/\Delta\text{CO}$ slopes in Mexico City, the Southeast U.S., and the Po Valley (despite outlier filtering for major non-vehicular events in some studies) (26, 31-33).

Our derived SOA yields are intended to model the first several generations of photochemical oxidation, which corresponds to the extent of oxidation effectively constrained by experimental measurements. It is highly plausible that the continued increase in $\Delta\text{OA}/\Delta\text{CO}$ ratios beyond our predictions is caused by the continued oxidation of multi-generation oxidation products in the gas-phase. In this study, we have refrained from estimating SOA yields for these highly-aged air masses as doing so would require excessive extrapolation with high uncertainties. A re-evaluation of gasoline and diesel SOA yields is encouraged once these data become available.

References and Notes

- 1 M. Hallquist *et al.*, The formation, properties and impact of secondary organic aerosol: current and emerging issues. *Atmos. Chem. Phys.* **9**, 5155 (2009).
- 2 U.S. Environmental Protection Agency, *U.S. Clean Air Act (and subsequent amendments/rulings)* (<http://www.epa.gov/air/caa/>)
- 3 J. L. Jimenez *et al.*, Evolution of Organic Aerosols in the Atmosphere. *Science* **326**, 1525 (2009).
- 4 D. R. Worton *et al.*, Embracing Complexity: Deciphering Origins and Transformations of Atmospheric Organics through Speciated Measurements (Viewpoint). *Environ. Sci. Technol.* **46**, 5265 (2012).
- 5 A. L. Robinson *et al.*, Rethinking organic aerosols: Semivolatile emissions and photochemical aging. *Science* **315**, 1259 (2007).
- 6 R. Bahreini *et al.*, Gasoline emissions dominate over diesel in formation of secondary organic aerosol mass. *Geophys. Res. Lett.* **39**, L06805 (2012).
- 7 E. A. Weitkamp *et al.*, Laboratory Measurements of the Heterogeneous Oxidation of Condensed-Phase Organic Molecular Markers for Motor Vehicle Exhaust. *Environ. Sci. Technol.* **42**, 7950 (2008).
- 8 H. O. T. Pye, G. A. Pouliot, Modeling the Role of Alkanes, Polycyclic Aromatic Hydrocarbons, and Their Oligomers in Secondary Organic Aerosol Formation. *Environ. Sci. Technol.* **46**, 6041 (2012).

- 9 Please see the supplementary material for extensive information on methods, supporting results, figures, and tables giving detailed composition data on gasoline and diesel fuel.
- 10 U.S. Energy Information Administration, *National fuel sales data* (2010 data, http://www.eia.gov/dnav/pet/pet_cons_prim_dcunus_a.htm)
- 11 California Department of Transportation, *California Motor Vehicle Stock Travel, and Fuel Forecast (MVSTAFF) 2008 Report* (<http://www.dot.ca.gov/hq/tsip/smb/documents/mvstaff/mvstaff08.pdf>)
- 12 T. W. Kirchstetter *et al.*, Impact of Oxygenated Gasoline Use on California Light-Duty Vehicle Emissions. *Environ. Sci. Technol.* **30**, 661 (1996).
- 13 J. J. Schauer *et al.*, Measurement of Emissions from Air Pollution Sources. 2. C1 through C30 Organic Compounds from Medium Duty Diesel Trucks. *Environ. Sci. Technol.* **33**, 1578 (1999).
- 14 D. R. Gentner *et al.*, Diurnal and Seasonal Variability of Gasoline-Related Volatile Organic Compound Emissions in Riverside, California. *Environ. Sci. Technol.* **43**, 4247 (2009).
- 15 G. Isaacman *et al.*, Improved resolution of hydrocarbon structures and constitutional isomers in complex mixtures using gas chromatography-vacuum ultraviolet-mass spectrometry. *Anal. Chem.* **84**, 2335 (2012).
- 16 J. G. Watson *et al.*, The effective variance weighting for least squares calculations applied to the mass balance receptor model. *Atmos. Env.* **18**, 1347 (1984).
- 17 W. R. Leppard *et al.*, "Effects of gasoline composition on vehicle engineout and tailpipe hydrocarbon emissions," *SAE Tech. Pap. Ser. No. 920329* (1992).
- 18 California Air Resources Board, *Motor Vehicle Emission Factor/Emission Inventory Model - EMFAC 2011* (<http://www.arb.ca.gov/msei/msei.htm>)
- 19 S. Liu *et al.*, Secondary organic aerosol formation from fossil fuel sources contribute majority of summertime organic mass at Bakersfield. *J. Geophys. Res.* in review.
- 20 A. Hodzic *et al.*, Modeling organic aerosols in a megacity: potential contribution of semi-volatile and intermediate volatility primary organic compounds to secondary organic aerosol formation. *Atmos. Chem. Phys.* **10**, 5491 (2010).
- 21 J. A. de Gouw *et al.*, Sources of particulate matter in the northeastern United States: 1. Direct emissions and secondary formation of organic matter in urban plumes. *J. Geophys. Res.* **113**, D08301 (2008).
- 22 K. Dzepina *et al.*, Modeling the Multiday Evolution and Aging of Secondary Organic Aerosol During MILAGRO 2006. *Environ. Sci. Technol.* **45**, 3496 (2011).
- 23 D. Johnson *et al.*, Simulating regional scale secondary organic aerosol formation during the TORCH 2003 campaign in the southern UK. *Atmos. Chem. Phys.* **6**, 403 (2006).
- 24 California Air Resources Board, *California Diesel Fuel and Reformulated Gasoline Regulations (with subsequent amendments)* (<http://www.arb.ca.gov/fuels/fuels.htm>)
- 25 N. Takegawa *et al.*, Seasonal and diurnal variations of submicron organic aerosol in Tokyo observed using the Aerodyne aerosol mass spectrometer. *J. Geophys. Res.* **111**, D11206 (2006).
- 26 L. I. Kleinman *et al.*, The time evolution of aerosol composition over the Mexico City plateau. *Atmos. Chem. Phys.* **8**, 1559 (2008).
- 27 A. R. Russell *et al.*, Space-based Constraints on Spatial and Temporal Patterns of NO_x Emissions in California, 2005-2008. *Environ. Sci. Technol.* **44**, 3608 (2010).

- 28 C. D. Cappa, K. R. Wilson, Multi-generation gas-phase oxidation, equilibrium partitioning, and the formation and evolution of secondary organic aerosol. *Atmos. Chem. Phys. Discuss.* **12**, 3295 (2012).
- 29 B. Ervens, B. J. Turpin, R. J. Weber, Secondary organic aerosol formation in cloud droplets and aqueous particles (aqSOA): a review of laboratory, field and model studies. *Atmos. Chem. Phys.* **11**, 11069 (2011).
- 30 A. W. Rollins *et al.*, Nighttime growth of particulate organic nitrates: a significant source of atmospheric secondary organic aerosols. *Science* in review.
- 31 R. J. Weber *et al.*, A study of secondary organic aerosol formation in the anthropogenic-influenced southeastern United States. *J. Geophys. Res.* **112**, D13302 (2007).
- 32 P. F. DeCarlo *et al.*, Fast airborne aerosol size and chemistry measurements above Mexico City and Central Mexico during the MILAGRO Campaign. *Atmos. Chem. Phys.* **8**, 4027 (2008).
- 33 J. Crosier *et al.*, Chemical composition of summertime aerosol in the Po Valley (Italy), northern Adriatic and Black Sea. *Q. J. R. Meteorol. Soc.* **113**, 61 (2007).
- 34 J. de Gouw, J. L. Jimenez, Organic aerosols in the Earth's atmosphere. *Environ. Sci. Technol.* **43**, 7614 (2009).
- 35 J. Pollmann, J. Ortega, D. Helmig, Analysis of atmospheric sesquiterpenes: Sampling losses and mitigation of ozone interferences, *Environ. Sci. Technol.*, **39**, 9620 (2005).
- 36 D. B. Millet *et al.*, Atmospheric volatile organic compound measurements during the Pittsburgh Air Quality Study: Results, interpretations, and quantification of primary and secondary contributions. *J. Geophys. Res.* **110**, D07S07 (2005).
- 37 T. R. Dallmann *et al.*, On-Road Measurement of Gas and Particle Phase Pollutant Emission Factors for Individual Heavy-Duty Diesel Trucks. *Environ. Sci. Technol.* in review.
- 38 R. A. Harley, S. C. Coulter-Burke, T. S. Yeung, Relating liquid fuel and headspace vapor composition in California reformulated gasoline samples containing ethanol. *Environ. Sci. Technol.* **34**, 4088 (2000).
- 39 U.S. Environmental Protection Agency, *EPA-CMB8.2* (http://www.epa.gov/scram001/receptor_cmb.htm)
- 40 C. E. Jordan *et al.*, Modeling SOA formation from OH reactions with C8–C17 n-alkanes. *Atmos. Environ.* **42**, 8015 (2008).
- 41 J. H. Kroll, J. H. Seinfeld, Chemistry of secondary organic aerosol: Formation and evolution of low-volatility organics in the atmosphere. *Atmos. Environ.* **42**, 3593 (2008).
- 42 Y. B. Lim, P. J. Ziemann, Effects of molecular structure on aerosol yields from OH radical-initiated reactions of linear, branched, and cyclic alkanes in the presence of NO_x. *Environ. Sci. Technol.* **43**, 2328 (2009).
- 43 J. F. Pankow, W. E. Asher, SIMPOL.1: a simple group contribution method for predicting vapor pressures and enthalpies of vaporization of multifunctional organic compounds. *Atmos. Chem. Phys.*, **8**, 2773 (2008).
- 44 G. Isaacman *et al.*, Understanding evolution of product composition and volatility distribution through in-situ GC × GC analysis: a case study of longifolene ozonolysis. *Atmos. Chem. Phys.*, **11**, 5335 (2011).
- 45 D. A. Hinckley *et al.*, Determination of Vapor Pressures for Nonpolar and Semipolar Organic Compounds from Gas Chromatographic Retention Data. *J. Chem. Eng. Data* **35**, 232 (1990).

- 46 J. Lee-Taylor *et al.*, Explicit modeling of organic chemistry and secondary organic aerosol partitioning for Mexico City and its outflow plume. *Atmos. Chem. Phys.*, **11**, 13219 (2011).
- 47 N. L. Ng *et al.*, Secondary organic aerosol formation from *m*-xylene, toluene, and benzene. *Atmos. Chem. Phys.* **7**, 3909 (2007).
- 48 K. P. Wyche *et al.*, Gas phase precursors to anthropogenic secondary organic aerosol: detailed observations of 1,3,5-trimethylbenzene photooxidation, *Atmos. Chem. Phys.*, **9**, 635 (2009).
- 49 A. W. H. Chan *et al.*, Secondary organic aerosol formation from photooxidation of naphthalene and alkylnaphthalenes: implications for oxidation of intermediate volatility organic compounds (IVOCs). *Atmos. Chem. Phys.* **9**, 3049 (2009).
- 50 California Air Resources Board, *Estimated annual average emissions, 2010*. (<http://www.arb.ca.gov/ei/emsmain/emsmain.htm>).

Figures and Tables

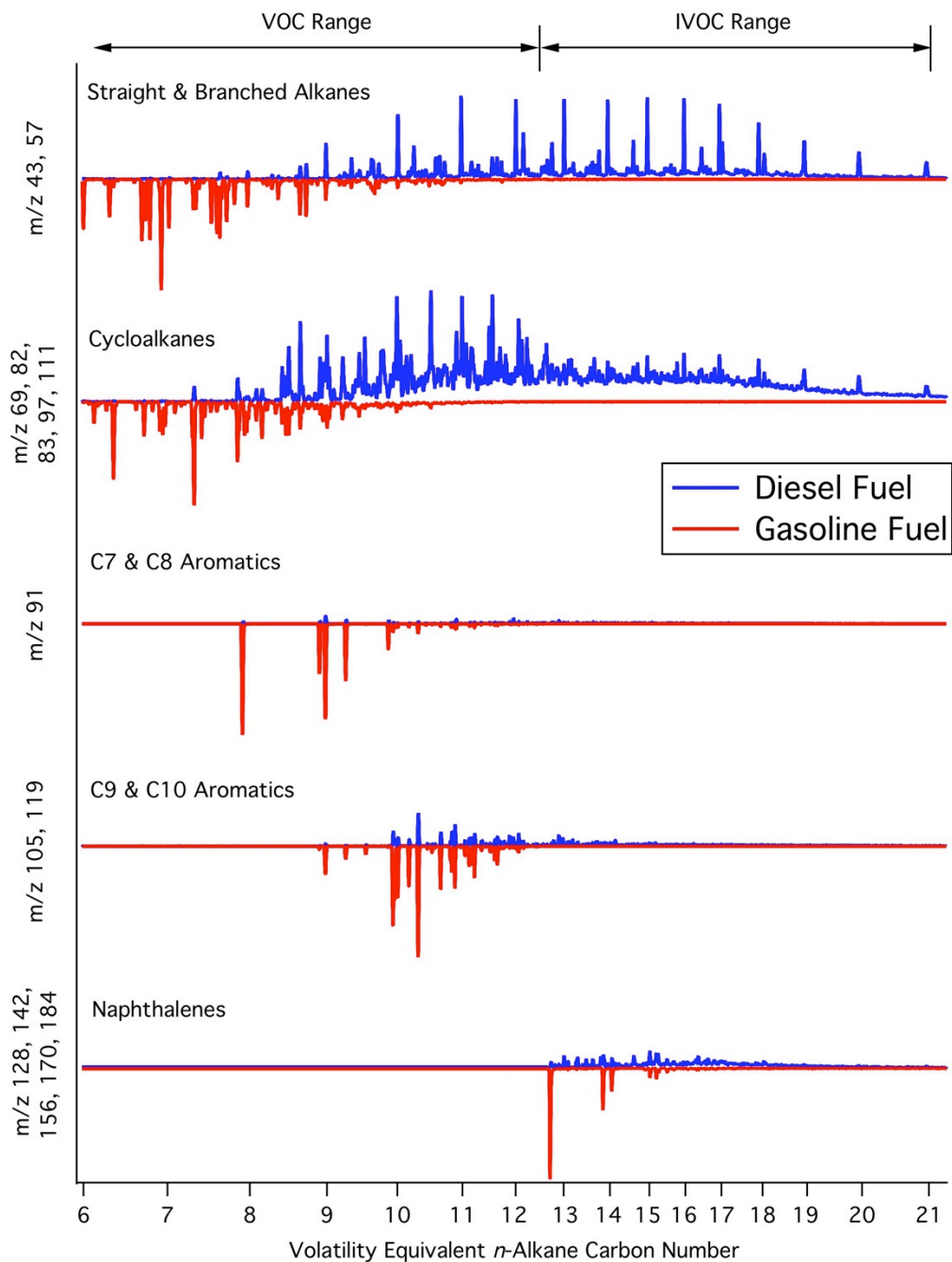


Figure 4.1. Distributions of chemical classes for diesel (blue) and gasoline (red) are distinct with some overlap as shown via gas chromatography/mass spectrometry for representative fuel samples. Fuels span both the VOC and IVOC volatility ranges. Chemical classes are represented by their dominant mass fragments and shown as a function of *n*-alkane carbon number.

Table 4.1. Distribution of mass and SOA potential by chemical class for diesel exhaust, gasoline exhaust, and non-tailpipe gasoline

| Compound Class | Weight Percent by Carbon [WtC%] | | | Potential SOA Formation [Wt% SOA] | | |
|---|--|-------------------------|------------------------------|--|-------------------------|------------------------------|
| | Diesel Exhaust | Gasoline Exhaust | Non-Tailpipe Gasoline | Diesel Exhaust | Gasoline Exhaust | Non-Tailpipe Gasoline |
| Total Aliphatic | 68 ± 8 | 58 ± 2 | 85 ± 4 | 47 ± 4 | 0.38 ± 0.07 | 0.9 ± 0.4 |
| <i>Straight-chain Alkanes</i> | 7 ± 1 | 7.7 ± 0.3 | 20 ± 1 | 11 ± 2 | 0.09 ± 0.003 | 0.02 ± 0.001 |
| <i>Branched Alkanes</i> | 23 ± 2 | 40 ± 1 | 60 ± 3 | 14 ± 2 | 0.12 ± 0.003 | 0.13 ± 0.01 |
| <i>Cycloalkanes (Single Straight Alkyl Chain)</i> | 2.5 ± 0.2 | 4.3 ± 0.1 | 1.03 ± 0.04 | 1.2 ± 0.3 | 0.13 ± 0.07 | 0.7 ± 0.4 |
| <i>Cycloalkanes (Branched or Multiple Alkyl Chain(s))</i> | 18 ± 2 | 6.2 ± 0.3 | 5.0 ± 0.2 | 11 ± 2 | 0.04 ± 0.02 | 0.05 ± 0.03 |
| <i>Bicycloalkanes</i> | 13 ± 1 | 0 | 0 | 6 ± 1 | 0 | 0 |
| <i>Tricycloalkanes</i> | 4.8 ± 0.6 | 0 | 0 | 4 ± 1 | 0 | 0 |
| Single-ring Aromatics | 19 ± 2 | 29 ± 1 | 2.7 ± 0.1 | 36 ± 9 | 96 ± 22 | 99 ± 6 |
| Polycyclic Aromatic Compounds | 4 ± 2 | 0.32 ± 0.02 | 0.0003 | 17 ± 8 | 3.2 ± 0.9 | 0.01 ± 0.01 |
| Alkenes (Straight, Branched, & Cyclic) | 0 | 3.6 ± 0.1 | 7.4 ± 0.3 | 0 | 0 | 0 |
| Ethanol | 0 | 6.9 ± 0.5 | 4.4 ± 0.4 | 0 | 0 | 0 |

Note: Wt% by total mass for each source can be found in the supplementary material (Table 4.3).

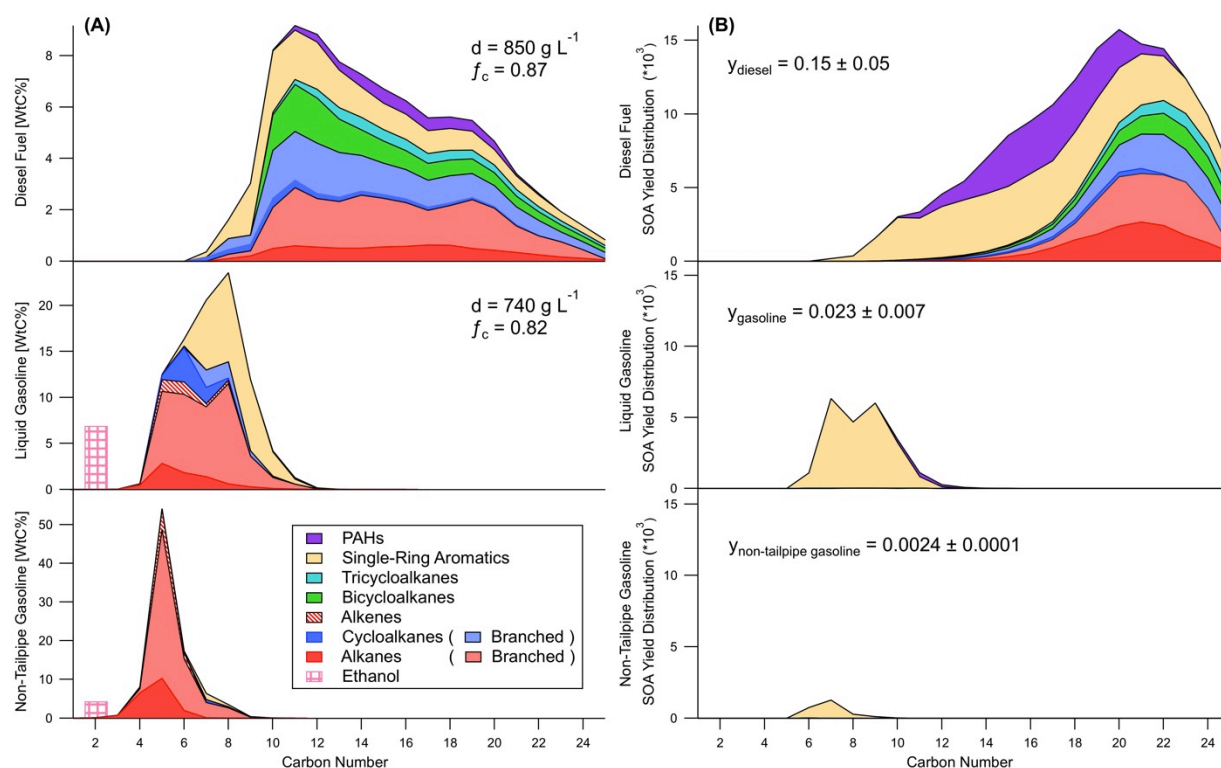


Figure 4.2. Distribution of mass **(A)** and SOA formation potential [$\mu\text{gSOA } \mu\text{g}^{-1}$] **(B)** in diesel and gasoline fuel (representative of exhaust) and non-tailpipe gasoline emissions. Distributions in both panels are colored by chemical class. Fuel properties (density, carbon fraction) and bulk SOA yields (at $M = 10 \mu\text{g m}^{-3}$) are superposed on panels A and B, respectively. Predicted SOA from gasoline exhaust is much lower than diesel and dominated solely by aromatic content, whereas diesel SOA is produced from a mix of aromatic and aliphatic compounds. A distribution of the SOA potential uncertainties can be found in Fig. 4.10.

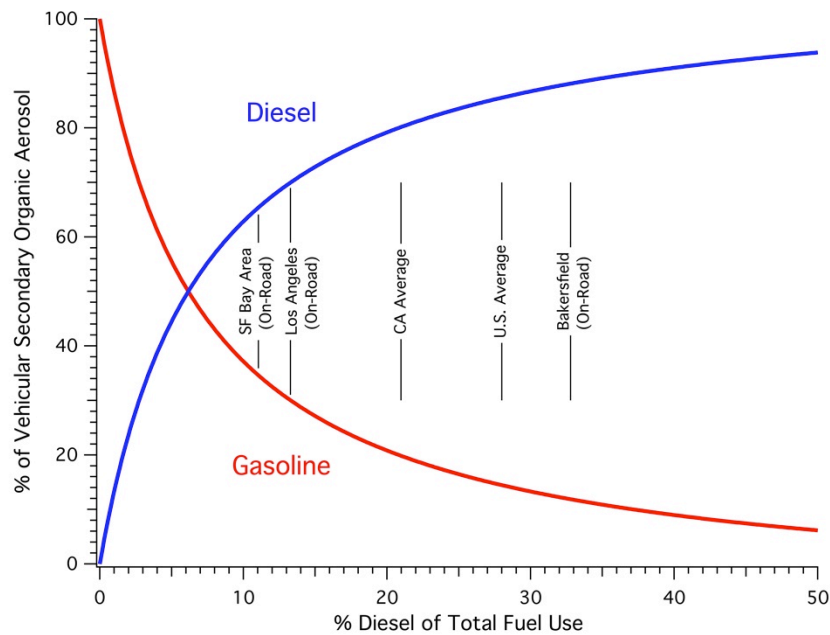


Figure 4.3. The percent contribution of gasoline and diesel exhaust to SOA over 0-50% diesel fuel use demonstrates the predominance of diesel sources for SOA formation. SOA contributions from the two sources are equivalent at 6% diesel fuel use. The U.S. and CA state averages shown are based on total on- and off-road use. The urban areas in CA shown are for on-road fuel use only; off-road contributions will increase the diesel fraction of total use by several percent, but are not available at this scale.

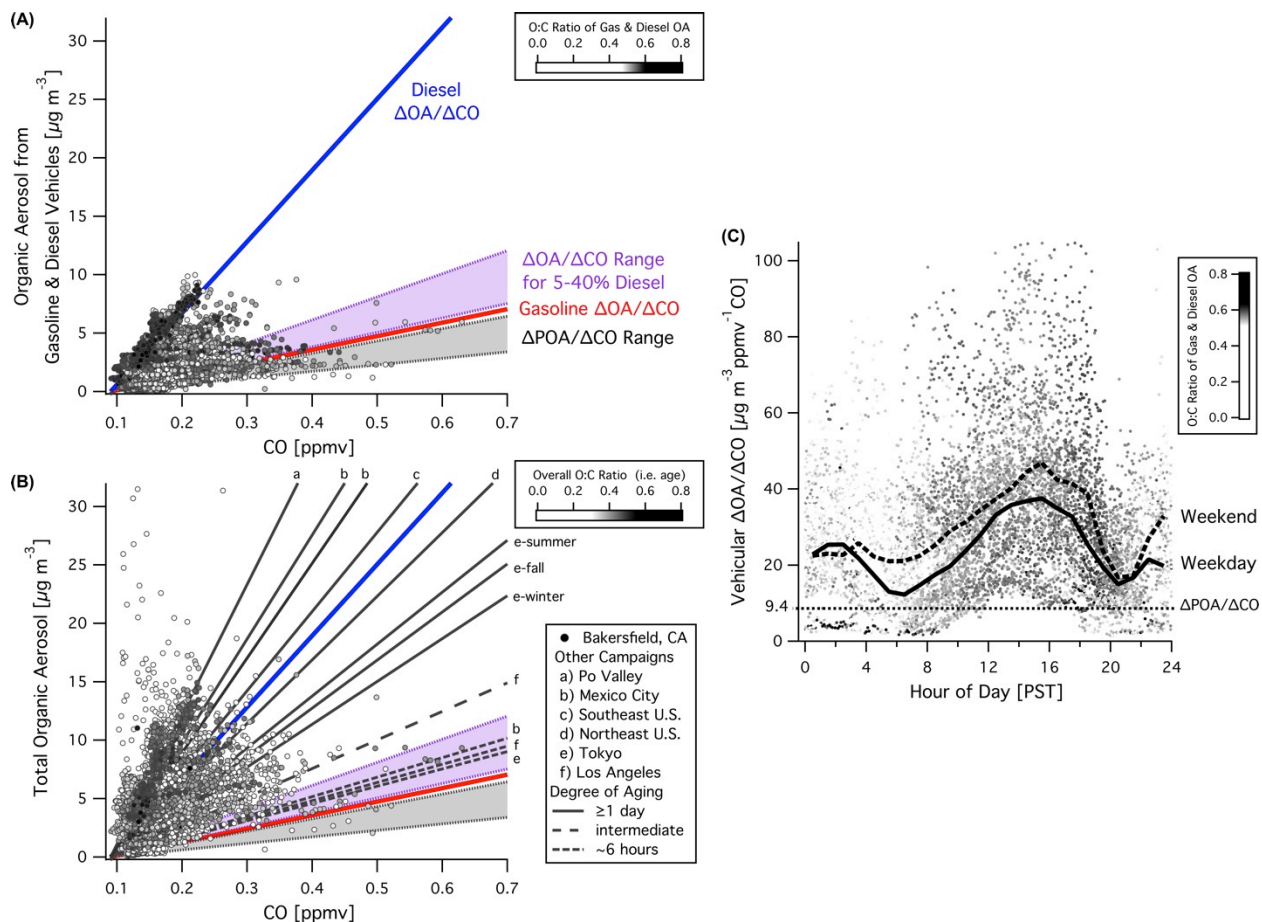


Figure 4.4. Comparisons of Organic Aerosol (OA) vs. carbon monoxide (CO) show the behavior of primary and secondary OA in the atmosphere and are used to examine vehicular OA and total OA in the San Joaquin Valley (Bakersfield) and numerous other urban sites (6, 19, 21, 25-33). Photochemical aging increases $\Delta\text{OA}/\Delta\text{CO}$ ratios and is represented by increased oxygen:carbon (O:C) ratios shaded in each panel. **(A)** Best estimates for $\Delta\text{OA}/\Delta\text{CO}$ ratios expected for pure gasoline and diesel emissions are added to a $\Delta\text{POA}/\Delta\text{CO}$ value of $9.4 \mu\text{g m}^{-3} \text{ ppmv}^{-1} \text{ CO}$ to account for primary OA and shown with a range of $\Delta\text{POA}/\Delta\text{CO}$ values (21, 34). Vehicular OA is determined from AMS factor analysis and observations are well constrained at Bakersfield with the exception of the most aged air parcels whose $\Delta\text{OA}/\Delta\text{CO}$ ratios are greater than expected for the mix of gasoline and diesel use. **(B)** Predicted $\Delta\text{OA}/\Delta\text{CO}$ slopes for a range of fuel mixtures ranging from 5 to 40% diesel agree with observations of relatively young aerosol in urban areas and vehicular OA at Bakersfield. Observed $\Delta\text{OA}/\Delta\text{CO}$ ratios increase with degree of aging and/or the influence of other SOA precursor sources that do not emit CO, which are prominent at Bakersfield and sites a-c. **(C)** Weekday and weekend diurnal averages of vehicular $\Delta\text{OA}/\Delta\text{CO}$ show greater ratios in the afternoon and over the weekend due to increased photochemical aging. Ratios are calculated with a 90 ppbv CO background and standard deviations are shown in Fig. 4.13.

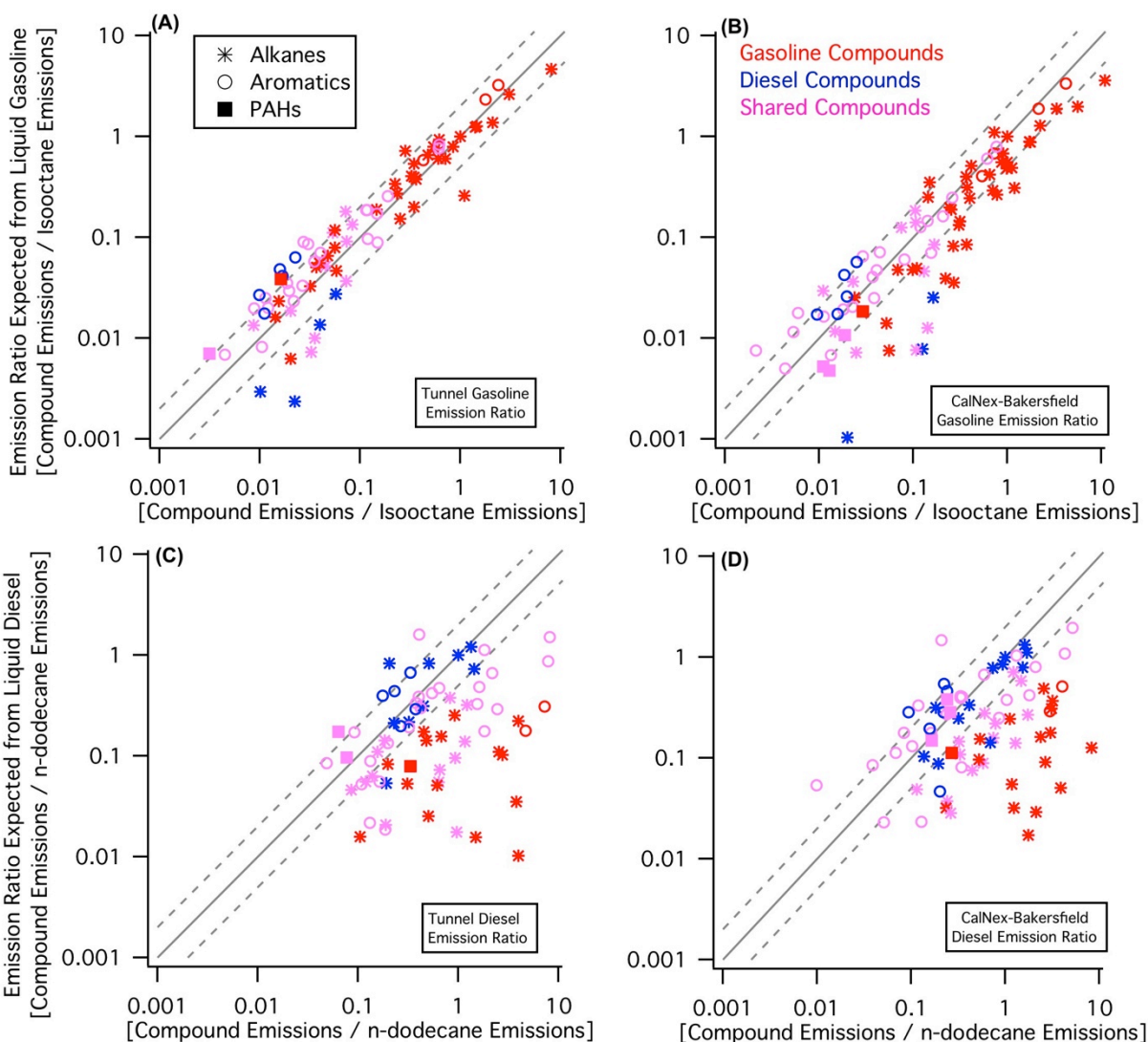


Figure 4.5: Demonstration of compositional consistency between gasoline and diesel fuel to gasoline and diesel exhaust, respectively, at both **(A, C)** the Caldecott tunnel and Bakersfield **(B, D)** using regressions to gasoline (isooctane) and diesel (n-dodecane) tracers. Similar to Figure 4.1, compounds dominated by gasoline (red) are most consistent with the liquid gasoline profile. Conversely, those dominated by diesel (blue) agree most with diesel fuel. Compounds shared by gasoline and diesel (pink) vary in degree of covariance with each source depending on relative content in each fuel and relative magnitude of each source at each field site.

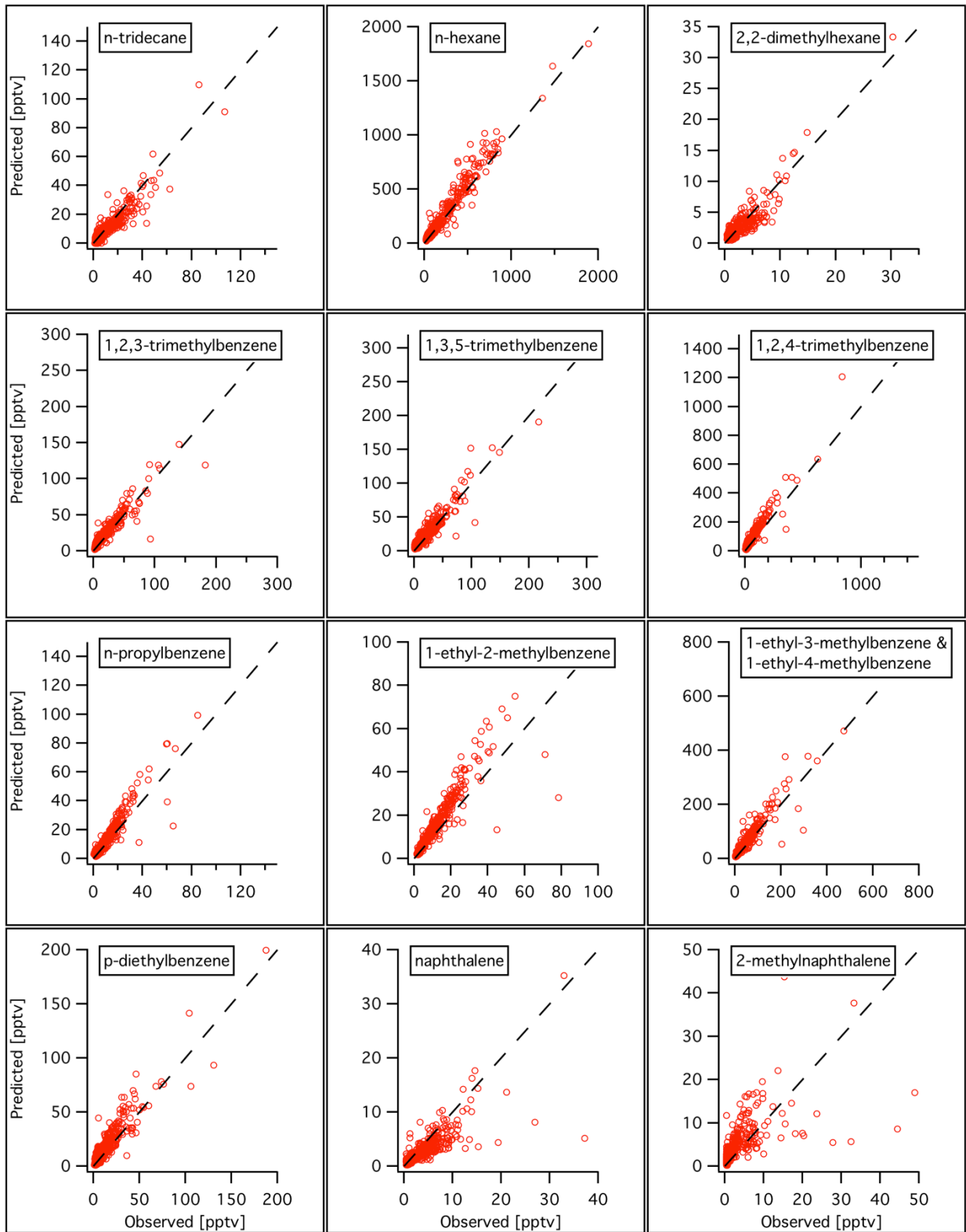


Figure 4.6: Verification of model performance at CalNex-Bakersfield by comparing predicted compound concentrations with observations of independent compounds not included in model. The 1:1 line is shown in each panel as a dashed line.

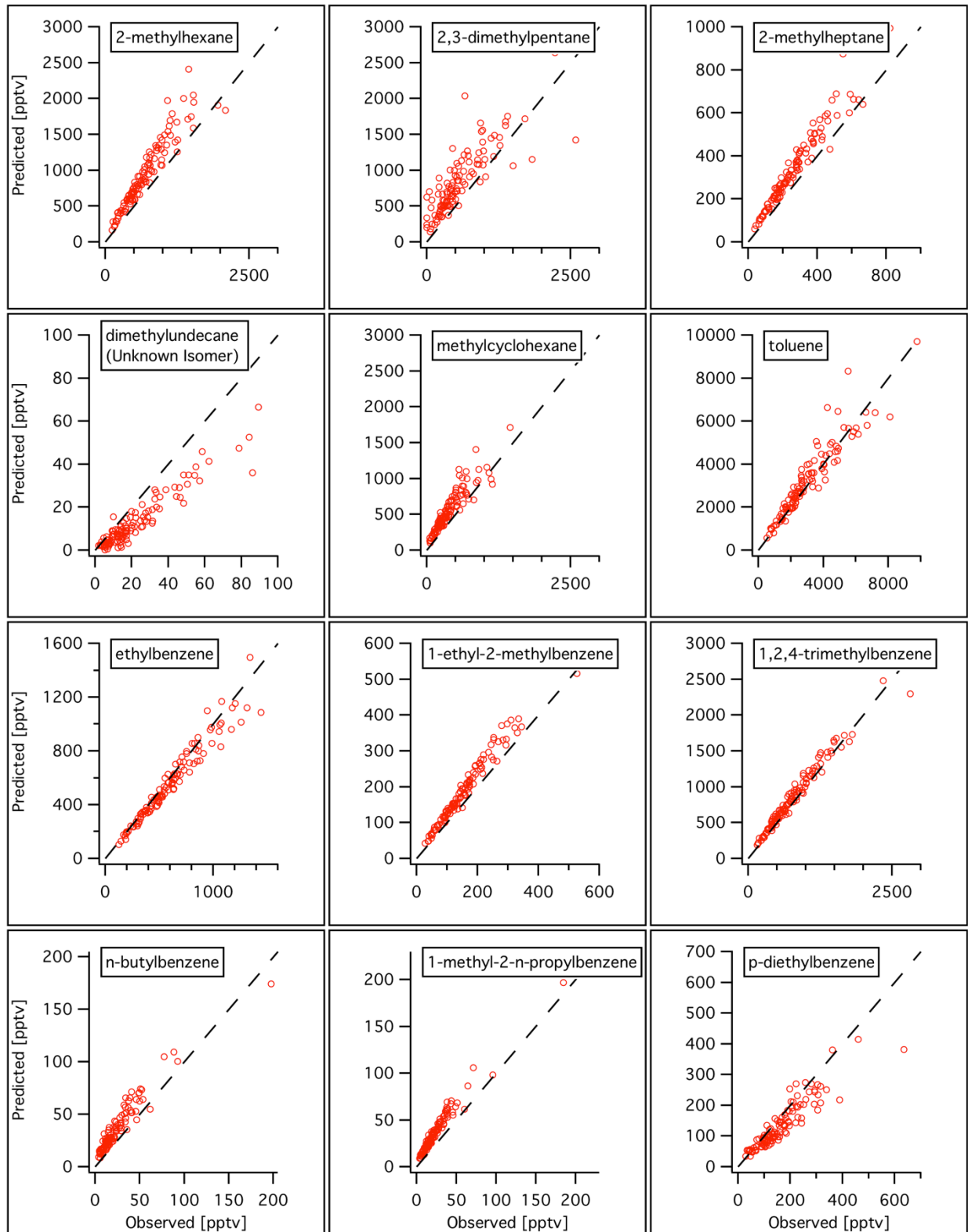


Figure 4.7: Verification of model performance at the Caldecott Tunnel (Oakland, CA) by comparing predicted compound concentrations with observations of independent compounds not included in model. The 1:1 line is shown in each panel as a dashed line.

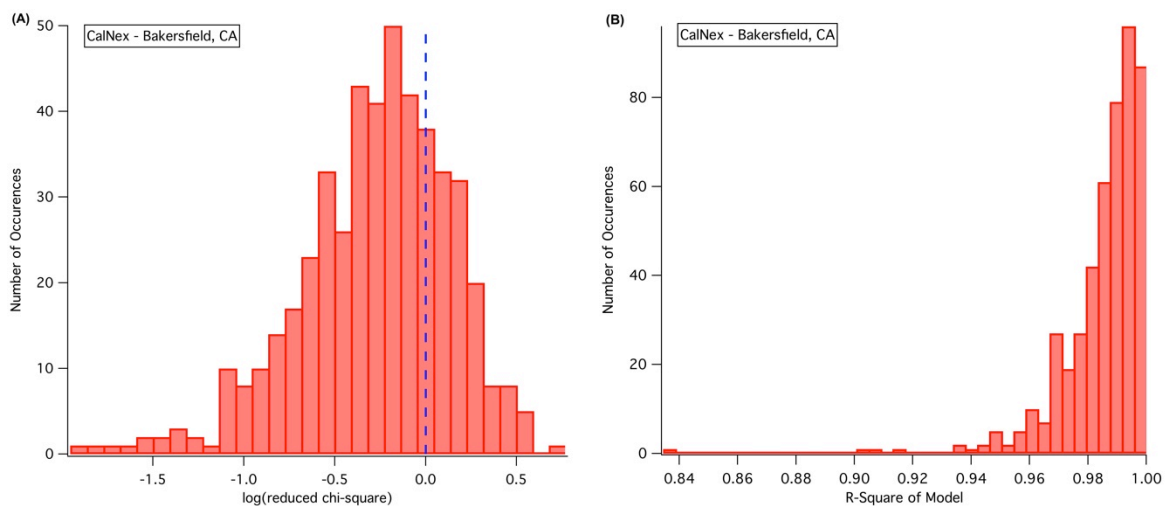


Figure 4.8: Internal model diagnostics for CalNex-Bakersfield site (N=476). Panel A shows the log of the reduced chi-square test where ≤ 0 indicates a good fit of model data. Similarly, Panel B shows the overall coefficient of determination (r^2) of compounds used in the model and values close to 1.0 indicate robust model performance.

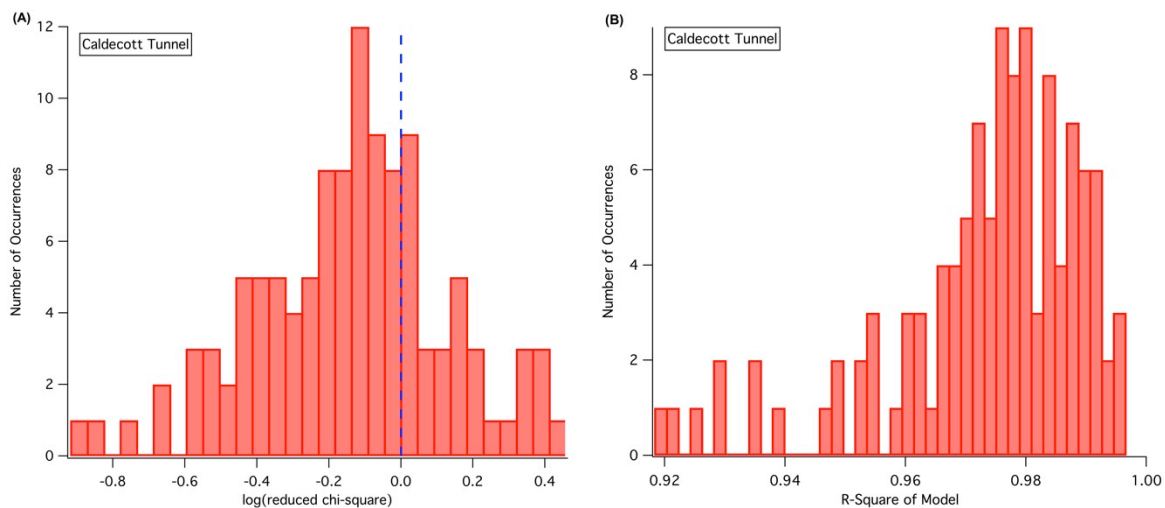


Figure 4.9: Internal model validation for the Caldecott tunnel (N=114). Description same as Figure 4.8.

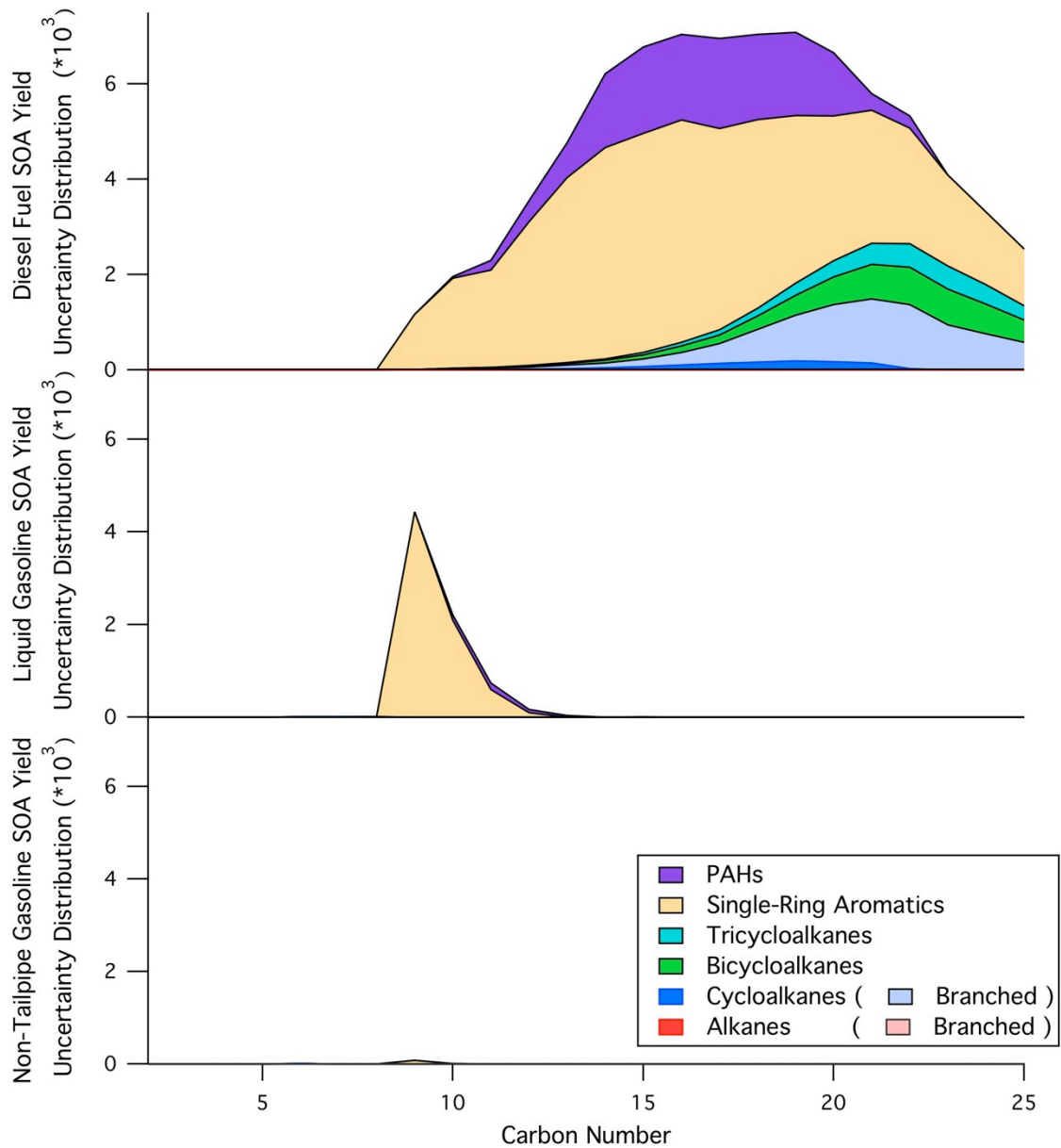


Figure 4.10: Distributions of SOA yield uncertainties [$\mu\text{gSOA } \mu\text{g}^{-1}$] from each source where uncertainties are based on Monte Carlo analysis. Diesel exhasut has greatest uncertainty due to insufficient studies on intermediate volatility compounds likely to form SOA, with the exception of straight and branched alkanes.

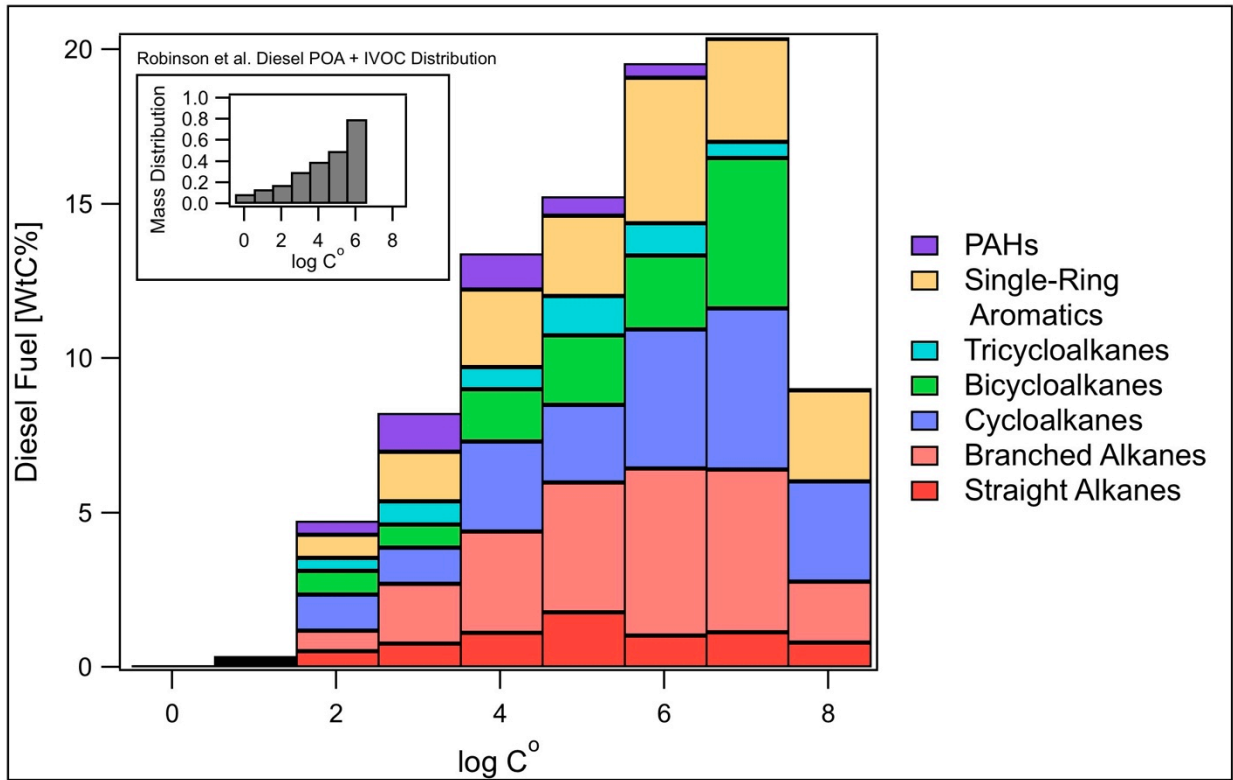


Figure 4.11: Volatility basis set distribution of diesel fuel broken down by chemical class. Inset shows SVOC and IVOC distribution used in current models (5), which does not include the $C^\circ=10^7 \mu\text{g m}^{-3}$ and $C^\circ=10^8 \mu\text{g m}^{-3}$ volatility bins, which contain C_{9-11} aromatics. The magnitude of the $C^\circ=1 \mu\text{g m}^{-3}$ and $C^\circ=10 \mu\text{g m}^{-3}$ volatility bins are accurately larger in current models as they include primary gases and particles emanating from motor oil.

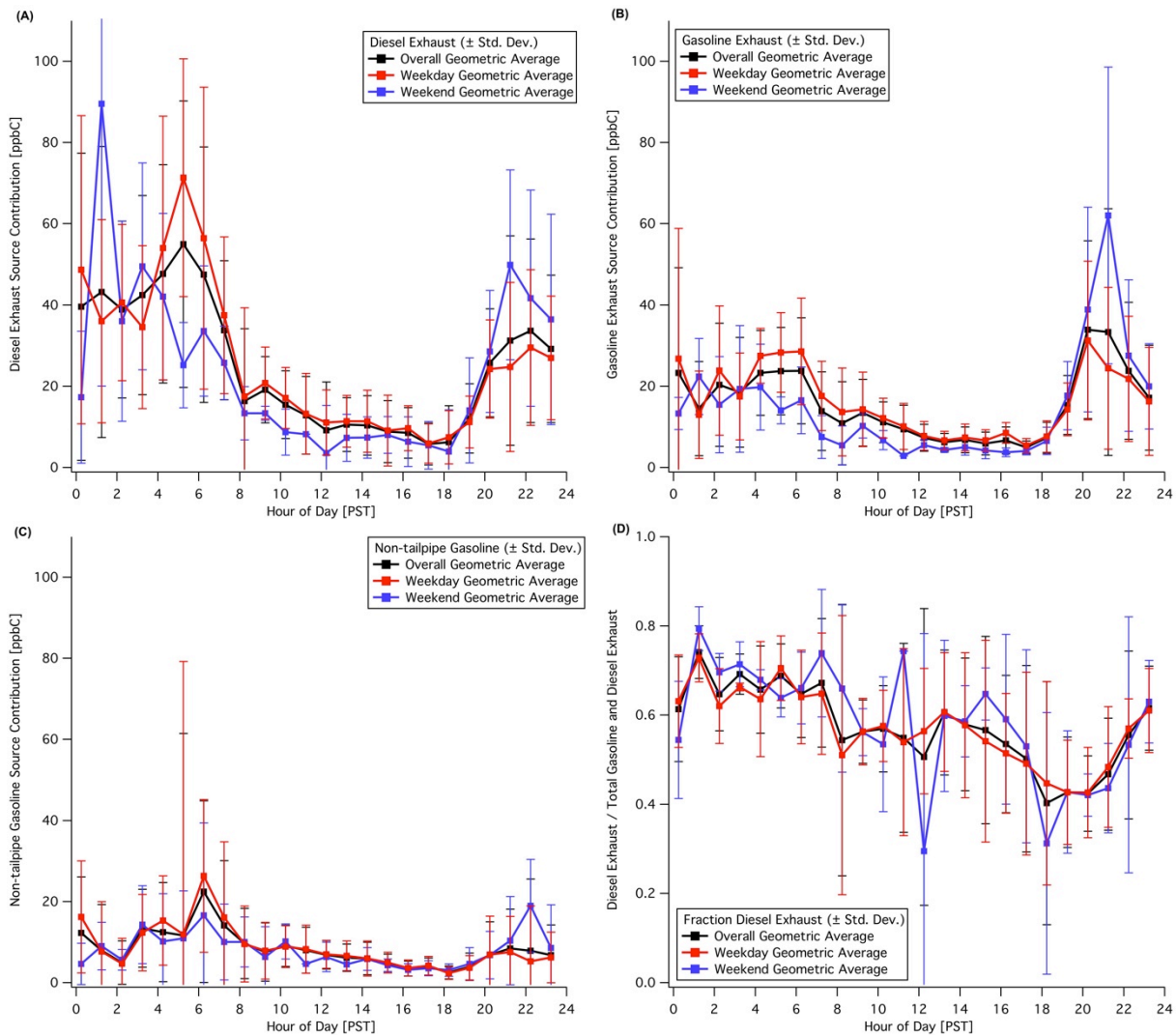


Figure 4.12: Weekday/weekend diurnal profiles of diesel exhaust (A), gasoline exhaust (B), and non-tailpipe gasoline source contributions (C), and ratio of diesel to gasoline exhaust (D) during the early summer in Bakersfield (includes 5 weekends). The source contributions of gasoline and diesel (A-B) have greater daytime values during the week. The diesel exhaust fraction (D) shows some diurnal variability, there is no strong weekday/weekend effect in the relative fraction of each fuel due to equivalent decreases in both gasoline and diesel.

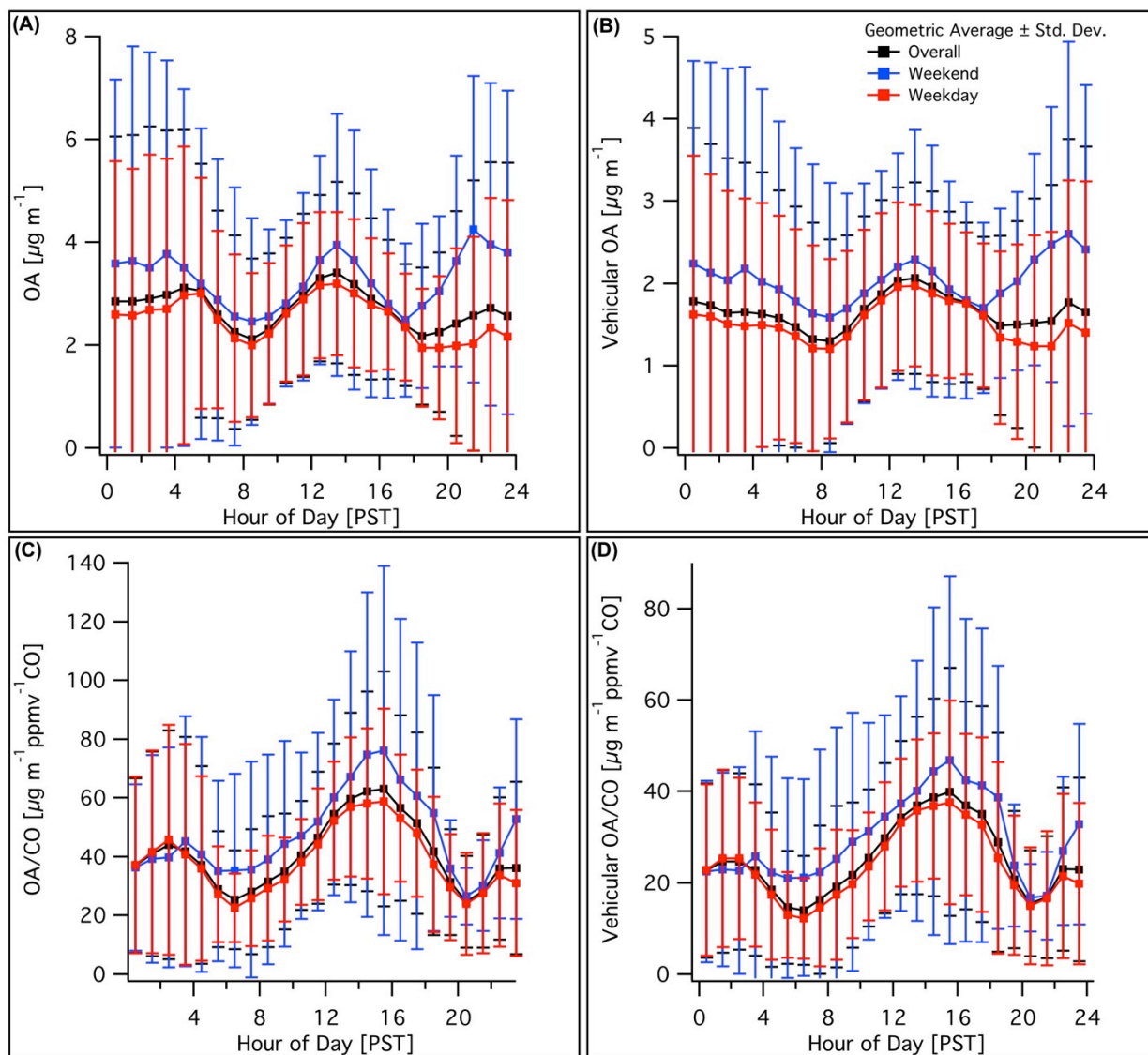


Figure 4.13: **(A-B)** Overall, weekday, and weekend diurnal patterns for total and vehicular organic aerosol at Bakersfield, CA during the early summer. Vehicular OA is determined from AMS positive matrix factor analysis (19). **(C-D)** Overall, weekday, and weekend diurnal patterns for $\Delta\text{OA}/\Delta\text{CO}$ ratios for total and vehicular organic aerosol. In all cases, daytime weekend values are higher, but within the large variability observed across the 6-week campaign. Total and vehicular OA are higher over the weekend due to increased photochemical processing (as shown by increased $\Delta\text{OA}/\Delta\text{CO}$ ratios) associated with decreased NO_x emissions from diesel sources and is not a function of changes in the distribution of fuel use.

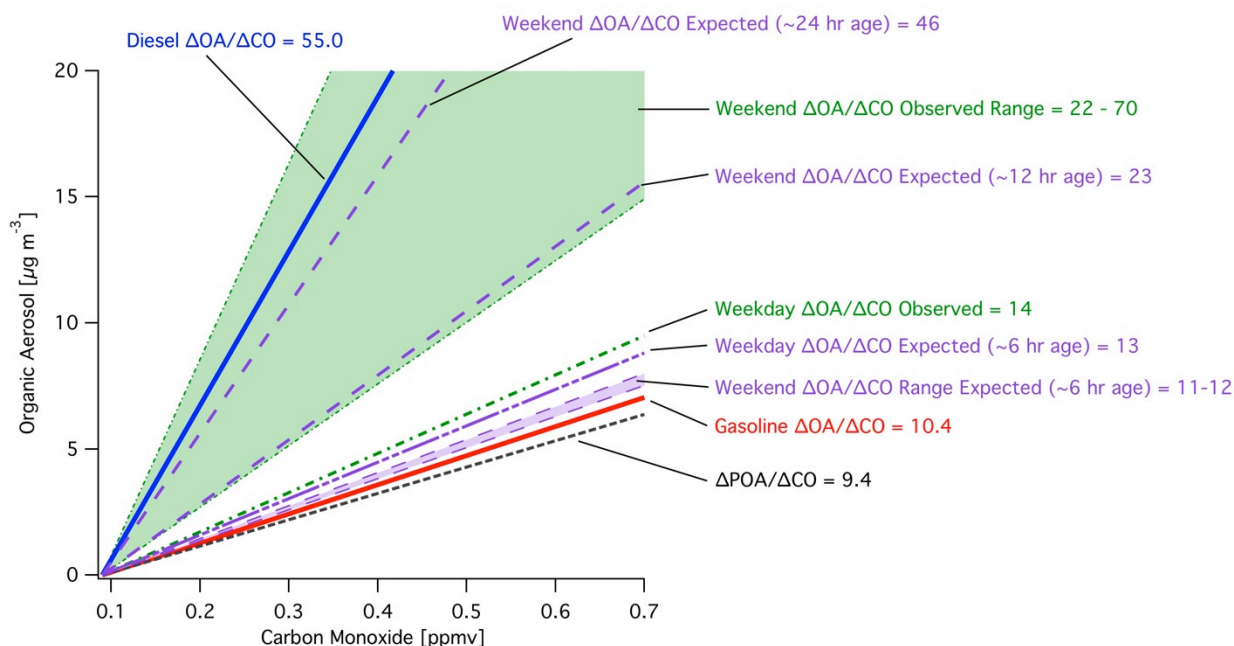


Figure 4.14: Weekday/weekend behavior of $\Delta\text{OA}/\Delta\text{CO}$ ratios in Los Angeles, CA (Summer 2010) with best estimates for $\Delta\text{OA}/\Delta\text{CO}$ ratios expected for pure gasoline and diesel emissions added to an average POA/CO value of $9.4 \mu\text{g m}^{-3} \text{ppmv}^{-1} \text{CO}$ (21). Calculated weekday $\Delta\text{OA}/\Delta\text{CO}$ slope (17% diesel) for Los Angeles agrees with observed value. Weekend values show varying degrees of aging ranging from 12 hours to 1 day based on reported photochemical ages, which roughly correspond to a 2-4x increase in $\Delta\text{OA}/\Delta\text{CO}$ ratios (6, 20, 26). Approximate aged weekend values with 5-10% diesel use are shown and are consistent with observations. While Los Angeles is dominated by motor vehicle emissions, contributions of SOA precursors from other non-CO related sources would elevate predicted $\Delta\text{OA}/\Delta\text{CO}$ ratios further.

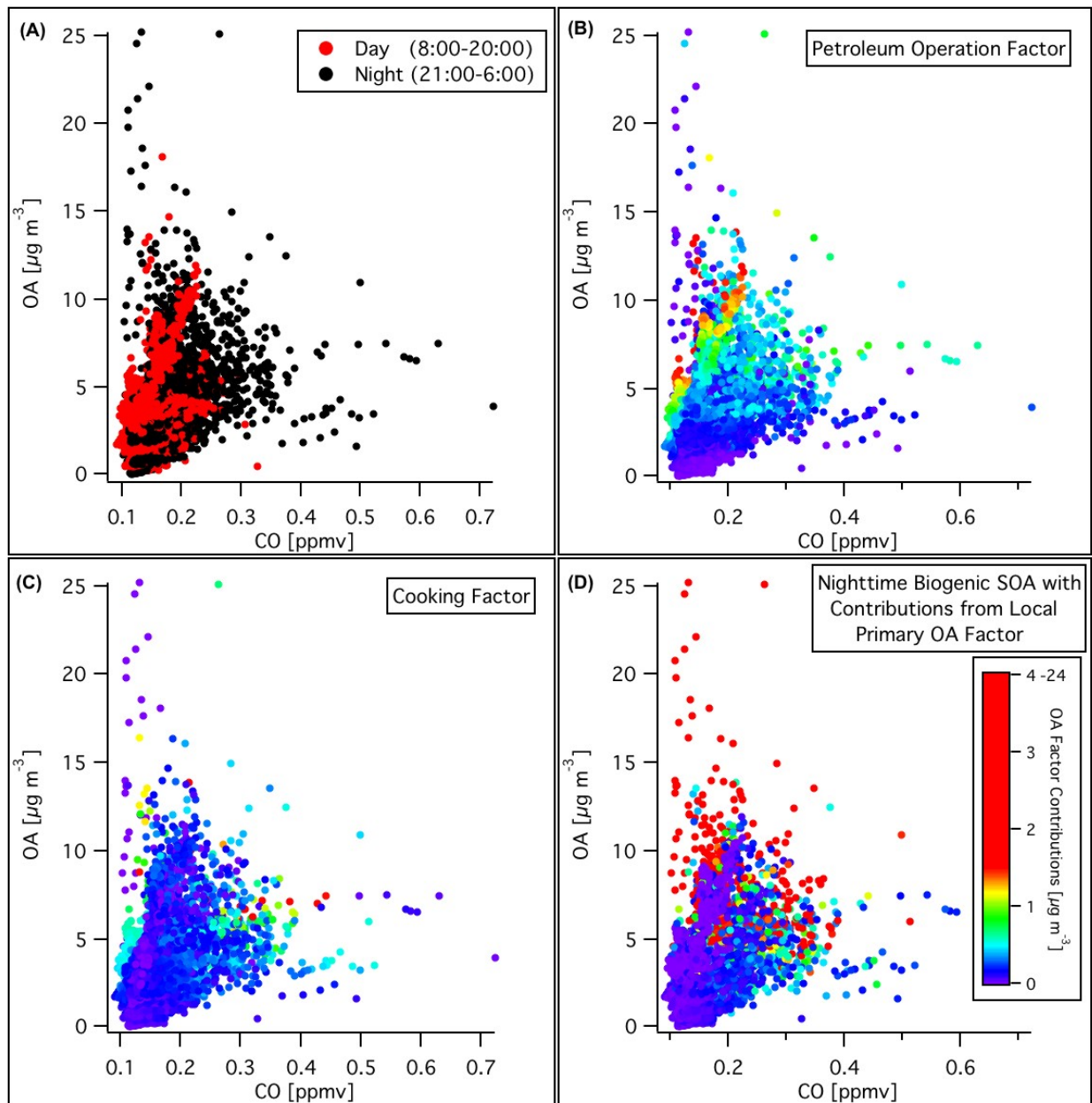


Figure 4.15: Observed organic aerosol vs. carbon monoxide at Bakersfield, CA during the early summer. Panel A shows day and night ratios, with increased daytime $\Delta\text{OA}/\Delta\text{CO}$ slopes associated with greater aging, while nighttime values show less aged air masses and episodic contributions to OA without CO from non-vehicular sources. Panels B-D show color-shaded contributions for major non-vehicular sources as determined by factor analysis of AMS data (19).

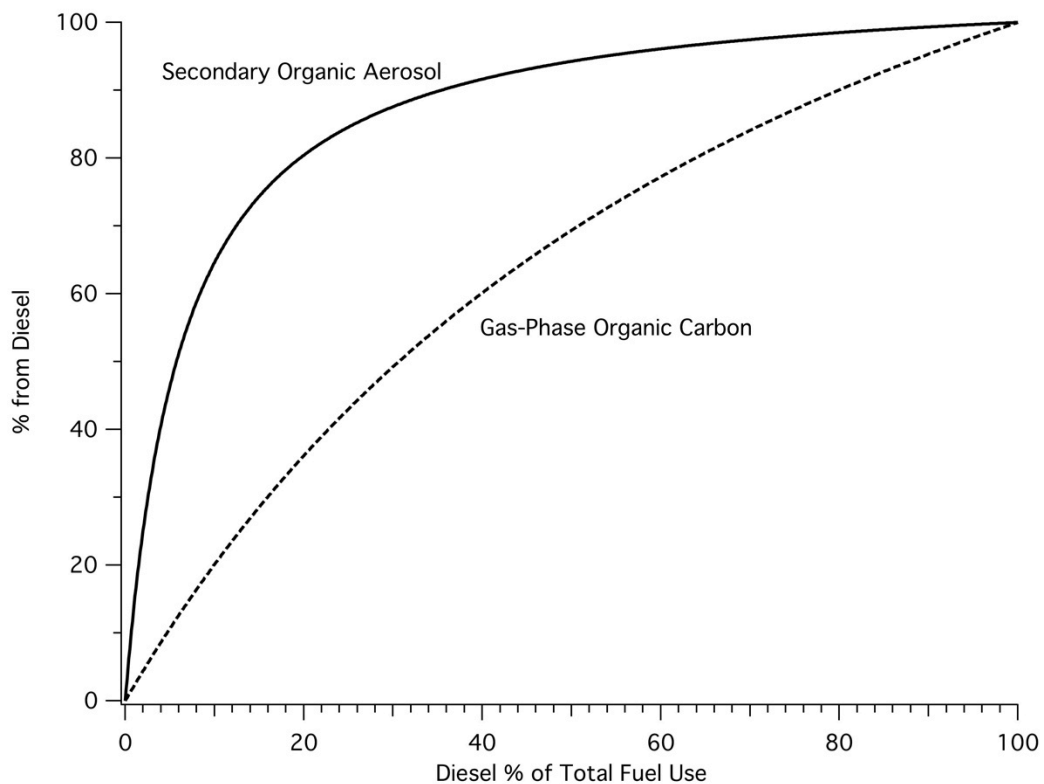


Figure 4.16: The percent contribution of diesel exhaust to SOA over percent diesel fuel use. The percent diesel contribution to gas-phase organic carbon is shown as well and has greater contributions from gasoline with a equivalence point at 31% diesel fuel use. The percent contribution from gasoline can be determined via the difference of diesel. The gas-phase organic carbon line does not consider contributions from non-tailpipe gasoline sources since contributions will vary depending on location and time of year.

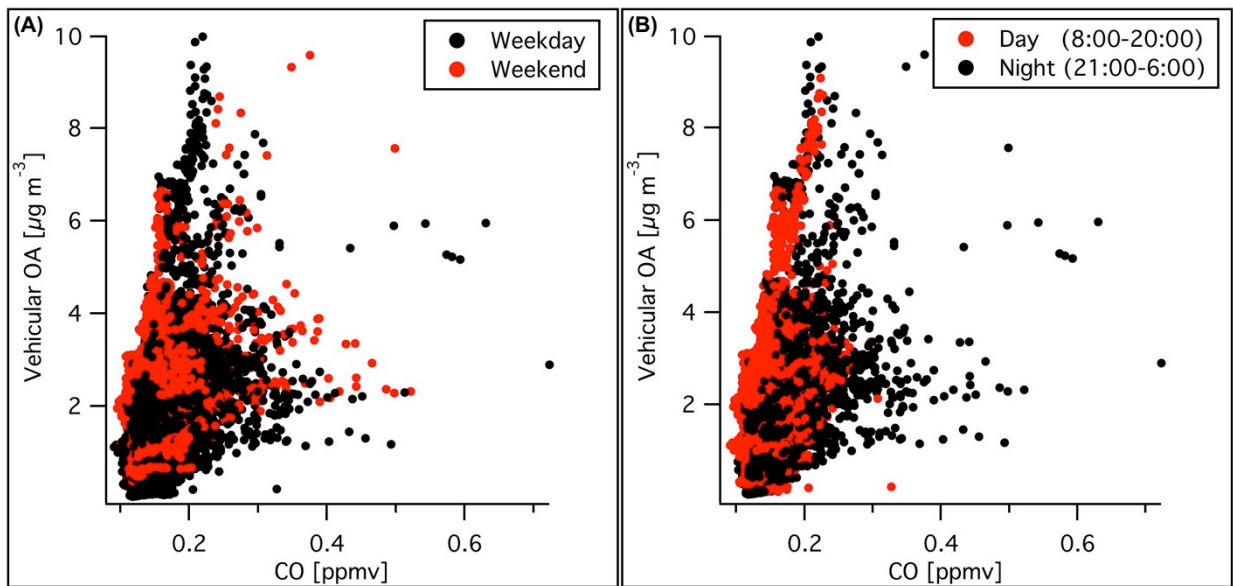


Figure 4.17: Vehicular organic aerosol vs. carbon monoxide at Bakersfield, CA during the early summer. Vehicular OA is determined from AMS positive matrix factor analysis (19). Panel A shows minor weekday/weekend differences with considerable variability and is better displayed in Figure 4.13D. Panel B shows day and night ratios, with increased daytime $\Delta\text{OA}/\Delta\text{CO}$ slopes associated with greater aging, while nighttime values show a mix of air mass ages.

Table 4.2: Sales of on-road gasoline and diesel fuel in California and its counties (11)

| COUNTY | Total Gas and Diesel Sales [10 ⁶ gallons annually] | Percent Gasoline (by volume) | Percent Diesel (by volume) |
|-----------------|---|------------------------------|----------------------------|
| ALAMEDA | 772 | 84.2% | 15.8% |
| ALPINE | 3 | 89.5% | 10.5% |
| AMADOR | 24 | 86.8% | 13.2% |
| BUTTE | 97 | 85.3% | 14.7% |
| CALAVERAS | 21 | 89.0% | 11.0% |
| COLUSA | 43 | 64.6% | 35.4% |
| CONTRA COSTA | 432 | 89.4% | 10.6% |
| DEL NORTE | 16 | 77.8% | 22.2% |
| EL DORADO | 86 | 89.7% | 10.3% |
| FRESNO | 497 | 76.6% | 23.4% |
| GLENN | 40 | 57.7% | 42.3% |
| HUMBOLDT | 72 | 81.9% | 18.1% |
| IMPERIAL | 129 | 71.4% | 28.6% |
| INYO | 32 | 77.5% | 22.5% |
| KERN | 565 | 67.3% | 32.7% |
| KINGS | 92 | 71.0% | 29.0% |
| LAKE | 32 | 85.2% | 14.8% |
| LASSEN | 34 | 69.7% | 30.3% |
| LOS ANGELES | 4251 | 86.8% | 13.2% |
| MADERA | 102 | 71.0% | 29.0% |
| MARIN | 145 | 92.3% | 7.7% |
| MARIPOSA | 13 | 95.8% | 4.2% |
| MENDOCINO | 67 | 82.4% | 17.6% |
| MERCED | 164 | 73.1% | 26.9% |
| MODOC | 15 | 65.1% | 34.9% |
| MONO | 17 | 84.7% | 15.3% |
| MONTEREY | 213 | 79.5% | 20.5% |
| NAPA | 62 | 90.3% | 9.7% |
| NEVADA | 71 | 77.8% | 22.2% |
| ORANGE | 1415 | 89.3% | 10.7% |
| PLACER | 194 | 83.2% | 16.8% |
| PLUMAS | 23 | 71.9% | 28.1% |
| RIVERSIDE | 1154 | 78.6% | 21.4% |
| SACRAMENTO | 644 | 85.5% | 14.5% |
| SAN BENITO | 33 | 71.2% | 28.8% |
| SAN BERNARDINO | 1301 | 76.3% | 23.7% |
| SAN DIEGO | 1460 | 88.7% | 11.3% |
| SAN FRANCISCO | 171 | 93.9% | 6.1% |
| SAN JOAQUIN | 413 | 73.4% | 26.6% |
| SAN LUIS OBISPO | 161 | 85.4% | 14.6% |
| SAN MATEO | 336 | 92.3% | 7.7% |
| SANTA BARBARA | 203 | 86.8% | 13.2% |
| SANTA CLARA | 790 | 89.6% | 10.4% |
| SANTA CRUZ | 102 | 89.7% | 10.3% |
| SHASTA | 120 | 76.1% | 23.9% |
| SIERRA | 7 | 74.7% | 25.3% |
| SISKIYOU | 72 | 60.9% | 39.1% |
| SOLANO | 252 | 86.2% | 13.8% |
| SONOMA | 220 | 87.2% | 12.8% |
| STANISLAUS | 250 | 76.3% | 23.7% |
| SUTTER | 50 | 85.0% | 15.0% |
| TEHAMA | 64 | 71.0% | 29.0% |
| TRINITY | 13 | 68.8% | 31.2% |
| TULARE | 232 | 74.4% | 25.6% |
| TUOLUMNE | 35 | 85.8% | 14.2% |
| VENTURA | 364 | 87.2% | 12.8% |
| YOLO | 120 | 79.2% | 20.8% |
| YUBA | 36 | 86.4% | 13.6% |
| TOTAL | 18344 | 83.5% | 16.5% |

Table 4.3: Chemical class distribution of sources by total mass

| Compound Class | Weight Percent by mass (\pm St. Dev) | | |
|---|--|------------------------|------------------------------|
| | Diesel Fuel | Liquid Gasoline | Non-Tailpipe Gasoline |
| Straight-chain Alkanes | 7.3 \pm 1.2 | 7.6 \pm 0.3 | 19 \pm 0.9 |
| Branched Alkanes | 23 \pm 2.5 | 39 \pm 0.9 | 58 \pm 3 |
| Cycloalkanes (Single Straight Alkyl Chain) | 2.5 \pm 0.2 | 4.2 \pm 0.1 | 0.98 \pm 0.04 |
| Cycloalkanes (Branched or Multiple Alkyl Chain(s)) | 18 \pm 1.8 | 6.0 \pm 0.3 | 4.8 \pm 0.2 |
| Bicycloalkanes | 12 \pm 1.3 | 0 | 0 |
| Tricycloalkanes | 4.7 \pm 0.6 | 0 | 0 |
| Single-ring Aromatics | 17.7 \pm 1.6 | 26.7 \pm 0.7 | 2.5 \pm 0.1 |
| Polycyclic Aromatic Compounds | 3.8 \pm 1.6 | 0.29 \pm 0.02 | 0.0003 |
| Alkenes (Straight, Branched, & Cyclic) | 0 | 3.5 \pm 0.1 | 7.0 \pm 0.3 |
| Ethanol | 0 | 10.9 \pm 0.9 | 6.9 \pm 0.6 |

Table 4.4: Summary of compounds used in source receptor modeling at Bakersfield

| Master Set | Confirmation Set #1 | Confirmation Set #2 | Confirmation Set #3 | Confirmation Set #4 |
|---|---|--|--|--|
| n-butane isopentane n-pentane n-heptane isooctane m&p-xylene o-xylene n-nonane n-undecane n-dodecane | n-butane n-pentane isopentane n-heptane isooctane m&p-xylene n-nonane n-undecane | n-butane isopentane 2,2-dimethylbutane n-heptane 2-methylhexane 3-methylhexane m&p-xylene n-nonane n-tridecane | n-butane n-pentane 2,2-dimethylbutane methylcyclopentane n-heptane isooctane m&p-xylene n-nonane 1-ethyl-3(+4)-methylbenzene n-dodecane | n-butane n-pentane isopentane toluene isooctane o-xylene n-undecane n-dodecane naphthalene |

Table 4.5: Summary of compounds used in source receptor modeling at the Caldecott Tunnel

| Master Set | Confirmation Set #1 | Confirmation Set #2 | Confirmation Set #3 | Confirmation Set #4 |
|--|---|--|---|---|
| isopentane isooctane m&p-xylene o-xylene n-nonane 1,2,3-trimethylbenzene 1,3,5-trimethylbenzene n-propylbenzene n-undecane n-dodecane | isopentane n-hexane isooctane m&p-xylene o-xylene n-nonane n-dodecane | n-pentane 2,2-dimethylbutane n-hexane 3-methylpentane o-xylene n-nonane 1,2,4-trimethylbenzene 1-ethyl-2-methylbenzene n-tridecane | n-pentane 2,2-dimethylbutane n-hexane 3-methylpentane ethylcyclopentane methylcyclohexane 2,3-dimethylheptane 1-ethyl-2-methylbenzene n-tridecane | n-pentane n-heptane n-nonane 1,2,3-trimethylbenzene n-undecane n-tridecane |

Table 4.6: Mass and chemical class distribution of diesel fuel (in weight percent by carbon)

| Carbon Number | Straight-chain Alkanes | Branched Alkanes | Cycloalkanes (Single Straight Alkyl Chain) | Cycloalkanes (Branched or Multiple Alkyl Chain(s)) | Bicycloalkanes | Tricycloalkanes | Aromatics | Polycyclic Aromatic Compounds |
|---------------|------------------------|------------------|--|--|----------------|-----------------|-----------|-------------------------------|
| 1 | 0 | 0 | 0 | 0 | 0 | 0 | 0 | 0 |
| 2 | 0 | 0 | 0 | 0 | 0 | 0 | 0 | 0 |
| 3 | 0 | 0 | 0 | 0 | 0 | 0 | 0 | 0 |
| 4 | 0 | 0 | 0 | 0 | 0 | 0 | 0 | 0 |
| 5 | 0 | 0 | 0 | 0 | 0 | 0 | 0 | 0 |
| 6 | 0 | 0 | 0 | 0 | 0 | 0 | 0 | 0 |
| 7 | 0 | 0 | 0.15 | 0 | 0 | 0 | 0.21 | 0 |
| 8 | 0.10 | 0.17 | 0.19 | 0.42 | 0 | 0 | 0.73 | 0 |
| 9 | 0.21 | 0.20 | 0.26 | 0.35 | 0 | 0 | 2.02 | 0 |
| 10 | 0.50 | 1.60 | 0.35 | 1.87 | 1.38 | 0.11 | 2.38 | 0.03 |
| 11 | 0.60 | 2.27 | 0.29 | 1.90 | 1.82 | 0.21 | 1.91 | 0.18 |
| 12 | 0.55 | 1.89 | 0.20 | 1.96 | 1.76 | 0.34 | 1.83 | 0.30 |
| 13 | 0.51 | 1.81 | 0.17 | 1.74 | 1.30 | 0.44 | 1.46 | 0.32 |
| 14 | 0.51 | 2.06 | 0.15 | 1.39 | 1.00 | 0.49 | 1.18 | 0.49 |
| 15 | 0.56 | 1.89 | 0.15 | 1.22 | 0.86 | 0.45 | 1.03 | 0.56 |
| 16 | 0.58 | 1.70 | 0.14 | 1.14 | 0.74 | 0.44 | 0.99 | 0.51 |
| 17 | 0.64 | 1.35 | 0.12 | 1.05 | 0.65 | 0.39 | 0.89 | 0.50 |
| 18 | 0.62 | 1.55 | 0.10 | 1.06 | 0.62 | 0.37 | 0.84 | 0.45 |
| 19 | 0.50 | 1.90 | 0.08 | 0.94 | 0.57 | 0.34 | 0.73 | 0.42 |
| 20 | 0.43 | 1.63 | 0.06 | 0.82 | 0.50 | 0.30 | 0.61 | 0.32 |
| 21 | 0.34 | 1.03 | 0.05 | 0.70 | 0.42 | 0.25 | 0.53 | 0.08 |
| 22 | 0.25 | 0.73 | 0.01 | 0.59 | 0.33 | 0.21 | 0.45 | 0.06 |
| 23 | 0.16 | 0.60 | 0 | 0.38 | 0.26 | 0.17 | 0.35 | 0 |
| 24 | 0.11 | 0.34 | 0 | 0.31 | 0.21 | 0.14 | 0.28 | 0 |
| 25 | 0.06 | 0.04 | 0 | 0.25 | 0.16 | 0.11 | 0.22 | 0 |

Table 4.7: Mass and chemical class distribution of liquid gasoline (in weight percent by carbon)

| Carbon Number | Straight-chain Alkanes | Branched Alkanes | Cycloalkanes (Single Straight Alkyl Chain) | Cycloalkanes (Branched or Multiple Alkyl Chain(s)) | Bicycloalkanes | Tricycloalkanes | Aromatics | Polycyclic Aromatic Compounds |
|---------------|------------------------|------------------|--|--|----------------|-----------------|-----------|-------------------------------|
| 1 | 0 | 0 | 0 | 0 | 0 | 0 | 0 | 0 |
| 2 | 0.0003 | 0 | 0 | 0 | 0 | 0 | 0 | 0 |
| 3 | 0.014 | 0 | 0 | 0 | 0 | 0 | 0 | 0 |
| 4 | 0.500 | 0.057 | 0 | 0 | 0 | 0 | 0 | 0 |
| 5 | 2.84 | 7.83 | 0.475 | 0 | 0 | 0 | 0 | 0 |
| 6 | 1.84 | 8.51 | 3.75 | 0 | 0 | 0 | 0.750 | 0 |
| 7 | 1.39 | 7.60 | 1.76 | 1.89 | 0 | 0 | 7.59 | 0 |
| 8 | 0.621 | 10.89 | 0.214 | 1.78 | 0 | 0 | 9.69 | 0 |
| 9 | 0.278 | 3.33 | 0.043 | 0.536 | 0 | 0 | 7.74 | 0 |
| 10 | 0.116 | 1.20 | 0 | 0.126 | 0 | 0 | 2.63 | 0.130 |
| 11 | 0.063 | 0.516 | 0 | 0 | 0 | 0 | 0.558 | 0.127 |
| 12 | 0.017 | 0.040 | 0 | 0 | 0 | 0 | 0.060 | 0.048 |
| 13 | 0.008 | 0 | 0 | 0 | 0 | 0 | 0 | 0.016 |
| 14 | 0.004 | 0.007 | 0 | 0 | 0 | 0 | 0.001 | 0 |
| 15 | 0.004 | 0.006 | 0 | 0 | 0 | 0 | 0 | 0.002 |
| 16 | 0 | 0 | 0 | 0 | 0 | 0 | 0 | 0.0004 |
| 17 | 0 | 0 | 0 | 0 | 0 | 0 | 0 | 0 |
| 18 | 0 | 0 | 0 | 0 | 0 | 0 | 0 | 0 |
| 19 | 0 | 0 | 0 | 0 | 0 | 0 | 0 | 0 |
| 20 | 0 | 0 | 0 | 0 | 0 | 0 | 0 | 0 |
| 21 | 0 | 0 | 0 | 0 | 0 | 0 | 0 | 0 |
| 22 | 0 | 0 | 0 | 0 | 0 | 0 | 0 | 0 |
| 23 | 0 | 0 | 0 | 0 | 0 | 0 | 0 | 0 |
| 24 | 0 | 0 | 0 | 0 | 0 | 0 | 0 | 0 |
| 25 | 0 | 0 | 0 | 0 | 0 | 0 | 0 | 0 |

Table 4.8: Mass and chemical class distribution of non-tailpipe gasoline (in weight percent by carbon)

| Carbon Number | Straight-chain Alkanes | Branched Alkanes | Cycloalkanes (Single Straight Alkyl Chain) | Cycloalkanes (Branched or Multiple Alkyl Chain(s)) | Bicycloalkanes | Tricycloalkanes | Aromatics | Polycyclic Aromatic Compounds |
|---------------|------------------------|------------------|--|--|----------------|-----------------|-----------|-------------------------------|
| 1 | 0 | 0 | 0 | 0 | 0 | 0 | 0 | 0 |
| 2 | 0.0987 | 0 | 0 | 0 | 0 | 0 | 0 | 0 |
| 3 | 0.690 | 0 | 0 | 0 | 0 | 0 | 0 | 0 |
| 4 | 6.54 | 1.07 | 0 | 0 | 0 | 0 | 0 | 0 |
| 5 | 10.3 | 38.4 | 1.07 | 0 | 0 | 0 | 0 | 0 |
| 6 | 1.97 | 13.4 | 3.35 | 0 | 0 | 0 | 0.506 | 0 |
| 7 | 0.137 | 3.89 | 0.562 | 0.774 | 0 | 0 | 1.52 | 0 |
| 8 | 0.0616 | 2.59 | 0.0194 | 0.257 | 0 | 0 | 0.564 | 0 |
| 9 | 0.0085 | 0.262 | 0.0014 | 0 | 0 | 0 | 0.139 | 0 |
| 10 | 0.0012 | 0 | 0 | 0.0003 | 0 | 0 | 0.0085 | 0.0002 |
| 11 | 0.0002 | 0 | 0 | 0 | 0 | 0 | 0.0001 | 0 |
| 12 | 0 | 0 | 0 | 0 | 0 | 0 | 0 | 0 |
| 13 | 0 | 0 | 0 | 0 | 0 | 0 | 0 | 0 |
| 14 | 0 | 0 | 0 | 0 | 0 | 0 | 0 | 0 |
| 15 | 0 | 0 | 0 | 0 | 0 | 0 | 0 | 0 |
| 16 | 0 | 0 | 0 | 0 | 0 | 0 | 0 | 0 |
| 17 | 0 | 0 | 0 | 0 | 0 | 0 | 0 | 0 |
| 18 | 0 | 0 | 0 | 0 | 0 | 0 | 0 | 0 |
| 19 | 0 | 0 | 0 | 0 | 0 | 0 | 0 | 0 |
| 20 | 0 | 0 | 0 | 0 | 0 | 0 | 0 | 0 |
| 21 | 0 | 0 | 0 | 0 | 0 | 0 | 0 | 0 |
| 22 | 0 | 0 | 0 | 0 | 0 | 0 | 0 | 0 |
| 23 | 0 | 0 | 0 | 0 | 0 | 0 | 0 | 0 |
| 24 | 0 | 0 | 0 | 0 | 0 | 0 | 0 | 0 |
| 25 | 0 | 0 | 0 | 0 | 0 | 0 | 0 | 0 |

Table 4.9: Average high-NO_x SOA yields with uncertainties (\pm st. dev) constructed from scenarios and Monte Carlo analysis

| Carbon Number | Straight-chain Alkanes | Branched Alkanes | Cycloalkanes (Single Straight Alkyl Chain) | Cycloalkanes (Branched or Multiple Alkyl Chain(s)) | Bicycloalkanes | Tricycloalkanes | Aromatics | Polycyclic Aromatic Compounds |
|---------------|------------------------|------------------|--|--|---------------------|---------------------|-------------------|-------------------------------|
| 1 | -- | -- | -- | -- | -- | -- | -- | -- |
| 2 | -- | -- | -- | -- | -- | -- | -- | -- |
| 3 | -- | -- | -- | -- | -- | -- | -- | -- |
| 4 | -- | -- | -- | -- | -- | -- | -- | -- |
| 5 | -- | -- | -- | -- | -- | -- | -- | -- |
| 6 | -- | -- | 0.0004 \pm 0.0003 | -- | -- | -- | 0.14 | -- |
| 7 | -- | -- | 0.0007 \pm 0.0006 | 0.0001 \pm 0.0001 | -- | -- | 0.083 | -- |
| 8 | 0.0006 | 0.0001 | 0.0015 \pm 0.0011 | 0.0002 \pm 0.0002 | -- | -- | 0.048 | -- |
| 9 | 0.0012 | 0.0002 | 0.0031 \pm 0.0020 | 0.0005 \pm 0.0003 | 0.0005 \pm 0.0002 | -- | 0.077 \pm 0.057 | -- |
| 10 | 0.0026 | 0.0004 | 0.0059 \pm 0.0039 | 0.0010 \pm 0.0006 | 0.0010 \pm 0.0005 | -- | 0.12 \pm 0.08 | 0.17 \pm 0.09 |
| 11 | 0.0053 | 0.0008 | 0.010 \pm 0.006 | 0.0018 \pm 0.0011 | 0.0018 \pm 0.0008 | -- | 0.15 \pm 0.11 | 0.23 \pm 0.11 |
| 12 | 0.010 | 0.0017 | 0.016 \pm 0.010 | 0.0034 \pm 0.0022 | 0.0031 \pm 0.0015 | 0.0032 \pm 0.0015 | 0.19 \pm 0.16 | 0.28 \pm 0.15 |
| 13 | 0.019 | 0.0035 | 0.026 \pm 0.016 | 0.0062 \pm 0.0042 | 0.0056 \pm 0.0029 | 0.0057 \pm 0.0030 | 0.26 \pm 0.27 | 0.40 \pm 0.23 |
| 14 | 0.033 | 0.0070 | 0.041 \pm 0.026 | 0.011 \pm 0.008 | 0.0097 \pm 0.0056 | 0.0098 \pm 0.0057 | 0.33 \pm 0.38 | 0.49 \pm 0.31 |
| 15 | 0.055 | 0.013 | 0.064 \pm 0.042 | 0.019 \pm 0.014 | 0.016 \pm 0.010 | 0.017 \pm 0.010 | 0.39 \pm 0.45 | 0.62 \pm 0.32 |
| 16 | 0.089 | 0.024 | 0.099 \pm 0.071 | 0.031 \pm 0.024 | 0.026 \pm 0.017 | 0.027 \pm 0.018 | 0.43 \pm 0.47 | 0.70 \pm 0.35 |
| 17 | 0.14 | 0.042 | 0.16 \pm 0.11 | 0.053 \pm 0.039 | 0.044 \pm 0.028 | 0.045 \pm 0.028 | 0.46 \pm 0.48 | 0.75 \pm 0.37 |
| 18 | 0.23 | 0.073 | 0.24 \pm 0.17 | 0.088 \pm 0.065 | 0.072 \pm 0.045 | 0.073 \pm 0.045 | 0.51 \pm 0.47 | 0.79 \pm 0.40 |
| 19 | 0.37 | 0.12 | 0.36 \pm 0.23 | 0.14 \pm 0.10 | 0.12 \pm 0.07 | 0.12 \pm 0.07 | 0.56 \pm 0.48 | 0.82 \pm 0.42 |
| 20 | 0.56 | 0.20 | 0.50 \pm 0.26 | 0.22 \pm 0.15 | 0.19 \pm 0.12 | 0.19 \pm 0.12 | 0.61 \pm 0.50 | 0.82 \pm 0.42 |
| 21 | 0.77 | 0.32 | 0.66 \pm 0.27 | 0.33 \pm 0.19 | 0.29 \pm 0.17 | 0.30 \pm 0.18 | 0.65 \pm 0.52 | 0.82 \pm 0.42 |
| 22 | 0.96 | 0.47 | 0.82 \pm 0.26 | 0.45 \pm 0.23 | 0.43 \pm 0.24 | 0.43 \pm 0.24 | 0.67 \pm 0.54 | 0.82 \pm 0.42 |
| 23 | 1.08 | 0.61 | 0.94 \pm 0.23 | 0.57 \pm 0.25 | 0.56 \pm 0.28 | 0.57 \pm 0.28 | 0.68 \pm 0.55 | 0.82 \pm 0.42 |
| 24 | 1.14 | 0.70 | 1.03 \pm 0.20 | 0.67 \pm 0.25 | 0.66 \pm 0.29 | 0.67 \pm 0.30 | 0.68 \pm 0.55 | 0.82 \pm 0.42 |
| 25 | 1.16 | 0.75 | 1.09 \pm 0.17 | 0.73 \pm 0.23 | 0.74 \pm 0.28 | 0.74 \pm 0.28 | 0.68 \pm 0.55 | 0.82 \pm 0.42 |

Table 4.10: Compound specific liquid gasoline speciation for California in Summer 2010

| Compound | Weight percentage in fuel [% weight by carbon (\pm St. Dev)] | | | | | Molar percentage in fuel [% mol (\pm St. Dev)] | | | | |
|-----------------------|---|-------------|-------------|-------------|-------------|---|-------------|--------------|-------------|-------------|
| | Statewide | Bakersfield | Berkeley | Pasadena | Sacramento | Statewide | Bakersfield | Berkeley | Pasadena | Sacramento |
| ethane | 0.000±0.000 | 0.001±0.000 | 0.000±0.000 | 0.000±0.000 | 0.000±0.000 | 0.001±0.000 | 0.004±0.001 | 0.000±0.000 | 0.001±0.000 | 0.000±0.000 |
| propane | 0.014±0.001 | 0.030±0.003 | 0.006±0.002 | 0.006±0.001 | 0.012±0.003 | 0.027±0.002 | 0.060±0.006 | 0.012±0.003 | 0.011±0.002 | 0.024±0.006 |
| n-butane | 0.500±0.038 | 0.692±0.049 | 0.420±0.074 | 0.478±0.098 | 0.411±0.074 | 0.747±0.057 | 1.025±0.073 | 0.626±0.110 | 0.722±0.148 | 0.615±0.110 |
| n-pentane | 2.839±0.220 | 3.920±0.207 | 2.487±0.484 | 2.582±0.533 | 2.366±0.459 | 3.376±0.261 | 4.635±0.247 | 2.957±0.574 | 3.080±0.634 | 2.830±0.548 |
| n-hexane | 1.837±0.156 | 2.117±0.037 | 1.715±0.351 | 1.841±0.386 | 1.674±0.341 | 1.821±0.155 | 2.085±0.037 | 1.698±0.347 | 1.832±0.383 | 1.668±0.340 |
| n-heptane | 1.385±0.116 | 1.538±0.026 | 1.652±0.329 | 1.093±0.214 | 1.257±0.248 | 1.177±0.099 | 1.299±0.022 | 1.403±0.279 | 0.933±0.182 | 1.074±0.211 |
| n-octane | 0.621±0.052 | 0.690±0.015 | 0.710±0.141 | 0.493±0.097 | 0.593±0.119 | 0.462±0.039 | 0.510±0.011 | 0.527±0.105 | 0.368±0.072 | 0.444±0.089 |
| n-nonane | 0.278±0.024 | 0.303±0.012 | 0.298±0.061 | 0.237±0.047 | 0.275±0.056 | 0.184±0.016 | 0.199±0.008 | 0.197±0.040 | 0.158±0.031 | 0.182±0.037 |
| n-decane | 0.116±0.011 | 0.100±0.003 | 0.099±0.020 | 0.147±0.030 | 0.117±0.023 | 0.069±0.006 | 0.059±0.002 | 0.059±0.012 | 0.088±0.018 | 0.070±0.014 |
| n-undecane | 0.063±0.007 | 0.034±0.002 | 0.054±0.012 | 0.098±0.022 | 0.065±0.013 | 0.034±0.004 | 0.018±0.001 | 0.029±0.006 | 0.054±0.012 | 0.036±0.007 |
| n-dodecane | 0.017±0.003 | 0.004±0.000 | 0.010±0.002 | 0.045±0.011 | 0.011±0.003 | 0.009±0.001 | 0.002±0.000 | 0.005±0.001 | 0.022±0.005 | 0.006±0.001 |
| n-tridecane | 0.008±0.001 | 0.002±0.000 | 0.002±0.000 | 0.025±0.005 | 0.004±0.001 | 0.004±0.001 | 0.001±0.000 | 0.001±0.000 | 0.012±0.003 | 0.002±0.000 |
| n-tetradecane | 0.004±0.001 | 0.001±0.000 | 0.001±0.000 | 0.011±0.002 | 0.002±0.000 | 0.002±0.000 | 0.000±0.000 | 0.000±0.000 | 0.005±0.001 | 0.001±0.000 |
| n-pentadecane | 0.004±0.001 | 0.002±0.000 | 0.003±0.001 | 0.007±0.002 | 0.003±0.000 | 0.002±0.000 | 0.001±0.000 | 0.001±0.000 | 0.003±0.001 | 0.001±0.000 |
| 2-methylpropane | 0.057±0.006 | 0.085±0.009 | 0.043±0.011 | 0.078±0.018 | 0.023±0.004 | 0.085±0.009 | 0.125±0.014 | 0.064±0.017 | 0.119±0.027 | 0.034±0.006 |
| 2-methylbutane | 7.821±0.646 | 7.166±0.192 | 8.426±1.555 | 7.475±1.393 | 8.216±1.508 | 9.321±0.770 | 8.470±0.219 | 10.032±1.849 | 8.946±1.661 | 9.838±1.803 |
| 2,2-dimethylpropane | 0.008±0.001 | 0.009±0.001 | 0.007±0.001 | 0.007±0.002 | 0.008±0.001 | 0.009±0.001 | 0.011±0.001 | 0.009±0.002 | 0.009±0.002 | 0.010±0.002 |
| 2-methylpentane | 3.858±0.344 | 3.283±0.246 | 4.323±0.832 | 3.922±0.776 | 3.906±0.736 | 3.829±0.341 | 3.231±0.238 | 4.287±0.824 | 3.904±0.769 | 3.895±0.733 |
| 3-methylpentane | 2.412±0.212 | 2.097±0.135 | 2.664±0.511 | 2.408±0.474 | 2.479±0.466 | 2.394±0.210 | 2.064±0.131 | 2.642±0.505 | 2.399±0.470 | 2.473±0.464 |
| 2,2-dimethylbutane | 0.902±0.106 | 0.585±0.107 | 1.303±0.304 | 0.728±0.201 | 0.991±0.186 | 0.894±0.105 | 0.575±0.104 | 1.291±0.300 | 0.721±0.199 | 0.989±0.185 |
| 2,3-dimethylbutane | 1.341±0.109 | 1.196±0.064 | 1.327±0.237 | 1.418±0.254 | 1.423±0.256 | 1.333±0.109 | 1.178±0.062 | 1.318±0.235 | 1.417±0.253 | 1.421±0.255 |
| 2-methylhexane | 1.339±0.137 | 1.164±0.078 | 1.813±0.386 | 1.090±0.266 | 1.288±0.270 | 1.136±0.116 | 0.981±0.065 | 1.538±0.328 | 0.925±0.225 | 1.100±0.230 |
| 3-methylhexane | 1.981±0.174 | 1.883±0.053 | 2.368±0.474 | 1.850±0.359 | 1.823±0.355 | 1.685±0.148 | 1.590±0.044 | 2.011±0.402 | 1.579±0.305 | 1.557±0.303 |
| 3-ethylpentane | 0.087±0.011 | 0.108±0.012 | 0.142±0.036 | 0.054±0.019 | 0.045±0.016 | 0.074±0.010 | 0.091±0.010 | 0.120±0.031 | 0.045±0.016 | 0.038±0.014 |
| 2,2-dimethylpentane | 0.113±0.010 | 0.129±0.002 | 0.121±0.027 | 0.113±0.024 | 0.089±0.017 | 0.096±0.008 | 0.109±0.002 | 0.103±0.023 | 0.096±0.020 | 0.076±0.014 |
| 2,3-dimethylpentane | 2.720±0.218 | 3.048±0.124 | 1.999±0.348 | 3.581±0.671 | 2.251±0.418 | 2.324±0.188 | 2.579±0.107 | 1.704±0.296 | 3.086±0.580 | 1.927±0.358 |
| 2,4-dimethylpentane | 1.200±0.093 | 1.292±0.051 | 0.874±0.148 | 1.516±0.269 | 1.116±0.204 | 1.025±0.080 | 1.093±0.044 | 0.745±0.126 | 1.304±0.232 | 0.956±0.174 |
| 3,3-Dimethylpentane | 0.112±0.010 | 0.133±0.002 | 0.111±0.029 | 0.112±0.023 | 0.093±0.018 | 0.095±0.009 | 0.112±0.001 | 0.094±0.025 | 0.096±0.019 | 0.080±0.015 |
| 2,2,3-Trimethylbutane | 0.044±0.003 | 0.044±0.000 | 0.042±0.007 | 0.044±0.008 | 0.044±0.008 | 0.037±0.003 | 0.037±0.000 | 0.036±0.006 | 0.038±0.007 | 0.038±0.007 |
| 2-Methylheptane | 0.940±0.078 | 0.990±0.013 | 0.976±0.191 | 0.913±0.176 | 0.882±0.171 | 0.700±0.058 | 0.731±0.010 | 0.726±0.141 | 0.683±0.132 | 0.660±0.128 |
| 3-Methylheptane | 1.014±0.083 | 1.115±0.015 | 1.089±0.213 | 0.917±0.180 | 0.936±0.181 | 0.754±0.062 | 0.824±0.011 | 0.809±0.158 | 0.684±0.134 | 0.700±0.135 |
| 4-Methylheptane | 0.427±0.034 | 0.456±0.005 | 0.443±0.085 | 0.399±0.076 | 0.409±0.077 | 0.318±0.026 | 0.337±0.004 | 0.330±0.063 | 0.299±0.056 | 0.306±0.058 |
| 2,2-dimethylhexane | 0.059±0.005 | 0.080±0.004 | 0.068±0.015 | 0.045±0.009 | 0.045±0.008 | 0.044±0.004 | 0.059±0.003 | 0.050±0.011 | 0.033±0.007 | 0.033±0.006 |
| 2,4-dimethylhexane | 0.622±0.047 | 0.630±0.011 | 0.575±0.099 | 0.638±0.112 | 0.645±0.114 | 0.464±0.035 | 0.466±0.008 | 0.429±0.074 | 0.479±0.084 | 0.483±0.086 |
| 2,5-dimethylhexane | 0.604±0.046 | 0.599±0.012 | 0.544±0.092 | 0.585±0.101 | 0.688±0.121 | 0.451±0.034 | 0.443±0.009 | 0.406±0.069 | 0.439±0.075 | 0.516±0.091 |
| 3,3-dimethylhexane | 0.070±0.006 | 0.097±0.005 | 0.078±0.016 | 0.050±0.010 | 0.054±0.010 | 0.052±0.004 | 0.072±0.004 | 0.058±0.012 | 0.037±0.007 | 0.041±0.008 |
| 2-Me-3-Et-pentane | 0.572±0.043 | 0.577±0.011 | 0.503±0.086 | 0.596±0.104 | 0.611±0.109 | 0.427±0.032 | 0.427±0.009 | 0.375±0.064 | 0.448±0.078 | 0.458±0.081 |
| 2,2,3-triMe-pentane | 0.167±0.014 | 0.152±0.005 | 0.146±0.026 | 0.145±0.025 | 0.226±0.040 | 0.125±0.010 | 0.113±0.004 | 0.109±0.019 | 0.109±0.019 | 0.170±0.030 |
| 2,2,4-triMe-pentane | 3.639±0.293 | 3.171±0.123 | 2.871±0.496 | 4.106±0.706 | 4.406±0.786 | 2.724±0.220 | 2.346±0.090 | 2.148±0.371 | 3.094±0.532 | 3.306±0.590 |
| 2,3,3-triMe-pentane | 1.374±0.112 | 1.261±0.042 | 1.168±0.205 | 1.161±0.202 | 1.904±0.340 | 1.026±0.084 | 0.934±0.031 | 0.873±0.153 | 0.871±0.152 | 1.428±0.255 |
| 2,3,4-triMe-pentane | 1.405±0.111 | 1.330±0.043 | 1.153±0.195 | 1.325±0.227 | 1.810±0.324 | 1.050±0.083 | 0.985±0.032 | 0.862±0.146 | 0.998±0.171 | 1.357±0.243 |
| 2,2,5-trimethylhexane | 0.894±0.083 | 0.896±0.041 | 0.874±0.205 | 0.656±0.117 | 1.148±0.228 | 0.594±0.055 | 0.590±0.028 | 0.582±0.137 | 0.438±0.078 | 0.767±0.152 |
| 2,3,5-trimethylhexane | 0.183±0.016 | 0.194±0.008 | 0.174±0.038 | 0.141±0.025 | 0.225±0.043 | 0.122±0.010 | 0.128±0.005 | 0.116±0.025 | 0.094±0.017 | 0.150±0.028 |
| 2,4,4-trimethylhexane | 0.089±0.008 | 0.072±0.003 | 0.072±0.014 | 0.109±0.021 | 0.104±0.019 | 0.059±0.005 | 0.047±0.002 | 0.048±0.009 | 0.073±0.014 | 0.069±0.013 |
| 2,4-dimethylheptane | 0.115±0.009 | 0.144±0.007 | 0.118±0.023 | 0.090±0.018 | 0.105±0.019 | 0.076±0.006 | 0.095±0.004 | 0.078±0.015 | 0.060±0.012 | 0.070±0.013 |
| 2,6-dimethylheptane | 0.186±0.018 | 0.165±0.003 | 0.168±0.035 | 0.227±0.050 | 0.184±0.036 | 0.123±0.012 | 0.108±0.002 | 0.111±0.023 | 0.152±0.033 | 0.122±0.024 |
| 2,5-dimethylheptane | 0.009±0.001 | 0.010±0.000 | 0.010±0.002 | 0.008±0.002 | 0.010±0.002 | 0.006±0.001 | 0.006±0.000 | 0.006±0.001 | 0.005±0.001 | 0.007±0.001 |

| | | | | | | | | | | |
|------------------------------|-------------|-------------|-------------|-------------|-------------|-------------|-------------|-------------|-------------|-------------|
| 3,5-dimethylheptane | 0.391±0.031 | 0.448±0.016 | 0.360±0.069 | 0.383±0.073 | 0.375±0.071 | 0.259±0.021 | 0.294±0.010 | 0.238±0.046 | 0.255±0.049 | 0.249±0.047 |
| 2,3-dimethylheptane | 0.121±0.009 | 0.130±0.004 | 0.119±0.022 | 0.108±0.020 | 0.129±0.023 | 0.080±0.006 | 0.085±0.003 | 0.079±0.014 | 0.071±0.013 | 0.086±0.016 |
| 3,4-dimethylheptane | 0.058±0.005 | 0.057±0.001 | 0.053±0.010 | 0.063±0.013 | 0.060±0.011 | 0.038±0.003 | 0.037±0.001 | 0.035±0.007 | 0.042±0.008 | 0.040±0.007 |
| 3,3-dimethylheptane | 0.039±0.004 | 0.029±0.001 | 0.028±0.006 | 0.059±0.013 | 0.039±0.008 | 0.026±0.003 | 0.019±0.001 | 0.019±0.004 | 0.040±0.009 | 0.026±0.005 |
| 4,4-dimethylheptane | 0.030±0.003 | 0.024±0.002 | 0.022±0.004 | 0.047±0.010 | 0.027±0.006 | 0.020±0.002 | 0.016±0.001 | 0.014±0.003 | 0.032±0.007 | 0.018±0.004 |
| 2-methyloctane | 0.323±0.027 | 0.343±0.007 | 0.313±0.063 | 0.322±0.063 | 0.314±0.063 | 0.214±0.018 | 0.225±0.005 | 0.207±0.042 | 0.214±0.042 | 0.209±0.042 |
| 3-methyloctane | 0.400±0.033 | 0.437±0.014 | 0.382±0.076 | 0.389±0.074 | 0.393±0.076 | 0.265±0.022 | 0.287±0.009 | 0.253±0.050 | 0.259±0.049 | 0.261±0.050 |
| 4-methyloctane | 0.274±0.023 | 0.312±0.011 | 0.269±0.054 | 0.260±0.051 | 0.257±0.051 | 0.182±0.015 | 0.205±0.007 | 0.178±0.036 | 0.173±0.034 | 0.171±0.034 |
| 3-ethylheptane | 0.090±0.008 | 0.098±0.003 | 0.092±0.019 | 0.078±0.017 | 0.094±0.019 | 0.060±0.005 | 0.064±0.002 | 0.061±0.012 | 0.051±0.011 | 0.062±0.013 |
| 4-ethylheptane | 0.054±0.004 | 0.064±0.003 | 0.053±0.010 | 0.048±0.009 | 0.051±0.010 | 0.036±0.003 | 0.043±0.002 | 0.035±0.007 | 0.032±0.006 | 0.034±0.007 |
| 2,2-dimethylheptane | 0.024±0.002 | 0.040±0.003 | 0.024±0.005 | 0.015±0.003 | 0.017±0.003 | 0.016±0.001 | 0.026±0.002 | 0.016±0.003 | 0.010±0.002 | 0.011±0.002 |
| 3-Me-4-Et-hexane | 0.029±0.002 | 0.037±0.002 | 0.030±0.006 | 0.020±0.004 | 0.028±0.005 | 0.019±0.001 | 0.024±0.001 | 0.020±0.004 | 0.013±0.003 | 0.019±0.003 |
| 2,2,3-trimethylhexane | 0.020±0.003 | 0.047±0.005 | 0.022±0.009 | 0.000±0.000 | 0.012±0.004 | 0.013±0.002 | 0.031±0.003 | 0.014±0.006 | 0.000±0.000 | 0.008±0.002 |
| 2-methylnonane | 0.111±0.010 | 0.101±0.002 | 0.105±0.022 | 0.120±0.025 | 0.119±0.025 | 0.066±0.006 | 0.060±0.001 | 0.062±0.013 | 0.072±0.015 | 0.071±0.015 |
| 3-methylnonane | 0.110±0.010 | 0.108±0.004 | 0.104±0.022 | 0.114±0.023 | 0.113±0.023 | 0.065±0.006 | 0.064±0.002 | 0.062±0.013 | 0.068±0.014 | 0.068±0.014 |
| 4-methylnonane | 0.145±0.015 | 0.207±0.006 | 0.116±0.030 | 0.074±0.023 | 0.182±0.046 | 0.086±0.009 | 0.123±0.004 | 0.069±0.018 | 0.044±0.014 | 0.109±0.027 |
| 3-ethyloctane | 0.004±0.001 | 0.000±0.000 | 0.001±0.001 | 0.010±0.003 | 0.005±0.002 | 0.003±0.000 | 0.000±0.000 | 0.001±0.000 | 0.006±0.002 | 0.003±0.001 |
| 4-ethyloctane | 0.048±0.004 | 0.044±0.002 | 0.043±0.008 | 0.054±0.011 | 0.050±0.010 | 0.029±0.003 | 0.026±0.001 | 0.026±0.005 | 0.033±0.006 | 0.030±0.006 |
| 2,2-dimethyloctane | 0.055±0.005 | 0.057±0.003 | 0.050±0.010 | 0.058±0.012 | 0.055±0.011 | 0.033±0.003 | 0.034±0.002 | 0.030±0.006 | 0.035±0.007 | 0.033±0.007 |
| 2,3-dimethyloctane | 0.042±0.004 | 0.038±0.002 | 0.035±0.007 | 0.053±0.012 | 0.040±0.008 | 0.025±0.003 | 0.022±0.001 | 0.021±0.004 | 0.032±0.008 | 0.024±0.005 |
| 2,6-dimethyloctane | 0.019±0.003 | 0.004±0.001 | 0.011±0.004 | 0.037±0.010 | 0.024±0.006 | 0.011±0.002 | 0.002±0.001 | 0.006±0.002 | 0.022±0.006 | 0.014±0.004 |
| 4,4-dimethyloctane | 0.022±0.002 | 0.021±0.001 | 0.020±0.004 | 0.026±0.005 | 0.023±0.005 | 0.013±0.001 | 0.012±0.000 | 0.012±0.002 | 0.015±0.003 | 0.014±0.003 |
| 2-methyldecane | 0.046±0.004 | 0.053±0.002 | 0.031±0.006 | 0.043±0.008 | 0.059±0.011 | 0.025±0.002 | 0.029±0.001 | 0.017±0.003 | 0.024±0.004 | 0.032±0.006 |
| 3-methyldecane | 0.033±0.004 | 0.020±0.001 | 0.030±0.008 | 0.048±0.011 | 0.036±0.008 | 0.018±0.002 | 0.010±0.001 | 0.016±0.004 | 0.026±0.006 | 0.020±0.004 |
| 2,6-dimethylnonane | 0.025±0.004 | 0.012±0.001 | 0.018±0.004 | 0.047±0.012 | 0.024±0.005 | 0.014±0.002 | 0.007±0.000 | 0.010±0.002 | 0.026±0.007 | 0.013±0.003 |
| C-11 Isoparaffins | 0.012±0.001 | 0.009±0.000 | 0.010±0.002 | 0.017±0.003 | 0.013±0.002 | 0.006±0.001 | 0.005±0.000 | 0.005±0.001 | 0.009±0.002 | 0.007±0.001 |
| C-11 Isoparaf alkyl | 0.026±0.003 | 0.019±0.001 | 0.018±0.004 | 0.041±0.010 | 0.026±0.006 | 0.014±0.002 | 0.011±0.001 | 0.010±0.002 | 0.022±0.006 | 0.014±0.003 |
| 223-triMethylheptane | 0.068±0.006 | 0.070±0.003 | 0.062±0.012 | 0.070±0.014 | 0.069±0.014 | 0.041±0.003 | 0.042±0.002 | 0.037±0.007 | 0.042±0.008 | 0.041±0.008 |
| 224-triMe-heptane | 0.031±0.002 | 0.029±0.001 | 0.026±0.005 | 0.030±0.005 | 0.039±0.007 | 0.019±0.001 | 0.017±0.001 | 0.016±0.003 | 0.018±0.003 | 0.023±0.004 |
| 225-triMe-heptane | 0.067±0.007 | 0.046±0.010 | 0.067±0.014 | 0.085±0.017 | 0.069±0.013 | 0.040±0.004 | 0.027±0.006 | 0.040±0.008 | 0.051±0.011 | 0.041±0.008 |
| 236-triMe-heptane | 0.077±0.006 | 0.082±0.004 | 0.058±0.010 | 0.088±0.016 | 0.079±0.014 | 0.046±0.004 | 0.049±0.002 | 0.035±0.006 | 0.053±0.009 | 0.047±0.008 |
| 244-triMe-heptane | 0.152±0.019 | 0.093±0.007 | 0.124±0.029 | 0.235±0.058 | 0.157±0.039 | 0.091±0.011 | 0.055±0.004 | 0.074±0.017 | 0.142±0.035 | 0.094±0.023 |
| 245-triMe-heptane | 0.029±0.002 | 0.026±0.001 | 0.021±0.004 | 0.036±0.007 | 0.030±0.005 | 0.017±0.001 | 0.016±0.001 | 0.013±0.002 | 0.022±0.004 | 0.018±0.003 |
| 246-triMe-heptane | 0.026±0.003 | 0.022±0.000 | 0.020±0.004 | 0.035±0.008 | 0.028±0.005 | 0.016±0.002 | 0.013±0.000 | 0.012±0.002 | 0.021±0.005 | 0.017±0.003 |
| 255-triMe-heptane | 0.120±0.010 | 0.116±0.005 | 0.089±0.015 | 0.147±0.027 | 0.128±0.023 | 0.072±0.006 | 0.069±0.003 | 0.053±0.009 | 0.088±0.016 | 0.077±0.014 |
| 335-triMe-heptane | 0.000±0.000 | 0.000±0.000 | 0.000±0.000 | 0.001±0.000 | 0.000±0.000 | 0.000±0.000 | 0.000±0.000 | 0.000±0.000 | 0.000±0.000 | 0.000±0.000 |
| 22466pentMe-heptane | 0.008±0.002 | 0.000±0.000 | 0.005±0.002 | 0.019±0.006 | 0.007±0.002 | 0.004±0.001 | 0.000±0.000 | 0.003±0.001 | 0.010±0.003 | 0.004±0.001 |
| C-10 Isoparaffin O | 0.027±0.003 | 0.019±0.001 | 0.016±0.003 | 0.047±0.010 | 0.027±0.005 | 0.016±0.002 | 0.011±0.000 | 0.010±0.002 | 0.029±0.006 | 0.016±0.003 |
| 2-Me-3-Et-heptane | 0.047±0.006 | 0.018±0.004 | 0.049±0.010 | 0.066±0.017 | 0.057±0.012 | 0.028±0.004 | 0.011±0.002 | 0.029±0.006 | 0.040±0.011 | 0.034±0.007 |
| 2,6-diMe-hendecane | 0.007±0.001 | 0.005±0.000 | 0.006±0.001 | 0.012±0.002 | 0.006±0.001 | 0.004±0.000 | 0.002±0.000 | 0.003±0.001 | 0.006±0.001 | 0.003±0.001 |
| 2,6,10triM-hendecane | 0.007±0.001 | 0.004±0.000 | 0.004±0.001 | 0.014±0.003 | 0.007±0.001 | 0.004±0.000 | 0.002±0.000 | 0.002±0.000 | 0.007±0.001 | 0.003±0.001 |
| 2,6,10triMe-dodecane | 0.006±0.001 | 0.001±0.000 | 0.005±0.001 | 0.011±0.002 | 0.005±0.001 | 0.003±0.000 | 0.000±0.000 | 0.002±0.001 | 0.005±0.001 | 0.002±0.000 |
| C-9 Naphthenes | 0.047±0.004 | 0.047±0.001 | 0.045±0.009 | 0.047±0.009 | 0.050±0.009 | 0.031±0.003 | 0.031±0.001 | 0.029±0.006 | 0.031±0.006 | 0.033±0.006 |
| Cyclopentane | 0.475±0.037 | 0.615±0.028 | 0.466±0.092 | 0.385±0.079 | 0.432±0.081 | 0.565±0.044 | 0.727±0.033 | 0.554±0.109 | 0.459±0.094 | 0.518±0.097 |
| Methylcyclopentane | 2.669±0.220 | 3.037±0.051 | 2.734±0.550 | 2.470±0.491 | 2.435±0.482 | 2.648±0.219 | 2.992±0.052 | 2.708±0.544 | 2.463±0.488 | 2.428±0.480 |
| Ethylcyclopentane | 0.332±0.029 | 0.369±0.009 | 0.299±0.063 | 0.346±0.070 | 0.314±0.064 | 0.283±0.024 | 0.312±0.007 | 0.254±0.054 | 0.297±0.060 | 0.269±0.055 |
| 1T2-diMecyclopentane | 0.617±0.050 | 0.986±0.079 | 0.529±0.118 | 0.483±0.101 | 0.470±0.096 | 0.525±0.042 | 0.833±0.067 | 0.450±0.100 | 0.414±0.087 | 0.402±0.082 |
| 1C3-diMecyclopentane | 0.679±0.058 | 0.814±0.031 | 0.655±0.146 | 0.638±0.128 | 0.610±0.124 | 0.578±0.050 | 0.687±0.026 | 0.557±0.124 | 0.547±0.110 | 0.521±0.106 |
| 1T3-diMecyclopentane | 0.592±0.050 | 0.741±0.032 | 0.558±0.124 | 0.555±0.112 | 0.515±0.105 | 0.504±0.043 | 0.626±0.027 | 0.474±0.105 | 0.475±0.096 | 0.440±0.090 |
| Propylcyclopentane | 0.024±0.002 | 0.024±0.001 | 0.018±0.004 | 0.029±0.006 | 0.023±0.005 | 0.018±0.002 | 0.018±0.000 | 0.013±0.003 | 0.022±0.005 | 0.018±0.003 |

| | | | | | | | | | | |
|-----------------------------|-------------|-------------|-------------|-------------|-------------|-------------|-------------|-------------|-------------|-------------|
| 112-triMeCyPentane | 0.007±0.001 | 0.006±0.001 | 0.005±0.001 | 0.011±0.002 | 0.006±0.001 | 0.005±0.001 | 0.004±0.000 | 0.004±0.001 | 0.008±0.002 | 0.005±0.001 |
| 113-triMeCyPentane | 0.146±0.012 | 0.204±0.010 | 0.111±0.023 | 0.154±0.032 | 0.117±0.024 | 0.109±0.009 | 0.151±0.007 | 0.083±0.017 | 0.116±0.024 | 0.087±0.018 |
| 1C2C3-triMeCyPentane | 0.004±0.000 | 0.003±0.000 | 0.003±0.001 | 0.005±0.001 | 0.004±0.001 | 0.003±0.000 | 0.002±0.000 | 0.002±0.001 | 0.004±0.001 | 0.003±0.001 |
| 1C2T3-triMeCyPentane | 0.013±0.001 | 0.016±0.000 | 0.013±0.003 | 0.013±0.003 | 0.011±0.002 | 0.010±0.001 | 0.012±0.000 | 0.009±0.002 | 0.010±0.002 | 0.009±0.002 |
| 1T2C3-triMeCyPentane | 0.149±0.012 | 0.221±0.015 | 0.104±0.022 | 0.156±0.034 | 0.113±0.023 | 0.111±0.009 | 0.164±0.011 | 0.078±0.016 | 0.117±0.026 | 0.084±0.017 |
| 1C2C4-triMeCyPentane | 0.005±0.001 | 0.004±0.001 | 0.003±0.001 | 0.008±0.002 | 0.003±0.001 | 0.003±0.000 | 0.002±0.000 | 0.002±0.001 | 0.006±0.001 | 0.003±0.001 |
| 1T2C4-triMeCyPentane | 0.239±0.021 | 0.268±0.007 | 0.189±0.040 | 0.288±0.060 | 0.211±0.044 | 0.178±0.016 | 0.198±0.005 | 0.141±0.030 | 0.216±0.045 | 0.158±0.033 |
| Cyclohexane | 1.076±0.100 | 1.147±0.044 | 1.313±0.289 | 0.820±0.178 | 1.024±0.210 | 1.066±0.099 | 1.130±0.044 | 1.299±0.285 | 0.815±0.177 | 1.021±0.209 |
| Methylcyclohexane | 1.424±0.123 | 1.542±0.028 | 1.361±0.284 | 1.473±0.299 | 1.322±0.267 | 1.212±0.105 | 1.302±0.023 | 1.157±0.241 | 1.262±0.256 | 1.129±0.228 |
| Ethylcyclohexane | 0.191±0.022 | 0.125±0.011 | 0.134±0.032 | 0.312±0.070 | 0.192±0.043 | 0.142±0.017 | 0.092±0.008 | 0.100±0.024 | 0.235±0.053 | 0.144±0.032 |
| 1,1-diMecyclohexane | 0.031±0.003 | 0.041±0.002 | 0.026±0.006 | 0.031±0.007 | 0.026±0.005 | 0.023±0.002 | 0.030±0.002 | 0.019±0.004 | 0.023±0.005 | 0.019±0.004 |
| 1C2-diMecyclohexane | 0.060±0.006 | 0.045±0.002 | 0.047±0.011 | 0.089±0.020 | 0.062±0.013 | 0.045±0.005 | 0.033±0.002 | 0.035±0.008 | 0.067±0.015 | 0.046±0.010 |
| 1T2-diMecyclohexane | 0.121±0.012 | 0.113±0.005 | 0.094±0.019 | 0.164±0.035 | 0.111±0.022 | 0.090±0.009 | 0.083±0.004 | 0.070±0.014 | 0.123±0.027 | 0.083±0.016 |
| 1C3-diMecyclohexane | 0.259±0.027 | 0.220±0.014 | 0.204±0.044 | 0.375±0.082 | 0.239±0.050 | 0.193±0.020 | 0.163±0.010 | 0.151±0.033 | 0.281±0.062 | 0.178±0.037 |
| 1T3-diMecyclohexane | 0.208±0.022 | 0.157±0.011 | 0.161±0.036 | 0.311±0.066 | 0.204±0.042 | 0.155±0.016 | 0.115±0.008 | 0.120±0.027 | 0.233±0.050 | 0.152±0.032 |
| 1C4-diMecyclohexane | 0.051±0.005 | 0.043±0.004 | 0.032±0.007 | 0.085±0.018 | 0.046±0.009 | 0.038±0.004 | 0.032±0.003 | 0.024±0.005 | 0.064±0.014 | 0.034±0.007 |
| Propylcyclohexane | 0.043±0.005 | 0.027±0.001 | 0.032±0.007 | 0.069±0.017 | 0.044±0.010 | 0.029±0.003 | 0.018±0.000 | 0.021±0.005 | 0.046±0.011 | 0.029±0.006 |
| iso-Bu-Cyclohexane | 0.004±0.000 | 0.003±0.000 | 0.004±0.001 | 0.004±0.001 | 0.006±0.001 | 0.003±0.000 | 0.002±0.000 | 0.002±0.001 | 0.003±0.001 | 0.004±0.001 |
| sec-Bu-Cyclohexane | 0.017±0.002 | 0.011±0.000 | 0.014±0.003 | 0.023±0.005 | 0.019±0.004 | 0.010±0.001 | 0.007±0.000 | 0.008±0.002 | 0.014±0.003 | 0.011±0.002 |
| 113-t4-tetraMeCyPent | 0.113±0.011 | 0.108±0.002 | 0.090±0.020 | 0.143±0.030 | 0.111±0.023 | 0.075±0.007 | 0.071±0.001 | 0.060±0.014 | 0.096±0.020 | 0.074±0.015 |
| 1Me-1EtCyclopentane | 0.100±0.010 | 0.109±0.004 | 0.072±0.017 | 0.136±0.031 | 0.082±0.020 | 0.074±0.008 | 0.080±0.003 | 0.053±0.013 | 0.103±0.023 | 0.061±0.015 |
| 1Me-C2EtCyclopentane | 0.055±0.006 | 0.040±0.002 | 0.050±0.012 | 0.069±0.014 | 0.063±0.013 | 0.041±0.004 | 0.030±0.001 | 0.037±0.009 | 0.052±0.011 | 0.047±0.010 |
| 1MeC3EtCyclopentane | 0.165±0.016 | 0.143±0.005 | 0.135±0.031 | 0.219±0.046 | 0.165±0.035 | 0.123±0.012 | 0.106±0.003 | 0.100±0.023 | 0.165±0.034 | 0.123±0.026 |
| 1-M-t-3-Et Cypentane | 0.164±0.016 | 0.149±0.005 | 0.126±0.028 | 0.223±0.045 | 0.161±0.033 | 0.123±0.012 | 0.110±0.004 | 0.093±0.020 | 0.167±0.034 | 0.120±0.024 |
| 1MeC3EtCyclohexane | 0.082±0.008 | 0.095±0.004 | 0.055±0.011 | 0.086±0.018 | 0.091±0.022 | 0.054±0.005 | 0.063±0.003 | 0.037±0.008 | 0.057±0.012 | 0.061±0.015 |
| 1MeC4EtCyclohexane | 0.011±0.001 | 0.007±0.001 | 0.009±0.002 | 0.015±0.003 | 0.013±0.002 | 0.007±0.001 | 0.005±0.000 | 0.006±0.001 | 0.010±0.002 | 0.009±0.002 |
| 1MeT4Etcyclohexane | 0.032±0.003 | 0.025±0.000 | 0.026±0.006 | 0.044±0.010 | 0.034±0.007 | 0.022±0.002 | 0.016±0.000 | 0.017±0.004 | 0.030±0.007 | 0.023±0.005 |
| 113-triMecyclohexane | 0.048±0.004 | 0.045±0.001 | 0.043±0.009 | 0.056±0.011 | 0.048±0.009 | 0.032±0.003 | 0.030±0.000 | 0.029±0.006 | 0.037±0.007 | 0.032±0.006 |
| 1C2C3-triMeCyhexane | 0.000±0.000 | 0.000±0.000 | 0.000±0.000 | 0.000±0.000 | 0.000±0.000 | 0.000±0.000 | 0.000±0.000 | 0.000±0.000 | 0.000±0.000 | 0.000±0.000 |
| 1C2T3-triMeCyhexane | 0.023±0.002 | 0.021±0.002 | 0.018±0.004 | 0.029±0.006 | 0.023±0.005 | 0.015±0.001 | 0.014±0.001 | 0.012±0.003 | 0.019±0.004 | 0.015±0.003 |
| 1C3T5-triMeCyhexane | 0.142±0.015 | 0.105±0.004 | 0.106±0.022 | 0.215±0.047 | 0.144±0.028 | 0.095±0.010 | 0.069±0.003 | 0.070±0.014 | 0.144±0.032 | 0.096±0.018 |
| 1-M-t2-PropCyHexane | 0.062±0.006 | 0.049±0.002 | 0.042±0.007 | 0.089±0.017 | 0.069±0.012 | 0.037±0.003 | 0.029±0.001 | 0.025±0.004 | 0.053±0.010 | 0.041±0.007 |
| C-9 Naphthene A | 0.013±0.001 | 0.010±0.001 | 0.009±0.002 | 0.019±0.004 | 0.014±0.003 | 0.008±0.001 | 0.006±0.001 | 0.006±0.002 | 0.013±0.003 | 0.009±0.002 |
| C-9 Naphthene B | 0.011±0.001 | 0.011±0.000 | 0.008±0.002 | 0.014±0.003 | 0.011±0.002 | 0.007±0.001 | 0.007±0.000 | 0.005±0.001 | 0.009±0.002 | 0.007±0.001 |
| C-9 Naphthene I | 0.014±0.002 | 0.012±0.003 | 0.014±0.004 | 0.004±0.001 | 0.025±0.005 | 0.009±0.001 | 0.008±0.002 | 0.009±0.002 | 0.003±0.001 | 0.017±0.003 |
| C-10 Cyclohexane AA | 0.014±0.002 | 0.003±0.001 | 0.009±0.003 | 0.029±0.008 | 0.013±0.003 | 0.009±0.002 | 0.002±0.001 | 0.006±0.002 | 0.019±0.005 | 0.009±0.002 |
| C-10 Cyclohexane BB | 0.027±0.004 | 0.013±0.001 | 0.017±0.004 | 0.054±0.016 | 0.025±0.005 | 0.016±0.003 | 0.008±0.000 | 0.010±0.002 | 0.032±0.009 | 0.015±0.003 |
| 2MePropylCyclohexane | 0.001±0.001 | 0.000±0.000 | 0.000±0.000 | 0.005±0.003 | 0.000±0.000 | 0.001±0.000 | 0.000±0.000 | 0.000±0.000 | 0.003±0.002 | 0.000±0.000 |
| Benzene | 0.750±0.063 | 0.800±0.017 | 0.725±0.145 | 0.805±0.154 | 0.669±0.134 | 0.744±0.062 | 0.788±0.017 | 0.719±0.143 | 0.804±0.153 | 0.667±0.133 |
| Toluene | 7.523±0.596 | 9.344±0.470 | 8.219±1.614 | 5.710±1.100 | 6.818±1.280 | 6.397±0.506 | 7.904±0.400 | 6.980±1.368 | 4.874±0.935 | 5.829±1.093 |
| Ethylbenzene | 1.433±0.124 | 1.280±0.041 | 1.677±0.324 | 1.302±0.251 | 1.475±0.278 | 1.067±0.092 | 0.946±0.030 | 1.246±0.240 | 0.973±0.187 | 1.103±0.208 |
| o-Xylene | 2.209±0.186 | 2.148±0.027 | 2.455±0.474 | 1.984±0.382 | 2.251±0.423 | 1.645±0.138 | 1.588±0.020 | 1.825±0.352 | 1.483±0.284 | 1.684±0.316 |
| m-Xylene | 4.881±0.409 | 4.831±0.069 | 5.533±1.077 | 4.191±0.804 | 4.969±0.933 | 3.633±0.305 | 3.571±0.053 | 4.113±0.800 | 3.132±0.598 | 3.717±0.698 |
| p-Xylene | 1.168±0.094 | 1.196±0.010 | 1.228±0.232 | 1.082±0.203 | 1.165±0.216 | 0.869±0.070 | 0.884±0.008 | 0.913±0.173 | 0.809±0.151 | 0.871±0.162 |
| Cumene | 0.097±0.009 | 0.090±0.004 | 0.114±0.022 | 0.088±0.018 | 0.096±0.018 | 0.064±0.006 | 0.059±0.002 | 0.076±0.015 | 0.058±0.012 | 0.064±0.012 |
| 1-Me-2-Et-benzene | 0.545±0.046 | 0.519±0.011 | 0.609±0.118 | 0.494±0.096 | 0.556±0.106 | 0.360±0.031 | 0.341±0.007 | 0.403±0.078 | 0.328±0.064 | 0.370±0.070 |
| 1-Me-3-Et-benzene | 1.575±0.133 | 1.501±0.015 | 1.739±0.337 | 1.434±0.274 | 1.626±0.309 | 1.042±0.088 | 0.986±0.010 | 1.149±0.223 | 0.953±0.181 | 1.081±0.205 |
| 1-Me-4-Et-benzene | 0.681±0.057 | 0.667±0.006 | 0.748±0.145 | 0.614±0.118 | 0.695±0.132 | 0.451±0.038 | 0.438±0.004 | 0.494±0.096 | 0.408±0.078 | 0.462±0.087 |
| 123-triMe-benzene | 0.587±0.049 | 0.581±0.012 | 0.606±0.117 | 0.575±0.111 | 0.586±0.112 | 0.388±0.032 | 0.382±0.007 | 0.400±0.077 | 0.382±0.073 | 0.389±0.074 |
| 124-TriMe-benzene | 2.629±0.213 | 2.824±0.044 | 2.705±0.522 | 2.417±0.463 | 2.568±0.485 | 1.739±0.141 | 1.856±0.029 | 1.787±0.344 | 1.606±0.307 | 1.708±0.322 |

| | | | | | | | | | | |
|-----------------------------|-------------|-------------|-------------|-------------|-------------|-------------|-------------|-------------|-------------|-------------|
| 135-triMe-benzene | 0.800±0.065 | 0.881±0.028 | 0.836±0.163 | 0.704±0.133 | 0.781±0.148 | 0.530±0.043 | 0.579±0.019 | 0.552±0.108 | 0.468±0.088 | 0.519±0.098 |
| Butylbenzene | 0.071±0.008 | 0.027±0.008 | 0.084±0.019 | 0.077±0.017 | 0.095±0.020 | 0.042±0.005 | 0.016±0.005 | 0.050±0.011 | 0.047±0.010 | 0.057±0.012 |
| Isobutylbenzene | 0.085±0.007 | 0.071±0.002 | 0.072±0.012 | 0.112±0.021 | 0.087±0.016 | 0.051±0.004 | 0.042±0.001 | 0.043±0.007 | 0.068±0.013 | 0.052±0.009 |
| Sec-butylbenzene | 0.042±0.004 | 0.029±0.002 | 0.050±0.010 | 0.036±0.008 | 0.051±0.011 | 0.025±0.002 | 0.017±0.001 | 0.030±0.006 | 0.022±0.005 | 0.031±0.006 |
| T-butylbenzene | 0.006±0.003 | 0.000±0.000 | 0.000±0.000 | 0.024±0.012 | 0.000±0.000 | 0.004±0.002 | 0.000±0.000 | 0.000±0.000 | 0.015±0.007 | 0.000±0.000 |
| o-Cymene | 0.019±0.002 | 0.012±0.001 | 0.016±0.003 | 0.033±0.007 | 0.014±0.003 | 0.011±0.001 | 0.007±0.001 | 0.010±0.002 | 0.020±0.005 | 0.008±0.002 |
| m-Cymene | 0.066±0.006 | 0.046±0.004 | 0.071±0.014 | 0.075±0.014 | 0.073±0.014 | 0.040±0.004 | 0.027±0.003 | 0.043±0.008 | 0.045±0.009 | 0.044±0.008 |
| p-Cymene | 0.020±0.002 | 0.014±0.001 | 0.021±0.004 | 0.022±0.004 | 0.022±0.004 | 0.012±0.001 | 0.008±0.001 | 0.013±0.003 | 0.013±0.003 | 0.013±0.003 |
| 1234-tetMe-benzene | 0.071±0.006 | 0.068±0.002 | 0.063±0.013 | 0.084±0.016 | 0.067±0.013 | 0.042±0.004 | 0.041±0.001 | 0.038±0.007 | 0.050±0.009 | 0.040±0.007 |
| 1235-tetMe-benzene | 0.230±0.019 | 0.226±0.004 | 0.229±0.044 | 0.249±0.047 | 0.214±0.040 | 0.137±0.011 | 0.134±0.002 | 0.137±0.026 | 0.149±0.028 | 0.128±0.024 |
| 1245-tetMe-benzene | 0.170±0.014 | 0.168±0.003 | 0.173±0.033 | 0.178±0.033 | 0.159±0.030 | 0.101±0.008 | 0.099±0.002 | 0.103±0.020 | 0.107±0.020 | 0.095±0.018 |
| Pentamethylbenzene | 0.015±0.001 | 0.012±0.000 | 0.011±0.002 | 0.023±0.004 | 0.012±0.002 | 0.008±0.001 | 0.007±0.000 | 0.006±0.001 | 0.013±0.002 | 0.007±0.001 |
| Propylbenzene | 0.499±0.043 | 0.453±0.008 | 0.557±0.109 | 0.488±0.093 | 0.498±0.096 | 0.330±0.029 | 0.297±0.005 | 0.368±0.072 | 0.325±0.062 | 0.331±0.064 |
| 1,3-diethylbenzene | 0.108±0.010 | 0.081±0.004 | 0.120±0.024 | 0.113±0.021 | 0.117±0.023 | 0.064±0.006 | 0.048±0.002 | 0.071±0.014 | 0.068±0.013 | 0.070±0.014 |
| 1-Me-3-Pr-benzene | 0.291±0.026 | 0.238±0.008 | 0.321±0.063 | 0.298±0.057 | 0.307±0.060 | 0.174±0.016 | 0.141±0.005 | 0.191±0.037 | 0.179±0.034 | 0.184±0.036 |
| 1-Me-4-Pr-benzene | 0.182±0.016 | 0.172±0.003 | 0.197±0.039 | 0.186±0.035 | 0.175±0.033 | 0.109±0.009 | 0.102±0.002 | 0.117±0.023 | 0.111±0.021 | 0.104±0.020 |
| Indan | 0.274±0.024 | 0.255±0.006 | 0.278±0.055 | 0.265±0.050 | 0.298±0.059 | 0.181±0.016 | 0.167±0.004 | 0.184±0.037 | 0.176±0.033 | 0.198±0.039 |
| 1,4-diethylbenzene | 0.329±0.029 | 0.279±0.005 | 0.349±0.068 | 0.347±0.066 | 0.341±0.065 | 0.196±0.017 | 0.165±0.003 | 0.208±0.040 | 0.208±0.039 | 0.204±0.039 |
| 1-Me-2-Pr-benzene | 0.099±0.009 | 0.077±0.004 | 0.106±0.021 | 0.113±0.022 | 0.100±0.019 | 0.059±0.005 | 0.045±0.002 | 0.063±0.012 | 0.068±0.013 | 0.060±0.011 |
| 14-diMe2Et-benzene | 0.237±0.022 | 0.187±0.006 | 0.253±0.051 | 0.255±0.049 | 0.253±0.050 | 0.141±0.013 | 0.110±0.003 | 0.151±0.030 | 0.153±0.029 | 0.151±0.030 |
| 13-diMe4Et-benzene | 0.193±0.017 | 0.160±0.004 | 0.207±0.041 | 0.201±0.038 | 0.203±0.039 | 0.115±0.010 | 0.095±0.002 | 0.123±0.024 | 0.120±0.023 | 0.122±0.023 |
| 12-diMe4Et-benzene | 0.297±0.026 | 0.256±0.005 | 0.326±0.064 | 0.305±0.058 | 0.302±0.058 | 0.177±0.015 | 0.151±0.003 | 0.194±0.038 | 0.182±0.034 | 0.180±0.035 |
| 13-diMe2Et-benzene | 0.026±0.002 | 0.020±0.001 | 0.025±0.005 | 0.033±0.007 | 0.027±0.005 | 0.016±0.001 | 0.012±0.001 | 0.015±0.003 | 0.020±0.004 | 0.016±0.003 |
| Indene | 0.035±0.003 | 0.027±0.001 | 0.027±0.005 | 0.051±0.011 | 0.035±0.007 | 0.023±0.002 | 0.018±0.001 | 0.018±0.003 | 0.035±0.007 | 0.023±0.004 |
| 12-diMe3Et-benzene | 0.087±0.008 | 0.065±0.003 | 0.091±0.018 | 0.104±0.020 | 0.089±0.017 | 0.052±0.005 | 0.039±0.002 | 0.054±0.011 | 0.062±0.012 | 0.053±0.010 |
| 1-Me35diEt-benzene | 0.032±0.003 | 0.018±0.001 | 0.030±0.007 | 0.047±0.010 | 0.033±0.007 | 0.017±0.002 | 0.010±0.001 | 0.017±0.004 | 0.026±0.005 | 0.018±0.004 |
| 1-Phenyl-2Me butane | 0.031±0.003 | 0.021±0.001 | 0.030±0.005 | 0.040±0.008 | 0.035±0.006 | 0.017±0.002 | 0.011±0.001 | 0.016±0.003 | 0.022±0.004 | 0.019±0.003 |
| 1-Phenyl-3Me butane | 0.014±0.001 | 0.011±0.000 | 0.010±0.002 | 0.019±0.004 | 0.016±0.003 | 0.008±0.001 | 0.006±0.000 | 0.006±0.001 | 0.010±0.002 | 0.009±0.002 |
| 124-triMe-5Etbenzene | 0.026±0.002 | 0.022±0.001 | 0.022±0.004 | 0.036±0.007 | 0.025±0.005 | 0.014±0.001 | 0.012±0.000 | 0.012±0.002 | 0.020±0.004 | 0.013±0.003 |
| 123-triMe-5Etbenzene | 0.024±0.003 | 0.015±0.000 | 0.018±0.004 | 0.045±0.009 | 0.018±0.004 | 0.013±0.001 | 0.008±0.000 | 0.010±0.002 | 0.025±0.005 | 0.010±0.002 |
| 124-triMe-3Etbenzene | 0.006±0.001 | 0.003±0.000 | 0.004±0.001 | 0.011±0.002 | 0.006±0.001 | 0.003±0.000 | 0.002±0.000 | 0.002±0.000 | 0.006±0.001 | 0.003±0.001 |
| 12-diMe-3Pr-benzene | 0.040±0.004 | 0.029±0.001 | 0.039±0.008 | 0.054±0.011 | 0.038±0.008 | 0.022±0.002 | 0.015±0.000 | 0.021±0.005 | 0.030±0.006 | 0.021±0.004 |
| 135-triMe-2Etbenzene | 0.026±0.002 | 0.022±0.001 | 0.022±0.004 | 0.030±0.005 | 0.029±0.005 | 0.014±0.001 | 0.012±0.000 | 0.012±0.002 | 0.016±0.003 | 0.016±0.003 |
| Tetralin | 0.010±0.002 | 0.001±0.000 | 0.001±0.000 | 0.027±0.009 | 0.011±0.004 | 0.006±0.001 | 0.000±0.000 | 0.001±0.000 | 0.016±0.005 | 0.007±0.002 |
| 1-Me-3Bu-benzene | 0.054±0.006 | 0.034±0.002 | 0.054±0.011 | 0.079±0.018 | 0.048±0.010 | 0.029±0.003 | 0.018±0.001 | 0.029±0.006 | 0.043±0.010 | 0.026±0.005 |
| 12-diMe-4Pr-benzene | 0.055±0.005 | 0.045±0.002 | 0.044±0.008 | 0.069±0.012 | 0.061±0.011 | 0.033±0.003 | 0.027±0.001 | 0.026±0.005 | 0.041±0.007 | 0.036±0.006 |
| 125-triMe-3Etbenzene | 0.027±0.003 | 0.020±0.001 | 0.024±0.005 | 0.039±0.007 | 0.024±0.005 | 0.016±0.002 | 0.012±0.000 | 0.014±0.003 | 0.023±0.004 | 0.014±0.003 |
| 123-triMe4Et-benzene | 0.004±0.001 | 0.002±0.000 | 0.003±0.001 | 0.009±0.003 | 0.004±0.001 | 0.003±0.000 | 0.001±0.000 | 0.002±0.000 | 0.006±0.002 | 0.002±0.000 |
| C-11 Aromatic K | 0.017±0.002 | 0.013±0.001 | 0.013±0.002 | 0.026±0.005 | 0.017±0.003 | 0.011±0.001 | 0.008±0.000 | 0.008±0.001 | 0.016±0.003 | 0.010±0.002 |
| Cis-hydrindane | 0.015±0.001 | 0.014±0.001 | 0.013±0.003 | 0.017±0.004 | 0.016±0.003 | 0.010±0.001 | 0.009±0.000 | 0.009±0.002 | 0.012±0.002 | 0.010±0.002 |
| C-7 cyclopentene A | 0.036±0.004 | 0.026±0.003 | 0.019±0.005 | 0.064±0.013 | 0.034±0.007 | 0.030±0.003 | 0.022±0.002 | 0.016±0.004 | 0.055±0.011 | 0.029±0.006 |
| C-7 cyclopentene B | 0.034±0.004 | 0.025±0.003 | 0.018±0.005 | 0.062±0.013 | 0.033±0.007 | 0.029±0.003 | 0.021±0.002 | 0.015±0.004 | 0.053±0.011 | 0.028±0.006 |
| C-11 Aromatic E | 0.059±0.006 | 0.032±0.002 | 0.057±0.012 | 0.086±0.018 | 0.061±0.013 | 0.033±0.003 | 0.018±0.001 | 0.032±0.007 | 0.048±0.010 | 0.033±0.007 |
| C-12 Aromatic A | 0.002±0.000 | 0.003±0.000 | 0.001±0.000 | 0.003±0.002 | 0.001±0.000 | 0.001±0.000 | 0.001±0.000 | 0.000±0.000 | 0.002±0.001 | 0.001±0.000 |
| C-12 Aromatic E | 0.001±0.000 | 0.000±0.000 | 0.001±0.000 | 0.004±0.002 | 0.000±0.000 | 0.001±0.000 | 0.000±0.000 | 0.000±0.000 | 0.002±0.001 | 0.000±0.000 |
| C-12 Aromatic F | 0.005±0.001 | 0.003±0.000 | 0.003±0.001 | 0.011±0.002 | 0.004±0.001 | 0.003±0.000 | 0.001±0.000 | 0.002±0.000 | 0.006±0.001 | 0.002±0.000 |
| Ocetylbenzene | 0.001±0.000 | 0.000±0.000 | 0.000±0.000 | 0.001±0.000 | 0.001±0.000 | 0.000±0.000 | 0.000±0.000 | 0.000±0.000 | 0.000±0.000 | 0.000±0.000 |
| 1-Methylindane | 0.101±0.010 | 0.068±0.003 | 0.097±0.020 | 0.136±0.028 | 0.101±0.020 | 0.060±0.006 | 0.040±0.002 | 0.058±0.012 | 0.081±0.017 | 0.061±0.012 |
| 2-Methylindane | 0.151±0.015 | 0.102±0.004 | 0.149±0.030 | 0.202±0.041 | 0.151±0.031 | 0.090±0.009 | 0.061±0.002 | 0.089±0.018 | 0.122±0.025 | 0.090±0.018 |
| 4-Methylindane | 0.002±0.000 | 0.002±0.001 | 0.004±0.001 | 0.000±0.000 | 0.002±0.001 | 0.001±0.000 | 0.001±0.001 | 0.003±0.001 | 0.000±0.000 | 0.001±0.001 |

| | | | | | | | | | | |
|------------------------------|-------------|-------------|-------------|-------------|-------------|--------------|--------------|--------------|--------------|--------------|
| Dimethylindane A | 0.017±0.002 | 0.011±0.000 | 0.013±0.002 | 0.031±0.006 | 0.014±0.003 | 0.009±0.001 | 0.006±0.000 | 0.007±0.001 | 0.017±0.003 | 0.008±0.001 |
| Dimethylindane B | 0.029±0.004 | 0.012±0.001 | 0.021±0.005 | 0.056±0.012 | 0.025±0.005 | 0.016±0.002 | 0.006±0.000 | 0.012±0.003 | 0.031±0.007 | 0.014±0.003 |
| Dimethylindane C | 0.016±0.002 | 0.006±0.000 | 0.011±0.003 | 0.034±0.008 | 0.014±0.003 | 0.009±0.001 | 0.003±0.000 | 0.006±0.001 | 0.019±0.004 | 0.007±0.002 |
| Dimethylindane E | 0.020±0.003 | 0.009±0.000 | 0.013±0.003 | 0.040±0.009 | 0.017±0.004 | 0.011±0.001 | 0.004±0.000 | 0.007±0.002 | 0.022±0.005 | 0.009±0.002 |
| Dimethylindane F | 0.030±0.003 | 0.017±0.001 | 0.021±0.004 | 0.057±0.012 | 0.024±0.005 | 0.016±0.002 | 0.009±0.000 | 0.012±0.002 | 0.031±0.006 | 0.013±0.002 |
| Dimethylindane G | 0.021±0.003 | 0.009±0.001 | 0.011±0.002 | 0.055±0.011 | 0.011±0.002 | 0.012±0.002 | 0.005±0.000 | 0.006±0.001 | 0.030±0.006 | 0.006±0.001 |
| C-11 Indane H | 0.012±0.002 | 0.006±0.000 | 0.008±0.002 | 0.029±0.006 | 0.008±0.002 | 0.007±0.001 | 0.003±0.000 | 0.004±0.001 | 0.016±0.003 | 0.004±0.001 |
| Biphenyl | 0.005±0.001 | 0.002±0.000 | 0.004±0.001 | 0.007±0.002 | 0.007±0.001 | 0.003±0.000 | 0.001±0.000 | 0.002±0.000 | 0.003±0.001 | 0.004±0.001 |
| Naphthalene | 0.130±0.013 | 0.073±0.005 | 0.140±0.029 | 0.179±0.035 | 0.129±0.026 | 0.078±0.008 | 0.043±0.003 | 0.083±0.017 | 0.108±0.021 | 0.077±0.016 |
| 1-Methylnaphthalene | 0.038±0.004 | 0.022±0.001 | 0.028±0.006 | 0.069±0.014 | 0.032±0.006 | 0.021±0.002 | 0.012±0.001 | 0.015±0.004 | 0.037±0.007 | 0.017±0.003 |
| 2-Methylnaphthalene | 0.090±0.010 | 0.047±0.002 | 0.075±0.016 | 0.168±0.034 | 0.069±0.013 | 0.049±0.005 | 0.025±0.001 | 0.041±0.008 | 0.092±0.019 | 0.038±0.007 |
| 12-DiMe-naphthalene | 0.003±0.000 | 0.002±0.000 | 0.002±0.001 | 0.006±0.001 | 0.003±0.001 | 0.002±0.000 | 0.001±0.000 | 0.001±0.000 | 0.003±0.001 | 0.001±0.000 |
| 13-DiMe-naphthalene | 0.014±0.002 | 0.008±0.000 | 0.012±0.003 | 0.025±0.005 | 0.011±0.002 | 0.007±0.001 | 0.004±0.000 | 0.006±0.001 | 0.013±0.003 | 0.006±0.001 |
| 14-DiMe-naphthalene | 0.000±0.000 | 0.000±0.000 | 0.001±0.000 | 0.001±0.000 | 0.001±0.000 | 0.000±0.000 | 0.000±0.000 | 0.000±0.000 | 0.000±0.000 | 0.000±0.000 |
| 15-DiMe-naphthalene | 0.001±0.000 | 0.000±0.000 | 0.000±0.000 | 0.002±0.000 | 0.001±0.000 | 0.000±0.000 | 0.000±0.000 | 0.000±0.000 | 0.001±0.000 | 0.000±0.000 |
| 16-DiMe-naphthalene | 0.008±0.001 | 0.005±0.000 | 0.006±0.001 | 0.014±0.003 | 0.007±0.001 | 0.004±0.000 | 0.002±0.000 | 0.003±0.001 | 0.007±0.001 | 0.003±0.001 |
| 17-DiMe-naphthalene | 0.000±0.000 | 0.000±0.000 | 0.000±0.000 | 0.000±0.000 | 0.000±0.000 | 0.000±0.000 | 0.000±0.000 | 0.000±0.000 | 0.000±0.000 | 0.000±0.000 |
| 18-DiMe-naphthalene | 0.000±0.000 | 0.000±0.000 | 0.000±0.000 | 0.001±0.000 | 0.000±0.000 | 0.000±0.000 | 0.000±0.000 | 0.000±0.000 | 0.000±0.000 | 0.000±0.000 |
| 23-DiMe-naphthalene | 0.007±0.001 | 0.004±0.000 | 0.006±0.001 | 0.012±0.003 | 0.006±0.001 | 0.003±0.000 | 0.002±0.000 | 0.003±0.001 | 0.006±0.001 | 0.003±0.001 |
| 26-DiMe-naphthalene | 0.002±0.000 | 0.002±0.000 | 0.001±0.000 | 0.003±0.001 | 0.001±0.000 | 0.001±0.000 | 0.001±0.000 | 0.000±0.000 | 0.002±0.000 | 0.001±0.000 |
| 27-DiMe-naphthalene | 0.001±0.000 | 0.001±0.000 | 0.001±0.000 | 0.002±0.000 | 0.002±0.001 | 0.001±0.000 | 0.001±0.000 | 0.000±0.000 | 0.001±0.000 | 0.001±0.000 |
| 1-Ethyl-naphthalene | 0.003±0.000 | 0.002±0.000 | 0.001±0.000 | 0.006±0.001 | 0.003±0.001 | 0.002±0.000 | 0.001±0.000 | 0.001±0.000 | 0.003±0.001 | 0.002±0.000 |
| 2-Ethyl-naphthalene | 0.006±0.001 | 0.003±0.000 | 0.006±0.001 | 0.011±0.002 | 0.004±0.001 | 0.003±0.000 | 0.001±0.000 | 0.003±0.001 | 0.005±0.001 | 0.002±0.000 |
| Acenaphthylene | 0.000±0.000 | 0.000±0.000 | 0.000±0.000 | 0.000±0.000 | 0.000±0.000 | 0.000±0.000 | 0.000±0.000 | 0.000±0.000 | 0.000±0.000 | 0.000±0.000 |
| Acenaphthene | 0.001±0.000 | 0.001±0.000 | 0.000±0.000 | 0.001±0.000 | 0.001±0.000 | 0.000±0.000 | 0.000±0.000 | 0.000±0.000 | 0.000±0.000 | 0.000±0.000 |
| Ethanol | 6.925±0.549 | 7.038±0.031 | 6.854±1.261 | 6.929±1.277 | 6.877±1.267 | 20.638±1.639 | 20.808±0.084 | 20.396±3.745 | 20.763±3.819 | 20.584±3.787 |
| Propene | 0.000±0.000 | 0.000±0.000 | 0.000±0.000 | 0.001±0.000 | 0.000±0.000 | 0.001±0.000 | 0.001±0.000 | 0.000±0.000 | 0.002±0.000 | 0.001±0.000 |
| 1-butene | 0.005±0.001 | 0.003±0.000 | 0.003±0.001 | 0.009±0.002 | 0.004±0.001 | 0.007±0.001 | 0.005±0.000 | 0.005±0.001 | 0.013±0.003 | 0.006±0.001 |
| Cis-2-butene | 0.027±0.004 | 0.017±0.002 | 0.015±0.005 | 0.055±0.013 | 0.020±0.005 | 0.040±0.005 | 0.025±0.002 | 0.022±0.007 | 0.084±0.019 | 0.029±0.007 |
| Trans-2-butene | 0.025±0.003 | 0.015±0.001 | 0.018±0.005 | 0.044±0.010 | 0.022±0.005 | 0.037±0.005 | 0.022±0.002 | 0.026±0.008 | 0.067±0.015 | 0.033±0.008 |
| 2-methylpropene | 0.003±0.000 | 0.002±0.000 | 0.002±0.001 | 0.006±0.001 | 0.003±0.001 | 0.005±0.001 | 0.003±0.000 | 0.003±0.001 | 0.009±0.002 | 0.004±0.001 |
| 1-pentene | 0.102±0.012 | 0.061±0.007 | 0.075±0.023 | 0.168±0.033 | 0.103±0.023 | 0.122±0.014 | 0.072±0.009 | 0.089±0.027 | 0.203±0.040 | 0.124±0.027 |
| Cis-2-pentene | 0.161±0.018 | 0.097±0.011 | 0.121±0.032 | 0.261±0.051 | 0.164±0.036 | 0.192±0.021 | 0.114±0.013 | 0.144±0.038 | 0.314±0.061 | 0.197±0.043 |
| trans-2-pentene | 0.310±0.035 | 0.177±0.021 | 0.252±0.066 | 0.473±0.092 | 0.339±0.077 | 0.371±0.041 | 0.209±0.025 | 0.300±0.078 | 0.569±0.111 | 0.405±0.092 |
| 2-methyl-1-butene | 0.200±0.023 | 0.113±0.015 | 0.154±0.045 | 0.324±0.064 | 0.208±0.046 | 0.239±0.028 | 0.134±0.018 | 0.183±0.053 | 0.391±0.078 | 0.249±0.055 |
| 3-methyl-1-butene | 0.029±0.004 | 0.016±0.003 | 0.024±0.009 | 0.045±0.009 | 0.031±0.007 | 0.034±0.004 | 0.018±0.003 | 0.028±0.010 | 0.054±0.011 | 0.037±0.009 |
| 2-methyl-2-butene | 0.447±0.049 | 0.243±0.028 | 0.386±0.097 | 0.665±0.130 | 0.494±0.109 | 0.534±0.059 | 0.287±0.033 | 0.459±0.115 | 0.800±0.157 | 0.591±0.130 |
| 1-hexene | 0.037±0.004 | 0.029±0.003 | 0.024±0.005 | 0.063±0.012 | 0.031±0.006 | 0.037±0.004 | 0.028±0.003 | 0.024±0.005 | 0.063±0.012 | 0.031±0.006 |
| Cis-2-hexene | 0.074±0.007 | 0.058±0.006 | 0.053±0.011 | 0.100±0.019 | 0.086±0.015 | 0.074±0.007 | 0.057±0.006 | 0.053±0.011 | 0.100±0.019 | 0.086±0.015 |
| Trans-2-hexene | 0.171±0.016 | 0.131±0.017 | 0.135±0.030 | 0.178±0.033 | 0.238±0.044 | 0.170±0.016 | 0.130±0.017 | 0.135±0.030 | 0.178±0.033 | 0.238±0.045 |
| Cis-3-hexene | 0.097±0.009 | 0.076±0.009 | 0.071±0.015 | 0.123±0.023 | 0.117±0.021 | 0.097±0.009 | 0.075±0.008 | 0.071±0.015 | 0.123±0.023 | 0.118±0.021 |
| 2-Me-1-pentene | 0.099±0.009 | 0.075±0.008 | 0.077±0.017 | 0.126±0.024 | 0.118±0.021 | 0.099±0.009 | 0.074±0.008 | 0.077±0.016 | 0.127±0.024 | 0.118±0.021 |
| 4-methyl-1-pentene | 0.044±0.004 | 0.031±0.003 | 0.033±0.007 | 0.066±0.013 | 0.046±0.008 | 0.044±0.004 | 0.031±0.003 | 0.033±0.007 | 0.066±0.013 | 0.046±0.008 |
| 2-methyl-2-pentene | 0.324±0.037 | 0.246±0.047 | 0.293±0.075 | 0.207±0.039 | 0.548±0.112 | 0.322±0.037 | 0.243±0.047 | 0.291±0.075 | 0.207±0.039 | 0.548±0.112 |
| C-3Me-2-pentene | 0.073±0.008 | 0.054±0.006 | 0.048±0.012 | 0.123±0.023 | 0.067±0.014 | 0.073±0.007 | 0.053±0.006 | 0.047±0.012 | 0.123±0.023 | 0.067±0.014 |
| T-3Me-2-pentene | 0.104±0.012 | 0.062±0.013 | 0.061±0.019 | 0.196±0.037 | 0.096±0.022 | 0.103±0.012 | 0.061±0.013 | 0.061±0.019 | 0.196±0.037 | 0.096±0.022 |
| C-4Me-2-pentene | 0.016±0.002 | 0.010±0.002 | 0.013±0.004 | 0.011±0.003 | 0.030±0.008 | 0.016±0.002 | 0.010±0.002 | 0.013±0.004 | 0.011±0.003 | 0.030±0.008 |
| T-4Me-2-pentene | 0.148±0.018 | 0.108±0.024 | 0.138±0.037 | 0.077±0.015 | 0.269±0.057 | 0.147±0.018 | 0.107±0.023 | 0.137±0.037 | 0.077±0.015 | 0.269±0.057 |
| 2-Et-1-butene | 0.026±0.003 | 0.020±0.002 | 0.017±0.004 | 0.046±0.009 | 0.022±0.004 | 0.026±0.003 | 0.020±0.002 | 0.017±0.004 | 0.047±0.009 | 0.022±0.004 |
| 2,3-dimethyl-1-butene | 0.037±0.003 | 0.026±0.003 | 0.030±0.007 | 0.043±0.008 | 0.048±0.009 | 0.037±0.003 | 0.025±0.003 | 0.030±0.007 | 0.043±0.008 | 0.048±0.009 |

| | | | | | | | | | | |
|-------------------------------|-------------|-------------|-------------|-------------|-------------|-------------|-------------|-------------|-------------|-------------|
| 3,3-dimethylbutene | 0.003±0.000 | 0.002±0.000 | 0.002±0.001 | 0.005±0.001 | 0.003±0.001 | 0.003±0.000 | 0.002±0.000 | 0.002±0.001 | 0.005±0.001 | 0.003±0.001 |
| 2,3-dimethyl-2-butene | 0.053±0.005 | 0.039±0.006 | 0.044±0.010 | 0.050±0.009 | 0.078±0.015 | 0.053±0.005 | 0.039±0.006 | 0.044±0.010 | 0.050±0.009 | 0.078±0.015 |
| Nonenes | 0.009±0.001 | 0.012±0.000 | 0.008±0.002 | 0.009±0.002 | 0.007±0.002 | 0.006±0.000 | 0.008±0.000 | 0.005±0.001 | 0.006±0.001 | 0.005±0.001 |
| Undecenes | 0.001±0.000 | 0.000±0.000 | 0.000±0.000 | 0.000±0.000 | 0.003±0.001 | 0.001±0.000 | 0.000±0.000 | 0.000±0.000 | 0.000±0.000 | 0.002±0.001 |
| Tridecenes | 0.001±0.000 | 0.001±0.000 | 0.001±0.000 | 0.001±0.001 | 0.000±0.000 | 0.000±0.000 | 0.000±0.000 | 0.000±0.000 | 0.001±0.000 | 0.000±0.000 |
| Tetradecenes | 0.002±0.000 | 0.002±0.000 | 0.001±0.000 | 0.002±0.000 | 0.002±0.000 | 0.001±0.000 | 0.000±0.000 | 0.000±0.000 | 0.001±0.000 | 0.001±0.000 |
| C-1,3-pentadiene | 0.003±0.000 | 0.002±0.000 | 0.003±0.001 | 0.005±0.001 | 0.003±0.001 | 0.004±0.000 | 0.002±0.000 | 0.003±0.001 | 0.006±0.001 | 0.004±0.001 |
| T-1,3-pentadiene | 0.006±0.001 | 0.004±0.000 | 0.005±0.001 | 0.009±0.002 | 0.006±0.001 | 0.007±0.001 | 0.004±0.000 | 0.006±0.002 | 0.011±0.002 | 0.008±0.002 |
| 2-Me-1,3-butadiene | 0.006±0.001 | 0.004±0.000 | 0.005±0.002 | 0.009±0.002 | 0.007±0.001 | 0.007±0.001 | 0.004±0.000 | 0.006±0.002 | 0.011±0.002 | 0.008±0.002 |
| T-1Me-1,3-pentadiene | 0.000±0.000 | 0.000±0.000 | 0.000±0.000 | 0.000±0.000 | 0.000±0.000 | 0.000±0.000 | 0.000±0.000 | 0.000±0.000 | 0.000±0.000 | 0.000±0.000 |
| 1,7-Octadiene | 0.001±0.000 | 0.001±0.000 | 0.001±0.000 | 0.003±0.001 | 0.001±0.000 | 0.001±0.000 | 0.001±0.000 | 0.001±0.000 | 0.002±0.000 | 0.001±0.000 |
| Cyclopentadiene | 0.004±0.000 | 0.002±0.000 | 0.003±0.001 | 0.007±0.001 | 0.004±0.001 | 0.005±0.001 | 0.003±0.000 | 0.003±0.001 | 0.008±0.002 | 0.005±0.001 |
| 1-Me-cyclopentadiene | 0.006±0.002 | 0.000±0.000 | 0.011±0.004 | 0.011±0.005 | 0.000±0.000 | 0.005±0.002 | 0.000±0.000 | 0.011±0.004 | 0.011±0.005 | 0.000±0.000 |
| Octadiene A | 0.029±0.003 | 0.020±0.002 | 0.020±0.005 | 0.041±0.008 | 0.034±0.007 | 0.021±0.002 | 0.014±0.002 | 0.015±0.004 | 0.031±0.006 | 0.025±0.005 |
| 23-diMe-1-pentene | 0.009±0.001 | 0.007±0.001 | 0.006±0.001 | 0.017±0.003 | 0.007±0.001 | 0.008±0.001 | 0.006±0.001 | 0.005±0.001 | 0.014±0.003 | 0.006±0.001 |
| 24-dime-1-pentene | 0.006±0.001 | 0.005±0.001 | 0.003±0.001 | 0.012±0.002 | 0.004±0.001 | 0.005±0.001 | 0.004±0.001 | 0.003±0.001 | 0.010±0.002 | 0.003±0.001 |
| 33-DiMe-1-pentene | 0.002±0.000 | 0.002±0.000 | 0.002±0.000 | 0.004±0.001 | 0.002±0.000 | 0.002±0.000 | 0.002±0.000 | 0.001±0.000 | 0.004±0.001 | 0.002±0.000 |
| 3,4-Dimethyl-2-Pentene | 0.000±0.000 | 0.000±0.000 | 0.001±0.000 | 0.000±0.000 | 0.000±0.000 | 0.000±0.000 | 0.000±0.000 | 0.001±0.000 | 0.000±0.000 | 0.000±0.000 |
| 44-diMe-1-pentene | 0.009±0.001 | 0.004±0.001 | 0.005±0.001 | 0.024±0.005 | 0.003±0.001 | 0.008±0.001 | 0.003±0.001 | 0.004±0.001 | 0.021±0.004 | 0.003±0.001 |
| 23-diMe-2-pentene | 0.037±0.004 | 0.028±0.004 | 0.025±0.006 | 0.061±0.011 | 0.036±0.008 | 0.032±0.003 | 0.024±0.003 | 0.021±0.005 | 0.052±0.010 | 0.031±0.006 |
| 24Dimethyl-2-Pentene | 0.002±0.000 | 0.002±0.000 | 0.001±0.000 | 0.004±0.001 | 0.001±0.000 | 0.002±0.000 | 0.001±0.000 | 0.001±0.000 | 0.004±0.001 | 0.001±0.000 |
| 34-diMe-c2-pentene | 0.009±0.001 | 0.007±0.001 | 0.007±0.002 | 0.015±0.003 | 0.009±0.002 | 0.008±0.001 | 0.006±0.001 | 0.006±0.001 | 0.013±0.002 | 0.008±0.002 |
| 44-diMe-c2-pentene | 0.004±0.000 | 0.003±0.000 | 0.002±0.000 | 0.008±0.002 | 0.003±0.001 | 0.004±0.000 | 0.003±0.000 | 0.002±0.000 | 0.007±0.001 | 0.003±0.001 |
| 3-Et-1-pentene | 0.000±0.000 | 0.000±0.000 | 0.000±0.000 | 0.001±0.000 | 0.000±0.000 | 0.000±0.000 | 0.000±0.000 | 0.000±0.000 | 0.000±0.000 | 0.000±0.000 |
| 3-Et-2-pentene | 0.075±0.008 | 0.055±0.007 | 0.046±0.011 | 0.128±0.025 | 0.070±0.014 | 0.064±0.007 | 0.046±0.006 | 0.040±0.010 | 0.110±0.021 | 0.060±0.012 |
| 2-Me-1-hexene | 0.020±0.002 | 0.016±0.002 | 0.012±0.003 | 0.036±0.007 | 0.015±0.003 | 0.017±0.002 | 0.014±0.002 | 0.011±0.003 | 0.031±0.006 | 0.013±0.003 |
| 3-Me-1-hexene | 0.003±0.000 | 0.002±0.000 | 0.002±0.001 | 0.006±0.001 | 0.002±0.001 | 0.003±0.000 | 0.002±0.000 | 0.002±0.000 | 0.005±0.001 | 0.002±0.000 |
| 5-Me-1-hexene | 0.012±0.001 | 0.010±0.001 | 0.008±0.002 | 0.021±0.004 | 0.010±0.002 | 0.011±0.001 | 0.008±0.001 | 0.007±0.002 | 0.018±0.003 | 0.009±0.002 |
| 2-Me-2-hexene | 0.041±0.004 | 0.031±0.004 | 0.027±0.007 | 0.065±0.012 | 0.038±0.008 | 0.035±0.004 | 0.026±0.003 | 0.023±0.006 | 0.056±0.010 | 0.033±0.007 |
| 5-Me-t2-hexene | 0.000±0.000 | 0.000±0.000 | 0.000±0.000 | 0.001±0.000 | 0.000±0.000 | 0.000±0.000 | 0.000±0.000 | 0.000±0.000 | 0.001±0.000 | 0.000±0.000 |
| 2-Me-t3-hexene | 0.020±0.002 | 0.016±0.002 | 0.012±0.003 | 0.037±0.007 | 0.015±0.003 | 0.017±0.002 | 0.013±0.002 | 0.011±0.003 | 0.032±0.006 | 0.013±0.003 |
| 3-Me-c3-hexene | 0.028±0.003 | 0.021±0.003 | 0.019±0.005 | 0.045±0.009 | 0.027±0.006 | 0.024±0.002 | 0.018±0.002 | 0.016±0.004 | 0.039±0.007 | 0.023±0.005 |
| 3-Me-t3-hexene | 0.017±0.002 | 0.013±0.002 | 0.012±0.003 | 0.028±0.005 | 0.016±0.003 | 0.015±0.002 | 0.011±0.001 | 0.010±0.003 | 0.024±0.005 | 0.013±0.003 |
| 1-Heptene | 0.019±0.002 | 0.015±0.003 | 0.010±0.003 | 0.033±0.007 | 0.016±0.004 | 0.016±0.002 | 0.013±0.003 | 0.008±0.003 | 0.028±0.006 | 0.014±0.003 |
| Cis-2-heptene | 0.000±0.000 | 0.000±0.000 | 0.000±0.000 | 0.001±0.000 | 0.000±0.000 | 0.000±0.000 | 0.000±0.000 | 0.000±0.000 | 0.001±0.000 | 0.000±0.000 |
| Trans-2-heptene | 0.002±0.000 | 0.005±0.001 | 0.000±0.000 | 0.001±0.000 | 0.000±0.000 | 0.001±0.000 | 0.004±0.000 | 0.000±0.000 | 0.001±0.000 | 0.000±0.000 |
| T3-Heptene | 0.025±0.003 | 0.015±0.004 | 0.012±0.004 | 0.051±0.009 | 0.022±0.005 | 0.021±0.003 | 0.013±0.003 | 0.011±0.004 | 0.043±0.008 | 0.019±0.004 |
| C2-Octene | 0.015±0.001 | 0.011±0.002 | 0.012±0.003 | 0.015±0.003 | 0.021±0.004 | 0.011±0.001 | 0.008±0.001 | 0.009±0.002 | 0.011±0.002 | 0.016±0.003 |
| C4-Octene | 0.001±0.000 | 0.002±0.001 | 0.001±0.001 | 0.002±0.001 | 0.000±0.000 | 0.001±0.000 | 0.001±0.001 | 0.001±0.001 | 0.002±0.001 | 0.000±0.000 |
| 25-Dimethyl-1-hexene | 0.000±0.000 | 0.000±0.000 | 0.000±0.000 | 0.001±0.000 | 0.000±0.000 | 0.000±0.000 | 0.000±0.000 | 0.000±0.000 | 0.001±0.000 | 0.000±0.000 |
| 4-M-1-Heptene | 0.058±0.005 | 0.075±0.003 | 0.041±0.008 | 0.065±0.013 | 0.050±0.010 | 0.042±0.003 | 0.055±0.003 | 0.030±0.006 | 0.048±0.010 | 0.037±0.007 |
| t-4-M-2-Heptene | 0.001±0.000 | 0.001±0.000 | 0.002±0.000 | 0.001±0.000 | 0.002±0.000 | 0.001±0.000 | 0.001±0.000 | 0.001±0.000 | 0.001±0.000 | 0.002±0.000 |
| C-2-m-3-heptene | 0.137±0.014 | 0.114±0.009 | 0.107±0.023 | 0.202±0.043 | 0.126±0.026 | 0.102±0.011 | 0.084±0.006 | 0.079±0.017 | 0.151±0.033 | 0.095±0.019 |
| c-6-M-2-Heptene | 0.002±0.000 | 0.002±0.000 | 0.002±0.000 | 0.004±0.001 | 0.002±0.000 | 0.002±0.000 | 0.001±0.000 | 0.001±0.000 | 0.003±0.001 | 0.002±0.000 |
| t-6-M-2-Heptene | 0.001±0.001 | 0.000±0.000 | 0.000±0.000 | 0.000±0.000 | 0.004±0.002 | 0.001±0.000 | 0.000±0.000 | 0.000±0.000 | 0.000±0.000 | 0.003±0.002 |
| 2-Methyl-2-heptene | 0.042±0.004 | 0.034±0.001 | 0.032±0.007 | 0.058±0.012 | 0.043±0.009 | 0.031±0.003 | 0.025±0.001 | 0.023±0.005 | 0.043±0.009 | 0.032±0.007 |
| 2235TetMethylhexane | 0.000±0.000 | 0.000±0.000 | 0.001±0.000 | 0.000±0.000 | 0.000±0.000 | 0.000±0.000 | 0.000±0.000 | 0.000±0.000 | 0.000±0.000 | 0.000±0.000 |
| C-7 Olefin A | 0.006±0.001 | 0.005±0.001 | 0.003±0.001 | 0.011±0.002 | 0.004±0.001 | 0.005±0.001 | 0.004±0.001 | 0.003±0.001 | 0.010±0.002 | 0.003±0.001 |
| C-7 Olefin B | 0.001±0.000 | 0.001±0.000 | 0.000±0.000 | 0.002±0.000 | 0.001±0.000 | 0.001±0.000 | 0.001±0.000 | 0.000±0.000 | 0.001±0.000 | 0.000±0.000 |
| C-7 Olefin D | 0.002±0.000 | 0.002±0.000 | 0.001±0.000 | 0.004±0.001 | 0.001±0.000 | 0.002±0.000 | 0.001±0.000 | 0.001±0.000 | 0.004±0.001 | 0.001±0.000 |

| | | | | | | | | | | |
|--------------------------------------|-------------|-------------|-------------|-------------|-------------|-------------|-------------|-------------|-------------|-------------|
| Octene B | 0.003±0.000 | 0.002±0.000 | 0.002±0.000 | 0.005±0.001 | 0.003±0.001 | 0.002±0.000 | 0.002±0.000 | 0.001±0.000 | 0.004±0.001 | 0.003±0.001 |
| Octene C | 0.006±0.001 | 0.004±0.000 | 0.003±0.001 | 0.012±0.002 | 0.005±0.001 | 0.005±0.001 | 0.003±0.000 | 0.002±0.001 | 0.009±0.002 | 0.003±0.001 |
| Octene D | 0.008±0.001 | 0.006±0.001 | 0.004±0.001 | 0.016±0.003 | 0.007±0.001 | 0.006±0.001 | 0.004±0.001 | 0.003±0.001 | 0.012±0.003 | 0.005±0.001 |
| Octene F | 0.001±0.000 | 0.001±0.000 | 0.000±0.000 | 0.005±0.001 | 0.000±0.000 | 0.001±0.000 | 0.000±0.000 | 0.000±0.000 | 0.004±0.001 | 0.000±0.000 |
| Octene G | 0.001±0.000 | 0.001±0.000 | 0.001±0.000 | 0.002±0.000 | 0.001±0.000 | 0.001±0.000 | 0.001±0.000 | 0.001±0.000 | 0.002±0.000 | 0.001±0.000 |
| Octene H | 0.007±0.001 | 0.006±0.001 | 0.005±0.001 | 0.012±0.002 | 0.007±0.001 | 0.006±0.001 | 0.004±0.000 | 0.004±0.001 | 0.009±0.002 | 0.006±0.001 |
| Octene I | 0.011±0.001 | 0.008±0.001 | 0.008±0.002 | 0.016±0.003 | 0.010±0.002 | 0.008±0.001 | 0.006±0.001 | 0.006±0.001 | 0.012±0.002 | 0.008±0.002 |
| C-8 Olefin K | 0.013±0.001 | 0.024±0.002 | 0.008±0.002 | 0.012±0.003 | 0.008±0.002 | 0.009±0.001 | 0.017±0.001 | 0.006±0.001 | 0.009±0.002 | 0.006±0.001 |
| C-8 Olefin M | 0.027±0.003 | 0.021±0.002 | 0.022±0.005 | 0.034±0.007 | 0.031±0.006 | 0.020±0.002 | 0.015±0.001 | 0.016±0.004 | 0.025±0.005 | 0.022±0.005 |
| 44DiMe2neopen1pentene | 0.001±0.001 | 0.000±0.000 | 0.002±0.001 | 0.004±0.002 | 0.000±0.000 | 0.001±0.000 | 0.000±0.000 | 0.001±0.000 | 0.002±0.001 | 0.000±0.000 |
| 22466PentaMe3heptene | 0.000±0.000 | 0.000±0.000 | 0.001±0.001 | 0.000±0.000 | 0.000±0.000 | 0.000±0.000 | 0.000±0.000 | 0.001±0.000 | 0.000±0.000 | 0.000±0.000 |
| T-2-T-4-hexadiene | 0.005±0.001 | 0.004±0.000 | 0.003±0.001 | 0.010±0.002 | 0.004±0.001 | 0.004±0.000 | 0.003±0.000 | 0.002±0.000 | 0.009±0.002 | 0.003±0.001 |
| Cyclopentene | 0.065±0.007 | 0.041±0.004 | 0.042±0.011 | 0.114±0.023 | 0.063±0.013 | 0.078±0.009 | 0.048±0.005 | 0.050±0.013 | 0.138±0.028 | 0.076±0.016 |
| 1-Me-cyclopentene | 0.143±0.016 | 0.105±0.012 | 0.074±0.020 | 0.262±0.052 | 0.133±0.027 | 0.126±0.014 | 0.091±0.010 | 0.065±0.018 | 0.231±0.046 | 0.116±0.024 |
| 3-Me-cyclopentene | 0.036±0.004 | 0.026±0.003 | 0.020±0.005 | 0.072±0.014 | 0.027±0.005 | 0.032±0.004 | 0.023±0.003 | 0.017±0.004 | 0.064±0.013 | 0.024±0.005 |
| Sum of Unclassified Compounds | 2.589±0.007 | 1.417±0.000 | 1.540±0.003 | 3.174±0.014 | 2.113±0.006 | 1.433±0.002 | 0.782±0.000 | 0.849±0.001 | 1.755±0.004 | 1.174±0.002 |

Note: Compounds for which an exact isomer could not be determined are denoted and differentiated by a CAPITAL suffix.

Table 4.11: Compound specific diesel fuel speciation for California in Summer 2010

| Compound | Weight percentage in fuel [% weight by carbon (\pm St. Dev)] | | | | |
|-------------------------------|---|-------------------|-------------------|-------------------|-------------------|
| | Statewide | Bakersfield | Berkeley | Pasadena | Sacramento |
| n-octane | 0.104 \pm 0.069 | 0.046 \pm 0.003 | 0.057 \pm 0.045 | 0.180 \pm 0.071 | 0.132 \pm 0.035 |
| n-nonane | 0.209 \pm 0.111 | 0.120 \pm 0.031 | 0.125 \pm 0.095 | 0.330 \pm 0.095 | 0.263 \pm 0.012 |
| n-decane | 0.444 \pm 0.169 | 0.353 \pm 0.066 | 0.315 \pm 0.228 | 0.588 \pm 0.122 | 0.519 \pm 0.098 |
| n-undecane | 0.581 \pm 0.183 | 0.456 \pm 0.039 | 0.573 \pm 0.312 | 0.695 \pm 0.168 | 0.602 \pm 0.114 |
| n-dodecane | 0.478 \pm 0.115 | 0.364 \pm 0.032 | 0.520 \pm 0.167 | 0.565 \pm 0.094 | 0.466 \pm 0.033 |
| n-tridecane | 0.440 \pm 0.091 | 0.337 \pm 0.029 | 0.469 \pm 0.102 | 0.517 \pm 0.091 | 0.436 \pm 0.005 |
| n-tetradecane | 0.439 \pm 0.081 | 0.322 \pm 0.020 | 0.503 \pm 0.021 | 0.493 \pm 0.018 | 0.437 \pm 0.061 |
| n-pentadecane | 0.524 \pm 0.106 | 0.414 \pm 0.033 | 0.560 \pm 0.076 | 0.605 \pm 0.104 | 0.518 \pm 0.121 |
| n-hexadecane | 0.552 \pm 0.162 | 0.395 \pm 0.041 | 0.588 \pm 0.090 | 0.645 \pm 0.188 | 0.579 \pm 0.216 |
| n-heptadecane | 0.628 \pm 0.189 | 0.542 \pm 0.102 | 0.659 \pm 0.131 | 0.646 \pm 0.257 | 0.665 \pm 0.297 |
| n-octadecane | 0.556 \pm 0.161 | 0.507 \pm 0.083 | 0.600 \pm 0.117 | 0.543 \pm 0.243 | 0.576 \pm 0.236 |
| n-nonadecane | 0.400 \pm 0.182 | 0.215 \pm 0.028 | 0.506 \pm 0.130 | 0.413 \pm 0.217 | 0.464 \pm 0.209 |
| n-eicosane | 0.386 \pm 0.175 | 0.233 \pm 0.021 | 0.511 \pm 0.128 | 0.351 \pm 0.215 | 0.450 \pm 0.197 |
| 2-5-dimethylhexane | 0.009 \pm 0.004 | 0.012 \pm 0.002 | 0.005 \pm 0.004 | 0.009 \pm 0.002 | 0.010 \pm 0.003 |
| 2-4-dimethylhexane | 0.006 \pm 0.002 | 0.005 \pm 0.002 | 0.004 \pm 0.002 | 0.006 \pm 0.002 | 0.007 \pm 0.003 |
| 2-methylheptane | 0.057 \pm 0.021 | 0.047 \pm 0.008 | 0.038 \pm 0.030 | 0.075 \pm 0.007 | 0.067 \pm 0.013 |
| 4-methylheptane | 0.017 \pm 0.008 | 0.012 \pm 0.003 | 0.012 \pm 0.010 | 0.023 \pm 0.007 | 0.023 \pm 0.004 |
| 3-methylheptane | 0.052 \pm 0.022 | 0.034 \pm 0.003 | 0.036 \pm 0.026 | 0.070 \pm 0.010 | 0.068 \pm 0.014 |
| 2,6-dimethylheptane | 0.051 \pm 0.026 | 0.032 \pm 0.004 | 0.028 \pm 0.021 | 0.078 \pm 0.022 | 0.063 \pm 0.005 |
| 3-5-dimethylheptane | 0.028 \pm 0.015 | 0.014 \pm 0.002 | 0.019 \pm 0.011 | 0.040 \pm 0.012 | 0.041 \pm 0.011 |
| 2,3-dimethylheptane | 0.013 \pm 0.005 | 0.012 \pm 0.002 | 0.007 \pm 0.005 | 0.017 \pm 0.003 | 0.017 \pm 0.001 |
| 4&2-methyloctane | 0.056 \pm 0.031 | 0.024 \pm 0.005 | 0.037 \pm 0.024 | 0.081 \pm 0.018 | 0.084 \pm 0.012 |
| 3-methyloctane+3-ethylheptane | 0.079 \pm 0.039 | 0.038 \pm 0.007 | 0.054 \pm 0.038 | 0.117 \pm 0.011 | 0.108 \pm 0.005 |
| C10 Branched alkanes A | 0.057 \pm 0.020 | 0.043 \pm 0.008 | 0.040 \pm 0.015 | 0.067 \pm 0.020 | 0.076 \pm 0.010 |
| 2-6-dimethyloctane | 0.035 \pm 0.016 | 0.029 \pm 0.006 | 0.023 \pm 0.018 | 0.045 \pm 0.018 | 0.042 \pm 0.016 |
| C10 Branch alkanes B | 0.316 \pm 0.118 | 0.206 \pm 0.032 | 0.243 \pm 0.092 | 0.405 \pm 0.113 | 0.408 \pm 0.054 |
| C11 Branched Alkanes A | 0.046 \pm 0.014 | 0.030 \pm 0.002 | 0.050 \pm 0.006 | 0.049 \pm 0.022 | 0.054 \pm 0.002 |
| C11 Branched Alkanes B | 0.018 \pm 0.008 | 0.007 \pm 0.002 | 0.017 \pm 0.005 | 0.024 \pm 0.005 | 0.023 \pm 0.002 |
| dimethylundecane A | 0.174 \pm 0.067 | 0.225 \pm 0.012 | 0.176 \pm 0.083 | 0.163 \pm 0.088 | 0.133 \pm 0.055 |
| dimethylundecane B | 0.129 \pm 0.049 | 0.191 \pm 0.009 | 0.120 \pm 0.048 | 0.111 \pm 0.046 | 0.093 \pm 0.024 |
| methylcyclohexane | 0.127 \pm 0.050 | 0.156 \pm 0.025 | 0.067 \pm 0.050 | 0.142 \pm 0.031 | 0.141 \pm 0.048 |
| Ethylcyclopentane | 0.025 \pm 0.010 | 0.029 \pm 0.008 | 0.016 \pm 0.011 | 0.032 \pm 0.010 | 0.025 \pm 0.007 |
| n-propylcyclopentane | 0.031 \pm 0.016 | 0.018 \pm 0.002 | 0.018 \pm 0.011 | 0.051 \pm 0.014 | 0.036 \pm 0.002 |

| | | | | | |
|--|-------------|-------------|-------------|-------------|-------------|
| ethylcyclohexane | 0.157±0.068 | 0.111±0.021 | 0.088±0.053 | 0.221±0.045 | 0.207±0.017 |
| propylcyclohexane | 0.256±0.095 | 0.270±0.047 | 0.147±0.053 | 0.312±0.112 | 0.294±0.083 |
| cumene | 0.029±0.009 | 0.036±0.005 | 0.022±0.017 | 0.030±0.001 | 0.029±0.004 |
| n-propyl_benzene | 0.090±0.020 | 0.092±0.017 | 0.069±0.021 | 0.099±0.019 | 0.101±0.012 |
| 1-ethyl-4(and3)-methylbenzene | 0.389±0.091 | 0.348±0.049 | 0.339±0.107 | 0.452±0.131 | 0.415±0.029 |
| 1-3-5-trimethylbenzene | 0.150±0.045 | 0.197±0.027 | 0.114±0.057 | 0.145±0.034 | 0.145±0.022 |
| 1-ethyl-2-methylbenzene | 0.136±0.023 | 0.129±0.018 | 0.128±0.035 | 0.149±0.029 | 0.137±0.015 |
| 1-2-4-trimethylbenzene | 0.699±0.222 | 0.984±0.111 | 0.589±0.255 | 0.605±0.122 | 0.617±0.120 |
| 1-ethenyl-2-(or3)-methylbenzene | 0.019±0.009 | 0.020±0.002 | 0.020±0.015 | 0.021±0.012 | 0.015±0.002 |
| isobutylbenzene | 0.009±0.003 | 0.012±0.002 | 0.008±0.003 | 0.007±0.002 | 0.010±0.003 |
| m-cymene | 0.040±0.015 | 0.054±0.007 | 0.035±0.028 | 0.037±0.006 | 0.035±0.007 |
| p-cymene | 0.039±0.021 | 0.065±0.007 | 0.029±0.026 | 0.031±0.010 | 0.030±0.011 |
| m-diethylbenzene | 0.589±0.244 | 0.588±0.047 | 0.693±0.504 | 0.545±0.171 | 0.531±0.130 |
| 1-methyl-3-n-propylbenzene | 0.267±0.076 | 0.279±0.024 | 0.287±0.144 | 0.267±0.088 | 0.233±0.014 |
| indan | 0.142±0.060 | 0.152±0.015 | 0.150±0.104 | 0.152±0.083 | 0.112±0.013 |
| p-diethylbenzene | 0.415±0.172 | 0.417±0.034 | 0.487±0.357 | 0.383±0.120 | 0.374±0.088 |
| n-butylbenzene | 0.132±0.053 | 0.103±0.014 | 0.146±0.093 | 0.150±0.066 | 0.128±0.013 |
| o-diethylbenzene | 0.034±0.006 | 0.038±0.002 | 0.037±0.009 | 0.033±0.002 | 0.028±0.001 |
| 1-methyl-2-n-propylbenzene | 0.071±0.018 | 0.076±0.007 | 0.083±0.030 | 0.062±0.016 | 0.063±0.009 |
| 1,4-dimethyl-2-ethylbenzene | 0.162±0.047 | 0.164±0.022 | 0.204±0.078 | 0.149±0.027 | 0.130±0.022 |
| 1,3-dimethyl-4-ethylbenzene | 0.164±0.046 | 0.203±0.017 | 0.182±0.071 | 0.145±0.025 | 0.127±0.023 |
| 1,2-dimethyl-4-ethylbenzene | 0.108±0.040 | 0.116±0.007 | 0.130±0.080 | 0.098±0.023 | 0.088±0.015 |
| Trans-1-butenylbenzene | 0.009±0.003 | 0.012±0.002 | 0.009±0.004 | 0.008±0.002 | 0.007±0.002 |
| 1,3-dimethyl-2-ethylbenzene | 0.071±0.030 | 0.096±0.007 | 0.075±0.057 | 0.057±0.006 | 0.055±0.003 |
| 1,2-dimethyl-3-ethylbenzene | 0.052±0.016 | 0.069±0.004 | 0.058±0.022 | 0.042±0.005 | 0.040±0.006 |
| 1-2-4-5-tetramethylbenzene | 0.078±0.038 | 0.108±0.014 | 0.086±0.069 | 0.061±0.017 | 0.057±0.017 |
| 1-2-3-5-tetramethylbenzene | 0.114±0.046 | 0.160±0.014 | 0.126±0.066 | 0.087±0.022 | 0.082±0.020 |
| C11 Aromatics A | 0.020±0.007 | 0.026±0.005 | 0.023±0.012 | 0.017±0.002 | 0.016±0.002 |
| 1-methylindan | 0.113±0.072 | 0.085±0.015 | 0.171±0.131 | 0.114±0.060 | 0.083±0.009 |
| C11 Aromatics B | 0.010±0.003 | 0.015±0.001 | 0.010±0.003 | 0.008±0.002 | 0.008±0.001 |
| 1-2-3-4-tetramethylbenzene | 0.183±0.084 | 0.301±0.012 | 0.190±0.073 | 0.122±0.016 | 0.119±0.021 |
| 2-methylindan | 0.217±0.092 | 0.215±0.018 | 0.289±0.168 | 0.200±0.069 | 0.164±0.010 |
| toluene | 0.214±0.102 | 0.252±0.043 | 0.106±0.074 | 0.242±0.122 | 0.256±0.108 |
| ethylbenzene | 0.093±0.043 | 0.063±0.010 | 0.061±0.033 | 0.132±0.044 | 0.115±0.033 |
| m&p-xylene | 0.475±0.154 | 0.467±0.069 | 0.321±0.158 | 0.575±0.186 | 0.538±0.098 |
| o-xylene | 0.164±0.056 | 0.151±0.021 | 0.107±0.040 | 0.202±0.070 | 0.195±0.038 |

| | | | | | |
|--|-------------|-------------|-------------|-------------|-------------|
| 123-trimethylbenzene | 0.286±0.178 | 0.564±0.075 | 0.189±0.090 | 0.190±0.040 | 0.199±0.060 |
| dimethylnaphthalenes | 0.182±0.167 | 0.456±0.007 | 0.125±0.021 | 0.067±0.015 | 0.082±0.010 |
| trimethylnaphthalenes | 0.153±0.134 | 0.370±0.007 | 0.112±0.030 | 0.056±0.022 | 0.073±0.012 |
| naphthalene | 0.045±0.037 | 0.103±0.017 | 0.034±0.010 | 0.022±0.007 | 0.020±0.003 |
| 2-methylnaphthalene | 0.124±0.120 | 0.319±0.029 | 0.082±0.032 | 0.046±0.019 | 0.050±0.009 |
| 1-methylnaphthalene | 0.066±0.062 | 0.166±0.013 | 0.046±0.013 | 0.024±0.008 | 0.027±0.005 |
| C9 Cycloalkene A | 0.052±0.026 | 0.065±0.007 | 0.028±0.007 | 0.047±0.026 | 0.068±0.039 |
| ctc-1-2-4-trimethylcyclopentane | 0.016±0.006 | 0.023±0.004 | 0.009±0.005 | 0.017±0.002 | 0.016±0.002 |
| ctc-1,2,3-trimethylcyclopentane | 0.040±0.020 | 0.066±0.014 | 0.018±0.013 | 0.041±0.014 | 0.036±0.007 |
| ctt-1-2-4-trimethylcyclopentane | 0.010±0.004 | 0.012±0.001 | 0.006±0.003 | 0.013±0.005 | 0.010±0.001 |
| cis-1,3 & 1,1-dimethylcyclohexane | 0.099±0.043 | 0.072±0.010 | 0.054±0.036 | 0.135±0.027 | 0.135±0.010 |
| trans-1-2-dimethylcyclohexane | 0.118±0.048 | 0.100±0.010 | 0.060±0.041 | 0.154±0.027 | 0.157±0.013 |
| trans-1-3-dimethylcyclohexane | 0.078±0.034 | 0.050±0.005 | 0.049±0.030 | 0.112±0.024 | 0.100±0.006 |
| isopropylcyclopentane | 0.010±0.006 | 0.007±0.001 | 0.006±0.003 | 0.017±0.007 | 0.011±0.001 |
| ccc-1-3-5-trimethylcyclohexane | 0.052±0.048 | 0.020±0.003 | 0.025±0.014 | 0.065±0.045 | 0.100±0.066 |
| cis-1-2-dimethylcyclohexane | 0.049±0.025 | 0.030±0.005 | 0.029±0.015 | 0.078±0.024 | 0.060±0.011 |
| 1-1-3-trimethylcyclohexane | 0.096±0.047 | 0.128±0.018 | 0.043±0.029 | 0.105±0.050 | 0.109±0.050 |
| 1-1-4-trimethylcyclohexane | 0.027±0.011 | 0.020±0.002 | 0.018±0.007 | 0.031±0.004 | 0.040±0.010 |
| ctt-1,2,4-trimethylcyclohexane | 0.018±0.013 | 0.011±0.001 | 0.010±0.004 | 0.018±0.009 | 0.031±0.018 |
| ctc-1-2-4-trimethylcyclohexane | 0.099±0.057 | 0.091±0.014 | 0.056±0.022 | 0.102±0.046 | 0.149±0.091 |
| C9 cycloalkanes A | 0.008±0.003 | 0.007±0.001 | 0.005±0.001 | 0.011±0.004 | 0.010±0.001 |
| methyl-ethylcyclohexane isomer A | 0.010±0.004 | 0.011±0.002 | 0.008±0.002 | 0.010±0.007 | 0.012±0.005 |
| isopropylcyclohexane | 0.039±0.014 | 0.052±0.007 | 0.022±0.009 | 0.041±0.011 | 0.041±0.012 |
| C10 cyclohexanes A | 0.126±0.050 | 0.129±0.014 | 0.094±0.014 | 0.134±0.073 | 0.148±0.075 |

Note: This list only comprises a fraction of compounds in diesel. Compounds for which an exact isomer could not be determined are denoted and differentiated by a CAPITAL suffix.

Table 4.12: Compound specific non-tailpipe gasoline speciation for California in Summer 2010

| Compound | Weight percentage in fuel [% weight by carbon (\pm St. Dev)] | | | | | Molar percentage in fuel [% mol (\pm St. Dev)] | | | | |
|-----------------------|---|--------------------|--------------------|--------------------|--------------------|---|--------------------|--------------------|--------------------|--------------------|
| | Statewide | Bakersfield | Berkeley | Pasadena | Sacramento | Statewide | Bakersfield | Berkeley | Pasadena | Sacramento |
| ethane | 0.099 \pm 0.011 | 0.310 \pm 0.042 | 0.015 \pm 0.006 | 0.069 \pm 0.014 | 0.000 \pm 0.000 | 0.235 \pm 0.026 | 0.735 \pm 0.099 | 0.037 \pm 0.015 | 0.169 \pm 0.033 | 0.000 \pm 0.000 |
| propane | 0.690 \pm 0.059 | 1.534 \pm 0.156 | 0.315 \pm 0.088 | 0.287 \pm 0.063 | 0.624 \pm 0.143 | 1.105 \pm 0.095 | 2.430 \pm 0.242 | 0.511 \pm 0.141 | 0.461 \pm 0.100 | 1.020 \pm 0.234 |
| n-butane | 6.542 \pm 0.499 | 8.944 \pm 0.646 | 5.472 \pm 0.961 | 6.326 \pm 1.301 | 5.426 \pm 0.973 | 7.929 \pm 0.603 | 10.652 \pm 0.740 | 6.734 \pm 1.182 | 7.652 \pm 1.561 | 6.676 \pm 1.197 |
| n-pentane | 10.313 \pm 0.801 | 14.100 \pm 0.768 | 9.068 \pm 1.766 | 9.362 \pm 1.924 | 8.723 \pm 1.690 | 10.060 \pm 0.787 | 13.484 \pm 0.685 | 8.950 \pm 1.746 | 9.210 \pm 1.899 | 8.595 \pm 1.666 |
| n-hexane | 1.970 \pm 0.168 | 2.245 \pm 0.044 | 1.837 \pm 0.374 | 1.976 \pm 0.413 | 1.823 \pm 0.372 | 1.605 \pm 0.138 | 1.797 \pm 0.030 | 1.511 \pm 0.308 | 1.617 \pm 0.338 | 1.497 \pm 0.306 |
| n-heptane | 0.137 \pm 0.012 | 0.150 \pm 0.003 | 0.164 \pm 0.033 | 0.108 \pm 0.021 | 0.126 \pm 0.025 | 0.096 \pm 0.008 | 0.103 \pm 0.002 | 0.116 \pm 0.023 | 0.075 \pm 0.015 | 0.088 \pm 0.017 |
| n-octane | 0.062 \pm 0.005 | 0.067 \pm 0.002 | 0.071 \pm 0.014 | 0.049 \pm 0.010 | 0.059 \pm 0.012 | 0.038 \pm 0.003 | 0.040 \pm 0.001 | 0.044 \pm 0.009 | 0.030 \pm 0.006 | 0.037 \pm 0.007 |
| n-nonane | 0.008 \pm 0.001 | 0.009 \pm 0.000 | 0.009 \pm 0.002 | 0.007 \pm 0.001 | 0.008 \pm 0.002 | 0.005 \pm 0.000 | 0.005 \pm 0.000 | 0.005 \pm 0.001 | 0.004 \pm 0.001 | 0.005 \pm 0.001 |
| n-decane | 0.001 \pm 0.000 | 0.001 \pm 0.000 | 0.001 \pm 0.000 | 0.001 \pm 0.000 | 0.001 \pm 0.000 | 0.001 \pm 0.000 | 0.000 \pm 0.000 | 0.000 \pm 0.000 | 0.001 \pm 0.000 | 0.001 \pm 0.000 |
| 2-methylpropane | 1.072 \pm 0.111 | 1.569 \pm 0.176 | 0.807 \pm 0.212 | 1.484 \pm 0.341 | 0.428 \pm 0.076 | 1.293 \pm 0.134 | 1.859 \pm 0.206 | 0.994 \pm 0.260 | 1.791 \pm 0.408 | 0.527 \pm 0.094 |
| 2-methylbutane | 38.367 \pm 3.173 | 34.577 \pm 0.809 | 41.426 \pm 7.644 | 36.647 \pm 6.790 | 40.817 \pm 7.477 | 37.582 \pm 3.129 | 33.334 \pm 0.935 | 40.855 \pm 7.546 | 35.930 \pm 6.675 | 40.209 \pm 7.370 |
| 2,2-dimethylpropane | 0.072 \pm 0.006 | 0.083 \pm 0.005 | 0.066 \pm 0.012 | 0.066 \pm 0.014 | 0.074 \pm 0.013 | 0.071 \pm 0.006 | 0.080 \pm 0.004 | 0.065 \pm 0.012 | 0.065 \pm 0.014 | 0.073 \pm 0.013 |
| 2-methylpentane | 5.814 \pm 0.519 | 4.856 \pm 0.345 | 6.545 \pm 1.260 | 5.893 \pm 1.158 | 5.961 \pm 1.121 | 4.756 \pm 0.427 | 3.923 \pm 0.298 | 5.384 \pm 1.038 | 4.821 \pm 0.950 | 4.895 \pm 0.921 |
| 3-methylpentane | 3.247 \pm 0.286 | 2.774 \pm 0.169 | 3.598 \pm 0.688 | 3.235 \pm 0.633 | 3.381 \pm 0.634 | 2.655 \pm 0.235 | 2.238 \pm 0.147 | 2.960 \pm 0.567 | 2.646 \pm 0.519 | 2.776 \pm 0.521 |
| 2,2-dimethylbutane | 2.051 \pm 0.241 | 1.295 \pm 0.232 | 3.006 \pm 0.703 | 1.628 \pm 0.448 | 2.276 \pm 0.426 | 1.688 \pm 0.199 | 1.060 \pm 0.194 | 2.483 \pm 0.582 | 1.341 \pm 0.370 | 1.869 \pm 0.350 |
| 2,3-dimethylbutane | 2.247 \pm 0.183 | 1.967 \pm 0.099 | 2.231 \pm 0.399 | 2.377 \pm 0.425 | 2.413 \pm 0.433 | 1.834 \pm 0.151 | 1.583 \pm 0.087 | 1.835 \pm 0.329 | 1.937 \pm 0.347 | 1.980 \pm 0.356 |
| 2-methylhexane | 0.625 \pm 0.064 | 0.535 \pm 0.034 | 0.852 \pm 0.182 | 0.504 \pm 0.122 | 0.610 \pm 0.128 | 0.439 \pm 0.045 | 0.370 \pm 0.026 | 0.601 \pm 0.129 | 0.356 \pm 0.087 | 0.430 \pm 0.090 |
| 3-methylhexane | 0.867 \pm 0.076 | 0.811 \pm 0.020 | 1.042 \pm 0.209 | 0.808 \pm 0.156 | 0.808 \pm 0.157 | 0.607 \pm 0.054 | 0.559 \pm 0.017 | 0.735 \pm 0.148 | 0.566 \pm 0.110 | 0.568 \pm 0.111 |
| 3-ethylpentane | 0.036 \pm 0.005 | 0.044 \pm 0.005 | 0.059 \pm 0.015 | 0.022 \pm 0.008 | 0.019 \pm 0.007 | 0.025 \pm 0.003 | 0.030 \pm 0.003 | 0.042 \pm 0.011 | 0.015 \pm 0.006 | 0.013 \pm 0.005 |
| 2,2-dimethylpentane | 0.085 \pm 0.008 | 0.095 \pm 0.001 | 0.092 \pm 0.021 | 0.084 \pm 0.017 | 0.068 \pm 0.013 | 0.059 \pm 0.005 | 0.065 \pm 0.001 | 0.065 \pm 0.015 | 0.059 \pm 0.012 | 0.048 \pm 0.009 |
| 2,3-dimethylpentane | 1.338 \pm 0.108 | 1.474 \pm 0.061 | 0.985 \pm 0.171 | 1.775 \pm 0.334 | 1.118 \pm 0.208 | 0.929 \pm 0.075 | 1.007 \pm 0.040 | 0.693 \pm 0.121 | 1.229 \pm 0.230 | 0.786 \pm 0.146 |
| 2,4-dimethylpentane | 0.844 \pm 0.066 | 0.894 \pm 0.036 | 0.615 \pm 0.104 | 1.075 \pm 0.191 | 0.794 \pm 0.145 | 0.587 \pm 0.046 | 0.612 \pm 0.024 | 0.432 \pm 0.073 | 0.746 \pm 0.132 | 0.558 \pm 0.102 |
| 3,3-Dimethylpentane | 0.066 \pm 0.006 | 0.077 \pm 0.001 | 0.066 \pm 0.018 | 0.066 \pm 0.013 | 0.056 \pm 0.010 | 0.046 \pm 0.004 | 0.053 \pm 0.001 | 0.047 \pm 0.013 | 0.046 \pm 0.009 | 0.039 \pm 0.007 |
| 2,2,3-Trimethylbutane | 0.032 \pm 0.002 | 0.032 \pm 0.000 | 0.031 \pm 0.006 | 0.032 \pm 0.006 | 0.032 \pm 0.006 | 0.022 \pm 0.002 | 0.022 \pm 0.000 | 0.022 \pm 0.004 | 0.022 \pm 0.004 | 0.023 \pm 0.004 |
| 2-Methylheptane | 0.137 \pm 0.011 | 0.142 \pm 0.002 | 0.143 \pm 0.028 | 0.133 \pm 0.026 | 0.130 \pm 0.025 | 0.084 \pm 0.007 | 0.085 \pm 0.001 | 0.088 \pm 0.017 | 0.081 \pm 0.016 | 0.080 \pm 0.016 |
| 3-methylheptane | 0.140 \pm 0.012 | 0.152 \pm 0.002 | 0.151 \pm 0.030 | 0.127 \pm 0.025 | 0.131 \pm 0.025 | 0.086 \pm 0.007 | 0.091 \pm 0.001 | 0.093 \pm 0.018 | 0.078 \pm 0.015 | 0.081 \pm 0.016 |
| 4-Methylheptane | 0.062 \pm 0.005 | 0.066 \pm 0.001 | 0.065 \pm 0.012 | 0.058 \pm 0.011 | 0.060 \pm 0.011 | 0.038 \pm 0.003 | 0.039 \pm 0.000 | 0.040 \pm 0.008 | 0.036 \pm 0.007 | 0.037 \pm 0.007 |
| 2,2-dimethylhexane | 0.014 \pm 0.001 | 0.019 \pm 0.001 | 0.016 \pm 0.004 | 0.011 \pm 0.002 | 0.011 \pm 0.002 | 0.009 \pm 0.001 | 0.011 \pm 0.001 | 0.010 \pm 0.002 | 0.007 \pm 0.001 | 0.007 \pm 0.001 |
| 2,4-dimethylhexane | 0.135 \pm 0.010 | 0.134 \pm 0.003 | 0.125 \pm 0.022 | 0.139 \pm 0.024 | 0.141 \pm 0.025 | 0.082 \pm 0.006 | 0.081 \pm 0.001 | 0.077 \pm 0.013 | 0.085 \pm 0.015 | 0.087 \pm 0.015 |
| 2,5-dimethylhexane | 0.131 \pm 0.010 | 0.128 \pm 0.003 | 0.118 \pm 0.020 | 0.127 \pm 0.022 | 0.151 \pm 0.026 | 0.080 \pm 0.006 | 0.076 \pm 0.001 | 0.073 \pm 0.012 | 0.078 \pm 0.013 | 0.093 \pm 0.016 |
| 3,3-dimethylhexane | 0.014 \pm 0.001 | 0.020 \pm 0.001 | 0.016 \pm 0.003 | 0.010 \pm 0.002 | 0.011 \pm 0.002 | 0.009 \pm 0.001 | 0.012 \pm 0.001 | 0.010 \pm 0.002 | 0.006 \pm 0.001 | 0.007 \pm 0.001 |
| 2-Me-3-Et-pentane | 0.097 \pm 0.007 | 0.097 \pm 0.002 | 0.086 \pm 0.015 | 0.102 \pm 0.018 | 0.105 \pm 0.019 | 0.059 \pm 0.005 | 0.058 \pm 0.001 | 0.053 \pm 0.009 | 0.062 \pm 0.011 | 0.065 \pm 0.012 |
| 2,2,3-triMe-pentane | 0.038 \pm 0.003 | 0.034 \pm 0.001 | 0.033 \pm 0.006 | 0.033 \pm 0.006 | 0.052 \pm 0.009 | 0.023 \pm 0.002 | 0.020 \pm 0.001 | 0.020 \pm 0.004 | 0.020 \pm 0.004 | 0.032 \pm 0.006 |
| 2,2,4-triMe-pentane | 1.287 \pm 0.104 | 1.101 \pm 0.042 | 1.013 \pm 0.175 | 1.465 \pm 0.252 | 1.571 \pm 0.280 | 0.785 \pm 0.064 | 0.658 \pm 0.024 | 0.624 \pm 0.108 | 0.893 \pm 0.154 | 0.967 \pm 0.172 |
| 2,3,3-triMe-pentane | 0.265 \pm 0.022 | 0.240 \pm 0.008 | 0.224 \pm 0.039 | 0.224 \pm 0.039 | 0.371 \pm 0.066 | 0.162 \pm 0.013 | 0.144 \pm 0.005 | 0.138 \pm 0.024 | 0.137 \pm 0.024 | 0.229 \pm 0.041 |
| 2,3,4-triMe-pentane | 0.271 \pm 0.022 | 0.253 \pm 0.008 | 0.222 \pm 0.038 | 0.257 \pm 0.044 | 0.353 \pm 0.063 | 0.165 \pm 0.013 | 0.151 \pm 0.005 | 0.137 \pm 0.023 | 0.157 \pm 0.027 | 0.217 \pm 0.039 |
| 2,2,5-trimethylhexane | 0.106 \pm 0.010 | 0.105 \pm 0.005 | 0.104 \pm 0.024 | 0.078 \pm 0.014 | 0.138 \pm 0.027 | 0.058 \pm 0.005 | 0.056 \pm 0.002 | 0.057 \pm 0.013 | 0.042 \pm 0.008 | 0.075 \pm 0.015 |
| 2,3,5-trimethylhexane | 0.022 \pm 0.002 | 0.023 \pm 0.001 | 0.021 \pm 0.004 | 0.017 \pm 0.003 | 0.027 \pm 0.005 | 0.012 \pm 0.001 | 0.012 \pm 0.000 | 0.011 \pm 0.002 | 0.009 \pm 0.002 | 0.015 \pm 0.003 |
| 2,4,4-trimethylhexane | 0.011 \pm 0.001 | 0.008 \pm 0.000 | 0.008 \pm 0.002 | 0.013 \pm 0.003 | 0.012 \pm 0.002 | 0.006 \pm 0.001 | 0.004 \pm 0.000 | 0.005 \pm 0.001 | 0.007 \pm 0.001 | 0.007 \pm 0.001 |
| 2,4-dimethylheptane | 0.009 \pm 0.001 | 0.011 \pm 0.001 | 0.009 \pm 0.002 | 0.007 \pm 0.001 | 0.008 \pm 0.002 | 0.005 \pm 0.000 | 0.006 \pm 0.000 | 0.005 \pm 0.001 | 0.004 \pm 0.001 | 0.005 \pm 0.001 |
| 2,6-dimethylheptane | 0.015 \pm 0.001 | 0.013 \pm 0.000 | 0.013 \pm 0.003 | 0.018 \pm 0.004 | 0.015 \pm 0.003 | 0.008 \pm 0.001 | 0.007 \pm 0.000 | 0.007 \pm 0.001 | 0.010 \pm 0.002 | 0.008 \pm 0.002 |
| 3,5-dimethylheptane | 0.031 \pm 0.002 | 0.035 \pm 0.001 | 0.028 \pm 0.005 | 0.030 \pm 0.006 | 0.030 \pm 0.006 | 0.017 \pm 0.001 | 0.018 \pm 0.001 | 0.015 \pm 0.003 | 0.016 \pm 0.003 | 0.016 \pm 0.003 |
| 2,3-dimethylheptane | 0.009 \pm 0.001 | 0.010 \pm 0.000 | 0.009 \pm 0.002 | 0.008 \pm 0.002 | 0.010 \pm 0.002 | 0.005 \pm 0.000 | 0.005 \pm 0.000 | 0.005 \pm 0.001 | 0.005 \pm 0.001 | 0.006 \pm 0.001 |
| 3,4-dimethylheptane | 0.005 \pm 0.000 | 0.004 \pm 0.000 | 0.004 \pm 0.001 | 0.005 \pm 0.001 | 0.005 \pm 0.001 | 0.002 \pm 0.000 | 0.002 \pm 0.000 | 0.002 \pm 0.000 | 0.003 \pm 0.001 | 0.003 \pm 0.000 |
| 3,3-dimethylheptane | 0.003 \pm 0.000 | 0.002 \pm 0.000 | 0.002 \pm 0.000 | 0.005 \pm 0.001 | 0.003 \pm 0.001 | 0.002 \pm 0.000 | 0.001 \pm 0.000 | 0.001 \pm 0.000 | 0.003 \pm 0.001 | 0.002 \pm 0.000 |
| 4,4-dimethylheptane | 0.002 \pm 0.000 | 0.002 \pm 0.000 | 0.002 \pm 0.000 | 0.004 \pm 0.001 | 0.002 \pm 0.000 | 0.001 \pm 0.000 | 0.001 \pm 0.000 | 0.001 \pm 0.000 | 0.002 \pm 0.000 | 0.001 \pm 0.000 |
| 2-methyloctane | 0.015 \pm 0.001 | 0.016 \pm 0.000 | 0.014 \pm 0.003 | 0.015 \pm 0.003 | 0.015 \pm 0.003 | 0.008 \pm 0.001 | 0.008 \pm 0.000 | 0.008 \pm 0.002 | 0.008 \pm 0.002 | 0.008 \pm 0.002 |

| | | | | | | | | | | |
|------------------------------|-------------|-------------|-------------|-------------|-------------|--------------|--------------|--------------|--------------|--------------|
| 3-methyloctane | 0.018±0.002 | 0.020±0.001 | 0.018±0.003 | 0.018±0.003 | 0.018±0.004 | 0.010±0.001 | 0.011±0.000 | 0.010±0.002 | 0.010±0.002 | 0.010±0.002 |
| 4-methyloctane | 0.013±0.001 | 0.014±0.001 | 0.012±0.002 | 0.012±0.002 | 0.012±0.002 | 0.007±0.001 | 0.008±0.000 | 0.007±0.001 | 0.007±0.001 | 0.007±0.001 |
| 2,2-dimethylheptane | 0.002±0.000 | 0.003±0.000 | 0.002±0.000 | 0.001±0.000 | 0.001±0.000 | 0.001±0.000 | 0.002±0.000 | 0.001±0.000 | 0.001±0.000 | 0.001±0.000 |
| 2,2,3-trimethylhexane | 0.002±0.000 | 0.004±0.000 | 0.002±0.001 | 0.000±0.000 | 0.001±0.000 | 0.001±0.000 | 0.002±0.000 | 0.001±0.000 | 0.000±0.000 | 0.001±0.000 |
| Cyclopentane | 1.070±0.084 | 1.371±0.065 | 1.056±0.209 | 0.864±0.177 | 0.988±0.186 | 1.044±0.083 | 1.312±0.057 | 1.043±0.207 | 0.850±0.174 | 0.973±0.183 |
| Methylcyclopentane | 2.602±0.216 | 2.923±0.055 | 2.669±0.536 | 2.409±0.477 | 2.408±0.477 | 2.119±0.177 | 2.339±0.036 | 2.194±0.441 | 1.967±0.390 | 1.977±0.391 |
| Ethylcyclopentane | 0.095±0.008 | 0.104±0.003 | 0.084±0.018 | 0.099±0.020 | 0.091±0.019 | 0.066±0.006 | 0.071±0.001 | 0.059±0.012 | 0.069±0.014 | 0.064±0.013 |
| 1T2-diMecyclopentane | 0.279±0.023 | 0.441±0.036 | 0.239±0.053 | 0.219±0.046 | 0.216±0.044 | 0.193±0.016 | 0.300±0.023 | 0.168±0.037 | 0.153±0.032 | 0.152±0.031 |
| 1C3-diMecyclopentane | 0.228±0.020 | 0.270±0.011 | 0.220±0.049 | 0.215±0.043 | 0.208±0.042 | 0.159±0.014 | 0.185±0.007 | 0.154±0.034 | 0.150±0.030 | 0.146±0.030 |
| 1T3-diMecyclopentane | 0.268±0.023 | 0.331±0.015 | 0.252±0.056 | 0.251±0.051 | 0.236±0.048 | 0.186±0.016 | 0.226±0.009 | 0.177±0.039 | 0.175±0.035 | 0.166±0.034 |
| Propylcyclopentane | 0.002±0.000 | 0.002±0.000 | 0.002±0.000 | 0.003±0.001 | 0.002±0.000 | 0.001±0.000 | 0.001±0.000 | 0.001±0.000 | 0.002±0.000 | 0.001±0.000 |
| 112-triMeCyPentane | 0.001±0.000 | 0.001±0.000 | 0.001±0.000 | 0.002±0.000 | 0.001±0.000 | 0.001±0.000 | 0.001±0.000 | 0.001±0.000 | 0.001±0.000 | 0.001±0.000 |
| 113-triMeCyPentane | 0.041±0.003 | 0.057±0.003 | 0.031±0.006 | 0.044±0.009 | 0.034±0.007 | 0.025±0.002 | 0.034±0.002 | 0.019±0.004 | 0.027±0.006 | 0.021±0.004 |
| 1C2T3-triMeCyPentane | 0.003±0.000 | 0.004±0.000 | 0.003±0.001 | 0.003±0.001 | 0.003±0.001 | 0.002±0.000 | 0.002±0.000 | 0.002±0.000 | 0.002±0.000 | 0.002±0.000 |
| 1T2C3-triMeCyPentane | 0.034±0.003 | 0.051±0.004 | 0.024±0.005 | 0.036±0.008 | 0.027±0.005 | 0.021±0.002 | 0.030±0.002 | 0.015±0.003 | 0.022±0.005 | 0.016±0.003 |
| 1T2C4-triMeCyPentane | 0.055±0.005 | 0.061±0.002 | 0.044±0.009 | 0.067±0.014 | 0.050±0.010 | 0.034±0.003 | 0.037±0.001 | 0.027±0.006 | 0.041±0.008 | 0.031±0.006 |
| Cyclohexane | 0.747±0.070 | 0.787±0.031 | 0.915±0.202 | 0.567±0.122 | 0.722±0.148 | 0.611±0.058 | 0.632±0.027 | 0.754±0.167 | 0.465±0.101 | 0.593±0.122 |
| Methylcyclohexane | 0.468±0.041 | 0.500±0.009 | 0.445±0.092 | 0.486±0.099 | 0.441±0.089 | 0.326±0.028 | 0.343±0.005 | 0.313±0.065 | 0.339±0.069 | 0.310±0.063 |
| Ethylcyclohexane | 0.017±0.002 | 0.011±0.001 | 0.012±0.003 | 0.029±0.006 | 0.018±0.004 | 0.011±0.001 | 0.007±0.001 | 0.007±0.002 | 0.017±0.004 | 0.011±0.002 |
| 1,1-diMecyclohexane | 0.005±0.000 | 0.006±0.000 | 0.004±0.001 | 0.005±0.001 | 0.004±0.001 | 0.003±0.000 | 0.004±0.000 | 0.003±0.001 | 0.003±0.001 | 0.003±0.001 |
| 1C2-diMecyclohexane | 0.006±0.001 | 0.004±0.000 | 0.004±0.001 | 0.009±0.002 | 0.006±0.001 | 0.004±0.000 | 0.003±0.000 | 0.003±0.000 | 0.003±0.001 | 0.004±0.001 |
| 1T2-diMecyclohexane | 0.017±0.002 | 0.015±0.001 | 0.013±0.003 | 0.023±0.005 | 0.016±0.003 | 0.010±0.001 | 0.009±0.000 | 0.008±0.002 | 0.014±0.003 | 0.010±0.002 |
| 1C3-diMecyclohexane | 0.040±0.004 | 0.033±0.002 | 0.031±0.007 | 0.057±0.013 | 0.037±0.008 | 0.024±0.002 | 0.020±0.001 | 0.019±0.004 | 0.035±0.008 | 0.023±0.005 |
| 1T3-diMecyclohexane | 0.032±0.003 | 0.024±0.002 | 0.024±0.005 | 0.048±0.010 | 0.032±0.007 | 0.020±0.002 | 0.014±0.001 | 0.015±0.003 | 0.029±0.006 | 0.020±0.004 |
| 1C4-diMecyclohexane | 0.007±0.001 | 0.006±0.000 | 0.004±0.001 | 0.011±0.002 | 0.006±0.001 | 0.004±0.000 | 0.003±0.000 | 0.003±0.001 | 0.007±0.001 | 0.004±0.001 |
| Propylcyclohexane | 0.001±0.000 | 0.001±0.000 | 0.001±0.000 | 0.002±0.001 | 0.001±0.000 | 0.001±0.000 | 0.000±0.000 | 0.001±0.000 | 0.001±0.000 | 0.001±0.000 |
| 1Me-1EtCyclopentane | 0.014±0.001 | 0.015±0.001 | 0.010±0.002 | 0.019±0.004 | 0.012±0.003 | 0.009±0.001 | 0.009±0.000 | 0.006±0.001 | 0.012±0.003 | 0.007±0.002 |
| Benzene | 0.506±0.042 | 0.532±0.012 | 0.491±0.098 | 0.544±0.103 | 0.457±0.091 | 0.412±0.035 | 0.426±0.008 | 0.404±0.081 | 0.445±0.085 | 0.375±0.075 |
| Toluene | 1.521±0.121 | 1.878±0.099 | 1.665±0.328 | 1.149±0.220 | 1.393±0.261 | 1.061±0.085 | 1.286±0.066 | 1.174±0.232 | 0.806±0.155 | 0.980±0.184 |
| Ethylbenzene | 0.097±0.008 | 0.086±0.003 | 0.114±0.022 | 0.088±0.017 | 0.102±0.019 | 0.060±0.005 | 0.052±0.002 | 0.071±0.014 | 0.054±0.010 | 0.062±0.012 |
| o-Xylene | 0.104±0.009 | 0.100±0.001 | 0.116±0.022 | 0.094±0.018 | 0.108±0.020 | 0.064±0.005 | 0.060±0.001 | 0.072±0.014 | 0.057±0.011 | 0.066±0.012 |
| m-Xylene | 0.289±0.024 | 0.282±0.005 | 0.329±0.064 | 0.248±0.047 | 0.298±0.056 | 0.177±0.015 | 0.169±0.003 | 0.203±0.040 | 0.152±0.029 | 0.183±0.034 |
| p-Xylene | 0.073±0.006 | 0.073±0.001 | 0.077±0.015 | 0.067±0.013 | 0.073±0.014 | 0.044±0.004 | 0.044±0.000 | 0.047±0.009 | 0.041±0.008 | 0.045±0.008 |
| Cumene | 0.003±0.000 | 0.003±0.000 | 0.004±0.001 | 0.003±0.001 | 0.003±0.001 | 0.002±0.000 | 0.002±0.000 | 0.002±0.000 | 0.002±0.000 | 0.002±0.000 |
| 1-Me-2-Et-benzene | 0.010±0.001 | 0.010±0.000 | 0.012±0.002 | 0.009±0.002 | 0.011±0.002 | 0.006±0.000 | 0.005±0.000 | 0.006±0.001 | 0.005±0.001 | 0.006±0.001 |
| 1-Me-3-Et-benzene | 0.035±0.003 | 0.033±0.000 | 0.039±0.008 | 0.032±0.006 | 0.037±0.007 | 0.019±0.002 | 0.018±0.000 | 0.021±0.004 | 0.017±0.003 | 0.020±0.004 |
| 1-Me-4-Et-benzene | 0.015±0.001 | 0.014±0.000 | 0.016±0.003 | 0.013±0.003 | 0.015±0.003 | 0.008±0.001 | 0.008±0.000 | 0.009±0.002 | 0.007±0.001 | 0.008±0.002 |
| 123-triMe-benzene | 0.007±0.001 | 0.007±0.000 | 0.007±0.001 | 0.007±0.001 | 0.007±0.001 | 0.004±0.000 | 0.004±0.000 | 0.004±0.001 | 0.004±0.001 | 0.004±0.001 |
| 124-TriMe-benzene | 0.041±0.003 | 0.043±0.001 | 0.042±0.008 | 0.038±0.007 | 0.040±0.008 | 0.022±0.002 | 0.023±0.000 | 0.023±0.004 | 0.020±0.004 | 0.022±0.004 |
| 135-triMe-benzene | 0.015±0.001 | 0.016±0.001 | 0.016±0.003 | 0.013±0.002 | 0.015±0.003 | 0.008±0.001 | 0.009±0.000 | 0.009±0.002 | 0.007±0.001 | 0.008±0.002 |
| Propylbenzene | 0.012±0.001 | 0.011±0.000 | 0.014±0.003 | 0.012±0.002 | 0.012±0.002 | 0.007±0.001 | 0.006±0.000 | 0.008±0.001 | 0.007±0.001 | 0.007±0.001 |
| 1,4-diethylbenzene | 0.002±0.000 | 0.002±0.000 | 0.003±0.001 | 0.003±0.000 | 0.003±0.000 | 0.001±0.000 | 0.001±0.000 | 0.001±0.000 | 0.001±0.000 | 0.001±0.000 |
| Ethanol | 4.387±0.351 | 4.363±0.014 | 4.392±0.810 | 4.374±0.805 | 4.421±0.815 | 10.726±0.863 | 10.485±0.035 | 10.831±2.000 | 10.701±1.973 | 10.885±2.008 |
| Propene | 0.029±0.004 | 0.031±0.002 | 0.012±0.004 | 0.047±0.014 | 0.025±0.006 | 0.046±0.006 | 0.049±0.004 | 0.020±0.006 | 0.076±0.022 | 0.041±0.010 |
| 1-butene | 0.077±0.010 | 0.052±0.004 | 0.048±0.014 | 0.142±0.033 | 0.067±0.016 | 0.094±0.012 | 0.062±0.005 | 0.059±0.017 | 0.173±0.040 | 0.082±0.019 |
| Cis-2-butene | 0.307±0.041 | 0.192±0.018 | 0.168±0.051 | 0.643±0.147 | 0.227±0.054 | 0.374±0.050 | 0.233±0.023 | 0.206±0.062 | 0.779±0.176 | 0.279±0.066 |
| 2-methylpropene | 0.052±0.007 | 0.033±0.002 | 0.033±0.009 | 0.096±0.023 | 0.048±0.011 | 0.063±0.008 | 0.039±0.003 | 0.040±0.011 | 0.116±0.028 | 0.059±0.013 |
| 1-pentene | 0.461±0.053 | 0.271±0.033 | 0.329±0.100 | 0.769±0.153 | 0.475±0.106 | 0.451±0.052 | 0.264±0.033 | 0.324±0.098 | 0.750±0.149 | 0.468±0.104 |
| Cis-2-pentene | 0.568±0.063 | 0.335±0.038 | 0.419±0.108 | 0.930±0.182 | 0.589±0.130 | 0.556±0.061 | 0.325±0.038 | 0.412±0.106 | 0.907±0.177 | 0.580±0.128 |
| trans-2-pentene | 1.118±0.125 | 0.626±0.075 | 0.889±0.229 | 1.718±0.336 | 1.239±0.281 | 1.095±0.123 | 0.609±0.075 | 0.875±0.226 | 1.676±0.327 | 1.219±0.277 |

| | | | | | | | | | | |
|------------------------------|-------------|-------------|-------------|-------------|-------------|-------------|-------------|-------------|-------------|-------------|
| 2-methyl-1-butene | 0.871±0.101 | 0.484±0.064 | 0.653±0.187 | 1.428±0.284 | 0.920±0.205 | 0.853±0.098 | 0.471±0.064 | 0.642±0.183 | 1.392±0.276 | 0.906±0.202 |
| 3-methyl-1-butene | 0.185±0.024 | 0.097±0.017 | 0.147±0.054 | 0.292±0.060 | 0.203±0.047 | 0.181±0.023 | 0.095±0.017 | 0.144±0.053 | 0.284±0.058 | 0.200±0.047 |
| 2-methyl-2-butene | 1.959±0.217 | 1.044±0.121 | 1.659±0.414 | 2.939±0.577 | 2.196±0.485 | 1.919±0.213 | 1.014±0.121 | 1.634±0.407 | 2.866±0.561 | 2.163±0.477 |
| 1-hexene | 0.049±0.005 | 0.037±0.004 | 0.032±0.007 | 0.084±0.016 | 0.041±0.008 | 0.040±0.004 | 0.030±0.003 | 0.026±0.006 | 0.068±0.013 | 0.034±0.006 |
| Cis-2-hexene | 0.079±0.007 | 0.061±0.006 | 0.056±0.012 | 0.107±0.020 | 0.093±0.017 | 0.065±0.006 | 0.049±0.005 | 0.046±0.010 | 0.087±0.016 | 0.076±0.014 |
| Trans-2-hexene | 0.188±0.018 | 0.143±0.019 | 0.148±0.033 | 0.197±0.037 | 0.266±0.050 | 0.154±0.015 | 0.116±0.016 | 0.120±0.027 | 0.161±0.030 | 0.218±0.041 |
| Cis-3-hexene | 0.114±0.010 | 0.087±0.010 | 0.083±0.018 | 0.145±0.027 | 0.140±0.025 | 0.093±0.009 | 0.071±0.008 | 0.068±0.015 | 0.118±0.022 | 0.114±0.021 |
| 2-Me-1-pentene | 0.111±0.010 | 0.082±0.009 | 0.086±0.018 | 0.143±0.027 | 0.135±0.024 | 0.091±0.008 | 0.067±0.008 | 0.070±0.015 | 0.116±0.022 | 0.110±0.020 |
| 4-methyl-1-pentene | 0.050±0.005 | 0.034±0.003 | 0.037±0.008 | 0.075±0.014 | 0.053±0.009 | 0.041±0.004 | 0.028±0.003 | 0.030±0.007 | 0.061±0.012 | 0.043±0.008 |
| 2-methyl-2-pentene | 0.363±0.042 | 0.273±0.053 | 0.323±0.083 | 0.234±0.044 | 0.624±0.127 | 0.296±0.034 | 0.222±0.043 | 0.263±0.067 | 0.190±0.036 | 0.510±0.104 |
| C-3Me-2-pentene | 0.082±0.008 | 0.059±0.006 | 0.053±0.014 | 0.138±0.026 | 0.076±0.016 | 0.067±0.007 | 0.048±0.005 | 0.044±0.011 | 0.112±0.021 | 0.062±0.013 |
| T-3Me-2-pentene | 0.103±0.012 | 0.060±0.013 | 0.061±0.019 | 0.196±0.037 | 0.097±0.022 | 0.084±0.010 | 0.049±0.011 | 0.050±0.016 | 0.159±0.030 | 0.080±0.018 |
| C-4Me-2-pentene | 0.028±0.004 | 0.018±0.004 | 0.022±0.008 | 0.019±0.005 | 0.053±0.014 | 0.023±0.003 | 0.015±0.003 | 0.018±0.006 | 0.015±0.004 | 0.044±0.011 |
| T-4Me-2-pentene | 0.235±0.029 | 0.169±0.037 | 0.214±0.057 | 0.123±0.023 | 0.432±0.091 | 0.191±0.024 | 0.138±0.030 | 0.174±0.046 | 0.100±0.019 | 0.354±0.074 |
| 2,3-dimethyl-1-butene | 0.066±0.006 | 0.046±0.006 | 0.053±0.012 | 0.078±0.015 | 0.087±0.016 | 0.054±0.005 | 0.037±0.005 | 0.044±0.009 | 0.063±0.012 | 0.071±0.013 |
| 3,3-dimethylbutene | 0.009±0.001 | 0.006±0.001 | 0.007±0.002 | 0.015±0.003 | 0.008±0.002 | 0.007±0.001 | 0.005±0.000 | 0.005±0.001 | 0.012±0.002 | 0.007±0.001 |
| 2,3-dimethyl-2-butene | 0.047±0.005 | 0.034±0.005 | 0.039±0.009 | 0.045±0.008 | 0.070±0.013 | 0.038±0.004 | 0.028±0.004 | 0.032±0.007 | 0.036±0.007 | 0.057±0.011 |
| C-1,3-pentadiene | 0.009±0.001 | 0.006±0.001 | 0.007±0.002 | 0.015±0.003 | 0.009±0.002 | 0.009±0.001 | 0.006±0.001 | 0.007±0.002 | 0.014±0.003 | 0.009±0.002 |
| T-1,3-pentadiene | 0.017±0.002 | 0.010±0.001 | 0.014±0.004 | 0.027±0.005 | 0.019±0.004 | 0.017±0.002 | 0.010±0.001 | 0.013±0.004 | 0.026±0.005 | 0.019±0.004 |
| 2-Me-1,3-butadiene | 0.024±0.003 | 0.014±0.002 | 0.020±0.006 | 0.036±0.007 | 0.027±0.006 | 0.024±0.003 | 0.014±0.002 | 0.019±0.006 | 0.035±0.007 | 0.026±0.006 |
| 1-Heptene | 0.007±0.001 | 0.006±0.001 | 0.004±0.001 | 0.013±0.003 | 0.006±0.001 | 0.005±0.001 | 0.004±0.001 | 0.003±0.001 | 0.009±0.002 | 0.005±0.001 |
| Trans-2-heptene | 0.001±0.000 | 0.002±0.000 | 0.000±0.000 | 0.000±0.000 | 0.000±0.000 | 0.000±0.000 | 0.001±0.000 | 0.000±0.000 | 0.000±0.000 | 0.000±0.000 |
| T3-Heptene | 0.010±0.001 | 0.006±0.001 | 0.005±0.002 | 0.020±0.004 | 0.009±0.002 | 0.007±0.001 | 0.004±0.001 | 0.004±0.001 | 0.014±0.003 | 0.006±0.001 |
| C2-Octene | 0.002±0.000 | 0.001±0.000 | 0.001±0.000 | 0.002±0.000 | 0.002±0.000 | 0.001±0.000 | 0.001±0.000 | 0.001±0.000 | 0.001±0.000 | 0.002±0.000 |
| Cyclopentene | 0.177±0.020 | 0.109±0.011 | 0.112±0.028 | 0.312±0.064 | 0.174±0.036 | 0.173±0.019 | 0.105±0.011 | 0.110±0.028 | 0.304±0.062 | 0.171±0.036 |

Chapter 5: Evidence for emissions from petroleum operations in California's San Joaquin Valley

Abstract

Petroleum operations are prominent in the southern San Joaquin Valley and concentrations of many associated hydrocarbons are well above other urban areas. Using a source receptor model with chemical mass balancing of Volatile Organic Compound (VOC) measurements from the CalNex-Bakersfield supersite, I present evidence of a large source of paraffinic hydrocarbons associated with unrefined petroleum gas. There are numerous VOCs presented that have limited previous *in situ* measurements and have not been associated with petroleum operations in the past, many of which are branched and cyclic alkanes. I use novel statistical modeling with Flexpart meteorological data and ground-based data to assess the spatial distribution of emissions in the southern San Joaquin Valley, which is consistent with aircraft measurements of propane and the locations of oil wells. Methane emissions associated with the petroleum gas are not significant despite very good agreement of other hydrocarbons with the unrefined natural gas composition measured at wells by the U.S. Geological Survey, which suggests that the emissions are predominantly from condensate storage tanks containing the non-methane liquids separated from the associated gas. The abundance of non-methane hydrocarbons due to petroleum gas ranges 30-150% of emissions from motor vehicles by carbon mass in Bakersfield. The non-methane hydrocarbon emissions from the petroleum gas source are an important source of hydrocarbon mass in the region and, given a calculated normalized reactivity of $0.67 \text{ gO}_3 \text{ g}^{-1}$, may have a minor effect on atmospheric chemistry. A rough comparison with the California Air Resources Board emission inventory validates the relative emissions of reactive organic gases compared to motor vehicles in the San Joaquin Valley and Kern County.

1. Introduction

California's San Joaquin Valley is an important region for oil and natural gas production in the United States. Operations include extraction, storage, transport, and processing; all of which may have varying degrees of fugitive emissions of methane and other gas-phase organic carbon, such as Volatile Organic Compounds (VOCs) (1, 2). Crude oil and unrefined natural gas are composed of a broad suite of organic compounds that span a range of vapor pressures, and are either produced by thermogenic or biogenic processes (3). Thermogenic gas is produced via the cracking of larger compounds in oil and can either be termed associated or non-associated depending on the presence of oil (3). The vast majority of wells in the San Joaquin Valley are oil wells and most have associated gas, also known as wet thermogenic gas (3). Thermogenic wet gas is predominately found in oil wells as the gas is geochemically produced from the cracking of larger molecules in oil, and thus contains substantial amounts of non-methane hydrocarbons ranging from 3 to 40% C_2 and greater content (Table 1) (3). Crude oil production in Kern County within the San Joaquin Valley is $450,000 \text{ barrels day}^{-1}$, which represents 69% of production within California and 8% of national production (4, 5).

Previous studies in the urban area of Houston, a prominent region for petroleum imports and refining have reported considerable emissions attributed to oil/gas operations and petrochemical production of other chemicals (1, 2). One evident source, termed oil/natural gas evaporation from refineries, was comprised of C_{2-7} straight and branched alkanes, as well as cyclopentane, cyclohexane, and methylcyclopentane. In one study, this source accounted for

27% of observed VOC mass at the urban site outside of the Houston shipping channel, and ranged from 10-40 ppbC diurnally (1).

The objective of this chapter is to examine the existence and magnitude of hydrocarbon emissions from petroleum operations in the San Joaquin Valley. This is accomplished using multiple VOC data sets and novel methods to assess the spatial distribution of sources (i.e. a statistical source footprint) via meteorological modeling. I will also examine the potential of petroleum operation emissions to impact air quality relative to motor vehicle emissions, and compare my results to the California Air Resources Board (CARB) emission inventory.

2. Materials & Methods

Using 6 weeks of VOC data collected in Bakersfield, CA as part of the CalNex (California at the Nexus of Air Quality and Climate Change) campaign, I assessed emissions from petroleum operations during Summer 2010. The magnitude of petroleum gas observed at the site was determined using source receptor modeling with chemical mass balancing; details on these methods and data collection have been described previously (Chapter 2). *A priori* source profile information for the model was constructed using U.S. Geological Survey data on associated thermogenic natural gas composition from wells in the San Joaquin Valley (Table 5.1) (3). The compounds used in the over-constrained model were propane, n-butane, n-pentane, isopentane, m/p-xylene, o-xylene, isooctane, n-nonane, n-undecane, n-dodecane to model motor vehicle and petroleum gas sources. Propane and n-butane were corrected for background values of 500 and 100 pptv, respectively. Standard errors were used as uncertainties in the model for the petroleum gas source as their standard deviations were ± 80 -300% given the variability between wells and sampling methods in the data compiled by the U.S.G.S. This was an order of magnitude greater than motor vehicle source profiles and would have otherwise been insufficient to constrain the petroleum source, so standard errors were used in this case to model the petroleum gas source.

Emissions of additional compounds from petroleum operations are inferred from an array of hydrocarbons not present in the initial limited petroleum gas profile that episodically exceed predicted concentrations from gasoline and diesel vehicles based on coincident fuel data from Bakersfield (Chapter 4). The residuals, or excess concentrations beyond contributions from motor vehicles, were filtered for values that exceed the uncertainties of model calculations, which are determined in part by the 10-20% variability in fuels. Measurements of a few light VOCs not measured *in situ* are included from canister measurements to further characterize the observed sources. Canisters were taken as 3-hour averages in the morning (5-8 PST) and analyzed via U.S. EPA methods for an array of organic compounds. Supporting methane measurements were made using integrated cavity output spectroscopy (Los Gatos Research, Fast Greenhouse Gas Analyzer) with 1-min time resolution. OH reactivities and ozone formation potentials are examined using literature OH reaction constants, and Maximum Incremental Reactivities (MIRs) (6, 7).

The spatial distribution of emissions is examined via two methods, using canister samples taken on NOAA's P3 aircraft and using ground measurements from the CalNex site coupled with meteorological modeling to assess the ground-level footprint of each 30-minute sample over the previous 6-12 hours. We generated 6- and 12-hour back-trajectory footprints with 4 km resolution for each hourly sample using the Flexpart Lagrangian dispersion meteorological modeling package as described in Chapter 2 (Figure 5.1). Here, I present the first integration of this meteorological modeling method with statistical back-trajectory analysis to explore the

distribution and relative magnitude of VOC sources at ground level. I contend that this method is superior to using single back trajectories (i.e. HYSPLIT), which do not directly inform the residence time of an air parcel at ground level or the distribution of residence time along a back trajectory or a collection of back trajectories during a campaign.

3. Results and Discussion

The reported non-methane composition of thermogenic wet gas (Table 5.1) accurately represented the observed petroleum gas source. The composition of the natural gas has substantial variability among all the wells sampled, but is consistent with atmospheric observations using both *in situ* and canister data at Bakersfield. The relative ratios of hydrocarbons in my *in situ* data, the canister data, and the thermogenic wet gas profile data are compared to strengthen the argument for petroleum gas as the observed source. Additionally, the ratios are also compared to a similar petroleum source factor from one of the Houston studies (1). The ethane to propane ratio expected from the thermogenic wet wells in the San Joaquin Valley is 1.2 in terms of mass carbon, which is similar to canister measurements at the Bakersfield site (1.4) and measurements in Houston (1.0) (Figure 5.2). Propane to n-butane ratios are all similar with 2.9, 3.0, 2.2 and 2.0 in the oil well data, in Houston, and at Bakersfield in canister and *in situ* data, respectively. Ratios of n-butane to isobutane also support the conclusion of a petroleum gas source as they are 1.7, 2.9, and 2.0 in the oil well, in Houston, and in canister measurements from Bakersfield. Comparisons of these ratios have considerable uncertainty when considering the variability among oil/gas wells within a region and compared to other regions.

The 25th percentiles for propane and n-butane are similar to other urban ground sites during the summer, but higher concentrations were observed for the 50th and 75th percentiles, by up to a factor of 2 compared to Pittsburgh, PA (2002) (8). The 75th percentiles in the San Joaquin Valley are even higher by 25-50% than values from Riverside, CA, a much more populated region, in summer 2005 (data from Chapter 3).

The over-constrained chemical mass balance model used in Chapter 4 effectively modeled emissions of most compounds in the tunnel study and many of the compounds that are most prevalent in gasoline and diesel at Bakersfield. Yet, in addition to the compounds known to be in natural gas, the model under-predicted numerous alkanes. These compounds are summarized in Table 5.2 and Figure 5.4, which shows their average unexplained concentrations and the percent of total mass that is unexplained as determined by the residuals in the source receptor model. Most of the mass of unexplained alkanes was well correlated ($r \geq 0.75$) with the petroleum gas signal, so it is attributed to this source. The presence of the branched and cyclic alkanes in unrefined petroleum gas is not surprising as there are significant amounts of C₅₋₇ straight chain alkanes in the reported composition (Table 5.1). Many of these compounds are reported here as *in-situ* measurements for the first time, especially many of the cyclic alkanes.

We assessed our model output to check for contributions from products of incomplete combustion. The only considerable impact was from cyclopentane as emissions in the Caldecott tunnel were higher than expected based on the abundance of cyclopentane in liquid gasoline. I determined that emissions of cyclopentane in gasoline exhaust due to formation from other precursors in the fuel were equivalent to those from cyclopentane present in unburned fuel, such that doubling the emission factor of cyclopentane accurately modeled emission in the on-road tunnel study. A similar, but larger increase is known for benzene (9). I did not observe any significant emission enhancement for cyclohexane.

The additional compounds attributed to the petroleum gas source profile increase the mass of emissions by 10% as shown by the regression of the correlated unexplained compounds with the petroleum gas source ($r=0.95$) (Figure 5.6). The weight fraction of each correlated compound in the “unexplained” mass is shown in Table 5.2 with similar fractions in the overall source profile as the known C_{5-7} compounds in petroleum gas. Using this new source profile, the ozone forming potential is calculated to be $0.67 \text{ gO}_3 \text{ g}^{-1}$ with the new compounds increasing the reactivity from $0.58 \text{ gO}_3 \text{ g}^{-1}$. In all, the interquartile range of the unrefined natural gas source contribution was 8.3-90 ppbC, with a diurnal pattern that was strongly dependent on meteorological dilution (Figure 5.5). The mass concentration of compounds from unrefined natural gas ranged from 30-40% to 100-150% of the sum of compounds from motor vehicles during the afternoon and nighttime, respectively (Figure 5.7).

The remaining branched and cyclic compounds that were not highly correlated with the petroleum gas source represent a relatively small amount of mass and a source could not be inferred for these compounds. The excess C_{13-16} branched alkanes were well-correlated ($r \geq 0.80$) with each other, but not with any of the other compounds. The excess concentrations of C_{10-11} branched alkanes are correlated with each other, and one of the compounds, 2,6-dimethylcyclooctane, is well-correlated ($r \geq 0.80$) with the three C_9 cycloalkanes that do not correlate well with the petroleum gas source. These remaining compounds have ozone formation potentials similar to other observed compounds, ranging from 0.6 to $1.6 \text{ gO}_3 \text{ g}^{-1}$, but their excess concentrations after modeling were minimal—average values from 0 to 0.15 ppbC (Figure 5.4).

Using Flexpart meteorological data for the region, distributions of back-trajectories were calculated for 6 and 12 hours prior to arrival and measurement at the Bakersfield site. Overall averages, as well as day and nighttime averages are shown for the entire campaign in Figure 5.1. At all times, the influence of local emissions near the site is important. Daytime measurements are largely impacted by the north-northwest due to consistent up-valley flows during the day. In contrast, at night the wind speeds and direction are more variable and irregular with flows that arrive from all directions, but originate from up-valley flows from the north-northwest. Extensive reviews of meteorology and flow patterns in the San Joaquin Valley found elsewhere are consistent with the results presented in this work (10, 11). Statistical meteorological modeling using ground site data resulted in a spatial distribution of petroleum gas emissions similar to that of oil wells in the southern San Joaquin Valley (Figure 5.8). Additionally, canister samples taken via aircraft in the region show higher propane (a major component of the source profile) concentrations for some points in the southern part of the valley (Figure 5.8C). Given the co-location of oil wells in the region and the spatial distribution of elevated concentrations of petroleum gas compounds, it is very likely that emissions occur at or near the wells during extraction/storage in addition to other potential emissions downstream in operations.

Observations of methane and the petroleum gas source are not well correlated (Figure 5.9) and the potential methane emissions expected from the thermogenic wet gas source profile would be equivalent to all of the methane enhancements above background concentrations. However, since non-methane compound ratios and chemical mass balance modeling agreed well with source profile for petroleum gas extracted in the region, I am confident that the source originates from unrefined petroleum gas, but excludes the methane. My observation of a major petroleum gas source with minimal coincident methane is consistent with measurements of emissions from condensate tanks, which contain the separated non-methane liquids and have been shown in two Texas-based studies to be dominated by non-methane hydrocarbons (12, 13). The studies demonstrated that condensate tanks emit 4-6 times more VOCs than methane

whereas all other emission pathways emit 3-15 times more methane than VOCs, and methane was on average only 15 ± 11 wt% of 20 vent gas samples from condensate tanks (12, 13).

A comparison of methane to non-vehicular ethanol (calculated via the CMB model) supports this claim that methane emissions from the petroleum source are relatively minor in the San Joaquin Valley as the two compounds are well correlated with no major methane spikes above the ratio inferred from the regression (Figure 5.10). Additionally, coloring the points by the petroleum gas factor showed no pattern towards higher ratios of methane to non-vehicular ethanol (not shown). Additional ethanol contributions are evident and have the strongest coincidence with high concentrations of chloroform. Carbon disulfide and ethanethiol (not shown) also show a similar trend as chloroform, but for different points that diverge from the line in Figure 5.10. Thus, it is evident that emissions of methane are dominated by the same source as non-vehicular ethanol and are relatively minor from the petroleum gas source. The reason methane is not co-emitted with other compounds in this source profile is because of the minor concentrations of methane in condensate storage tanks. Further work underway by CARB focused on quantifying emissions from these tanks will further constrain the source and strengthen the case for control through either vapor recovery systems or vent flares (14).

On a mass basis emissions of petroleum gas are important at the Bakersfield site as observed concentrations of petroleum gas were 30-40% of that from motor vehicles during the day and 100-150% at night. Yet, they represent a relatively minor contribution to potential ozone formation, as the MIR value is 3-5 times less than that of gasoline sources. Secondary organic aerosol (SOA) formation from this source is likely to be minimal given that the yields for all of the alkanes with 8 or less carbon atoms will be $0.002 \text{ gSOA g}^{-1}$ at most with an organic particle loading of $10 \mu\text{g m}^{-3}$ (Chapter 4). The CARB emissions inventory for the San Joaquin Valley reports an average of 35 tons ROG per day, which is equal to 28% of mobile source emissions in the air basin (15). This value is roughly consistent with the daytime ratio observed at the Bakersfield site, but is expectedly lower than nighttime ratios as Bakersfield is in much closer proximity to potential sources than many other portions of the air basin. A comparison on a smaller scale for the portion of Kern county in the San Joaquin Valley supports this as the CARB inventory has petroleum operations emitting 132% that of mobile sources with much of the San Joaquin Valley's petroleum operation emission in this county (15). This observation is consistent with the statistical footprints shown in this work as daytime footprints encompass a larger footprint that stretches into other counties while nighttime footprints are more heavily influenced by local emissions. This intercomparison, while rough, provides some validation of the CARB emission inventory for petroleum operations in the San Joaquin Valley.

References

1. Leucher M. and Rappengluck B. (2010) VOC source-receptor relationships in Houston during TexAQS-II, *Atmos. Environ.*, 44, 4056-4067.
2. Buzcu B. and Fraser M.P. (2006) Source identification and apportionment of volatile organic compounds in Houston, TX, *Atmos. Environ.*, 40, 2385-2400.
3. U.S. Geological Survey, Petroleum Systems of the San Joaquin Basin Province—Geochemical Characteristics of Gas Types by P.G. Lillis, A. Warden, G.E. Claypool, and L.B. Magoon, Chapter 10 in "Petroleum Systems and Geologic Assessment of Oil and Gas in the San Joaquin Basin Province, California" A.H. Scheirer ed., 2007 (<http://pubs.usgs.gov/pp/pp1713/>).

4. U.S. Energy Information Administration, *U.S. Crude Oil Production by State, 2004*. (http://www.eia.gov/dnav/pet/PET_CRD_CRPDN_ADC_MBBLPD_A.htm).
5. California Energy Commission, *California Crude Oil Production and Imports, 2006*, by M. Sheridan. (<http://www.energy.ca.gov/2006publications/CEC-600-2006-006/CEC-600-2006-006.PDF>).
6. Carter, W. P. L.: SAPRC Atmospheric Chemical Mechanisms and VOC Reactivity Scales (available at: <http://www.engr.ucr.edu/~carter/SAPRC/>)
7. Atkinson, R. and Arey, J. (2003) Atmospheric degradation of volatile organic compounds, *Chem. Rev.*, 103, 4605-4638.
8. Millet DB *et al.* (2005) Atmospheric volatile organic compound measurements during the Pittsburgh Air Quality Study: Results, interpretations, and quantification of primary and secondary contributions. *J. Geophys. Res.* 110:D07S07.
9. Leppard WR *et al.* (1992) Effects of gasoline composition on vehicle engineout and tailpipe hydrocarbon emissions. *SAE Tech. Pap. Ser.* No. 920329.
10. Bao J.W. *et al.* (2007) Observed and simulated low-level winds in a high ozone episode during the central California ozone study, *J. Applied Met. & Climate.*, 47, 2372-2394.
11. Beaver S. and Palazoglu A. (2009) Influence of synoptic and mesoscale meteorology on ozone pollution potential for San Joaquin Valley of California, *Atmos. Environ.*, 43, 1779-1788.
12. Armendariz A., "Emissions from Natural Gas Production in the Barnett Shale Area and Opportunities for Cost-Effective Improvements," Jan. 26, 2009. (http://www.edf.org/sites/default/files/9235_Barnett_Shale_Report.pdf) Accessed Oct. 2012.
13. Hendler A., Nunn J., Lundeen J., McKaskle R. "VOC Emissions from Oil and Condensate Storage Tanks – Final Report," a report prepared for the Houston Advanced Research Center. October 31, 2006. (<http://files.harc.edu/Projects/AirQuality/Projects/H051C/H051CFinalReport.pdf>) Accessed Oct. 2012.
14. California Air Resources Board, "Determination of Methane, Carbon Dioxide, and Volatile Organic Compounds from Crude Oil and Natural Gas Separation and Storage Tank Systems," June, 2012 Draft. (http://www.arb.ca.gov/cc/oil-gas/flash_protocol_dec29.pdf) Accessed Oct. 2012.
15. California Air Resources Board, *Estimated annual average emissions, 2010*. (<http://www.arb.ca.gov/ei/emsmain/emsmain.htm>) Accessed May 2012.

Tables and Figures

Table 5.1: Unrefined natural gas profile for thermogenic wet wells in the San Joaquin Valley from U.S.G.S. samples (N=49 wells)

| | wtC% | Std. Dev. | k_{OH} | MIR |
|-------------|-------------|------------------|-----------------------|------------|
| methane | 82.3 | 9.2 | 0.0064 | 0.014 |
| ethane | 5.33 | 3.46 | 0.248 | 0.28 |
| propane | 4.42 | 3.50 | 1.09 | 0.49 |
| isobutane | 0.920 | 0.837 | 2.12 | 1.23 |
| n-butane | 1.55 | 2.17 | 2.36 | 1.15 |
| isopentane | 0.223 | 0.401 | 3.6 | 1.45 |
| n-pentane | 0.273 | 0.405 | 3.80 | 1.31 |
| neo-pentane | 0.061 | 0.182 | 0.825 | 0.67 |
| n-hexane | 0.105 | 0.108 | 5.20 | 1.24 |
| n-heptane | 0.049 | 0.041 | 6.76 | 1.07 |

Notes: k_{OH} is in cm³ s⁻¹ molecules⁻¹ × 10¹² and are from Ref. 7

MIR is in gO₃ g⁻¹ and are from Ref. 6

Table 5.2: Interquartile ranges and MIRs for alkanes discussed in this work

| Compound Name | # in Fig. 5.3 | Interquartile Range [pptv] | WtC% of Unexplained Mass | MIR [$\text{gO}_3 \text{g}^{-1}$] |
|--|---------------|----------------------------|--------------------------|-------------------------------------|
| propane | - | 1133 - 5602 | | 0.49 |
| n-butane | - | 230 - 6397 | | 1.15 |
| n-pentane | - | 221 - 2127 | | 1.31 |
| 2-2-dimethylbutane | 1 | 28.0 - 76.6 | | 1.17 |
| 2-methylpentane & 2,3-dimethylbutane | 2 | 121.6 - 501.0 | 9.02 | 1.2 |
| 3-methylpentane | 3 | 50.1 - 253.9 | 7.41 | 1.80 |
| 2,4- & 2,2-dimethylpentane | 4 | 13.7 - 54.7 | | 1.3 |
| 3,3-dimethylpentane | 5 | 4.0 - 16.6 | | 1.20 |
| 2,3-dimethylpentane | 6 | 19.7 - 93.0 | | 1.34 |
| 2-methylhexane | 7 | 23.2 - 90.3 | 2.76 | 1.19 |
| 3-methylhexane | 8 | 28.0 - 124.6 | 3.48 | 1.61 |
| 2,2-dimethylhexane | 9 | 1.0 - 4.0 | | 1.02 |
| 2,5-dimethylhexane | 10 | 6.2 - 35.8 | 1.50 | 1.46 |
| 2,4-dimethylhexane | 11 | 7.4 - 32.0 | 0.88 | 1.73 |
| 2,2,3-trimethylpentane | 12 | 2.7 - 12.1 | | 1.22 |
| iso-octane | 13 | 39.1 - 115.3 | | 1.26 |
| 2,3,4-trimethylpentane & ctc-1,2,3-trimethylcyclopentane | 14 | 31.6 - 160.2 | 7.57 | 1.3 |
| 2,3,3-trimethylpentane & 2,3-dimethylhexane | 15 | 11.3 - 32.8 | | 1.1 |
| 2-methylheptane | 16 | 10.2 - 48.8 | 1.34 | 1.07 |
| 4-methylheptane | 17 | 4.3 - 20.7 | | 1.25 |
| 3-methylheptane | 18 | 9.3 - 43.6 | 1.84 | 1.24 |
| 2,2,5-trimethylhexane | 19 | 5.4 - 16.3 | | 1.13 |
| 2,6-dimethylheptane | 20 | 5.4 - 30.7 | 1.91 | 1.04 |
| 3,5-dimethylheptane | 21 | 2.2 - 10.3 | | 1.56 |
| 2,3-dimethylheptane | 22 | 0.9 - 4.7 | | 1.09 |
| 2- & 4-methyloctane | 23 | 2.9 - 12.7 | | 0.9 |
| 3-methyloctane & 4-ethylheptane | 24 | 3.1 - 12.9 | | 1.1 |
| 2,2,5-trimethylheptane | 25 | 0.7 - 1.7 | | 1.26 |
| 2,2,4-trimethylheptane | 26 | 0.8 - 2.6 | | 1.16 |
| C10 branched alkanes (5 unknown isomers) | 27 | 3.0 - 11.5 | | 0.94 |
| 2,6-dimethyloctane | 28 | 0.7 - 3.2 | | 1.08 |
| 2- & 3- & 4-methylnonane & 3- & 4-ethyloctane & 2,3-dimethyloctane | 29 | 6.9 - 24.6 | | 0.94 |
| C11 branched alkanes (3 unknown isomers) | 30 | 0.7 - 2.6 | | 0.73 |
| C11 branched alkanes (10 unknown isomers) | 31 | 5.4 - 17.5 | | 0.73 |
| dimethylundecane isomer #1 | 32 | 0.8 - 3.3 | | 0.6 |
| dimethylundecane isomer #2 | 33 | 0.8 - 2.6 | | 0.6 |
| C13 branched alkanes (2 unknown isomers) | 34 | 2.3 - 5.8 | | 0.6 |
| C14 branched alkanes (6 unknown isomers) | 35 | 4.4 - 11.3 | | 0.55 |
| C16 branched alkane (unknown) | 36 | 1.3 - 3.1 | | 0.47 |
| cyclopentane | 37 | 36.7 - 164.5 | 4.04 | 2.39 |
| methylcyclopentane | 38 | 57.4 - 315.3 | 8.86 | 2.19 |
| cis-1,3-dimethylcyclopentane | 39 | 14.8 - 100.1 | 5.23 | 1.94 |
| trans-1,3-dimethylcyclopentane | 40 | 16.4 - 177.7 | 7.86 | 1.94 |

| | | | | |
|---|----|--------------|------|------|
| ethylcyclopentane | 41 | 7.9 - 44.4 | 1.93 | 2.01 |
| ctc-1,2,4-trimethylcyclopentane | 42 | 5.4 - 52.2 | 4.19 | 1.53 |
| ctt-1,2,4-trimethylcyclopentane | 43 | 1.7 - 15.5 | 1.32 | 1.53 |
| Unknown methylethylcyclopentane | 44 | 0.7 - 4.3 | | 1.6 |
| iso-propylcyclopentane | 45 | 1.1 - 5.9 | 0.35 | 1.69 |
| n-propylcyclopentane | 46 | 2.1 - 10.0 | 0.58 | 1.69 |
| cyclohexane | 47 | 27.5 - 154.0 | 6.22 | 1.25 |
| methylcyclohexane | 48 | 20.4 - 147.0 | 7.30 | 1.70 |
| cis-1,3- & 1,1-dimethylcyclohexane | 49 | 4.6 - 38.4 | 3.02 | 1.4 |
| trans-1,2-dimethylcyclohexane | 50 | 4.6 - 42.4 | 3.37 | 1.41 |
| trans-1,3-dimethylcyclohexane | 51 | 2.9 - 17.8 | 0.95 | 1.52 |
| cis-1,2-dimethylcyclohexane | 52 | 1.9 - 9.8 | 0.52 | 1.41 |
| ethylcyclohexane | 53 | 4.8 - 31.9 | 2.36 | 1.47 |
| ccc-1,3,5-trimethylcyclohexane | 54 | 1.0 - 6.6 | | 1.15 |
| 1,1,3-trimethylcyclohexane | 55 | 2.0 - 20.4 | 2.32 | 1.19 |
| 1,1,4-trimethylcyclohexane | 56 | 1.1 - 8.8 | | 1.2 |
| ctt-1,2,4- & cct-1,3,5-trimethylcyclohexane | 57 | 0.7 - 3.9 | | 1.2 |
| ctc-1,2,4-trimethylcyclohexane | 58 | 1.2 - 9.6 | | 1.2 |
| 1,1,2-trimethylcyclohexane and isobutylcyclopentane | 59 | 0.7 - 2.0 | | 1.3 |
| methylethylcyclohexane isomer #1 | 60 | 0.8 - 4.5 | 0.32 | 1.4 |
| methylethylcyclohexane isomer #2 | 61 | 0.7 - 3.7 | 0.28 | 1.4 |
| iso-propylcyclohexane | 62 | 0.9 - 5.2 | | 1.3 |
| n-propylcyclohexane | 63 | 2.9 - 15.5 | | 1.29 |
| unidentified C10 cyclohexane | 64 | 2.5 - 7.8 | | 1.07 |
| unidentified C10 cyclohexanes | 65 | 0.7 - 2.7 | | 1.07 |
| unidentified C9 cycloalkane | 66 | 1.2 - 11.0 | 1.26 | 1.36 |

Table 5.3: Quartiles [ppbC] for ambient concentrations from major petroleum-based sources measured at the Bakersfield site

| | Q ₂₅ | Q ₅₀ | Q ₇₅ |
|----------------------------|-----------------|-----------------|-----------------|
| Gasoline Exhaust | 8.25 | 13.9 | 23.1 |
| Diesel Exhaust | 11.0 | 20.6 | 39.9 |
| Non-tailpipe Gasoline | 4.19 | 8.41 | 20.4 |
| Petroleum Gas Source (ROG) | 8.25 | 20.2 | 89.8 |

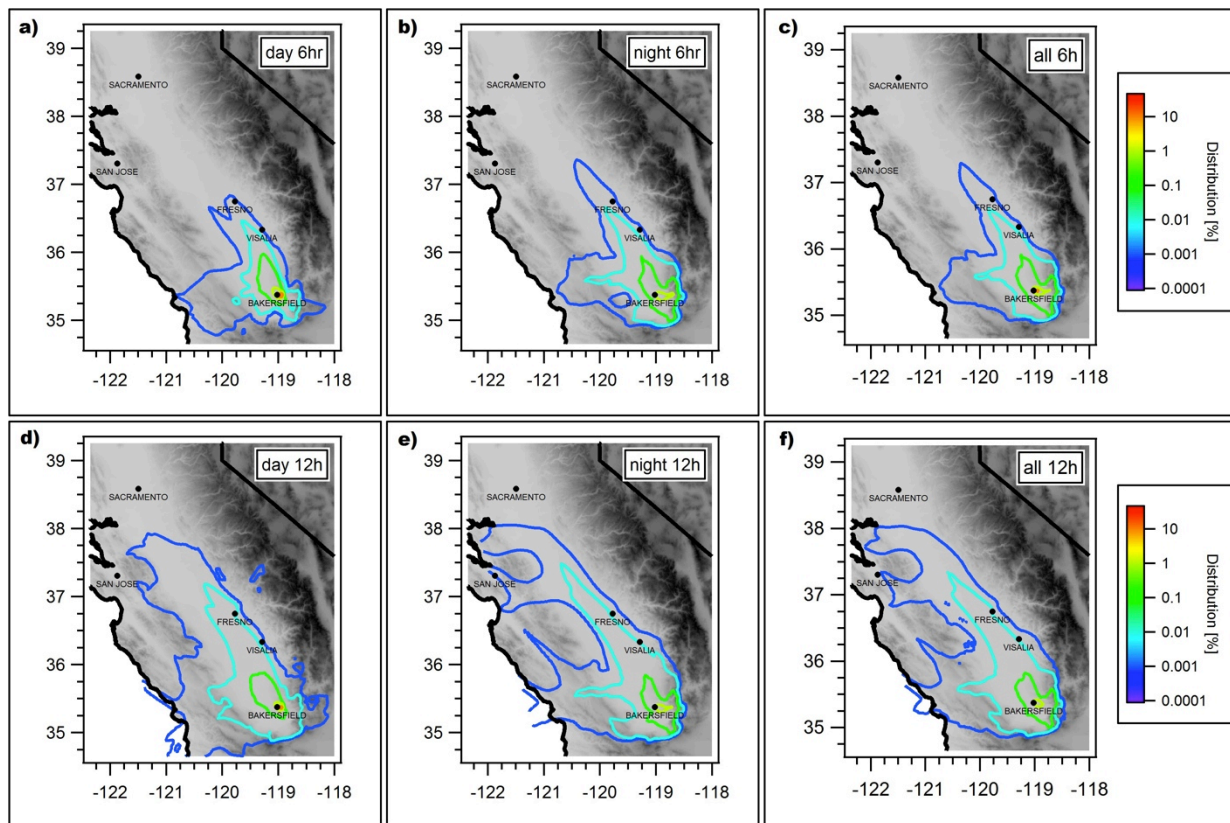


Figure 5.1: 6 and 12 hour statistical footprints for the Bakersfield ground site averaged across the entire CalNex campaign. Day (**a, d**) and nighttime (**b, e**) average are filtered for 08:00-20:00 PST and 21:00-06:00 PST, respectively, and are shown with overall averages (**c, f**).

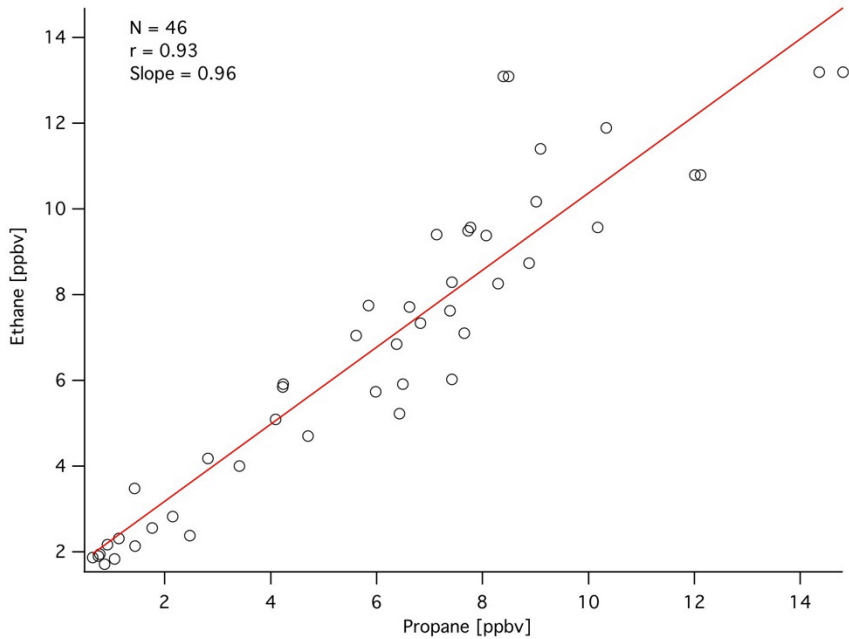


Figure 5.2: Observations of ethane vs. propane using canister measurements (5-8 PST) are well correlated with a ratio similar to that expected based on the petroleum gas source profile.

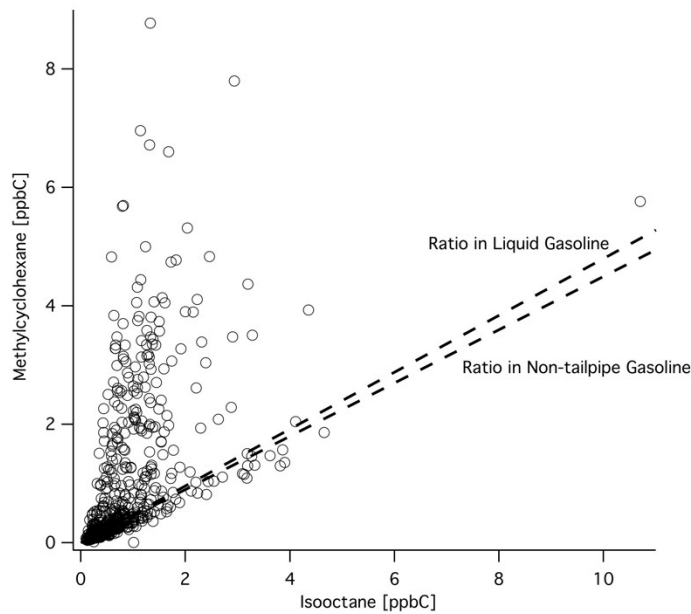


Figure 5.3: Comparison of methylcyclohexane and isooctane at the Bakersfield ground site. Isooctane is a prevalent tracer for gasoline emissions and its ratios to methylcyclohexane are roughly equivalent for exhaust and non-tailpipe emissions. Many points agree with these ratios, but numerous points have considerably more methylcyclohexane than expected. This result is similar for many other compounds whose observed values are episodically greater than predicted from gasoline and diesel sources.

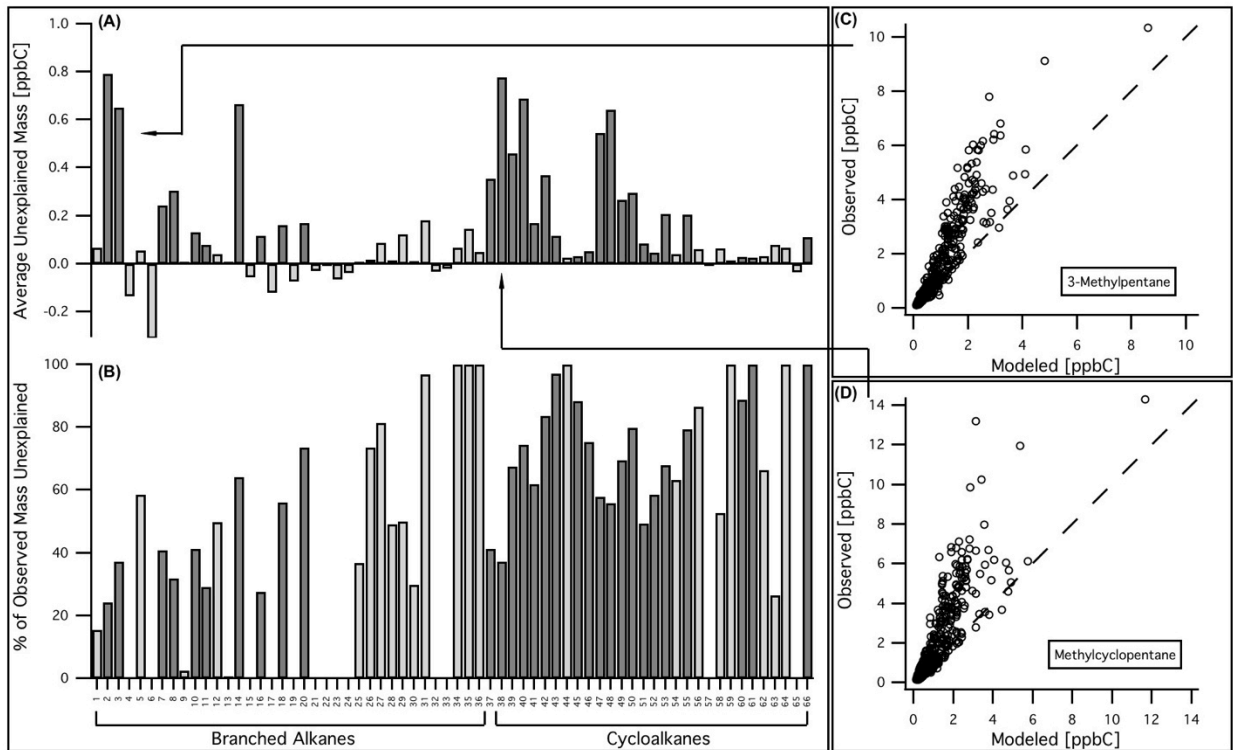


Figure 5.4: Many branched and cyclic alkanes exceeded predicted concentrations based on source profiles for motor vehicles. **(A-B)** The average unexplained concentration of each compound and the percentage of unexplained mass out of total observations. Compounds that are well correlated ($r \geq 0.75$) with the petroleum gas source are shown with shaded bars. A few compounds have negative residuals. **(C-D)** Examples of exceedances of observed over predicted values are shown with a 1:1 line.

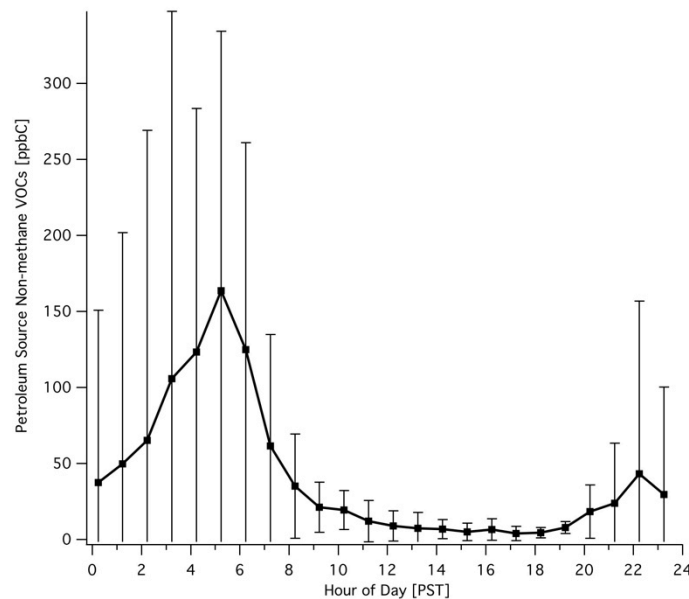


Figure 5.5: Average diurnal pattern for the petroleum gas source contribution (before “unexplained” mass is added)

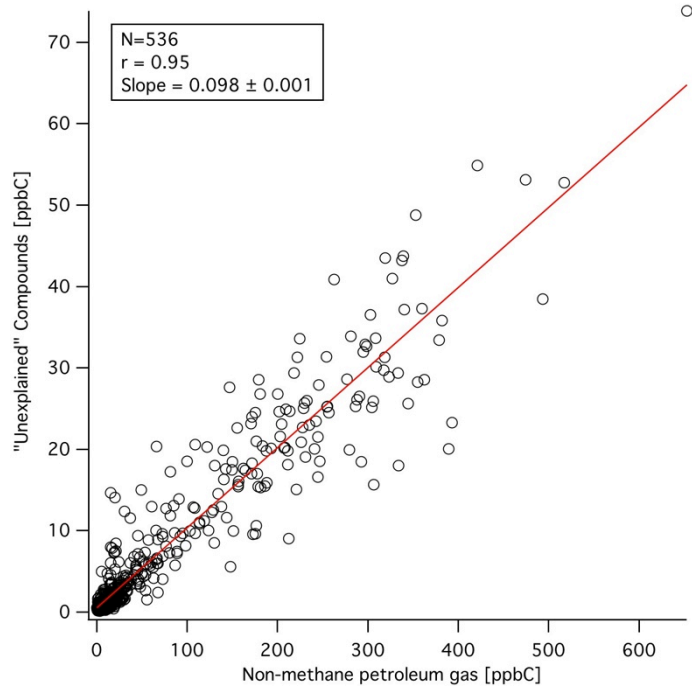


Figure 5.6: The sum of unexplained compounds that were correlated with the petroleum gas source is very well correlated with a slope of 0.098 increasing emissions by 10% from the original profile

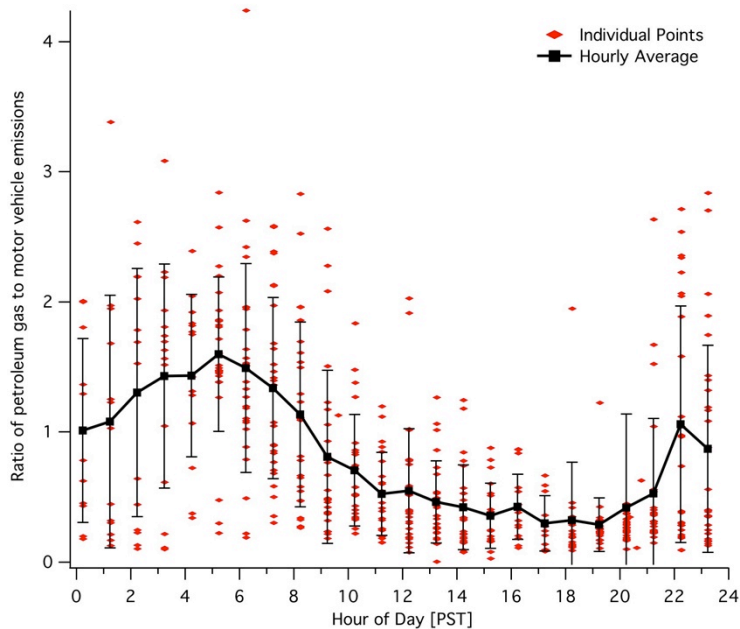


Figure 5.7: The diurnal average of the ratio of petroleum gas (including "unexplained" mass) to the sum of motor vehicle emissions.

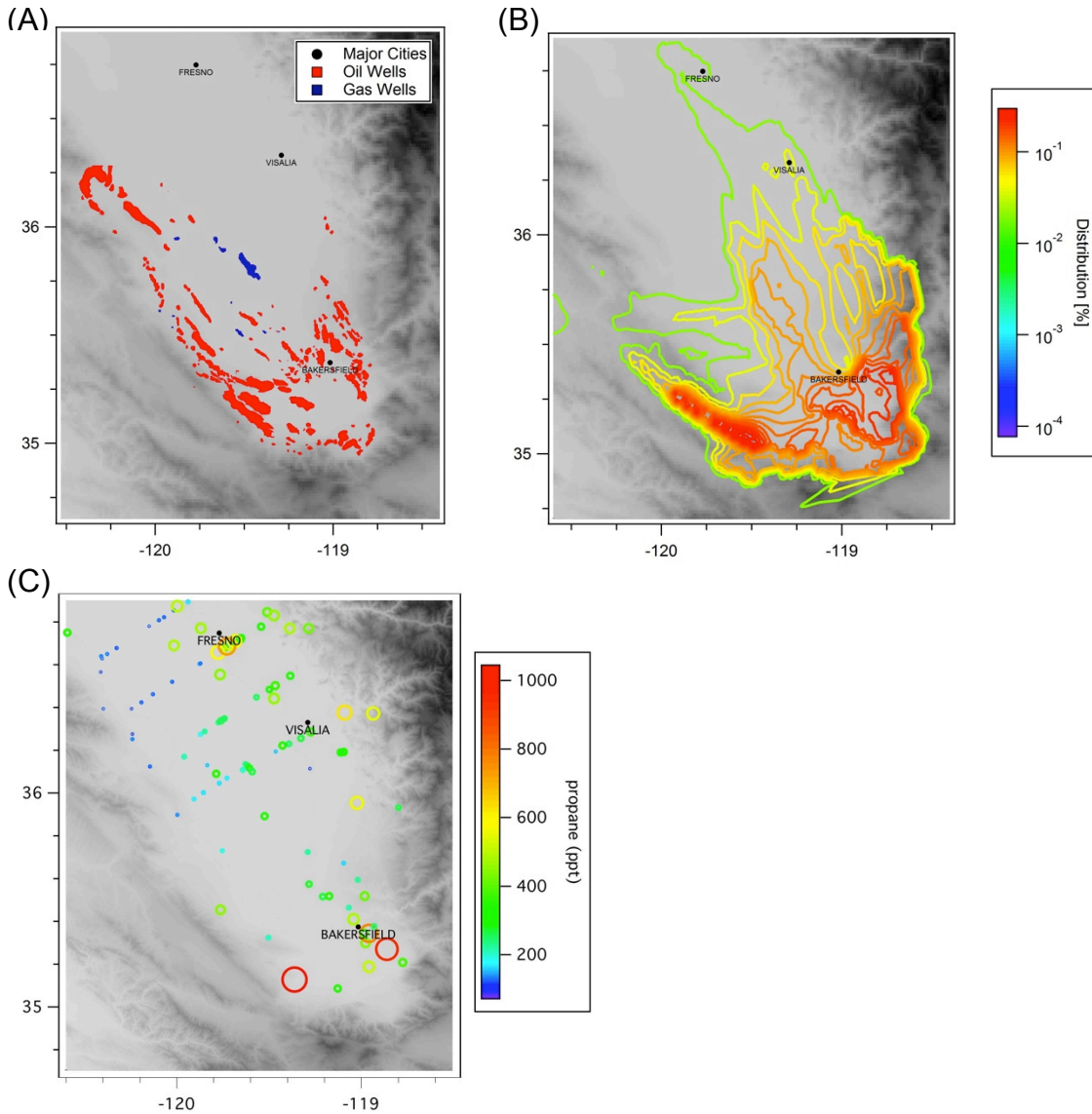


Figure 5.8: Maps of southern part of the San Joaquin Valley with **(A)** the location of oil and gas wells, **(B)** the spatial distribution of petroleum gas emissions determined using statistical footprint analysis, and **(C)** aircraft canister measurements of propane, sized and colored by concentration. Together the maps show a similar distribution of wells and emissions in the region.

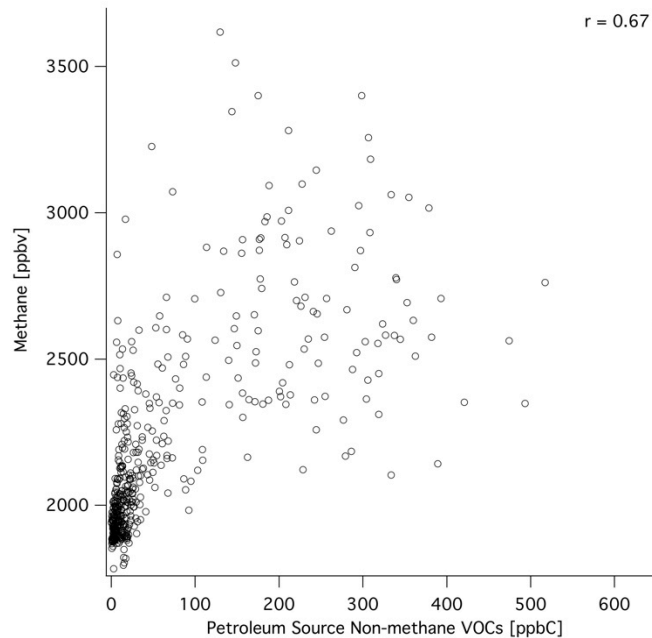


Figure 5.9: Observations of methane are not well correlated with the petroleum gas source and much of the observed correlation can be attributed to simultaneous dilution or concentration due to boundary layer effects.

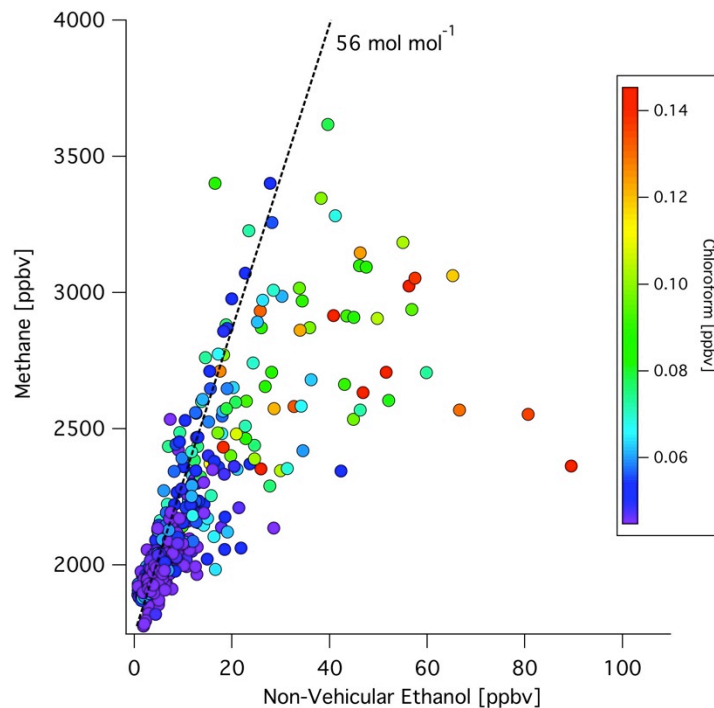


Figure 5.10: Observations of methane vs. non-vehicular ethanol are correlated. Enhancements of ethanol from another source than the dominant source of methane and ethanol are shown by enhancements in chloroform. No major enhancements of methane are observed beyond the inferred slope with non-vehicular ethanol. This, with Figure 5.9, suggests a minimal impact of petroleum gas emissions on methane concentrations in the region.

Chapter 6: Emissions of biogenic gas-phase organic carbon from agriculture and their implications for air quality

Portions adapted from reports to the California Air Resources Board and Citrus Research Board, “Flux measurements of biogenic precursors to ozone and particulate matter in the central valley” (contract no. 06-329) and “Measurements of ozone removal and VOC emissions in citrus trees with implications for regional air quality”, respectively.

Abstract

Agriculture comprises a substantial fraction of land cover in many regions of the world, including California’s San Joaquin Valley, which is out of compliance with state and federal standards for tropospheric ozone and PM_{2.5}, a substantial fraction of which is secondary organic aerosol. Using data from 3 measurement campaigns, I examine emissions of reactive gas-phase carbon from agricultural crops and their potential to impact regional air quality relative to anthropogenic emissions in California’s San Joaquin Valley. Emission rates for a suite of biogenic terpenoid compounds were measured for over 20 representative crops from California in a greenhouse in 2008, and ambient measurements of terpenoids and other biogenic compounds were made over an orange orchard in a rural area of the San Joaquin Valley during two seasons in 2010: summer and spring flowering. When accounting for both emissions of reactive precursors and the deposition of ozone to an orange crop, the net effect of the orange grove is a net source of ozone in the springtime during flowering, and relatively neutral for most of the summer until the fall when it becomes a sink. Flowering was a major emission event and caused a large increase in emissions including a suite of compounds that had not been measured in the atmosphere before. In the San Joaquin Valley during the summer, the mass of biogenic emissions and their formation potential for ozone and secondary organic aerosol are similar to anthropogenic emissions from motor vehicles and must be considered in air quality models and policy. Additionally, emission events, such as flowering, have significant potential to impact regional air quality as emissions increase by an order of magnitude.

1. Introduction

Biogenic compounds are emitted from vegetation with various purposes via several mechanisms. Emissions are typically associated with environmental parameters (light, temperature) or with specialized response functions to communicate with, attract or repel animals, insects, or other plants (1, 2). Biogenic emissions from plants are mostly in the gas-phase and span from 1 to over 20 carbon atoms in size (2). Examples include light hydrocarbons such as methanol and acetone, and an extensive number of compounds that are multiples of isoprene (C₅H₈) known as terpenoids, which sometimes contain 1-2 oxygen atoms (2). These olefinic compounds are referred to as monoterpenes (C₁₀H₁₆) or sesquiterpenes (C₁₅H₂₄), with their oxygenated counterparts included in the definition of monoterpeneoids and sesquiterpeneoids. Any given plant species can emit a number of these potential isomers with one or more double bonds and can include cyclic or bicyclic rings, but a certain suite of compounds have been observed more frequently (1, 2). Commonly reported monoterpenes include Δ-limonene, α-pinene, and Δ³-carene, and sesquiterpenes which are more difficult to measure include β-caryophyllene and α-humulene (1). Many terpenoids have a specific purpose and are responsible for the fragrances and flavors associated with various plants (1, 3-9). Some studies have also

shown plants or their flowers to contain other compounds containing aromatic rings (i.e. benzenoids), nitrogen or sulfur-containing functional groups (3-9).

Much work has been done to understand emissions of biogenic gas-phase organic carbon as most of the compounds are highly reactive and can produce considerable ozone and/or secondary organic aerosol (SOA) following reaction with atmospheric oxidants (10, 12). Understanding emissions from vegetation is important in California because of the complex interplay of anthropogenic emissions and biogenic emissions from both natural vegetation and agriculture. Agricultural plantings make up a major fraction of land cover in some regions such as California's San Joaquin Valley, which is an extreme non-attainment area for ozone and non-attainment area for PM_{2.5} (13). A summary of prominent agricultural plantings in the San Joaquin Valley is shown in Table 6.1. Biogenic emissions from many of these crops and other agricultural plants have not been sufficiently characterized. Larger scale models use information on emission factors from individual plant species; these models include the MEGAN (Model of Emissions of Gases and Aerosols from Nature) model and the BEIGIS model developed by the California Air Resources Board (14, 15).

This work focuses on a large number of agricultural plant species studied via enclosure measurements in a greenhouse (Table 6.2) to survey emissions and develop emission factors and emission parameters, and also assesses seasonal emissions in an orange orchard located in a rural area of the San Joaquin Valley. Further objectives of this work include characterizing emissions associated with spring flowering and examining the relative importance of biogenic emissions from agriculture on ozone and SOA formation in the San Joaquin Valley.

2. *Materials and methods*

This chapter uses measurements from the 2008 greenhouse enclosure measurements, both seasons at the Lindcove field site, and the urban Bakersfield site. Seasonal measurements at the Lindcove site included once in spring during flowering and once in summer coincident with warmer temperatures and higher levels of ambient ozone. FLEXPART footprint modeling is used to examine the transport of biogenic VOCs to the urban site in the southern San Joaquin Valley. Measurements of monoterpenes reported from greenhouse enclosure measurements were made in conjunction with a high-time resolution Proton-Transfer Mass-Spectrometer (PTR-MS) and had good agreement (16). Year-long measurements of ozone fluxes over the orange grove were made at the Lindcove site and are used in this work; methods have been described elsewhere (17).

Basal Emission Factors (BEF) are calculated as the standard emission factor for biogenic compounds from vegetation, and are adjusted based on the environmental parameters considered. BEFs were calculated for each compound class for each plant species studied in the greenhouse by taking the average of the data points with temperature = 30 ± 2 °C, and photosynthetically active radiation (PAR) > 800 $\mu\text{mol m}^{-2} \text{s}^{-1}$. If insufficient data existed at these basal conditions, data was logarithmically extrapolated from lower temperature data (see reference 18 for details).

Most compounds without specialized functions are characterized by two different emission mechanisms, described as dependence on light and temperature or just on temperature. Compounds that are emitted immediately after being synthesized in the leaves are light and temperature dependent, and emission rates (E_{L+T}) are determined using the algorithm developed by Guenther et al. (19).

$$E_{L+T} = BEF \left[\frac{\alpha C_L PAR}{\sqrt{1 + \alpha^2 PAR^2}} \right] * \left[\frac{\exp\left(\frac{C_{T1}(T - T_S)}{RT_S T}\right)}{0.961 + \exp\left(\frac{C_{T2}(T - T_M)}{RT_S T}\right)} \right] \quad (7.1)$$

where the empirical coefficients are α (0.0027), C_L (1.066), C_{T1} (95000 J mol⁻¹), C_{T2} (230000 J mol⁻¹), $C_{T3} = 0.961$, and T_M (314 K); R is the universal gas constant (8.314 J K⁻¹ mol⁻¹), T is the leaf temperature (K) and T_S is the leaf temperature at standard conditions (303 K). Emission rates, also referred to as fluxes, are in terms of compound mass per mass dry leaf matter per time (e.g. ngC gDM⁻¹ h⁻¹). Using information on the mass to area of a species' leaves and the leaf density of a canopy, this emission rate can be converted to carbon mass per area ground cover per time (e.g. gC m⁻² h⁻¹).

Emissions based solely on temperature are synthesized and stored in specific pools inside the leaves and/or stems, and are emitted via volatilization. Emission rates (E_T) are calculated based on Tingey et al., (20).

$$E_T = BEF \exp[\beta(T - T_s)] \quad (7.2)$$

where β (K⁻¹) is a coefficient that scales the exponential dependence on temperature and is calculated by inverting equation 7.2 using the estimated BEF.

For both methods, modeled fluxes from the greenhouse enclosure studies were compared to measured fluxes via linear correlation with slopes and coefficients of determination (r^2) to determine which modeling method best represents the emissions from each plant for each compound class.

At the Lindcove and Bakersfield sites, comparisons of biogenic to anthropogenic burdens of gas-phase organic carbon are done via chemical mass balancing methods (Chapters 2, 4) to model anthropogenic emissions from motor vehicles. Total emissions of anthropogenic hydrocarbons in the San Joaquin Valley from motor vehicles are determined using the emission factors derived in Chapter 4 and fuel use data for the seven counties of the air basin (21). Biogenic emissions for the region are compared to the California Air Resources Board emission inventory (22). The ozone formation potential of these emissions are compared using Maximum Incremental Reactivity (MIR) determined using the SAPRC VOC Reactivity Scales (10). Where available, literature values are presented for the reaction constants of biogenic compounds with atmospheric oxidants (11, 23). Otherwise, theoretical values are estimated using the U.S. EPA's EPI Suite program (24).

3. Results and discussion

3.1. Greenhouse measurements of individual species

There were numerous terpenoid compounds quantified in emissions from crops with considerable diversity between the plant species. Emission parameters and detailed chemical speciation for monoterpenes, oxygenated monoterpenes, and sesquiterpenes measured from the different crops in the greenhouse study are shown Tables 6.3-6.7. Monoterpene concentrations were measured as individual species via gas chromatography and as total monoterpenes with the PTR-MS, and agreed to within 20%. In addition to several well-studied monoterpenes, there was a considerable amount of β -myrcene, sabinene, and both isomers of β -ocimene. Oxygenated

monoterpene emissions were dominated by linalool and perillene, a little-studied furanoid. I observed only two sesquiterpenes, α -humulene and β -caryophyllene. Consistent with previous work, β -caryophyllene dominated the two, but it is likely that there were other sesquiterpenes outside of the observable range, at concentrations below the limit of detection, or were lost in the sampling system prior to detection. A broader suite of sesquiterpenes were measured using a cartridge method and emissions are reported by Ormeno et al. (25). Calculated BEFs and beta values for total monoterpenoids, oxygenated monoterpenes, and sesquiterpenes are summarized in Tables 6.3-6.4 with relevant statistical metrics.

3.1.1 Monoterpenes

Total emissions of monoterpenes were lowest ($< 100 \text{ ngC gDM}^{-1} \text{ h}^{-1}$) from almond, grape, olive, pistachio, plum and pomegranate (Table 6.3). For almond and cherry, the BEF for monoterpenes agreed with previous research (26). Emissions from grapes were very low (11 and 91 $\text{ngC gDM}^{-1} \text{ h}^{-1}$) whereas Winer et al. (26) did not detect any emission. The monoterpene BEF for peach, 1211 $\text{ngC gDM}^{-1} \text{ h}^{-1}$ was significantly higher than other plants in the *Prunus* genus (i.e. almond, plum) measured in this study.

Correlations between measured and modeled monoterpene emissions for both the temperature only and the light and temperature methods were significant for almond and olive (Table 6.4). Some plants, such as these, are known to have storage structures on their leaves where terpenes are typically stored (27). The existence of these “pools” of biogenic compounds is relevant as harvesting or pruning may cause emission if leaves are damaged during agricultural operations.

Among the herbaceous species, tomato was the highest monoterpene emitter (BEF = 742 $\text{ngC gDM}^{-1} \text{ h}^{-1}$). The measured BEF was within the range of previously reported values for Tomato (26, 28). Tomato is well known to have specialized structures (29, 30) filled with terpenes, and the emissions have been shown to dramatically increase after wounding or pathogen infestation (28), suggesting that higher emissions should be expected during harvesting.

Orange had the highest levels of monoterpene emissions, BEF = 2520 $\text{ngC gDM}^{-1} \text{ h}^{-1}$ and with β coefficient (temperature only) of 0.14 for monoterpenes from Parent Navel oranges without flowers. The range of observed emissions, the BEF, and β coefficient are consistent with previous published work on oranges (31). The composition of monoterpenes was dominated by β -myrcene and β -trans-ocimene, with small amounts of limonene, sabinene, and β -cis-ocimene. The correlation between measured and modeled emissions was significant for Parent Navel orange using both the light and temperature and temperature only methods.

Emissions of total monoterpenes from other citrus species in this study were very low; 22, 26, and 63 $\text{ngC gDM}^{-1} \text{ h}^{-1}$ for Eureka lemon, Clementine mandarin, and Murcott mandarin, respectively. For mandarins, the most abundant monoterpenes were β -cis and β -trans isomers of ocimene with minor amounts of limonene, sabinene, and pinene. The lemon and mandarins, which had negligible monoterpene emissions, also had lower β coefficients than orange. Previous work has shown much higher emission for Lisbon lemons (26), which suggests potential variability in emissions owing to genotypic and phenotypic factors.

Our measurements of Pistachio are considerably lower than previous work classifying Pistachio as a strong monoterpene emitter; our BEF is more than two orders of magnitude lower (26). Since pistachio acreage is substantial in the San Joaquin Valley, further studies on this crop are warranted as fundamental questions remain about pistachio's BEF. It is possible that

although the same variety was used in both studies, specific phenotypic traits of the individuals selected could cause such differences. It is the case here with Pistachio as with many other crop surveyed in our study that several replicates of a few individuals in a crops species were inadequate to capture the variability in biogenic emissions between different crops, individuals of the same species, and during different periods of an individual's life or annual cycles. Thus, it is important to note that the results presented from the greenhouse study are merely a survey of emissions from a broad suite of crops and more extensive measurements are critical to effectively characterize emissions from a particular crop species. Future users of this individual crop data should take caution of the variability between individuals of the same species and their seasonal cycles.

3.1.2 Oxygenated monoterpenes

Oxygenated monoterpene emissions have not been reported extensively in the past. The most prevalent oxygenated monoterpene observed in this study was perillene. Emissions of oxygenated monoterpenes were highest from flowering orange (BEF = 4600 ngC gDM⁻¹h⁻¹), followed by pima cotton and non-flowering orange (2700 and 1300 ngC gDM⁻¹h⁻¹, respectively). Lower emissions were observed from cherry, peach, almond, and Murcott mandarin, with very low emissions from the other crops (Table 6.3). Modeled and measured emissions of oxygenated monoterpenes from non-flowering orange leaves were not well correlated. The occurrence of perillene may suggest that neither of the modeling methods represent emissions of this furanoid. For flowering oranges, the temperature only method best describes the emission of oxygenated monoterpenes, mainly linalool, confirming the temperature dependency of emissions for this compound.

3.1.3 Sesquiterpenes

Almond was the highest sesquiterpene emitter of the crops studied according to the calculated BEF (10000 ngC gDM⁻¹h⁻¹), while the magnitude of the monoterpene and oxygenated monoterpene emissions were very low. This sesquiterpene BEF was anomalous, so I report it with low confidence. The calculated beta of 0.45 is very high, and all the measurements for almond were below 25 °C. Using a beta of 0.1, the BEF would be 1200 (a factor of 10 lower, but still a significant emission). Sesquiterpene emissions were very low or not detected for other non-citrus woody crops. Sesquiterpene emissions from tomato were 59 ngC gDM⁻¹h⁻¹, slightly lower than the range reported in previous work for different varieties (26).

Sesquiterpene emission rates for orange trees in this study are consistent with work by Hansen and Seufert (32), who measured emissions with a branch enclosure and agree with our finding that β -caryophyllene is the main sesquiterpene emitted by Navel orange. Our results suggest that temperature is a more important environmental parameter controlling the emission of sesquiterpenes in orange plants without flowers, consistent with previous characterization (33). The β coefficient for sesquiterpenes in oranges was on average 0.28, although recent literature suggests a β coefficient used for modeling purposes to be about half of that calculated in this study (14). Our value is however in agreement with previous estimates (31) and justified by the higher vaporization energy required to transfer β -caryophyllene from the liquid to the gas phase, owing to their lower vapor pressure relative to monoterpenes.

3.2. Emissions from flowering citrus trees

Flowering is an important phenomenon that occurs for most trees and herbaceous plants once or twice every year in locations such as California's central valley. Flowering dramatically increased emissions of monoterpenes from Navel orange to 5589 ngC gDM⁻¹ h⁻¹ in the greenhouse enclosure studies. The presence of flowers has been shown previously to dramatically influence the magnitude and composition of biogenic compounds emitted from oranges (31, 32, 34). Emissions from plant species that have the ability to store chemicals, such as *Citrus*, occur primarily via the volatilization of compounds accumulated within specific leaf reservoirs, where emissions depend more on temperature than on plant physiology. Whereas during flowering, the presence of flowers and their role as strong emitters caused a decoupling between photosynthesis and emissions in flowering oranges.

In the greenhouse study monoterpene species emitted from flowering and non-flowering branches were similar; β -myrcene was the dominant monoterpene followed by β -trans-ocimene (Table 6.3). For flowering plants, β -cis-ocimene was also observed. The β -ocimene isomers have been previously reported in emissions from flowering *Citrus* trees as a known attractant for pollinators (35). Linalool was the dominant oxygenated monoterpene observed from flowering plants (98%), which agrees with previous observations (31, 34). Perillene, a furanoid, was observed from both flowering and non-flowering plants. This is the first time perillene has been identified in plant emissions as volatile furanoids are rare in plants. Prior to this, cis- and trans-linalool oxide were the only furanoids observed from plants (36). β -caryophyllene was the main sesquiterpene emitted from both flowering and non-flowering oranges. For both the flowering and non-flowering plants, the temperature-only method better predicted emissions of β -caryophyllene. Increased emissions from the flowering orange tree were observed for all compounds measured, but there were no flowering individuals for the other *Citrus* species.

During the spring measurement campaign at the orange orchard, a broad array of gas-phase organic compounds was measured in ambient air (Table 2.1). The effect of flowering at the field site and in the region had a major impact on the distribution of biogenic compounds in ambient air. There was a dramatic increase in both the magnitude and diversity of chemical species emitted during the flowering process. Due to strong nocturnal inversions, many were measured at ppb-level concentrations at night owing to their build-up in the shallow boundary layer where ozone had been scavenged to concentrations below 10 ppb. Perhaps of more interest is that daytime concentrations averaged above 10 ppt for most compounds, when their emissions are most relevant to photochemistry. Additionally, several of the most prominent compounds had daytime concentrations that regularly exceeded 1 ppb, as summarized in Table 6.8.

β -myrcene was the principal monoterpene observed during flowering, while linalool was overall the most dominant terpenoid compounds observed. Yet, there were high concentrations of a wide variety of compounds during the flowering period (Table 6.8) that had strong diurnal patterns. While many of the biogenic compounds observed at the site were terpenoids, there was a diverse array of functionalized aromatic compounds that were clearly biogenic and associated with flowering (Table 6.8-6.9). This is evidenced by their strong correlations to β -myrcene and linalool (Table 6.10), which are known to be associated with flowering from the greenhouse studies. Of the compounds observed and measured, several have not been previously reported, to my knowledge, in other studies of ambient air. These compounds were initially identified through high quality matches to mass spectra libraries and Kovat's indices for appropriate retention times, and then later confirmed with authentic standards after the campaign. Table 6.9 summarizes their chemical structures, reactivity, and previous records of the compounds. Many

of the compounds I observed during flowering have been attributed to floral scents or essential oils from flowers in various botany and ecology studies, which include a variety of compounds with aromatic rings, nitrogen, sulfur, and oxygen-containing functional groups (3-9).

There were several previously unidentified peaks observed during measurements of the flowering Parent Navel orange in the greenhouse studies that have very good retention time matches to these flowering compounds measured at this site: indole, methyl anthranilate, benzeneethanol, benzyl nitrile, 2-aminobenzaldehyde, and possibly sabina ketone. In the greenhouse measurements, these compounds were observed only from the flowering specimen, supporting the conclusion that flowering is the source. Daytime concentrations of methyl anthranilate, indole, and benzyl nitrile were over 1 ppb, similar or greater than the dominant monoterpene β -myrcene. Lavender lactone, benzeneethanol, 2-amino-benzaldehyde, and benzeneacetaldehyde had significant median daytime concentrations at, or above, 100 ppt. Sabina ketone and methyl benzoate had lower concentrations similar to the linalool oxide isomers, but still appeared to be emitted in significant amounts. Cis-3-hexenyl acetate, a well-known plant-wounding compound, had considerable nighttime concentrations around 1 ppb despite no harvest or pruning activity, and correlated well with other flowering compounds suggesting that it is also released as part of the flowering process. In addition to these compounds, I also observed several high molecular weight straight alkanes and alkenes associated with flowering (e.g. n-heptadecane, 1-heptadecene), which have been reported in other floral and essential oil analyses (3-6, 9, 26). The diurnal patterns of the flowering-related compounds were similar to that of monoterpenes, but were more prevalent (Figures 6.1-6.2). A regression of the flowering related compounds to the sum of monoterpenes yielded a ratio of 4.0 (on a mass basis), but the sum of monoterpenes included compounds that were related to flowering (i.e. β -myrcene, sabinene, and both β -ocimenes).

There were several sesquiterpenes observed at the site during flowering, but the concentrations measured were considerably lower than many of the other terpenoids measured. I observed a number of sesquiterpenes, several of which I was not able to identify. The dominant observed sesquiterpenes were β -caryophyllene, aromadendrene, trans- β -farnesene, valencene and trans-nerolidol (all confirmed with standards). Given the high reactivity of sesquiterpenes, the lower magnitude of concentrations does not necessarily imply lower emissions, but could also be a result of sesquiterpene compounds reacting at more rapid rates in the atmosphere than other terpenoid compounds. Sampling methodology can sometimes underestimate ambient concentrations, but the sampling and measurement techniques used in this study are suitable for sesquiterpene measurements. It is very likely that only a fraction of the emitted sesquiterpenes were measured, as I was only able to detect and identify a few sesquiterpenes. Previous work (25) has shown that a wide array of sesquiterpenes are emitted from agricultural crops (flowering and non-flowering) and that emissions of sesquiterpenes should be roughly equivalent to those of monoterpenes. Our springtime measurements show that sesquiterpenes were 5% of monoterpenes, on average by carbon mass. Flowering is an episodic event and is not representative of an annual average. Previous work with the MEGAN model estimates sesquiterpene emission to be 9-16% of monoterpenes, but sesquiterpene data for input into the MEGAN model is limited (14). Figures 6.3 and 6.4 show the relative amounts of sesquiterpenes to monoterpenes and it is evident that there is a dynamic range of observed ratios that varies over the course of the day and it is quite possible that additional, unaccounted sesquiterpenes will increase the ratio.

The concentrations of sesquiterpenes during flowering were higher than previous work done in a ponderosa pine forest, where concentrations of individual sesquiterpenes were on the order of 10 ppt (1), but there are extremely few ambient air measurements of sesquiterpenes published with which to compare our observations. It should be noted that our summertime measurements did not have the capacity to measure sesquiterpenes due to chromatographic and detector difficulties.

3.3. Seasonal differences in biogenic VOCs

While there were considerable year-round concentrations of monoterpenes at the site, there was a strong increase in biogenic emissions during the flowering period. A comparison indicates the daytime concentration of monoterpenes was approximately three times greater during spring flowering compared to summer non-flowering conditions. The diurnal pattern of monoterpenes between the two seasons was similar, despite higher concentrations in the spring during flowering (Figures 6.5-6.7). Given the similarities between Δ -limonene during the two seasons, the difference can be attributed to the other monoterpenes associated with flowering. Over the summer, Δ -limonene was the predominant monoterpene, but during flowering β -myrcene, sabinene, and trans- β -ocimene were equally prevalent (Figures 6.5-6.6, Table 6.12). A variety of other monoterpenes were present during both seasons, but made up relatively minor fractions.

While I measured fewer biogenic compounds during the summer campaign relative to the spring, I still observed a variety of monoterpenes in ambient air. I did not observe many of the compounds that were associated with flowering including many of the oxygenated monoterpenes and benzenoids. There were similar diurnal patterns in the summer as in the spring due to boundary layer effects, with ambient ozone still getting below 10 ppb at night due to stomatal deposition, and reaction with BVOCs and NO.

The chemical speciation of monoterpenes is summarized in Table 6.12. There is a similar distribution and diversity of monoterpenes between the two seasons, with the exception of β -myrcene, sabinene and trans- β -ocimene, which increased significantly with flowering. Concentrations of total monoterpenes during the summer were similar to those observed at a California ponderosa pine forest in warm temperatures (26 °C daytime mean), but the distribution of monoterpenes was significantly different; there was much more Δ -limonene and less α - and β -pinene compared to the pine forest (1). Δ -limonene was the most prevalent monoterpene observed in the summer and its diurnal patterns and interquartile concentrations were slightly higher in the spring; 159-292 ppt vs. 184-365 ppt for daytime summer and spring concentrations, respectively, and 204-1606 ppt vs. 275-2251 ppt at night (Table 6.8). This slight increase during flowering is consistent with observations in the greenhouse for orange trees. The relatively comparable concentrations of several monoterpenes during the two measurement periods in the orange orchard imply similar emission rates during those two periods.

Δ -limonene concentrations were very similar between spring flowering and summer non-flowering periods, as shown in Figure 6.8. Para-cymene is a known non-flowering aromatic emitted from plants with a wide variety of sources and a few minor anthropogenic sources (e.g. gasoline). Similar to Δ -limonene, Figure 6.9 shows that it was similar between the two seasons in both prevalence and diurnal pattern. The potential anthropogenic contribution to para-cymene is negligible given the relatively lower concentrations of dominant gasoline components.

3.4 Transport of biogenic emissions in the San Joaquin Valley

The relative importance of biogenic versus anthropogenic emissions varies widely in the San Joaquin Valley depending on locations as shown by the comparison of Bakersfield to Lindcove (Figures 6.10-6.11). Given the geographic distributions of agriculture and urban areas in the San Joaquin Valley, the transport of biogenic emission from more vegetated areas is important and can affect atmospheric reactivity and secondary pollutant formation throughout the valley. By comparing various pairs of monoterpenes, I assessed the timescales for transport of biogenic emissions through their aging by the three primary atmospheric oxidants (OH, O₃, NO₃). Each monoterpene measured at Bakersfield reacts at different rates with each oxidant, so by picking monoterpene pairs appropriately, I determined the most important oxidants for aging and their timescales. A comparison of Δ -limonene to α -pinene shows a distribution of ratios (Figure 6.13). While some of this variability is possible due to differences in emissions, it is evident that aging is playing an important role in the variability of observed ratios. Δ -limonene reacts faster than α -pinene with all three atmospheric oxidants, but given the average concentrations of the oxidants, oxidation by OH is the fastest and will have the strongest influence on the observed ratios. 24-hour averages of the oxidants were 0.25 pptv, 41 ppbv, and 0.29 pptv for OH, O₃, and NO₃, respectively at the Bakersfield site. A comparison of Δ -limonene to para-cymene (not shown) similarly demonstrates the importance of aging by OH as the differences in reaction rates are more pronounced than between Δ -limonene and α -pinene. A similar comparison of camphene to α -pinene, demonstrates the constant initial emission ratio for the sources in the region and the effects of aging by ozone and nitrate radicals as there is less variability in the observations given that their OH reaction rates are identical (Figure 6.14). These observations indicate the presence of these oxidation mechanisms and show the predominance of oxidation by OH, but are dependent on the timescales and diurnal patterns of biogenic compounds arriving to Bakersfield. Nevertheless, my findings are consistent with recent work reporting the presence of nitrate chemistry and also a study showing the dominance of OH oxidation of biogenic emissions (37, 38).

It is evident from this analysis that the observed biogenic compounds are emitted within several hours of transport to the site, which can inform our exploration of their spatial distribution. Using the FLEXPART footprint modeling method, I determined the spatial distribution of biogenic sources that emit monoterpenes, which advect to the Bakersfield ground site. Figure 6.15 shows the distribution for the sum of monoterpenes over the 6 hours of transport and Figure 6.16 shows the distribution of individual chemical species. While many of the compounds appear to have similar sources in the San Joaquin Valley, some areas are stronger than others as emitters of different monoterpenes. Overall, there are three areas that emit monoterpenes that impact Bakersfield: cropland to the East/Southeast of the site, cropland to Northwest, and a relatively small patch of cropland in the mountains to the Southwest. The location of these sites appear to be consistent with the location of croplands, but influence from natural vegetation is expected especially in the case of areas near or in the mountains with pine trees and other significant natural emitters.

3.5 Impacts on air quality

The principal motivation for studying biogenic emissions from agriculture was to determine the impact of biogenic emissions on air quality in the San Joaquin Valley. Terpenoid compounds are known to be very reactive and have the potential to form both tropospheric ozone

and SOA. While our work has highlighted orange trees as major emitters, many other crops have been shown in this and other studies to have non-negligible emissions (26).

To provide a relative comparison for biogenic emissions in context of the region, I estimated the ambient concentration of anthropogenic emissions due to motor vehicles during the spring campaign using the source receptor modeling methods described in Chapter 2 and used in Chapters 4-5. Figures 6.10 and 6.11 show the diurnal pattern and relative prevalence of anthropogenic and biogenic source contributions for both Lindcove and Bakersfield. Biogenic sources are not very important in Bakersfield, but are very important at the Lindcove site, especially in the spring. This effect is due to the differences in the biogenic factor as the anthropogenic contribution is similar between the two sites except for major spikes due to commuting periods in Bakersfield (Figure 6.12). While a similar CMB analysis is not possible for the summer, a comparison of anthropogenic compounds (e.g. m/p-xylene, isooctane) between the two seasons shows that nighttime concentrations are similar, but daytime concentrations of motor vehicle emissions are ~30% lower. This could be due to either enhanced photochemical processing or dilution during the summer months. Nevertheless, it appears that during the summer anthropogenic emissions from motor vehicles will be slightly higher or the same order as biogenic emissions of terpenoids based on the sum of monoterpenes presented in Figure 6.7 and a similar abundance as the springtime anthropogenic vehicular contribution (Figure 6.12).

During flowering the mass of observed biogenic compounds was on average 14 times that of inferred anthropogenic compounds from vehicular emissions, as compared to Bakersfield where anthropogenic contributions for vehicles are 48 times monoterpenoids from biogenic sources. Contributions from isoprene or oxygenated VOCs from biogenic sources will slightly reduce this difference, but are not included as their source can not be attributed to agriculture. Daytime monoterpene concentrations at Lindcove were on average 6 ± 2 times greater during flowering than in the summer. This is consistent with observations from year-long PTR-MS measurements at the Lindcove site that reported a 10x increase in the monoterpene BEF between the flowering and non-flowering periods. Given that the concentration of flowering compounds was 4 times greater than the sum of monoterpenes, this indicates that flowering increases carbon emissions by ~25x in total. The source profile for flowering is shown in Table 6.11. This difference in emissions between flowering and non-flowering plants needs to be considered in emissions and air quality modeling, since during flowering periods the chemistry of the atmosphere may be significantly different. Given the changes in emissions, these seasonal events need to be taken into account to accurately model biogenic emissions from agriculture and air quality in the San Joaquin Valley. Important emission events were spring flowering, pruning, harvesting, and fertilizer application. During these events large increases in emissions of terpenoids were measured (monoterpenes, sesquiterpenes, and oxygenated terpenes).

To assess the ability of agricultural terpenoid emissions and flowering events to impact air quality via the contributions of reactive precursors to ozone and SOA, I developed metrics to compare them to motor vehicle emissions. The ability of a compound to produce ozone is quantified through the use of literature MIR values [$\text{gO}_3 \text{ g}^{-1} \text{ compound}$], which is used here despite differences in NO_x availability to compare sources on a similar basis in a valley with complex emissions and meteorology. The gasoline analyzed in this dissertation has ozone formation potentials (OFPs) on average of 3.0 and 2.1 for exhaust and non-tailpipe emissions, respectively. For the monoterpene profile observed during the spring (excluding β -myrcene, but including para-cymene), the OFP was calculated to be 4.1. For the presented flowering profile (Table 6.11), the OFP was 3.6-5.4 with the range based the range of potential values for

unknown values determined from compounds with similar structures and general values provided with the framework. Linalool, a dominant fraction of the flowering profile, has a known OFP of 5.4. These calculated values infer that per mass of emissions, the biogenic emissions have a greater ability to produce ozone than gasoline emissions, but this effect may be slightly reduced as some of the biogenic compounds are more reactive with ozone.

Predicting the exact SOA yields and formation from flowering-related compounds is not feasible given the high level of uncertainty associated with predicting SOA yields for these compounds as many of them have barely been studied. However their potential to form SOA can be estimated using literature on well-characterized Δ -limonene and α -pinene yields from OH oxidation and ozonolysis experiments (39, 40), and work by Ng et al. (12) that compares a suite of terpenoid compounds including Δ -limonene and α -pinene. SOA yields from Δ -limonene and α -pinene range from 0.25-0.35 and 0.1-0.2 g OA g⁻¹ compound, respectively, for ozonolysis at an organic particle loading of 10 $\mu\text{g m}^{-3}$ (39). SOA yields from OH oxidation at similar particle loadings are significantly lower at approximately 0.05 and 0.04 g OA g⁻¹ compound for Δ -limonene and α -pinene, respectively (40). Given the lifetimes to OH and O₃ presented in this work, that implies average SOA yields of 0.1 and 0.07 at OA=10 $\mu\text{g m}^{-3}$. Assessing the behavior of other monoterpenoids associated with flowering and their reaction rates with OH and O₃ suggests a slightly lower SOA yield for β -myrcene than α -pinene and an SOA yield for linalool below 0.01. So overall this infers that under similar loadings, the monoterpene emissions have a greater SOA yield than the gasoline exhaust, but not quite that of diesel based on the yields for gasoline and diesel derived in Chapter 4. Estimating SOA yields for the benzenoids associated with flowering is much more difficult given the uncertainties, but SOA yields for C₇₋₈ aromatics in Chapter 4 were approximately 0.05 g OA g⁻¹ compound for OH oxidation at an organic particle loading of 10 $\mu\text{g m}^{-3}$. So benzenoid compounds can be assumed to be 0.05 or greater given their decreased initial volatility due to functionalization.

Detailed modeling using spatially resolved chemical models coupled with emissions will be necessary to fully understand the relative impact of biogenic emissions on air quality using the new information derived in this dissertation, but here I estimate their contributions relative to motor vehicle emissions for the entire San Joaquin Valley. Spatial distribution of emissions and chemistry are essential to account for transport and NO_x emissions/chemistry, but the objective here is to inform the necessity of that future research. The work presented here addresses emissions of monoterpenoids and larger compounds, and does not include isoprene or small oxygenated VOCs and alcohols that can be emitted from vegetation. As the focus is on the relative impacts of agriculture, I do not consider the potential transport of emissions from natural vegetation (e.g. pine trees, oak trees) in the foothills or mountains. I use available metrics from literature to assess potential ozone and SOA formation with the caveat that they may not fully capture the differences in NO_x availability and thus the chemical regimes between urban and rural areas in the valley. The principal motivation is to use available information to make a back of the envelope calculation to demonstrate the need for further detailed modeling efforts based on the magnitude of emissions from agricultural vegetation and their potential to impact air quality.

Based on fuel sales for the valley, gas-phase gasoline exhaust emissions are 7.3×10^7 g day⁻¹, non-tailpipe gasoline emissions are 4.5×10^7 g day⁻¹, and diesel emissions are 3.4×10^7 g day⁻¹. Together this combines to 1.5×10^8 g day⁻¹ and an ozone formation potential of 3.8×10^8 gO₃ day⁻¹ (assuming a lower OFP=2 for diesel), with the reactivity dominated by gasoline

sources. Using the SOA yields from Chapter 4, potential SOA from motor vehicles is 6.7×10^6 gOA day⁻¹.

Biogenic emissions from agriculture are estimated using a range of emission factors from agriculture measured in the greenhouse study that is consistent with the range of input BEFs into the BEIGIS model; leaf scale emission factors of 80-3000 ngC gDM⁻¹ hr⁻¹ correspond to field-level emission factors of 0.1-2 nmol m⁻² s⁻¹, given a mean specific leaf area of 85 cm² g⁻¹ and a canopy leaf area index of 3.0 m² leaf area m⁻² land area (17). This range of estimates includes the summertime BEF measured in the orange grove (0.13 nmol m⁻² s⁻¹) (16). I assume a total land cover by agriculture of 3 million acres in the San Joaquin Valley (Table 6.1).

In terms of total mass from agricultural sources, baseline monoterpene emissions are on the same order as anthropogenic sources with a range of $0.1-3 \times 10^8$ g day⁻¹. The ARB emission inventory of 1.8×10^7 g monoterpenes day⁻¹ from agriculture in the San Joaquin Valley is at the low end of my estimated range. The estimated emission factor does not include emissions during flowering or other emission events, which will increase emissions by 24x and at least 2x, respectively.

With regard to the production of ozone from organic precursors, monoterpene emissions from agriculture have the ability to produce $1-12 \times 10^8$ gO₃ day⁻¹, making it equally important as organic emissions from motor vehicles, but further analysis with NO_x sensitivity is essential to elucidate the relative importance for the region. As this is a baseline value, it is evident that emissions occurring during flowering will have a major impact on ozone production given the substantial increase in emissions, and additional considerations for sesquiterpene emissions will increase ozone production as well.

Estimating SOA has a significant amount of uncertainty associated with it, but for comparison with motor vehicles I estimate that monoterpene emissions from agriculture can contribute $0.5-3 \times 10^7$ gOA day⁻¹, across the range of emissions and SOA yields (at 10 μg m⁻³). This means that baseline monoterpene emissions have a similar ability as motor vehicles (6.7×10^6 gOA day⁻¹) to produce SOA and does not include sesquiterpene emissions or other emission events such as flowering.

Many woody-plants, including orange trees, remove some ozone from the ambient atmosphere via uptake through their stomata. This process, stomatal deposition, coupled with the reaction of ozone with reactive biogenic compounds in the air produces a flux of ozone into the plant canopy, which was measured for a full year at the field site. Chemical deposition via reaction with BVOCs was estimated to be 10-26%, while stomatal deposition and soil deposition were each responsible for approximately ~30% of ozone losses (17). A full discussion of these fluxes and their partitioning into different mechanisms has been published elsewhere (17). To determine the net effect of the orange grove on regional ozone, I compared the measured ozone flux into the canopy with the amount of ozone to be produced downwind based on emissions and OFP values. Monoterpene BEFs from the field site for spring and summer were used from Fares *et al.* (16), with the summer flux multiplied by 2 during emission events (harvest, pruning, fertilizer application) when emissions measured by PTR-MS exceeded modeled emissions. Based on the work of Ormeno *et al.* (25) sesquiterpene emissions were assumed to be equivalent to monoterpene emissions and were assumed to have an OFP of 4. Emissions of floral compounds during the spring flowering period were estimated by multiplying monoterpene emissions by 4.0 per the results of Figure 6.2. Additionally, chemical removal of ozone, beyond the measured flux reported previously (17), was accounted for using the monoterpene emissions and the probability of reaction with ozone. Figure 6.17 summarizes the results of this analysis

with total emissions, ozone fluxes into the canopy, ozone production, and the net effect. The net effect on a weekly timescale of these processes is shown in Figure 6.18 over the period of ozone exceedances in the region. The orchard is a net source of ozone in the springtime during flowering, and is neither a major source nor sink for most of the summer. The orchard is a sink in the fall and in the early spring before flowering begins. Given that flowering occurs at different times for different crops throughout the valley, the time periods net ozone production or loss may not translate to a valley-wide effect. The net effect of ozone deposition was not included in the previous basin-wide comparison of agriculture to motor vehicles as exhaust emissions contain significant amounts of alkenes that can also remove ozone initially.

This work has demonstrated the importance of biogenic emissions relative to vehicular emissions for total emissions and the formation of ozone and SOA in the San Joaquin Valley, but highly resolved modeling of emissions and chemistry is warranted with this new information. When the magnitude of the flowering event is considered across the region, it will have a substantial effect on the biogenic emission inventory and likely on atmospheric composition and air quality during flowering periods in the valley. The newly characterized compounds should be included in the MEGAN and BEIGIS models since their emissions during flowering were on the same order as or greater than all the terpenoids observed. Further study is necessary to better characterize the basal emission factors, dependent parameters, and, in the case of the novel compounds, their ozone and SOA formation potential. Emissions due to flowering and other seasonal events need to be assessed for other major crops, and possibly natural vegetation.

References

1. Bouvier-Brown, N. C., Goldstein, A. H., Gilman, J.B., Kuster, W.C., and de Gouw J. A.: In-situ ambient quantification of monoterpenes, sesquiterpenes, and related oxygenated compounds during BEARPEX 2007: implications for gas- and particle-phase chemistry, *Atmos. Chem. Phys.*, 9, 5505-5518, 2009.
2. Goldstein, A. H. and Galbally, I. E.: Known and Unexplored Organic Constituents in the Earth's Atmosphere. *Environ. Sci. Technol.*, 41, 1514-1521, 2007.
3. Lewis, G.P., Knudsen, J. T., Klitgaard, B. B., and Pennington, R. T.: The floral scent of *Cyathostegia mathewsii* (Leguminosae, Papilionoideae) and preliminary observations on reproductive biology. *Biochemical Systematics and Ecology*, 31, 951-962, 2003.
4. Afsharypuor, S., and Jamali, M.: Volatile Constituents of the Flowering Aerial Parts, Fruits and Roots of *Cardaria draba* L., *J. Essent. Oil Res.*, 18, 674-675, 2006.
5. Bendimerad, N., Bendiab, S. A. T., Breme, K., and Fernandez, X.: Essential Oil Composition of Aerial Parts of *Sinapis arvensis* L. from Algeria, *J. Essent. Oil Res.*, 19, 206-208, 2007.
6. Bernhardt, P., Sage, T., Weston, P., Azuma, H., Lam, M., Thien, L. B., and Bruhl, J.: The pollination of *Trimenia moorei* (Trimeniaceae): floral volatiles, insect/wind pollen vectors and stigmatic self-incompatibility in a basal angiosperm, *Ann. Bot.*, 92, 445-58. 2003.
7. Azuma, H., Toyota, M., and Asakawa, Y.: Intraspecific Variation of Floral Scent Chemistry in *Magnolia kobus* DC. (Magnoliaceae), *J. Plant Res.*, 114, 411-422, 2001.
8. Omura, H., Honda, K., and Hayashi, N.: Chemical and chromatic bases for preferential visiting by the cabbage butterfly, *Pieris rapae*, to rape flowers, *J. Chem. Ecology*, 25, 1895-1906, 1999.

9. Kotze, M. J., Jürgens, A., Johnson, S. D., and Hoffmann, J. H.: Volatiles associated with different flower stages and leaves of *Acacia cyclops* and their potential role as host attractants for *Dasineura dielsi* (Diptera: Cecidomyiidae), *South African J. Botany*, 76, 701–709, 2010.
10. Carter, W. P. L.: SAPRC Atmospheric Chemical Mechanisms and VOC Reactivity Scales (available at: <http://www.engr.ucr.edu/~carter/SAPRC/>)
11. Atkinson, R. and Arey, J.: Gas-phase tropospheric chemistry of biogenic volatile organic compounds: A review, *Atmos. Environ.*, 37, S197–S219, 2003.
12. Ng, N. L., Kroll, J. H., Kenwood, M. D., Bahreini, R., Varutbangkul, V., Flagain, R. C., Seinfeld, J. H., Lee, A., and Goldstein, A. H.: Contribution of first- versus second-generation products to secondary organic aerosols formed in the oxidation of biogenic hydrocarbons, *Environ. Sci. Technol.*, 40, 2283–2297, 2006.
13. U.S. Environmental Protection Agency, *U.S. Clean Air Act (and subsequent amendments/rulings)* (<http://www.epa.gov/air/caa/>)
14. Sakulyanontvittaya, T., Duhl, T., Wiedinmyer, C. et al.: Monoterpene and Sesquiterpene Emission Estimates for the United States, *Environ. Sci. Technol.*, 42, 1623–1629 2008.
15. California Air Resources Board, Appendix B: Development of a biogenic hydrocarbon emission inventory for the Central California Ozone Study domain, in “Ozone SIP Modeling Documentation and Results for the Sacramento Region Using the July/August 2000 Central California Ozone Study Episode,” by K. I. Scott, Nov. 26 2003 (available at: http://eos.arb.ca.gov/eos/ARB_Modeling/JulyAug2000_SIP_Modeling_Doc_AppB_11-26-03.pdf).
16. Fares, S., Park, J. H., Gentner, D. R., Weber, R., Ormeño, E., Karlik, J., and Goldstein, A. H.: Seasonal Cycle of Biogenic Volatile Organic Compound Fluxes and Concentrations in a California Citrus Orchard, *Atmos. Chem. Phys. Discuss.*, 12, 17987–18027, 2012
17. Fares, S., Weber, R., Park, J. H., Gentner, D. R., Karlik, J., and Goldstein, A. H.: Ozone deposition to an orange orchard: Partitioning between stomatal and non-stomatal sinks, *Environ. Pollution*, 169, 258–266, 2012.
18. Fares, S., Gentner, D. R., Park, J. H., Ormeño, E., Karlik, J., and Goldstein, A. H.: Biogenic emissions from *Citrus* species in California, *Atmos. Environ.*, 45, 4557–4568, 2011.
19. Guenther, A., Zimmerman, P. R., Harley, P. C., Monson, R. K., and Fall, R.: Isoprene and monoterpene emission rate variability – model evaluations and sensitivity analyses, *J. Geophys. Res. – Atmospheres*, 98, 12609–12617, 1993.
20. Tingey, D., Manning, M., Grothaus, L., and Burns, W.: Influence of light and temperature on monoterpene emission rates from slash pine, *Plant Phys.*, 65, 797–801, 1980.
21. California Department of Transportation, *California Motor Vehicle Stock Travel, and Fuel Forecast (MVSTAFF) 2008 Report*
22. California Air Resources Board, *Estimated annual average emissions, 2010.* (<http://www.arb.ca.gov/ei/emsmain/emsmain.htm>).
23. Atkinson, R. and Arey, J.: Atmospheric degradation of volatile organic compounds, *Chem. Rev.*, 103, 4605–4638, 2003.
24. U.S. EPA, M.I.: Estimation Programs Interface Suite for Microsoft Windows, AOPWIN v.1.92, United States Environmental Protection Agency, Washington DC, USA, 2000.

25. E. Ormeno, Gentner, D. R., Fares, S. *et al.*: Sesquiterpenoid emissions from agricultural crops: correlations to monoterpenoid emissions and leaf terpene content, *Environ. Sci. Technol.*, 44, 3758–3764, 2010.
26. Winer, A. M., Arey, J., Atkinson, R., Aschmann, S. M., Long, W. D., Morrison, C. L., and Olszyk, D. M.: Emission rates of organics from vegetation in California's Central Valley, *Atmos. Environ.*, 26, 2647–2659, 1992.
27. Vieira, R. C., Delprete, P. G., Leitao, G. G., and Leitao, S. G.: Anatomical and chemical analyses of leaf secretory cavities of *Rustia formosa* (Rubiaceae), *American J. Botany* 88, 2151-2156, 2001.
28. Jansen R. M. C., Miebach, M., Kleist, E., van Henten, E. J., and Wildt, J.: Release of lipoxygenase products and monoterpenes by tomato plants as an indicator of *Botrytis cinerea*-induced stress, *Plant Bio.*, 11, 859-868, 2008.
29. Freitas, J. A., Maluf, W. R., Cardoso, M. D., Gomes, L. A. A., and Bearzotti, E.: Inheritance of foliar zingiberene contents and their relationship to trichome densities and whitefly resistance in tomatoes, *Euphytica*, 127, 275-287, 2002.
30. van Schie, C. C. N., Haring, M. A., and Schuurink, R.C.: Tomato linalool synthase is induced in trichomes by jasmonic acid, *Plant Molecular Biology*, 64, 251–263, 2007.
31. Ciccioli, P., Brancaleoni, E., Frattoni, M. *et al.*: Emission of reactive terpene compounds from orange orchards and their removal by within-canopy processes, *J. Geophys. Res.*, 104, 8077–8094, 1999.
32. Hansen, U., and Seufert, G.: Terpenoid emission from *Citrus sinensis* (L.) OSBECK under drought stress, *Physics and Chemistry of the Earth B – Hydrology Oceans and Atmosphere*, 24, 681-687, 2003.
33. Tingey, D. T., Turner, D. P., and Weber, L. C.: Factors controlling the emission of monoterpenes and other volatile organic compounds. In *Trace Gas Emissions by Plants*, vol. 65, ed. T.D. Sharkey, E.A. Holland, and H.A. Mooney, pp. 797–801. Academic Press, San Diego, California, 1991.
34. Arey, J., Corchnoy, S. B., and Atkinson, R.: Emission of linalool from Valencia orange blossoms and its observation in ambient air, *Atmos. Environ.*, 25, 1377–1381, 1991.
35. Dudareva, N. and Pichersky, E.: Biochemical and molecular aspects of floral scents. *Plant Physiology*, 122, 627–634, 2000.
36. Noe, S. M., Ciccioli, P., Brancaleoni, E., Loreto, F., and Niinemets, U.: Emissions of monoterpenes linalool and ocimene respond differently to environmental changes due to differences in physio-chemical characteristics, *Atmos. Environ.*, 40, 4649-4662, 2006.
37. Rollins A. W. *et al.*: Nighttime growth of particulate organic nitrates: a significant source of atmospheric secondary organic aerosols, *Science* in press, 2012.
38. Donahue, N. M., Henry, K.M., Mentel, T.F. *et al.*: Aging of biogenic secondary organic aerosol via gas-phase OH radical reactions, *Proc. Nat. Acad. Sci.*, 109, 13503-13508, 2012.
39. H. Saathoff, Naumann, K. H., Mohler, O. *et al.*: Temperature dependence of yields of secondary organic aerosols from the ozonolysis of α -pinene and limonene, *Atmos. Chem. Phys.*, 9, 1551–1577, 2009.
40. H. Kim, Barkey, B., Paulson, S. E.: Real Refractive Indices and Formation Yields of Secondary Organic Aerosol Generated from Photooxidation of Limonene and α -Pinene: The Effect of the HC/NO_x Ratio, *J. Phys. Chem. A*, 116, 6059–6067, 2012.

Figures and Tables

Table 6.1: Planted areas for permanent crops with largest land cover in the San Joaquin Valley.

| Crop | Acreage¹ |
|---------------------------|----------------------------|
| Cotton | 653,000 |
| Maize | 501,000 |
| Tomatoes | 222,000 |
| Grapes (Table Varieties) | 84,900 |
| Grapes (Raisin Varieties) | 241,000 |
| Almonds | 453,000 |
| Apples | 15,800 |
| Peaches | 51,300 |
| Pistachios | 97,024 |
| Walnuts | 124,000 |
| Navel Oranges | 124,000 |

¹ Data from 2002 crop reports, respective county Agriculture Commissioner's offices.

Table 6.2: Plants studied during greenhouse enclosure campaign

| Common Name | Scientific Name | Variety and Type |
|---------------------------------|-----------------------------------|--|
| <i>Herbaceous plants</i> | | |
| Alfalfa | <i>Medicago sativa</i> L. | Lucerne |
| Carrot 1 | <i>Daucus carota</i> L. | Bolero Nantes |
| Carrot 2 | <i>Daucus carota</i> L. | Red Label |
| Corn (Maize) | <i>Zea mays</i> L. | Eureka |
| Cotton 1 | <i>Gossypium barbadense</i> L. | Pima |
| Cotton 2 | <i>Gossypium hirsutum</i> L. | Upland |
| Onion | <i>Allium cepa</i> L. | Walla Walla |
| Potato | <i>Solanum tuberosum</i> L. | Red La Soda |
| Tomato | <i>Lycopersicon esculentum</i> L. | Mortgage Lifter |
| <i>Woody plants</i> | | |
| Almond | <i>Prunus dulcis</i> Mill. D.Webb | Nonpareil |
| Apricot | <i>Prunus armeniaca</i> L. | Blenheim |
| Cherry | <i>Prunus avium</i> L. | Bing |
| Grape 1 | <i>Vitis vinifera</i> L. | Crimson Seedless (Table Variety) |
| Grape 2 | <i>Vitis vinifera</i> L. | Pinot Noir (Wine Variety) |
| Lemon | <i>Citrus limon</i> L. | Allen Eureka (on Cuban Shaddock rootstock) |
| Mandarin | <i>Citrus reticulata</i> Blanco | W. Murcott (on C-35 rootstock) |
| Mandarin | <i>Citrus reticulata</i> Blanco | Clementine (on C-35 rootstock) |
| Olive | <i>Olea europaea</i> L. | Manzanillo |
| Orange | <i>Citrus sinensis</i> L. Osbeck | Parent Navel (on Volk rootstock) |
| Peach | <i>Prunus persica</i> L. Batsch. | Carson |
| Pistachio | <i>Pistacia vera</i> L. | Kerman |
| Plum | <i>Prunus salicina</i> Lindley | Satsuma |
| Pomegranate | <i>Punica granatum</i> L. | Wonderful |

Table 6.3: Basal emission factors (ngC gDM⁻¹ h⁻¹) and beta values for monoterpenes, oxygenated monoterpenes and sesquiterpenes from enclosure studies

| Crop | Monoterpenes | | Oxygenated Monoterpenes | | Sesquiterpenes | |
|-----------------------------|---------------------------------|--------------------|--------------------------------|-------------------|--------------------------------|------------------|
| | BEF±StDev (N) | Beta ®(N) | BEF±StDev (N) | Beta ®(N) | BEF±StDev (N) | Beta ®(N) |
| Alfalfa | 270±160 (2) | 0.10 (0.84)(11) | N.D. | | N.D. | |
| Almond | 68±51 (23) ^[24] | 0.065 (0.23)(157)* | 150±28 (6) ^[24] | 0.16 (0.90)(32) | 10000±3300 (6) ^[24] | 0.45 (0.92)(31) |
| Carrot (RL) | 78±45 (15) ^[25] | N.B. | 22±12 (3) ^[25] | 0.099 (0.51)(11) | N.D. | |
| Carrot (BN) | 48±36 (43) ^[27] | 0.063 (0.29)(166)* | | | 56±36 (3) ^[27] | N.B. |
| Cherry | 84±59 (26) ^[26] | 0.067 (0.34)(121)* | 670±250 (16) ^[26] | 0.30 (0.94)(40) | N.D. | |
| Corn | N.D. | | N.D. | | N.D. | |
| Cotton Pima | 47±21 (10) ^[27] | 0.027 (0.25)(31)* | 2700±3100 (5) | 0.13 (0.35)(26) | N.D. | |
| Cotton Upland | 41±16 (4) | 0.12 (0.74)(16) | 81±83 (4) | 0.18 (0.26)(7) | N.D. | |
| Table Grape | 11±4.9 (2) ^[28] | N.B. | 26±13 (5) | 0.029 (0.27)(23) | 45±15 (5) | 0.095 (0.69)(13) |
| Wine Grape | 91±50 (13) ^[27] | 0.17 (0.67)(20) | 44±10 (3) ^[25] | N.B. | 52±22 (8) ^[27] | N.B. |
| Liquidambar | 350±260 (31) ^[26] | 0.098 (0.35)(174)* | 47±4.8 (2) ^[26] | 0.19 (0.94)(4) | N.D. | |
| Miscanthus | 140±89 (17) ^[27] | 0.044 (0.20)(63)* | 48±19 (6) ^[28] | 0.16 (0.80)(11) | 180±31 (6) ^[28] | 0.076 (0.76)(11) |
| Olive | 60±32 (8) ^[26] | 0.15 (0.68)(28) | 7.5±0.91 (2) ^[26] | 0.066 (0.51)(4) | N.D. | |
| Onion | 350±110 (3) ^[28] | N.B. | N.D. | | N.D. | |
| Peach | 1200±270 (2) ^[24] | 0.23 (0.97)(10) | 240±55 (2) ^[24] | 0.23 (0.97)(10) | N.D. | |
| Pistachio | 40±22 (47) ^[28] | 0.098 (0.47)(207)* | 39±55 (15) ^[26] | 0.15 (0.36)(22)* | N.D. | |
| Plum | 37±20 (5) ^[26] | 0.010 (0.04)(26)* | 30±11 (4) ^[28] | 0.14 (0.68)(6) | N.D. | |
| Pomegranate | 32±26 (4) ^[25] | N.B. | 26±9.8 (4) ^[27] | 0.14 (0.78)(5) | 61±8.6 (5) ^[27] | 0.024 (0.23)(9)* |
| Potato | 150±9.8 (3) ^[24] | 0.064 (0.47)(16)* | 22±9.3 (3) ^[27] | N.B. | 40±13 (3) | N.B. |
| Tomato | 740±260 (7) ^[27] | 0.11 (0.31)(68)* | N.D. | | 59±15 (3) ^[27] | N.B. |
| Orange P.N. (No Flowers) | 2500±3400 (116) ^[26] | 0.14 (0.35)(522)* | 1300±1900 (33) ^[26] | N.B. | 1500±970 (20) ^[25] | 0.25 (0.74)(58) |
| Orange P.N. (Flowers) | 7800±4300 (36) ^[26] | 0.15 (0.71)(151) | 4600±1300 (11) ^[24] | 0.072 (0.38)(36)* | 3200±780 (11) ^[24] | 0.28 (0.92)(36) |
| Mandarin W. Murcott | 63±25 (20) ^[28] | 0.080 (0.47)(99)* | 150±190 (8) ^[29] | 0.23 (0.79)(20) | N.D. | |
| Mandarin Clementine | 26±18 (22) ^[26] | 0.064 (0.27)(141)* | N.D. | | N.D. | |
| Lemon Eureka | 22±22 (24) ^[25] | 0.036 (0.15)(166)* | N.M. | | N.M. | |

Notes: N.M.=No Measurements, N.D.=Below Detection Limit, N.A.=No Basal Condition Met, N.B.=Beta Value Analysis Inaccurate

When the BEF was determined at a lower temperature and adjusted, the temperature it was determined at is indicated after the BEF as ^[.C], the value was adjusted using the calculated beta unless the correlation coefficient for beta was below 0.5, then a default beta of 0.1 was used and the beta column is marked with *

Table 6.4: Statistics for modeling methods using light and temperature (L&T) and temperature only (T) from enclosure studies

| Crop | Monoterpenes | | | | Oxygenated Monoterpenes | | | | Sesquiterpenes | | | |
|---------------------|--------------|-------|-------|-------|-------------------------|-------|-------|-------|----------------|-------|-------|-------|
| | L&T | | T | | L&T | | T | | L&T | | T | |
| | r^2 | Slope | r^2 | Slope | r^2 | Slope | r^2 | Slope | r^2 | Slope | r^2 | Slope |
| Alfalfa | 0.72 | 1.36 | 0.7 | 0.92 | | | | | | | | |
| Almond | 0.6 | 0.36 | 0.61 | 0.27 | 0.72 | 1.41 | 0.84 | 0.89 | 0.62 | 3.26 | 0.94 | 0.81 |
| Carrot (RL) | N.S. | N.S. | N.S. | N.S. | N.S. | N.S. | N.S. | N.S. | | | | |
| Carrot (BN) | 0.14 | 0.4 | 0.11 | 0.24 | | | | | N.S. | N.S. | N.S. | N.S. |
| Cherry | 0.64 | 2.52 | 0.6 | 1.37 | 0.69 | 1.57 | 0.78 | 0.87 | | | | |
| Corn | | | | | | | | | | | | |
| Cotton Pima | N.S. | N.S. | N.S. | N.S. | 0.32 | 0.4 | 0.34 | 0.27 | | | | |
| Cotton Upland | 0.51 | 1.02 | 0.43 | 0.66 | N.S. | N.S. | N.S. | N.S. | | | | |
| Table Grape | N.S. | N.S. | N.S. | N.S. | 0.11 | 0.68 | 0.11 | 0.28 | 0.25 | 0.56 | 0.28 | 0.32 |
| Wine Grape | 0.11 | 0.43 | N.S. | N.S. | N.S. | N.S. | N.S. | N.S. | 0.14 | 0.35 | N.S. | N.S. |
| Liquidambar | 0.5 | 0.16 | 0.63 | 0.17 | 0.64 | 1.65 | 0.81 | 1.07 | | | | |
| Miscanthus | 0.7 | 1.23 | 0.73 | 0.97 | 0.25 | 0.94 | 0.5 | 0.7 | 0.35 | 1.18 | 0.47 | 0.7 |
| Olive | 0.98 | 0.26 | 0.84 | 0.16 | 0.47 | 1.4 | 0.28 | 0.42 | | | | |
| Onion | N.S. | N.S. | N.S. | N.S. | | | | | | | | |
| Peach | 0.96 | 1.78 | 0.97 | 1.17 | 0.93 | 1.84 | 0.95 | 1.21 | | | | |
| Pistachio | 0.15 | 0.18 | 0.17 | 0.16 | N.S. | N.S. | N.S. | N.S. | | | | |
| Plum | 0.13 | 0.21 | N.S. | N.S. | 0.4 | 1.08 | 0.25 | 0.69 | | | | |
| Pomegranate | N.S. | N.S. | N.S. | N.S. | 0.63 | 1.01 | 0.69 | 0.68 | 0.29 | 1.87 | N.S. | N.S. |
| Potato | 0.12 | 1.31 | 0.2 | 0.53 | 0.12 | 0.13 | N.S. | N.S. | N.S. | N.S. | N.S. | N.S. |
| Tomato | 0.33 | 0.18 | 0.27 | 0.11 | | | | | N.S. | N.S. | N.S. | N.S. |
| Orange (no flowers) | 0.57 | 0.74 | 0.63 | 0.61 | 0.44 | 0.84 | 0.68 | 0.87 | 0.88 | 2.14 | 0.8 | 1.17 |
| Orange (flowers) | 0.6 | 0.78 | 0.61 | 0.58 | 0.43 | 1.37 | 0.37 | 0.74 | 0.92 | 2.13 | 0.89 | 1.11 |
| Mandarin W. Murcott | 0.32 | 0.08 | 0.41 | 0.08 | 0.18 | 0.26 | 0.34 | 0.4 | | | | |
| Mandarin Clementine | N.S. | N.S. | N.S. | N.S. | | | | | | | | |
| Lemon Eureka | N.S. | N.S. | N.S. | N.S. | | | | | | | | |

N.S.: Results not significant ($r^2 < 0.10$ or negative slope)

Note: Table 6.3 gives information on sample size (N)

Table 6.5: Composition of monoterpene emissions measured in enclosure studies

| Crop | limonene | β -cis-ocimene | β -trans-ocimene | β -myrcene | α -phellandrene | β -phellandrene | Δ^3 -carene | Δ^2 -carene | α -terpinene | γ -terpinene | α -thujene | sabinene | α -pinene | β -pinene |
|---------------------|----------|----------------------|------------------------|------------------|------------------------|-----------------------|--------------------|--------------------|---------------------|---------------------|-------------------|----------|------------------|-----------------|
| Alfalfa | 0% | 0% | 58% | 0% | 0% | 0% | 0% | 0% | 0% | 0% | 0% | 0% | 42% | 0% |
| Almond | 9% | 0% | 23% | 36% | 2% | 0% | 26% | 0% | 0% | 0% | 0% | 0% | 3% | 0% |
| Carrot (RL) | 28% | 3% | 3% | 37% | 0% | 1% | 3% | 0% | 11% | 6% | 0% | 0% | 6% | 3% |
| Carrot (BN) | 2% | 19% | 1% | 23% | 0% | 0% | 4% | 0% | 0% | 0% | 0% | 15% | 34% | 1% |
| Cherry | 0% | 94% | 6% | 0% | 0% | 0% | 0% | 0% | 0% | 0% | 0% | 0% | 0% | 0% |
| Corn | | | | | | | | | | | | | | |
| Cotton Pima | 0% | 0% | 2% | 0% | 0% | 0% | 0% | 0% | 0% | 0% | 0% | 34% | 64% | 0% |
| Cotton Upland | 0% | 1% | 19% | 0% | 0% | 39% | 0% | 0% | 0% | 0% | 0% | 0% | 41% | 0% |
| Table Grape | 0% | 1% | 1% | 0% | 0% | 0% | 0% | 0% | 0% | 0% | 0% | 0% | 98% | 0% |
| Wine Grape | 0% | 0% | 23% | 0% | 0% | 0% | 0% | 0% | 0% | 6% | 0% | 64% | 3% | 4% |
| Liquidambar | 55% | 0% | 0% | 0% | 0% | 0% | 0% | 0% | 1% | 0% | 0% | 17% | 27% | 0% |
| Miscanthus | 48% | 4% | 23% | 0% | 0% | 0% | 0% | 0% | 0% | 21% | 0% | 2% | 2% | 0% |
| Olive | 0% | 5% | 93% | 0% | 0% | 0% | 1% | 0% | 0% | 0% | 0% | 1% | 0% | 0% |
| Onion | 85% | 0% | 15% | 0% | 0% | 0% | 0% | 0% | 0% | 0% | 0% | 0% | 0% | 0% |
| Peach | 0% | 0% | 100% | 0% | 0% | 0% | 0% | 0% | 0% | 0% | 0% | 0% | 0% | 0% |
| Pistachio | 87% | 5% | 1% | 1% | 0% | 0% | 1% | 0% | 0% | 0% | 3% | 0% | 1% | 1% |
| Plum | 0% | 0% | 100% | 0% | 0% | 0% | 0% | 0% | 0% | 0% | 0% | 0% | 0% | 0% |
| Pomegranate | | | | | | | | | | | | | | |
| Potato | 61% | 22% | 0% | 0% | 0% | 0% | 0% | 0% | 0% | 0% | 0% | 0% | 17% | 0% |
| Tomato | 0% | 0% | 0% | 0% | 7% | 75% | 1% | 14% | 2% | 0% | 0% | 0% | 2% | 0% |
| Orange (no flowers) | 7% | 4% | 27% | 56% | 0% | 0% | 0% | 0% | 0% | 0% | 0% | 3% | 1% | 0% |
| Orange (flowers) | 2% | 0% | 30% | 67% | 0% | 0% | 0% | 0% | 0% | 0% | 0% | 1% | 0% | 0% |
| Mand. W. Murcott | 13% | 33% | 32% | 1% | 0% | 0% | 1% | 0% | 0% | 4% | 0% | 9% | 2% | 4% |
| Mand. Clementine | 17% | 6% | 14% | 1% | 1% | 0% | 14% | 0% | 0% | 0% | 0% | 40% | 5% | 3% |
| Lemon Eureka | | | | | | | | | | | | | | |

Table 6.6: Composition of oxygenated monoterpene emissions measured in enclosure studies

| Plant | Linalool | Perillene | Eucalyptol |
|--------------------------|-----------------|------------------|-------------------|
| Alfalfa | | | |
| Almond | 10% | 90% | 0% |
| Carrot (RL) | 94% | 6% | 0% |
| Carrot (BN) | | | |
| Cherry | 0% | 100% | 0% |
| Corn | | | |
| Cotton Pima | 0% | 100% | 0% |
| Cotton Upland | 4% | 96% | 0% |
| Table Grape | 0% | 100% | 0% |
| Wine Grape | 0% | 100% | 0% |
| Liquidambar | 0% | 100% | 0% |
| Miscanthus | 26% | 0% | 74% |
| Olive | 0% | 100% | 0% |
| Onion | | | |
| Peach | 0% | 100% | 0% |
| Pistachio | 16% | 84% | 0% |
| Plum | 3% | 97% | 0% |
| Pomegranate | 0% | 100% | 0% |
| Potato | 0% | 100% | 0% |
| Tomato | 100% | 0% | 0% |
| Orange P.N. (No Flowers) | 93% | 6% | 1% |
| Orange P.N. (Flowers) | 97% | 2% | 1% |
| Mandarin W. Murcott | 6% | 94% | 0% |
| Mandarin Clementine | 46% | 54% | 0% |
| Lemon Eureka | | | |

Table 6.7: Composition of sesquiterpene emissions measured in enclosure studies

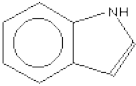
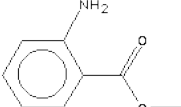
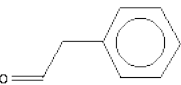
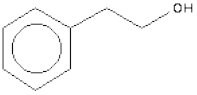
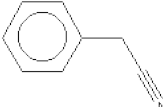
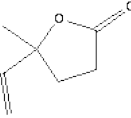
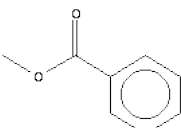
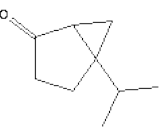
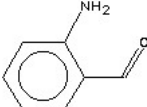
| Plant | β-caryophyllene | α-humulene |
|--------------------------|---|-------------------------------------|
| Alfalfa | | |
| Almond | 77% | 23% |
| Carrot (RL) | 100% | 0% |
| Carrot (BN) | 100% | 0% |
| Cherry | | |
| Corn | | |
| Cotton Pima | 54% | 46% |
| Cotton Upland | | |
| Table Grape | 69% | 31% |
| Wine Grape | 100% | 0% |
| Liquidambar | 100% | 0% |
| Miscanthus | 7% | 93% |
| Olive | 100% | 0% |
| Onion | | |
| Peach | | |
| Pistachio | 0% | 100% |
| Plum | | |
| Pomegranate | 90% | 10% |
| Potato | 98% | 2% |
| Tomato | 100% | 0% |
| Orange P.N. (No Flowers) | 100% | 0% |
| Orange P.N. (Flowers) | 100% | 0% |
| Mandarin W. Murcott | 33% | 67% |
| Mandarin Clementine | 17% | 83% |
| Lemon Eureka | | |

Table 6.8: Interquartile ranges for measured BVOC in spring and summer (in pptv).

| Compound | Spring (Flowering) | | Summer | |
|---------------------------|----------------------|-----------------------|----------------------|-----------------------|
| | Day (10:00-17:00) | Night (20:00-6:00) | Day (10:00-17:00) | Night (20:00-6:00) |
| isoprene | 24.8-67.4 | 55.5-375.8 | 61.3-197.8 | 107.4-852.8 |
| α -thujene | 3.8-13.7 | 16.4-122.0 | 2.5-3.7 | 4.6-19.1 |
| α -pinene | 6.9-13.0 | 12.6-90.8 | 3.2-6.8 | 5.4-20.7 |
| camphene | 4.4-6.8 | 6.2-40.2 | 3.7-7.7 | 7.0-26.5 |
| sabinene | 23.6-67.6 | 62.7-977.5 | 11.5-23.2 | 15.7-33.7 |
| β -myrcene | 324.1-1143.2 | 407.9-2285.4 | 4.4-9.3 | 8.4-49.8 |
| β -pinene | BDL-17.7 | 12.8-52.3 | | |
| α -phellandrene | 1.3-3.1 | 2.1-5.1 | 2.3-6.7 | 7.0-35.1 |
| cis-3-hexenyl acetate | 165.3-353.7 | 213.3-790.2 | | |
| Δ 3-carene | 23.0-51.1 | 37.0-162.0 | 3.2-5.2 | 5.2-38.5 |
| Benzaldehyde | 69.5-276.0 | 78.6-434.3 | | |
| α -terpinene | 5.3-12.0 | 12.0-102.1 | | |
| cis- β -ocimene | 23.9-65.9 | 39.5-162.5 | | |
| trans- β -ocimene | 134.8-380.3 | 197.6-1267.1 | | |
| Δ -limonene | 183.6-365.0 | 275.2-2250.5 | 158.9-271.9 | 204.1-1606.0 |
| p-cymene | 17.8-41.1 | 26.0-238.6 | 7.8-16.6 | 16.4-176.5 |
| γ -valeroactone | 6.2-11.3 | 11.2-103.3 | | |
| γ -terpinene | 16.4-32.4 | 30.6-247.6 | 1.6-7.5 | 4.1-15.5 |
| terpinolene | 6.7-15.6 | 14.2-85.8 | 1.7-2.7 | 6.8-22.2 |
| trans-linalool oxide | 1.7-5.1 | 3.3-18.0 | | |
| cis-linalool oxide | 9.2-14.9 | 11.6-50.6 | | |
| benzeneacetaldehyde | 57.1-242.4 | 86.8-455.7 | | |
| linalool | 1657.3-6037.5 | 2436.4-18342.1 | | |
| lavender lactone | 122.5-278.6 | 216.3-1033.1 | | |
| sabina ketone | 16.8-111.9 | 58.8-255.1 | | |
| 2-amino-benzaldehyde | 174.0-443.1 | 189.2-806.2 | | |
| indole | 984.6-2707.4 | 1408.4-3696.6 | | |
| methyl anthranilate | 906.6-2742.4 | 1151.8-6856.5 | | |
| benzeneethanol | 188.2-420.4 | 215.8-966.7 | | |
| benzyl nitrile | 836.6-1780.8 | 971.7-3212.2 | | |
| methyl benzoate | 14.9-32.8 | 19.8-57.6 | | |
| β -caryophyllene | 9.7-19.6 | 7.0-18.4 | | |
| aromadendrene | 7.2-25.0 | 10.2-31.9 | | |
| trans- β -farnesene | 3.1-21.5 | 6.9-41.7 | | |
| valencene | BDL-17.1 | 13.3-59.2 | | |
| trans-Nerolidol | 22.7-150.9 | 64.0-301.1 | | |
| n-pentadecane | 12.6-29.5 | 14.6-35.8 | | |
| n-hexadecane | 8.1-37.3 | 5.4-34.9 | | |
| n-heptadecane | 36.6-83.7 | 38.7-101.4 | | |
| 8-heptadecene | 1.2-7.1 | 2.0-52.0 | | |
| 1-heptadecene | 79.0-204.3 | 105.5-285.5 | | |
| hexanal | 35.8-162.7 | 81.0-337.8 | | |
| octanal | 11.6-25.3 | 17.3-73.9 | | |
| nonanal | 55.0-120.4 | 68.6-184.2 | | |
| decanal | 6.9-21.1 | 11.3-40.1 | | |

Notes: Entries left blank indicate that compound was not observed during the summer campaign
BDL: Below Detection Limit

Table 6.9 Novel compounds from measurements of ambient air during flowering

| Name(s) | Structure | k_{OH} [$\text{cm}^3 \text{s}^{-1}$ molecules $^{-1} * 10^{11}$] | Lifetime to OH oxidation [min] |
|---|---|---|-----------------------------------|
| Indole |  | 15.4 | 20 |
| Methyl Anthranilate (benzoic acid, 2-amino-, methyl ester) |  | 3.48 | 89 |
| Benzeneacetaldehyde (phenyl acetaldehyde) |  | 2.63 | 117 |
| Benzeneethanol (phenylethyl alcohol) |  | 0.957 | 323 |
| Benzyl Nitrile (benzneacetonitrile) |  | 0.962 | 321 |
| Lavender Lactone (γ -lactone, dihydro-5-methyl-5-vinyl- 2(3H)-furanone) |  | 2.76 | 112 |
| Methyl Benzoate (Methyl Benzenecarboxylate, Niobe Oil) |  | 0.0844 | 3660 |
| Sabina Ketone (5-isopropylbicyclo [3.1.0]hexan-2-one) |  | 0.626 | 493 |
| 2-amino-benzaldehyde |  | 5.23 | 59 |

Notes:

(Chemical Structures from NIST Chemistry WebBook <http://webbook.nist.gov/chemistry/>)

[OH] = 0.25 pptv

Table 6.10: Compounds highly correlated with flowering emissions (represented by β -myrcene)

| Compound | mol/mol β -myrcene | \pm Std. Dev. | Correlation Coeff. (r) |
|-------------------------|--------------------------|-----------------|------------------------|
| linalool | 7.1 | 0.2 | 0.92 |
| methyl anthranilate | 1.2 | 0.04 | 0.95 |
| indole | 0.62 | 0.02 | 0.93 |
| benzyl nitrile | 0.38 | 0.03 | 0.78 |
| Δ -limonene | 0.35 | 0.03 | 0.73 |
| trans- β -ocimene | 0.31 | 0.01 | 0.93 |
| benzeneacetaldehyde | 0.26 | 0.02 | 0.76 |
| 2-amino-benzaldehyde | 0.23 | 0.007 | 0.95 |
| benzeneethanol | 0.22 | 0.007 | 0.94 |
| lavender lactone | 0.18 | 0.01 | 0.78 |
| cis-3-hexenyl acetate | 0.15 | 0.006 | 0.93 |
| benzaldehyde | 0.081 | 0.006 | 0.78 |
| 1-heptadecene | 0.040 | 0.002 | 0.91 |
| cis- β -ocimene | 0.025 | 0.002 | 0.79 |
| Δ 3-carene | 0.023 | 0.002 | 0.79 |
| cis-linalool-oxide | 0.015 | 0.0005 | 0.93 |
| octanal | 0.014 | 0.0009 | 0.82 |
| n-heptadecane | 0.011 | 0.0006 | 0.85 |
| terpinolene | 0.0096 | 0.0009 | 0.70 |
| methyl benzoate | 0.0071 | 0.0006 | 0.75 |
| valencene | 0.0067 | 0.0005 | 0.83 |
| decanal | 0.0060 | 0.0006 | 0.71 |
| aromadendrene | 0.0048 | 0.0002 | 0.88 |
| n-pentadecane | 0.0041 | 0.0002 | 0.91 |
| trans-linalool oxide | 0.0032 | 0.0003 | 0.76 |
| β -caryophyllene | 0.0030 | 0.0002 | 0.83 |

Table 6.11: Source profile for flowering emissions from citrus trees

| Compound | |
|-----------------------|-------|
| linalool | 44.3% |
| methyl anthranilate | 17.0% |
| indole | 10.1% |
| benzyl nitrile | 8.0% |
| β -myrcene | 7.9% |
| cis-3-hexenyl acetate | 2.3% |
| benzeneethanol | 2.2% |
| lavender lactone | 1.9% |
| 2-amino-benzaldehyde | 1.9% |
| 1-heptadecene | 1.2% |
| benzaldehyde | 1.0% |
| benzeneacetaldehyde | 0.92% |
| sabina ketone | 0.61% |
| n-heptadecane | 0.44% |
| methyl benzoate | 0.17% |
| cis-linalool oxide | 0.12% |
| trans-linalool oxide | 0.04% |
| 8-heptadecene | 0.04% |

Table 6.12: Summary of monoterpene composition for both seasonal campaigns at Lindcove

| Compound | Spring (Flowering) | Summer |
|-------------------------|---------------------------|---------------|
| β -myrcene | 34.2% | 2.4% |
| sabinene | 12.8% | 2.2% |
| Δ -limonene | 24.2% | 87.6% |
| γ -terpinene | 2.0% | 1.0% |
| cis- β -ocimene | 2.9% | - |
| trans- β -ocimene | 13.6% | - |
| α -thujene | 1.7% | 1.1% |
| Δ 3-carene | 3.7% | 1.3% |
| α -pinene | 0.7% | 0.80% |
| α -terpinene | 0.77% | - |
| α -phellandrene | 0.93% | 1.3% |
| terpinolene | 0.84% | 0.7% |
| β -pinene | 0.91% | 2.60% |
| camphene | 0.70% | 1.6% |

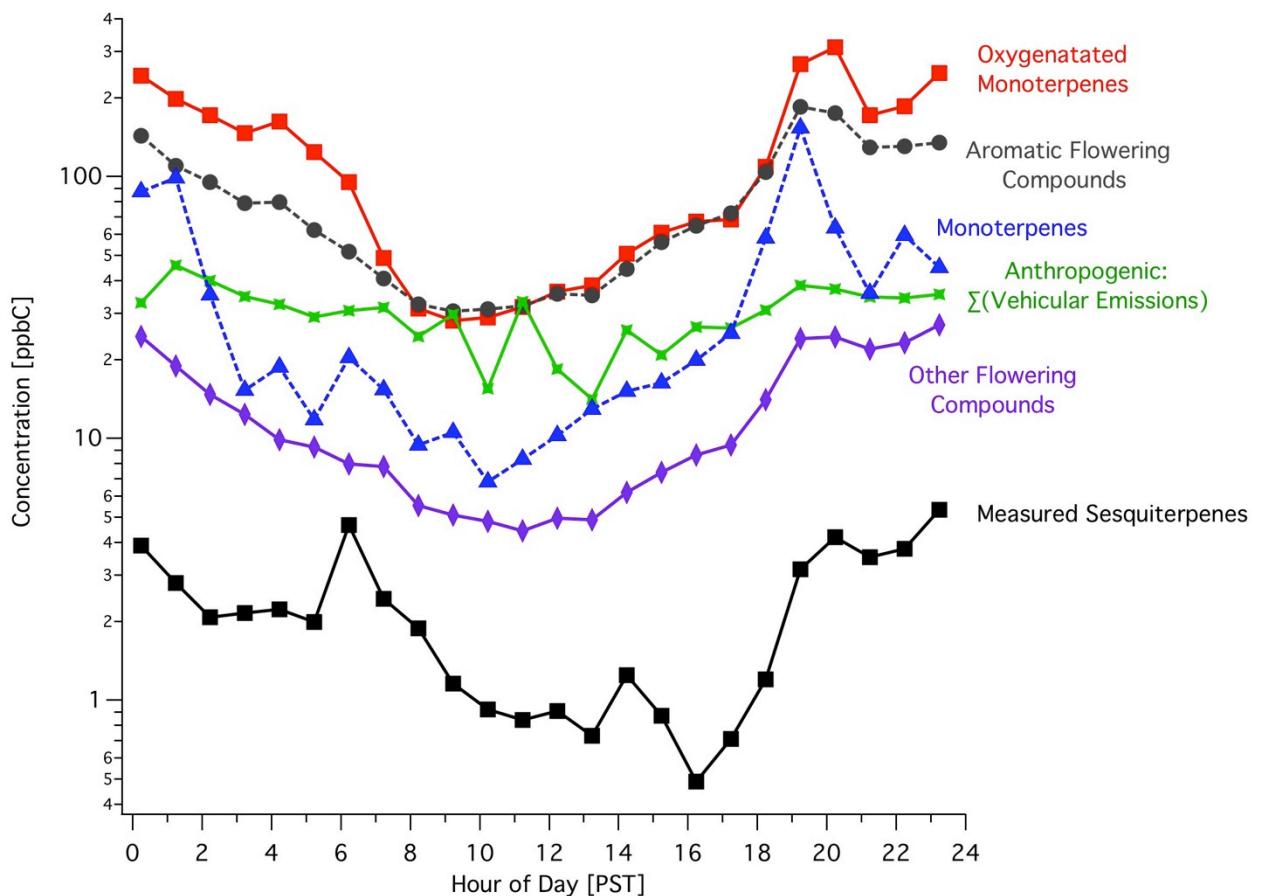


Figure 6.1: Average diurnal patterns of different compound classes shown on a logarithmic scale during flowering at the Lindcove site. Anthropogenic emissions from motor vehicles are shown for comparison. Floral emissions of oxygenated monoterpenes and aromatics dominate total biogenic emissions. Observed sesquiterpenes are lower than total sesquiterpenes as not all compounds were measured.

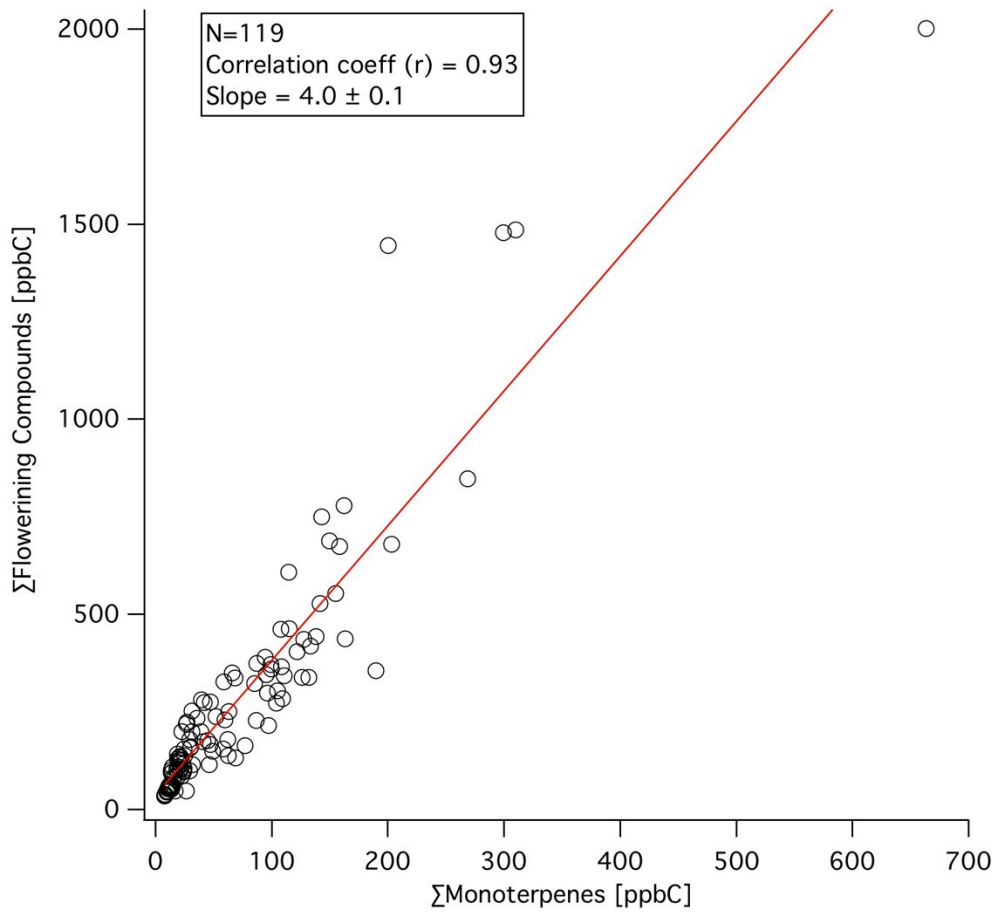


Figure 6.2: Comparison of total observed flowering compounds to the sum of monoterpenes during the spring at the Lindcove site. Concentrations were well correlated with a slope of 4.0, but can be expected to vary somewhat with the density of blossoms over the whole period of flowering.

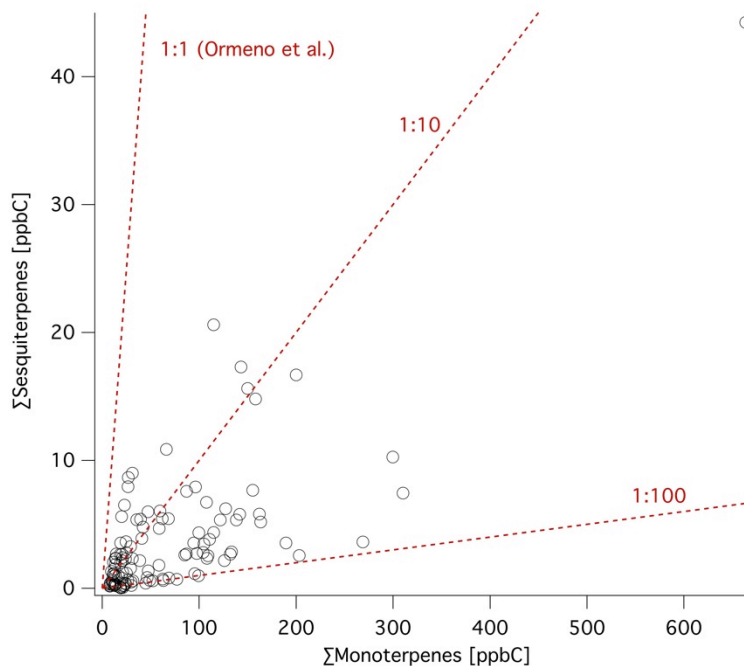


Figure 6.3: A comparison of observed sesquiterpenes to monoterpenes during the spring at Lindcove show considerable variance in their ratio to each other. The 1:1 ratio expected by Ormeno et al. (25) is shown, but is not reached due to measurements of a partial suite of sesquiterpenes and their greater atmospheric reactivity.

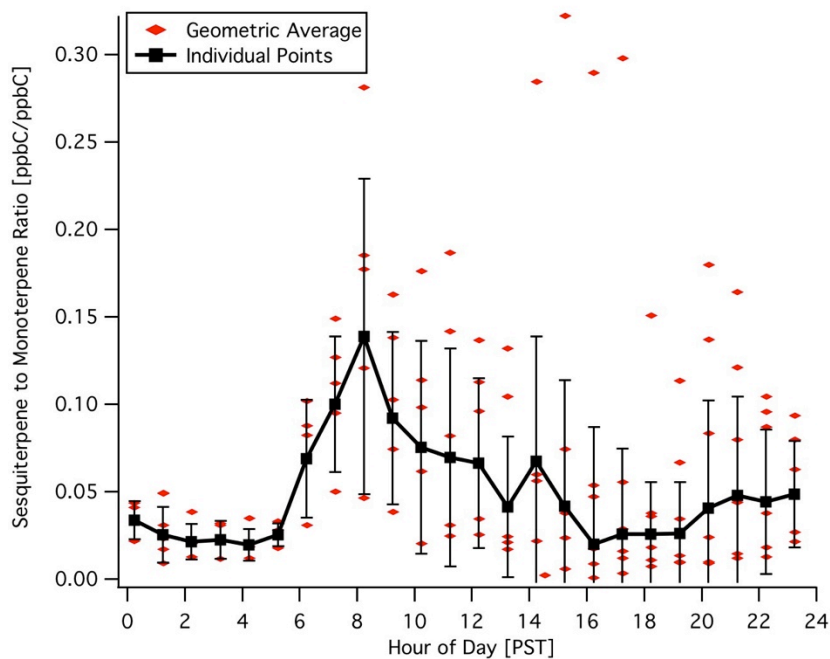


Figure 6.4: The diurnal pattern of sesquiterpenes to monoterpenes shows a higher ratio during the day than at night. Ratios are the highest early in the morning possibly due to lower levels of atmospheric oxidants (OH and O₃) in the morning.

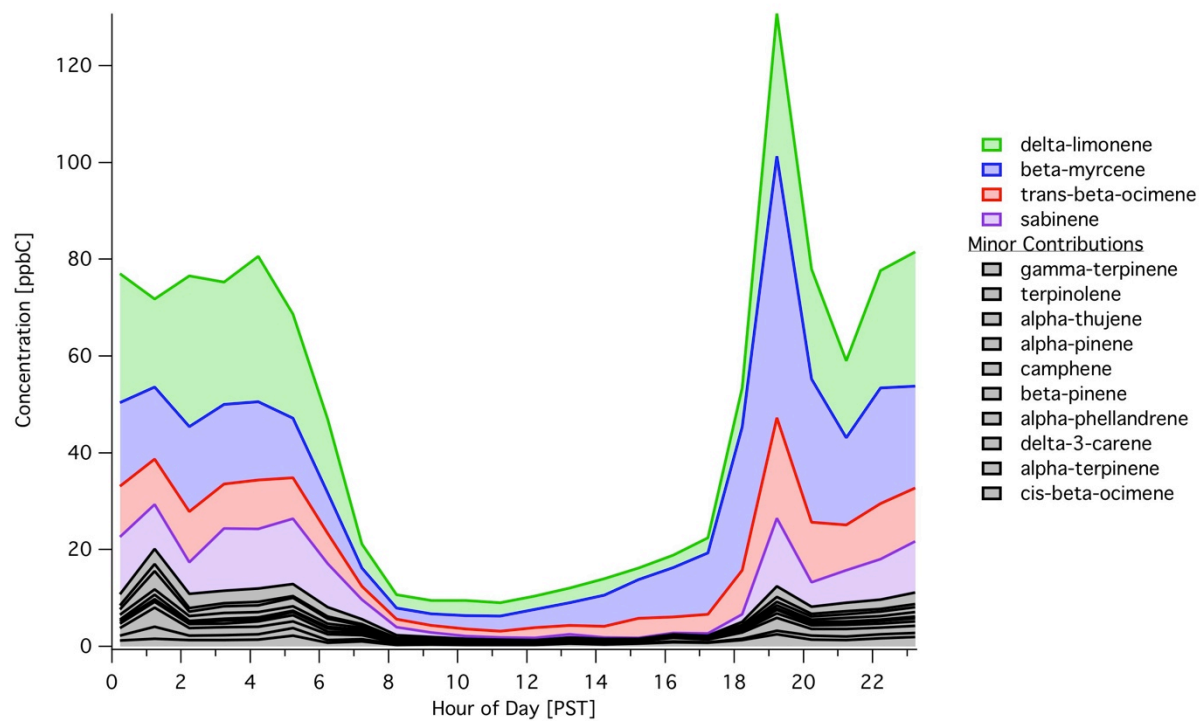


Figure 6.5: Diurnal pattern and composition of monoterpenes in spring during flowering.

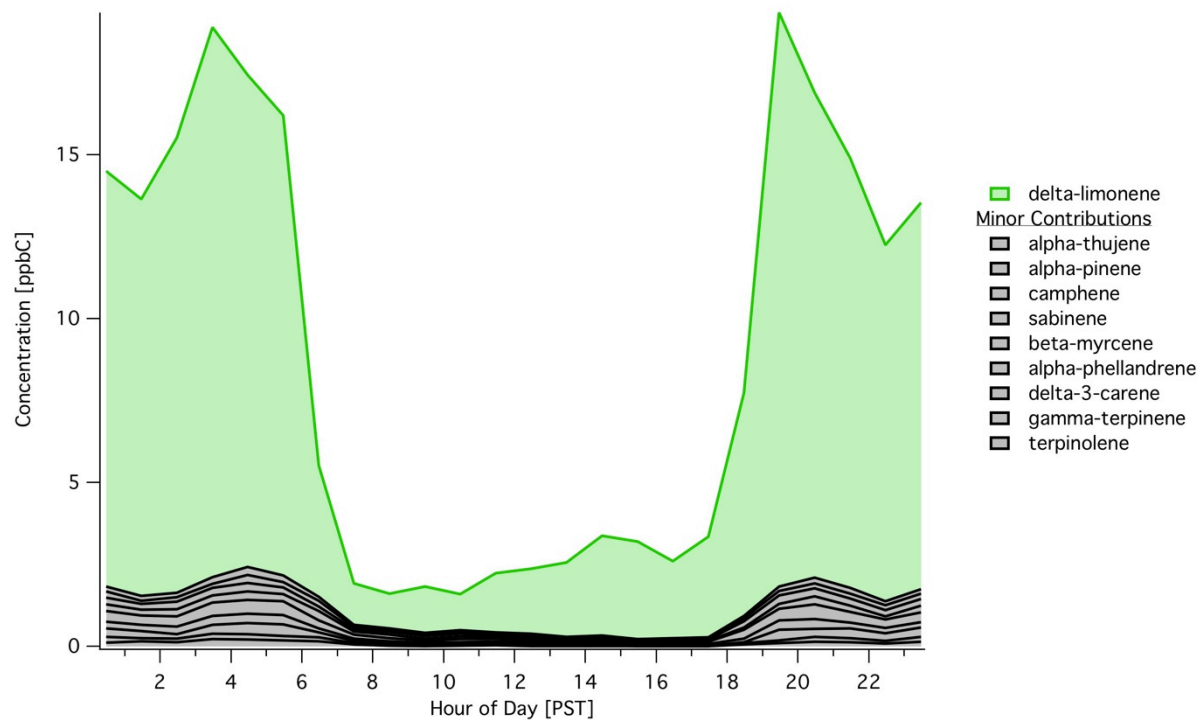


Figure 6.6: Diurnal pattern and composition of monoterpenes in summer.

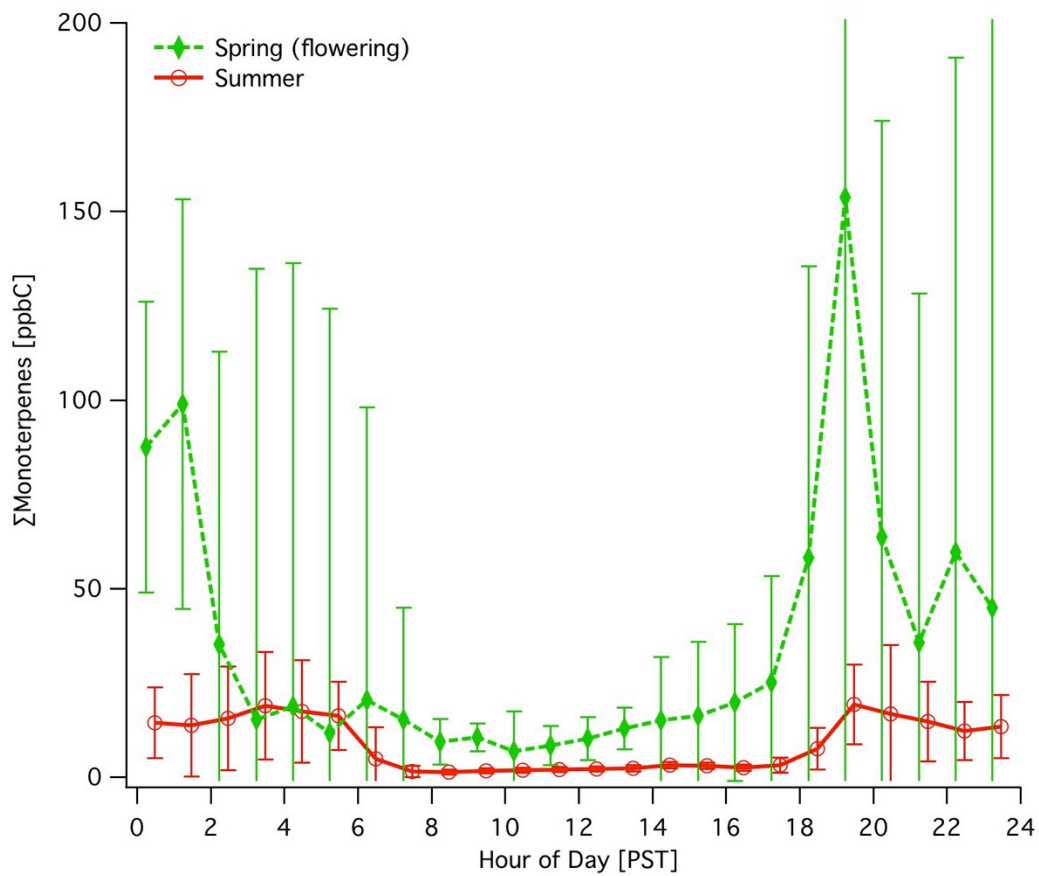


Figure 6.7: Seasonal comparison of diurnal monoterpene concentrations shown with standard deviations.

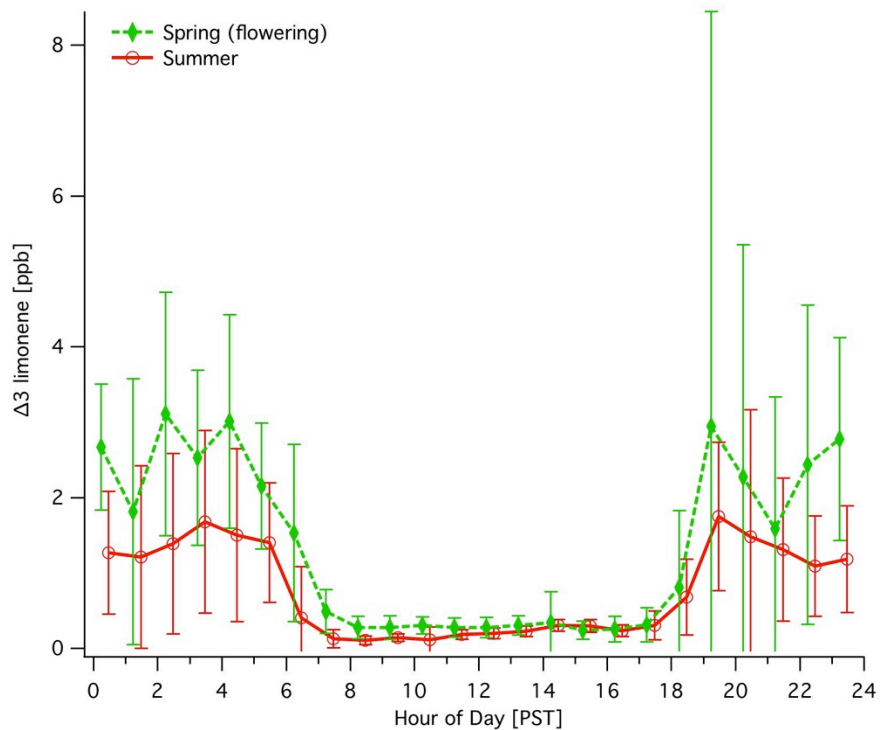


Figure 6.8: The seasonal comparison of diurnal limonene concentrations (shown with standard deviations) demonstrates similar concentrations that are slightly higher during flowering.

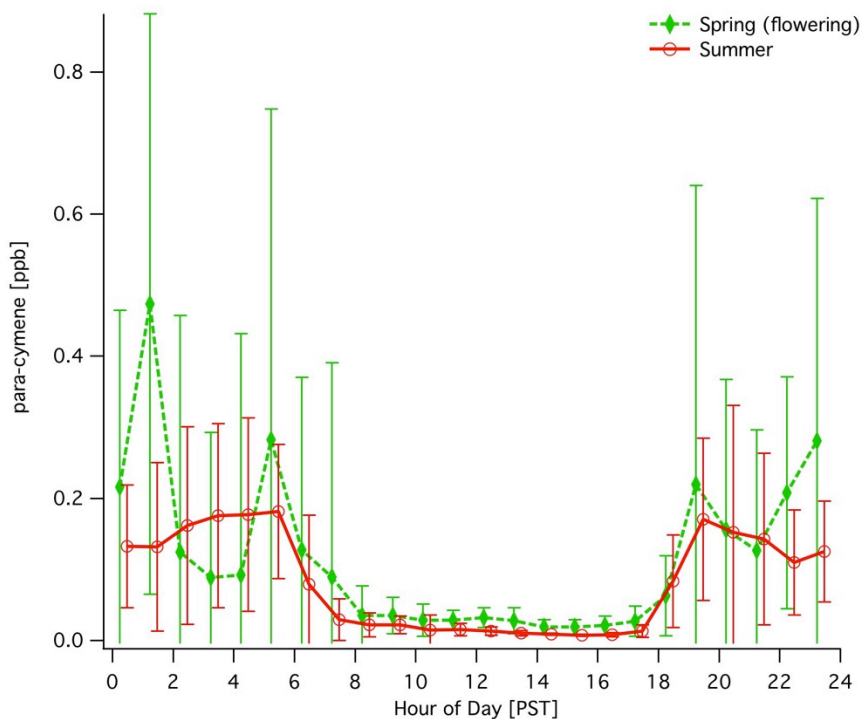


Figure 6.9: The seasonal comparison of diurnal p-cymene concentrations (shown with standard deviations) demonstrates similar levels between the two seasons.

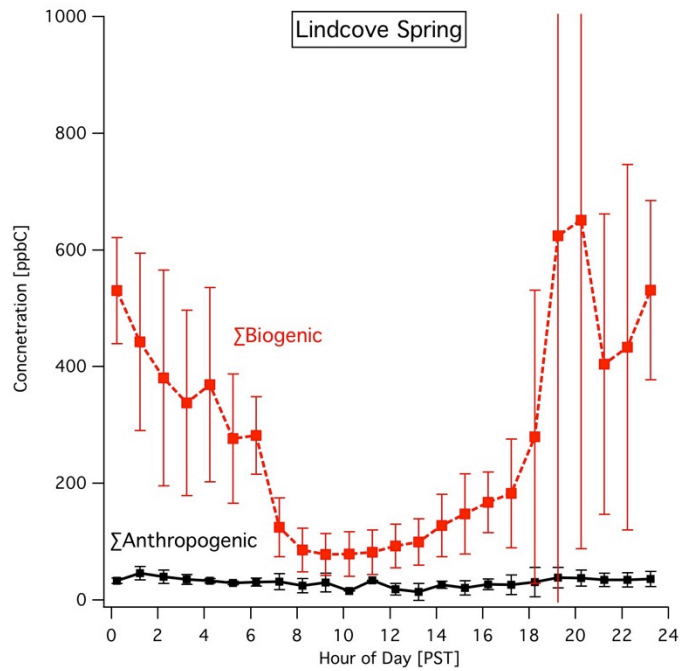


Figure 6.10: Diurnal patterns of the sum of biogenic compounds vs. anthropogenic compounds from motor vehicles at the Lindcove site in the spring.

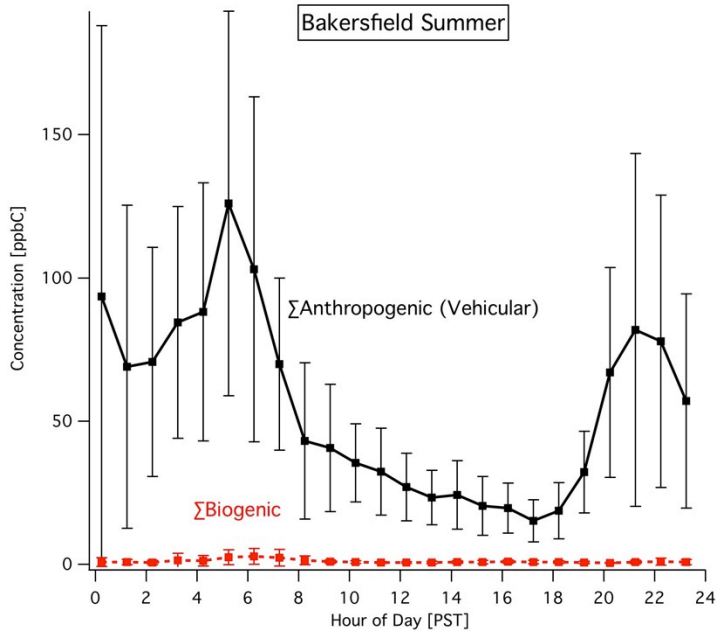


Figure 6.11: Sum of biogenic compounds (largely monoterpenes) observed at the urban Bakersfield site vs. the sum of compounds from motor vehicles. Shown for comparison to the previous figure at the rural Lindcove site during flowering.

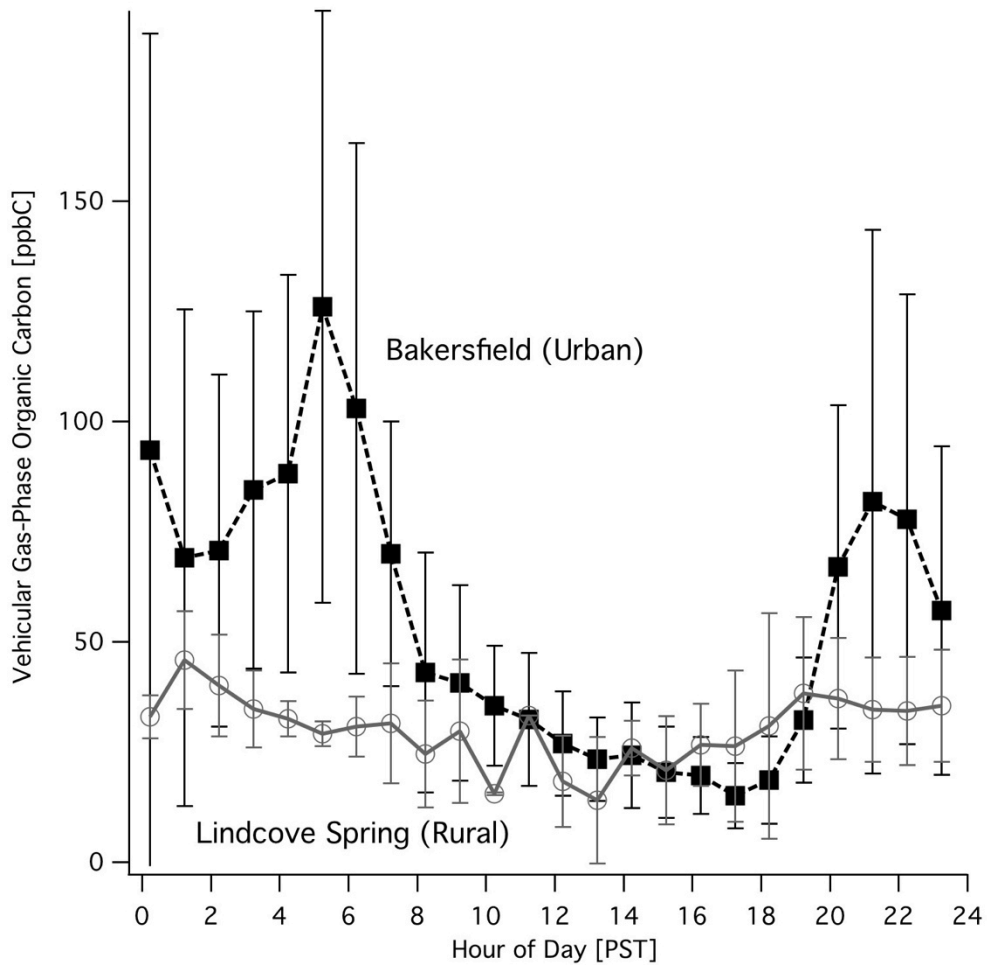


Figure 6.12: A comparison of motor vehicle compound concentrations between the urban Bakersfield site and the rural Lindcove site shows similar daytime levels, but nighttime and morning values vary due to the build-up of local emissions in the nocturnal boundary layer.

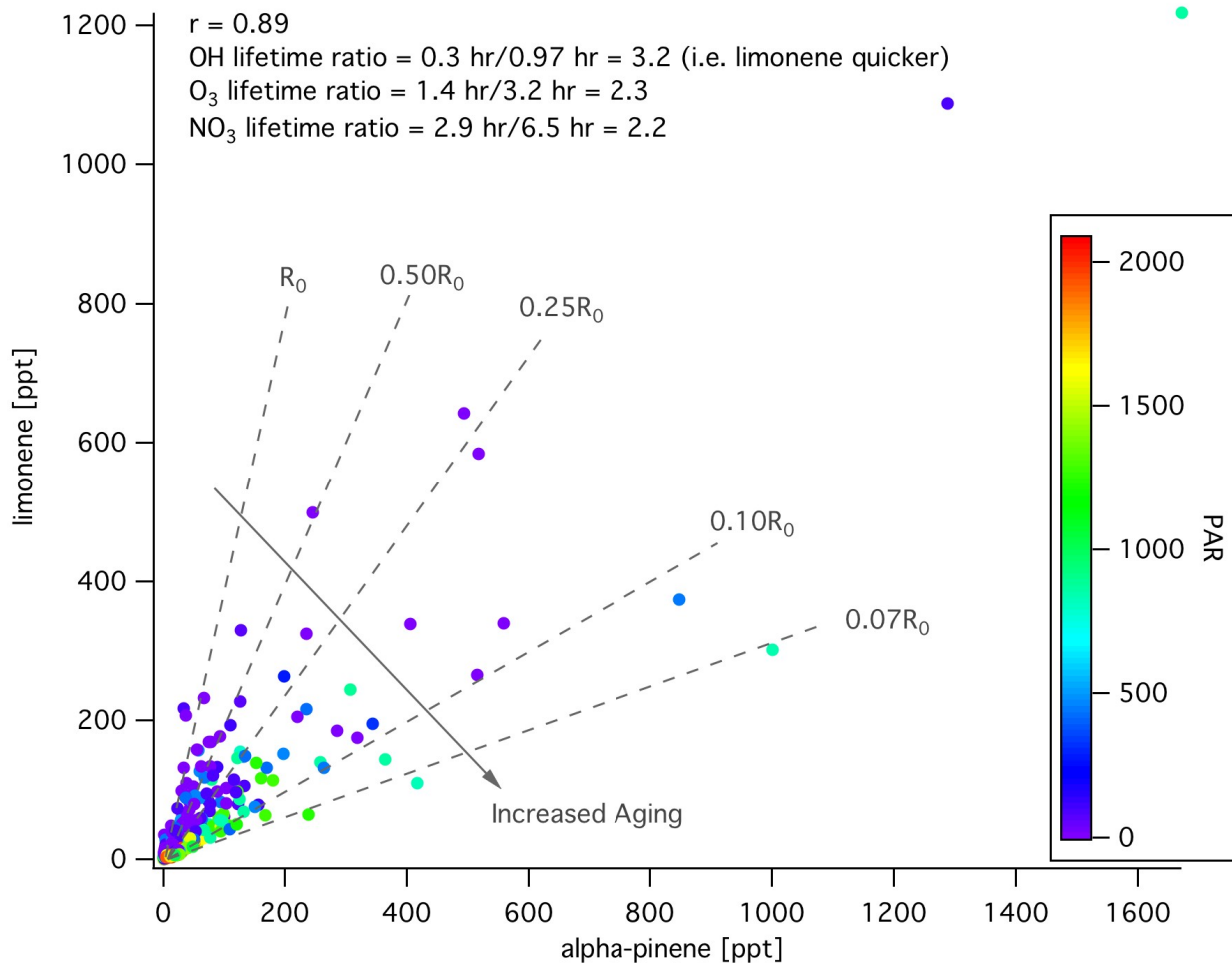


Figure 6.13: Observations of Δ -limonene vs. α -pinene at the Bakersfield site. Ratios of lifetimes to all three atmospheric oxidants show faster processing of Δ -limonene. Given the concentrations of radicals, OH oxidation has the fastest timescales and the importance of OH oxidation is also indicated by the most aged parcels coinciding with PAR (representative of OH production).

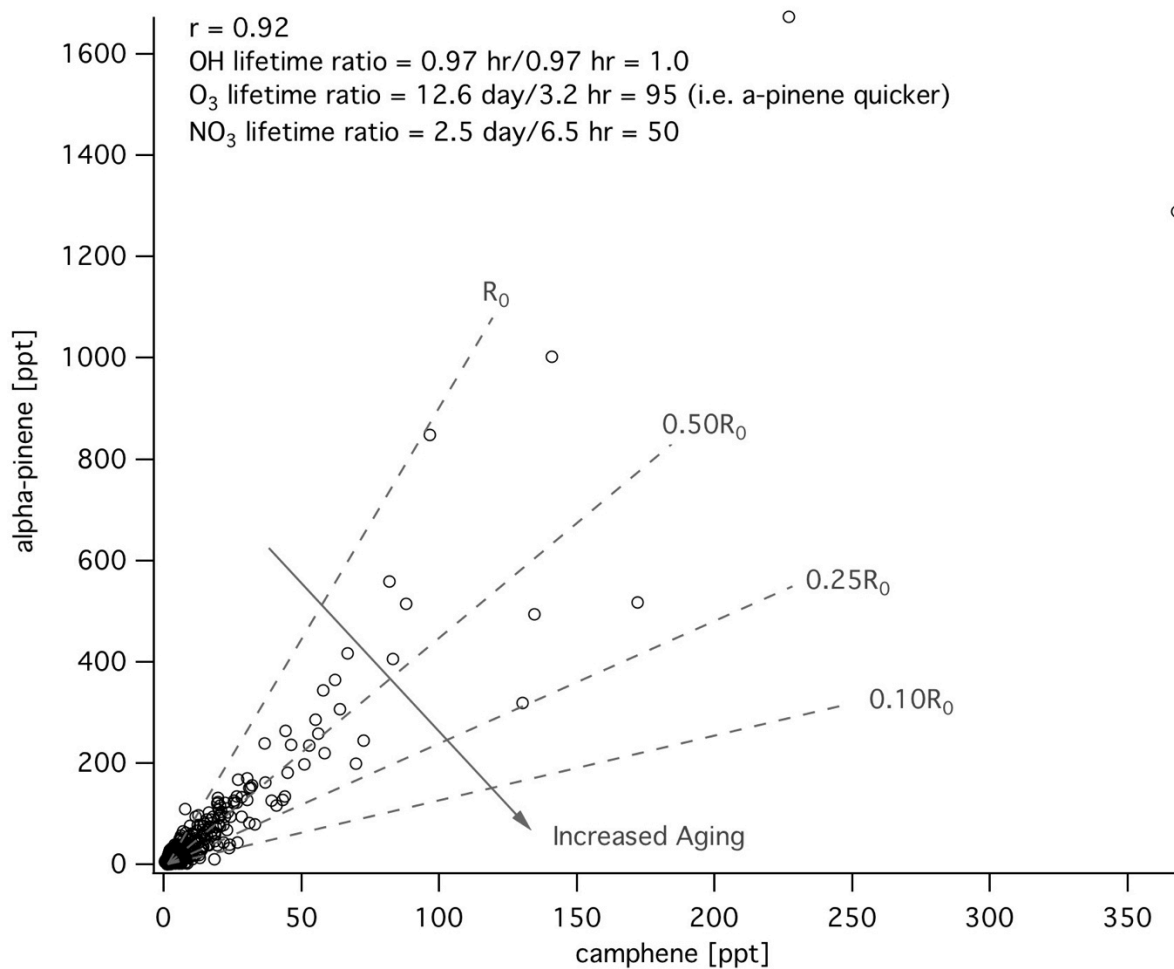


Figure 6.14: A comparison of α -pinene vs. camphene at Bakersfield shows evidence of aging by O_3 and NO_3 as α -pinene and camphene's lifetimes to OH are identical.

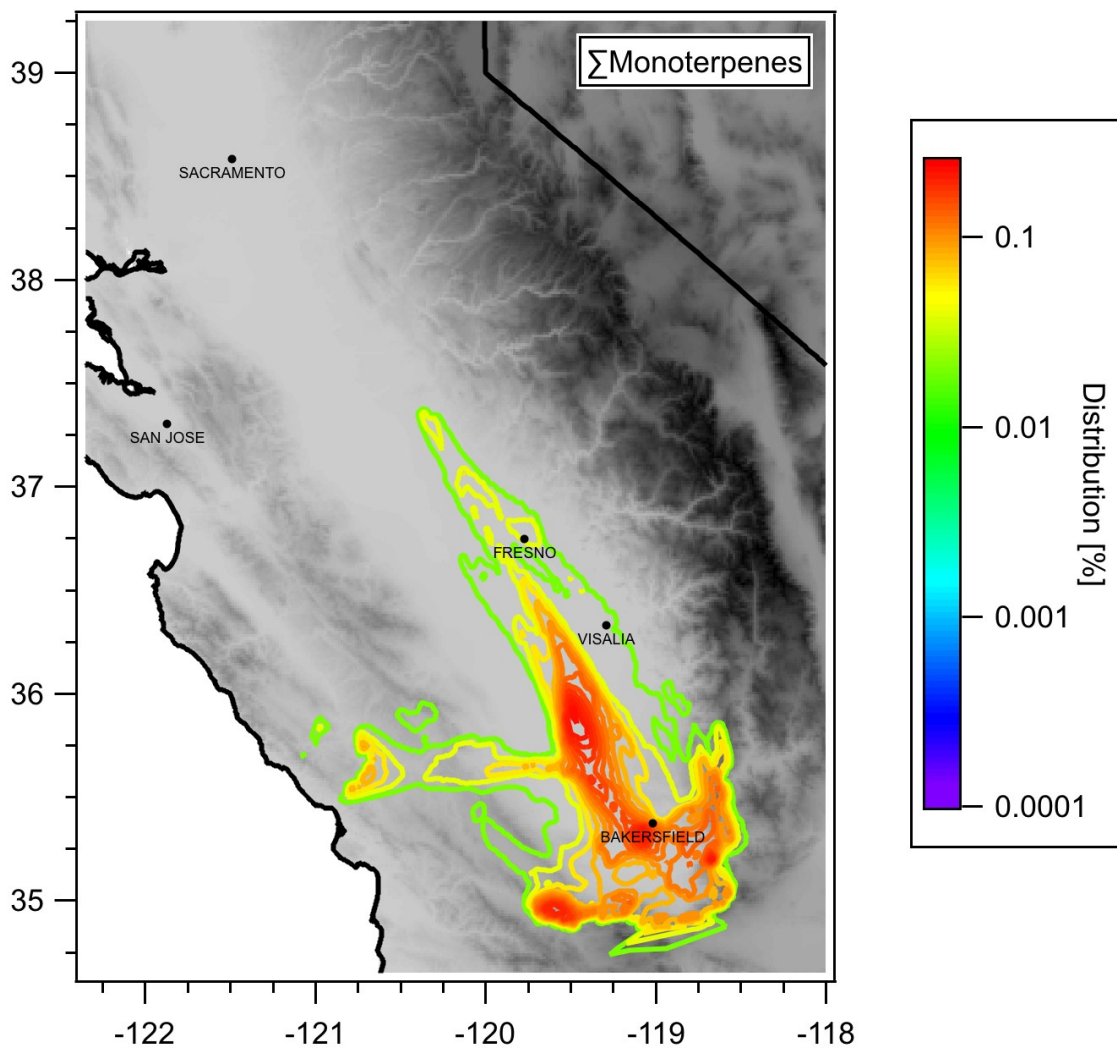


Figure 6.15: Spatial distribution of monoterpene sources in the southern San Joaquin Valley shown using the statistical source footprint of the sum of monoterpenes over 6 hours of transport prior to arrival at the ground site.

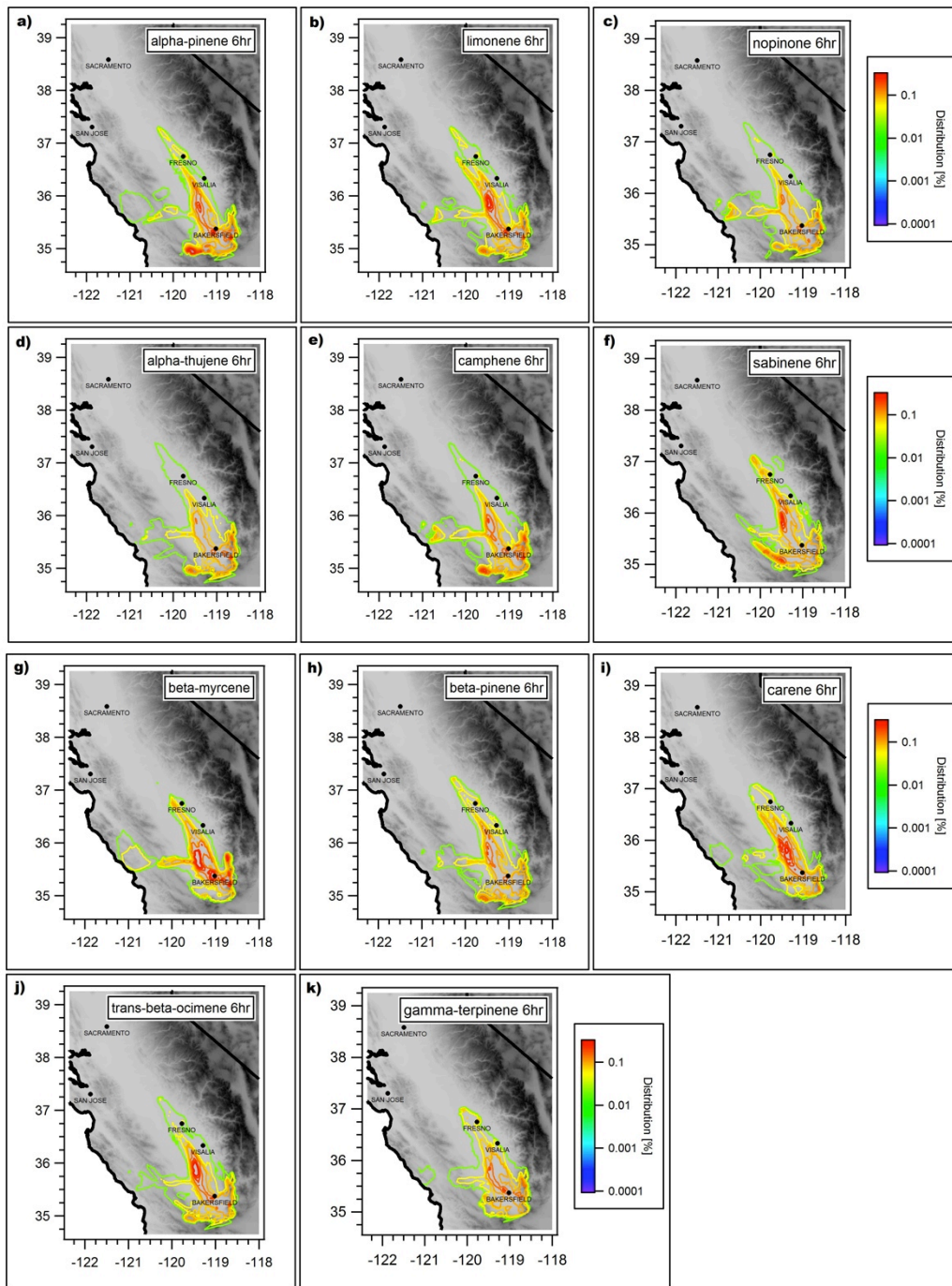


Figure 6.16: Similar to Figure 6.15, showing the spatial distribution of individual monoterpenes arriving to Bakersfield.

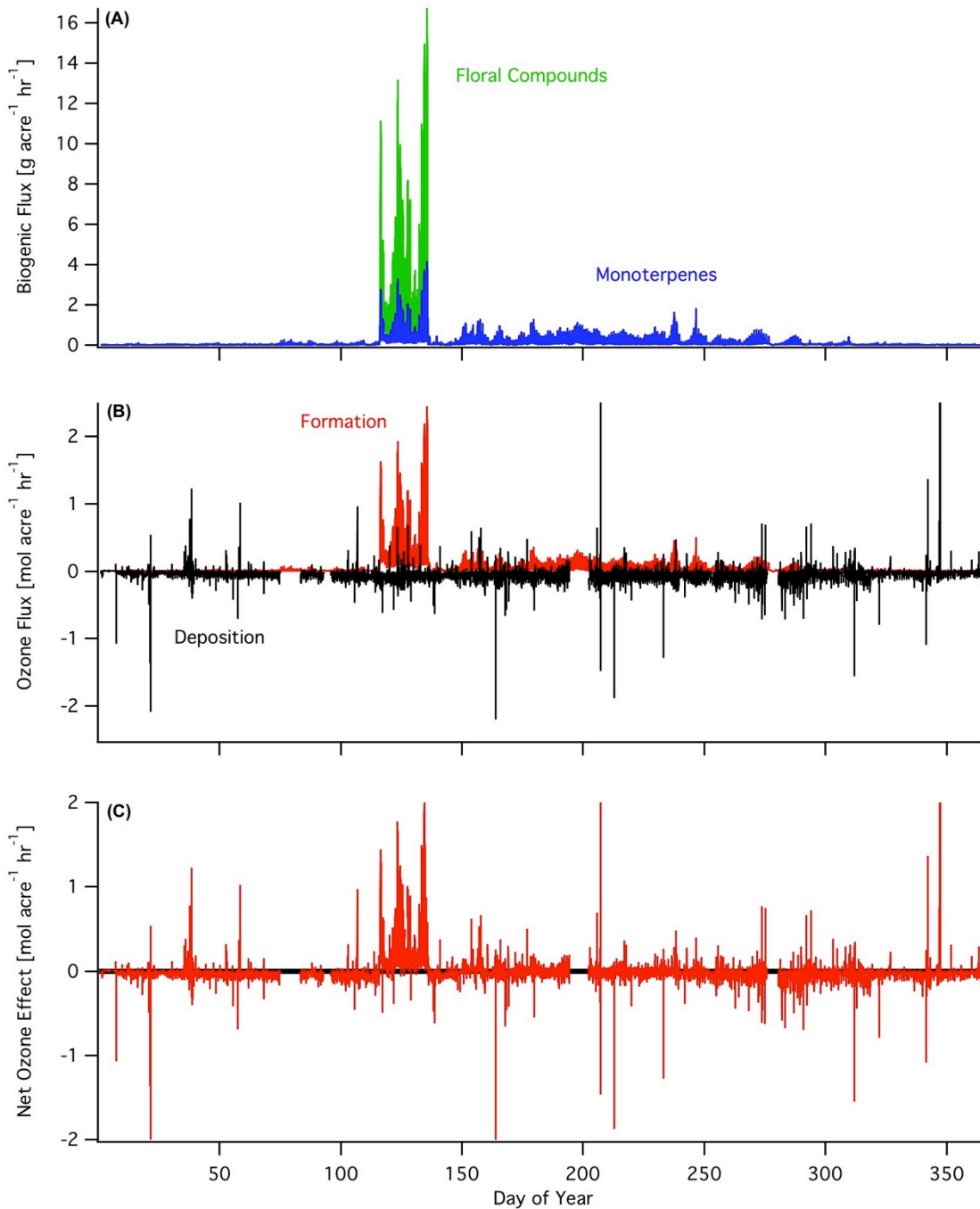


Figure 6.17: The components of the net ozone flux for the Lindcove orange grove. (A) Modeled fluxes of monoterpenes and floral compounds are greatest in the spring during flowering, but are significant throughout the summer. Sesquiterpene emissions are assumed to be equivalent to monoterpene emissions. (B) Ozone formation and deposition fluxes per acre throughout the year show variable ozone formation with more constant deposition (stomatal and chemical). Formation is calculated as potential O₃ (i.e. assuming a VOC-limited regime). (C) The combined effect of these fluxes produces a net flux into the canopy except when biogenic emissions are high.

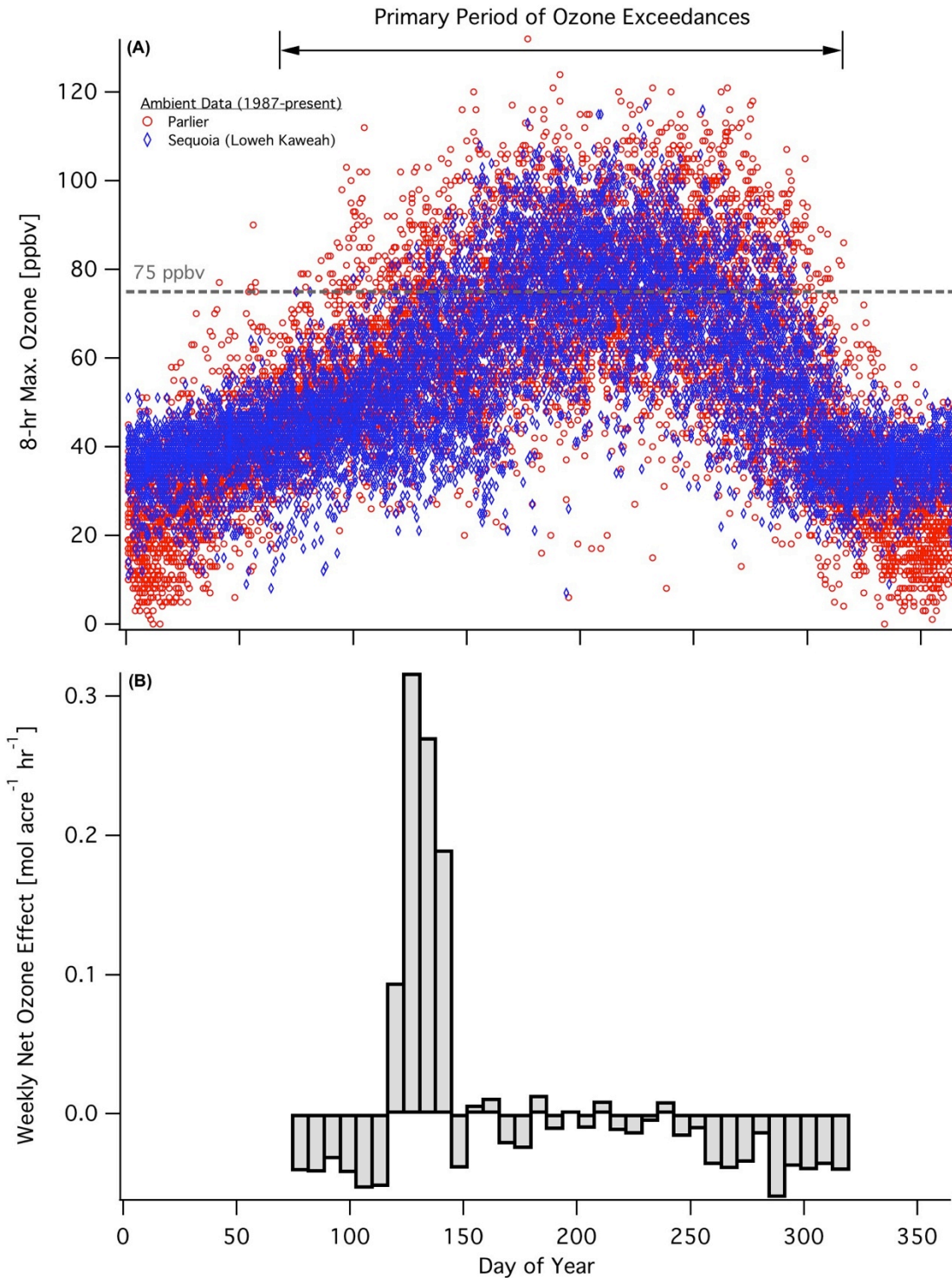


Figure 6.18: (A) Ambient ozone data since 1987 show exceedances above 75 ppbv at both the center of the valley and downwind in the Sierra Nevada mountains with the primary period of concern from day 70 to 320. No trends were apparent in the data from 1987 till present. (B) The weekly net effect of the orange grove on ozone over this period is shown to be net source of ozone in the springtime during flowering, and relatively neutral for most of the summer until the fall when it becomes a sink.

Chapter 7: Conclusions

Summary of major advancements and findings

I effectively developed instrumentation to measure a range of under-studied compounds that included Volatile Organic Compounds and Intermediate-Volatility Organic Compounds, which are hypothesized to have significant impacts on air quality through the formation of secondary organic aerosol (SOA) and tropospheric ozone. Using this instrument I was able to make the first *in-situ* measurements of numerous compounds in the ambient atmosphere from a mix of anthropogenic and biogenic sources. Measurements of gas-phase organic carbon were made at 5 field campaigns: U.C. Berkeley greenhouse plant enclosures, the CalNex (California at the Nexus of Air Quality and Climate Change) supersite in Bakersfield, CA, the Caldecott Tunnel in Oakland, CA, and two sets of seasonal measurements over an orange orchard in the rural town of Lindcove in California's San Joaquin Valley.

Several statistical methods were also developed/refined for use in this dissertation. This included a source receptor model based on chemical mass balancing with effective accounting of uncertainty and errors, which was a primary component of Chapters 4-5 and informed analyses in Chapter 6; a method for estimating bulk SOA yields from gasoline and diesel sources based on chemically speciated source profiles and a Monte Carlo analysis to incorporate yields of known compounds with under-studied compounds (Chapter 4); and statistical meteorological footprint modeling to evaluate the spatial distribution of sources. Statistical footprint modeling using the FLEXPART meteorological modeling platform provides a novel method for assessing meteorology in a region and determines the most important areas that will affect emissions and chemistry in a region. It also provides a powerful method to look at the spatial distribution of sources in a region that is much more effective than wind direction analysis, especially in cases of complex meteorology. The utility of this method is shown in Chapter 5-6 and informed the conclusions therein.

Using liquid fuel-based source profiles for gasoline exhaust and non-tailpipe (e.g. evaporative) emissions, I demonstrate the use of chemical mass balance source receptor modeling to characterize the importance of various sources to the atmosphere (Chapter 3). The study showed that non-tailpipe emissions accounted for $31 \pm 2\%$ of gasoline-related VOC in Riverside, CA, and validated California's emission factor model (EMFAC), which similarly estimates 31% of gasoline-related VOC emissions are fuel vapor. This analysis worked to set the stage for more complex subsequent analyses using source receptor modeling.

Through the use of extensive novel measurements at the CalNex Bakersfield ambient site and on-road measurements at the Caldecott Tunnel, I provide the most comprehensive assessment to date of organic carbon emissions from gasoline and diesel vehicles (Chapter 4). I provide unprecedented chemically speciated source profiles for gasoline and diesel fuel and use source receptor modeling and bulk SOA yield modeling to determine their relative importance for organic carbon emissions and SOA formation. I found that diesel exhaust forms 15 times more SOA than gasoline exhaust. Yet, both sources are important for air quality; depending on the gasoline vs. diesel fuel use in a region, diesel is responsible for 65-90% of vehicular-derived SOA, with substantial contributions from both aromatic and aliphatic hydrocarbons. The insights

from this study are likely to improve regional pollution control policies, fuel regulations, and methodologies for future measurement, laboratory, and modeling studies.

Further analysis of the Bakersfield data revealed evident a petroleum-related source on top of emissions from gasoline and diesel sources. Petroleum operations are prominent in the southern San Joaquin Valley and measurements of many associated hydrocarbons are well above typical rural or urban areas. Using statistical footprint modeling with FLEXPART meteorological data and ground-based Volatile Organic Compound measurements I examined emissions from petroleum operations. Statistical footprint modeling confirms the spatial distribution of the oil wells in the Southern San Joaquin Valley. Emissions include many VOCs that have limited previous *in situ* measurements and have not been associated with petroleum operations in the past, many of which are branched and cyclic alkanes. The abundance of non-methane hydrocarbons due to petroleum gas ranges 30-150% of emissions from motor vehicles by carbon mass in Bakersfield, which is roughly consistent with emission inventories. Emissions from the petroleum gas source likely originate from condensate tanks and are an important source of mass in the region and may have a minor effect on atmospheric chemistry.

To assess emissions of gas-phase organic carbon from agriculture, a major part of the California's central valley, emission rates for a suite of biogenic terpenoid compounds were measured for over 20 crops in enclosures and ambient measurements of terpenoids and other biogenic compounds were made over an orange orchard in a rural area of the central valley during two seasons. In the San Joaquin Valley during the summer, the mass of biogenic emissions and their formation potential for ozone and secondary organic aerosol are similar to anthropogenic emissions from motor vehicles and must be considered in air quality models and policy. Additionally, emission events, such as flowering, have significant potential to impact regional air quality as emissions increase by an order of magnitude. Flowering was a major emission event and caused a large increase in emissions and a suite of novel compounds that had not been measured in the atmosphere before. When accounting for both emissions of reactive precursors and the deposition of ozone to an orange crop, the canopy was determined to be a net source of ozone in the springtime during flowering, and had minimal effect either way for most of the summer until the fall when it became a sink.

In all, this dissertation has pushed the limits on *in situ* gas-phase organic carbon measurements and reports measurements of numerous compounds for the first time. Using these novel compounds and traditional measurements in conjunction with developed statistical techniques, I was able to characterize prominent sources with unprecedented detail and advance the state of understanding of the ozone and SOA formation potential from major gas-phase organic carbon sources. The work has assessed emissions of both novel and established compounds from a variety of biogenic and anthropogenic sources with a focus on air quality with the objective of informing policy to improve human health and the environment.

Recommendations for future research

Continued advances in instrument development are important to facilitate the progress on some of the pressing questions in atmospheric sciences and engineering—ranging from emissions to oxidation chemistry. Using the instrument development outlined in this dissertation, a valuable step for the community would be to extend the capabilities of instrumentation at field

campaigns and monitoring sites to measure a selection of chemically-speciated high molecular weight VOCs and IVOCs. As shown with the results presented in Chapter 4, exhaustive *in-situ* measurements are not always necessary to characterize emissions and atmospheric burdens from a suite of sources if measured compounds are selected insightfully. Nevertheless, periodic extensive measurements beyond the realm of typically measured species is necessary to improve atmospheric characterization, as shown in Chapters 4, 5, and 6 with emissions from motor vehicles, petroleum operations, and biogenic sources, respectively.

Efforts to comprehensively characterize source profiles for a suite of prominent and influential sources can then be used with source apportionment methods and a more limited set of ambient measurements to draw important conclusions about the impact of sources on atmospheric reactivity, secondary pollutant formation, and public health. One area that would benefit from additional attention would be the focus on techniques to measure highly reactive products of incomplete combustion (i.e. high-molecular weight alkenes and carbonyls) that are eluding current measurement methods either through reaction prior to measurement, loss in sampling systems/instrumentation (e.g. adsorption, losses on chromatography columns), or co-elution with large peaks in chromatograms. Similarly, further instrument development is necessary to adequately measure a broader array of oxygenated chemical species, including the aforementioned products of incomplete combustion and atmospheric oxidation products.

Additionally, the footprint analysis method using the FLEXPART meteorological modeling platform has been demonstrated as an effective method to accurately assess prominent flow patterns and the spatial distribution of sources in a region given a long enough period of data. Further implementation of this methodology to other campaigns and regions is recommended.

In this dissertation I have provided unprecedented information to characterize the relative importance of gasoline and diesel vehicles for organic carbon emissions and SOA formation, but considerable amount of work remains to assess and understand all the impacts of these sources as they make up a dominant fraction of AVOC emissions. My work in Chapters 3 & 4 focused on organic carbon emissions originating from fuels, but emissions of unburned motor oil from both gasoline and diesel vehicles represent an additional source of organic carbon. While total consumption of oil is minor relative to fuel, oil contributes gas and particle-phase compounds with lower volatilities than diesel fuel and needs to be better characterized with respect to chemical speciation and emission factors.

There remains a significant amount of work that needs to be done to characterize SOA yields from under-studied compounds and better include them in SOA models either explicitly or via parameterization. Chapter 4 outlines the compounds that need to be better examined in chamber studies, which include aromatics with 9 or more carbon atoms, branched alkanes, and cyclic alkanes with 5- and 6-membered rings as they all make up a considerable fraction of gasoline and diesel fuel, and potential SOA formation. I examined the compounds included in SOA models and found that 20-30% of the SOA formed from gasoline exhaust was not included in recent urban studies (Chapter 4). This exclusion needs to be rectified; as an example, C₉₋₁₁ aromatics from gasoline and diesel vehicles are important for SOA formation and need to be better represented in either explicit traditional SOA models or the extension of volatility basis set modeling to include the 10⁷ and 10⁸ μg m⁻³ C° bins that fall in the VOC range. Our ballpark estimations of traditional chemically-explicit SOA models (Chapter 4) demonstrated that

including “missing” SOA from gasoline and diesel sources dramatically improved model closure which has typically underestimated SOA in urban regions by 80-90%.

Due to regulations on NO_x control, significant progress is being made to improve heavy-duty diesel engine performance with post-combustion control technology. To better understand the future implications of motor vehicles we need to periodically assess changing emissions due to changes in gasoline and diesel fuel composition and the implementation of new engine technology and post-combustion pollution control methods. Additionally, to better characterize the relative impact of gasoline and diesel vehicles on urban and regional air quality, a similar analysis to that done for SOA is warranted for ozone formation. Furthermore, continued work on the oxidation chemistry of diesel and gasoline emissions are necessary especially with greater photochemical ages as we do not understand all the OA transformation processes that lead to the development of low-volatility OA observed in urban plumes globally. The predictive models in Chapter 4 are able to predict overall OA from motor vehicles well, but cannot effectively predict highly aged $\Delta\text{OA}/\Delta\text{CO}$ ratios in urban plumes.

As gasoline and diesel vehicles only comprise a fraction of total gas-phase organic carbon emissions, enumerating additional contributions from other anthropogenic and biogenic sources is important to elucidate ozone and SOA formation.

In chapter 5, I was able to identify a regional VOC source related to the production of crude oil and associated petroleum gas, but further work is necessary to characterize emissions from condensate tanks in the southern San Joaquin Valley and inform effective abatement methods. This will likely require field measurements on a mobile platform that closely examines individual parts of the extraction through refining process.

The characterization of biogenic emissions from a broad survey of agricultural crops in Chapter 6 demonstrated the variability in emissions from the individuals within a plant species or genus and the impact of seasonal cycles. If extensive crop level data is necessary, then further measurements are necessary across a large number of individuals at different points in their seasonal and life cycles to fully characterize emissions. Such a study could be done in a controlled setting (e.g. greenhouse) averaged over a large number of samples or over a crop field with flux measurements and detailed analysis of environmental parameters.

The importance of seasonal events such as flowering was shown to be important on regional scales and needs to be better accounted for in biogenic emission models, regional air quality models, and inventories. Further work is needed to incorporate these events into models, to characterize emission events of various types from different crops, such as flowering or different harvesting methods, and to understand their impacts on air quality.